IL
NUOVO CIMENTO
ORGANO DELLA SOCIETÀ ITALIANA DI FISICA
SOTTO GLI AUSPICI DEL CONSIGLIO NAZIONALE DELLE RICERCHE

VOL. XVII, N. 3 *Serie decima* 1° Agosto 1960

On the Inelastic Scattering by Deformed Nuclei.

Z. JANKOVIĆ

Faculty of Science, University of Zagreb and Institute « Rudjer Bošković » - Zagreb

(ricevuto il 21 Marzo 1960)

Summary. — A more general treatment of the nuclear inelastic scattering on even-even target nuclei is given particularly by introducing other collective target states besides rotational ones, the deformed diffuse nuclear and spin-orbit potentials and the Coulomb potential for the deformed target nucleus. In the first order approximation explicit expressions for the differential cross-section (18) and for the total cross-section (19) for the transition $0 \rightarrow 2$ are deduced.

In the last few years, the collective model description of the target nucleus was also applied in the attempts to explain the inelastic scattering of nuclear projectiles on nuclei with the excitation of rotational states and a direct interaction between the target nucleus and the projectile has been assumed ([1-3]). We try to generalize the above mentioned problem of inelastic scattering and particularly by introducing also other collective target states ([4]), the deformed

([1]) D. M. BRINK: *Proc. Phys. Soc.*, **68**, 994 (1955); S. HAYAKAWA and S. YOSHIDA: *Progr. Theor. Phys.*, **14**, 1 (1955).

([2]) S. YOSHIDA: *Proc. Phys. Soc.*, **69**, 668 (1956).

([3]) D. M. CHASE, L. WILETS and A. R. EDMONDS: *Phys. Rev.*, **110**, 1080 (1958).

([4]) Z. JANKOVIĆ: *Nuovo Cimento*, **14**, 1174 (1959). Another paper, with more details, to be published soon.

smooth tail nuclear and spin-orbit potentials and the Coulomb potential of the deformed target nucleus for charged projectiles.

Let the projectile a and the target nucleus X be described, in the center of mass system, by the sets of parameters ξ and α respectively. Then a Hamiltonian of the form

$$H = H(\xi) + H(\alpha) + H_{\text{int}}(\alpha, \xi) \tag{1}$$

describes the scattering of projectiles a on the targets X. Here, the first part $H(\xi)$ is simply the kinetic energy operator of the projectile.

The second term $H(\alpha)$ is the target nucleus Hamiltonian and we assume that the complete set of its orthonormalized eigenfunctions is at our disposal

$$(H(\alpha) - E_n)\Phi_n(\alpha) = 0\,, \qquad \int \Phi_n^*(\alpha)\,\Phi_k(\alpha)\,\mathrm{d}\tau_\alpha = \delta_{nk}\,. \tag{2}$$

For the collective model even-even target nucleus wave functions we have the general form [4]:

$$\Phi_n(\alpha) = \sum_K f_{Kn\beta}(\beta)\, g_{Kn\gamma}(\gamma)\, D^I_{\mu K}(\vartheta_i)\,, \qquad K\ (\text{even}) \leqslant I. \tag{3}$$

We quote the following special cases: *a*) for the rotational case, β and γ remain fixed and the sum (3) contains only one normalized $D^I_{\mu K}(\vartheta_i)$ function; *b*) for harmonic β stabilized vibrations the f wave function does not depend on K, unstabilized γ vibrations not having any n_γ quantum; *c*) for β and γ stabilized (an) harmonic vibrations (with the small or vanishing equilibrium values β_0, γ_0) the sum (3) reduces to one K term.

The third term in the Hamiltonian (1) represents the interaction between the projectile and the target nucleus and is composed of three terms originating from nuclear forces, Coulomb force and spin-orbit coupling, all being dependent on both sets of parameters α and ξ:

$$H_{\text{int}}(\alpha, \xi) = V_n(\alpha, \xi) + V_c(\alpha, \xi) + V_s(\alpha, \xi)\, \boldsymbol{l}\cdot\boldsymbol{s}\,. \tag{4}$$

For the collective model the sharp deformed surface has been originally introduced by

$$R = R_0\Big(1 + \sum_\nu a_\nu Y^\nu_2(\vartheta', \varphi')\Big)\,, \qquad R_0 = r_0\sqrt{A}\,. \tag{5}$$

a_ν being known functions of the deformation parameters β and γ, ϑ', φ' meaning the polar angles in the principal axes system. The nuclear forces

potential as well as the spin-orbit potential are functions of the distance $r - R$ and one can expand them in the following way

$$(6) \qquad V(r-R) = -\mathscr{V}_0 f(r-R) = -\mathscr{V}_0 \sum_k \frac{1}{k!} \frac{\mathrm{d}^k f(r-R_0)}{\mathrm{d}r^k} \left(-R_0 \sum_\nu a_\nu Y_2^\nu(\vartheta', \varphi')\right),$$

where $\mathscr{V}_0$ is a constant (may be depending on target atomic number and projectile's energy) and R (and R_0) has to be redefined as a mean value regarding the diffuse potential V. Thus, in the expression (6), we have a diffuse and deformed potential expanded in a power series of deformation parameters a_ν. Allowing a change of these parameters with time, the whole deformed and diffuse edge target, represented by the potential (6), executes vibrations and rotations.

The optical model suggests a complex nuclear potential, in order to take care of the target's absorption of the projectiles, which leads in the most simple case to put

$$(7) \qquad \mathscr{V}_0 = V_0 + iW_0 ,$$

where in general we could assume different r dependences both for real and imaginary parts, each part being then expanded like (6).

Thus, by choosing a smooth complex potential (*e.g.* of the Woods-Saxon type) we have in expression (6) its series expansion, the zero order term being of spherical symmetry.

For the square well potential we see from (6) that approximately, the first order term is represented by a spherical delta surface function which has been applied in [1] and [2].

By assuming a spatial distribution of protons the Coulomb potential can also be expanded in a power series of deformation parameters a_ν. The expansion problem being here more difficult, we assume as a good approximation the uniform charge distribution in the deformed target nucleus with the sharp surface (5), in which case the expansion can be made easily. For further application we quote the first order approximation:

$$(8) \qquad \begin{cases} V_C(\alpha, \xi) = \dfrac{4\pi R_0^3}{3r} \varrho \left[1 + \dfrac{3}{5}\left(\dfrac{R_0}{r}\right)^2 \sum_\nu a_\nu Y_2^\nu(\vartheta', \varphi')\right], & r \geqslant R_0 \\ V_C(\alpha, \xi) = 2\pi R_0^2 \varrho \left[1 - \left(\dfrac{r}{R_0}\right)^2\right] + \dfrac{4\pi}{5} r^2 \varrho \sum_\nu a_\nu Y_2^\nu(\vartheta', \varphi'), & r \leqslant R_0 , \end{cases}$$

where again the zero order terms are the known expressions for the Coulomb potential of a uniform spherically distributed charge.

To solve the scattering problem we expand the stationary solution of the Schrödinger equation

$$(H - E)\Psi(\alpha, \xi) = 0\,, \tag{9}$$

with H given by expression (1) and E representing the total energy of the projectile plus the target nucleus, into a series of the complete set of target wave functions

$$\Psi(\alpha, \xi) = \sum_n \Phi_n(\alpha)\, u_n(\xi)\,. \tag{10}$$

Inserting the expression (10) in the Schrödinger equation (9) we find that the projectile's wave functions have to satisfy this system of linear coupled second order differential equations

$$\frac{\hbar^2}{2m}\Delta u_n(\xi) + (E - E_n)\, u_n(\xi) - \sum_k H_{nk}(\xi)\, u_k(\xi) = 0\,, \tag{11}$$

m being the projectile's reduced mass, n the set of quantum numbers specifying completely the target quantum state and H_{nk} the following interaction Hamiltonian matrix elements

$$H_{nk}(\xi) = \int \Phi_n^*(\alpha)\, H_{\text{int}}(\alpha, \xi)\, \Phi_k(\alpha)\, \mathrm{d}\tau_\alpha\,. \tag{12}$$

By the known procedure ([5]) the differential cross-section for a transition $i \to f$ is expressed in the following way:

$$\mathrm{d}\sigma_{if}(\Omega) = \frac{v_f}{v_i} |r\,(u_f^{(+)}(\xi) - u_{\text{inc},i}^{(+)}(\xi)\,\delta_{fi})\,|^2_{\text{Asympt}}\,\mathrm{d}\Omega\,. \tag{13}$$

The system (11) contains in principle infinite number of differential equations and cannot be solved without approximations with regard first to the number of equations (*i.e.* the number of target states taken into account) and second to the order of approximation in calculating the matrix elements (12). The most simple case represents the two states case where the spinless projectile induces the target transition from the i to the f state, all other transitions neglected, and only the lowest order target deformation taken into

---

([5]) J. M. Blatt and L. C. Biedenharn: *Rev. Mod. Phys.*, **24**, 261 (1953); see also ref. ([6]).

account when calculating the matrix elements. Under these assumptions the system (11) reduces to the following two equations:

$$(14)\qquad \begin{cases} \dfrac{\hbar^2}{2m}\Delta u_i(\xi) + \left(E - E_i - V_n^{(0)}(r) - V_C^{(0)}(r)\right) u_i(\xi) = 0\,, \\ \dfrac{\hbar^2}{2m}\Delta u_f(\xi) + \left(E - E_f - V_n^{(0)}(r) - V_C^{(0)}(r)\right) u_f(\xi) = H_{fi}^{(1)}(\xi)\, u_i(\xi)\,, \end{cases}$$

where ξ means the projectile's spatial co-ordinate's and the matrix element (12) calculated with the first order target deformation a_ν terms. For the more specified transition: i (fundamental state $I = 0$, $\mu = K = 0$), f (first excited state $I = 2$, μ; $K = 0$) of an even-even target nucleus, one finds for the matrix element with wave functions (3):

$$(15)\qquad H_{fi}^{(1)}(\xi) = C\left(V_n^{(1)}(r) + V_C^{(1)}(r)\right) Y_2^{\mu *}(\vartheta, \varphi)\,,$$

where the constant C takes on different values according to the different specifications of the wave functions:

$$(16)\qquad \begin{cases} a) \quad C_r = \dfrac{a_0}{\sqrt{5}}\,, \\ b) \quad C_B = \dfrac{36}{\sqrt{\Gamma\left(\frac{5}{2}\right)\Gamma\left(\frac{7}{2}\right)}}\,\dfrac{\hbar}{B\omega}\,, \\ c) \quad C_g = \mathscr{I}(n_\beta, n_\gamma), \qquad n_\beta + n_\gamma = 1\,. \end{cases}$$

$\mathscr{I}$ representing an integral of the corresponding f and g wave functions. Each coefficient C can be numerically expressed when the collective model, *i.e.* the corresponding collective Hamiltonian, is completely specified.

After performing a series expansion in spherical harmonics for both functions $u_i(r, \vartheta, \varphi)$ and $u_f(r, \vartheta, \varphi)$

$$(17)\qquad u(r, \vartheta, \varphi) = \sum_{l=0}^{\infty} \sqrt{\pi(2l+1)}\,\frac{i^{l+1}}{kr}\, u_l(kr) Y_l^m(\vartheta, \varphi)\,,$$

one gets from (14) the radial wave equations: homogeneous for u_{i,l_i} and inhomogeneous u_{f,l_f}. There is a known procedure ([6]) to find the asymptotic form of the solution $u_{f,l_f}^{(+)}$ (and then by (17) also for $u_f^{(+)}$) needed for the calculation of the differential cross-section (13) $\mathrm{d}\sigma_{if}^{\mu}(\Omega)$.

([6]) N. F. MOTT and H. S. W. MASSEY: *The Theory of Atomic Collisions* (Oxford, 1952), p. 108.

A summation over the final state magnetic quantum number μ gives the differential cross-section for the transition i $(I = 0)$ to f $(I = 2)$:

$$(18) \qquad \mathrm{d}\sigma_{if}(\Omega) = \left(\frac{2m}{\hbar^2} C\right)^2 \frac{1}{64\pi k_f k_i^3} \sum_{l_f l_i l'_f l'_i L} i^{l_f + l_i - l'_f - l'_i} \cdot$$
$$\cdot (2l_f + 1)(2l'_f + 1)(2l_i + 1)(2l'_i + 1) I^*_{l_f l_i} I_{l'_f l'_i} \cdot$$
$$\cdot C(l_f l_i\, 2\,{:}\,00)\, C(l'_f l'_i\, 2\,{:}\,00)\, C(l'_f l_f\, L\,{:}\,00)\, C(l'_i l_i\, L\,{:}\,00) W(l_i l'_i l_f l'_f {:} L2)\, P_L(\cos\vartheta)\, \mathrm{d}\Omega$$

and the integration gives the total cross-section

$$(19) \qquad \sigma_{if} = \left(\frac{2m}{\hbar^2} C\right)^2 \frac{1}{16 k_f k_i^3} \sum_{l_f l_i} (2l_f + 1)(2l_i + 1) |I_{l_f l_i}|^2 C(l_f l_i\, 2\,{:}\,00)^2 .$$

Here $I_{l_f l_i}$ means the integral

$$(20) \qquad I_{l_f l_i} = \int_0^\infty \bar{u}_{f,\, l_f}(k_f r)\, \bar{u}_{i,\, l_i}(k_i r) \left(V_n^{(1)}(r) + V_C^{(1)}(r)\right) \mathrm{d}r ,$$

both dashed $\bar{u}$ functions meaning the stationary solutions of the elastic scattering problem (homogeneous differential equations in (14)) vanishing at the origin and behaving as $u_l^{(-)} - \eta_l u_l^{(+)}$ at the infinity, $u_l^{(\pm)}$ being the known asymptotic forms $\exp[\pm i(kr - \eta \ln 2kr - l(\pi/2))]$ for charged particles and with $\eta = 0$ for neutral particles. η_l is the factor describing nuclear and Coulomb scattering. Clebsch-Gordan coefficients take care of the conservation of the total angular momentum, only even or odd l values can combine because of the conservation of parity.

We see in this simple example, under assumptions which are essentially equivalent to the first order perturbation calculation, how the diffuseness, deformability and charge distribution of the target nucleus enter through the coefficient (20) into the differential and total cross-sections (18) and (19). The nature of the states i and f (k_i and k_f assumed to be the same) different under assumptions *a*), *b*) and *c*) influences only the absolute values of the differential and total cross-sections through the different coefficients C^2 given in (16) and has no influence on the angular distribution of the inelastically scattered projectiles.

* * *

This work has been done during the author's stay at the Centre d'Etudes Nucléaires de Saclay. The author wishes to express his appreciation of the

arrangements which made possible his stay at the Centre d'Etudes Nucléaires de Saclay and is very much indebted to Prof. J. THIRION for the hospitality at the Section des Réactions Nucléaires à Moyenne Energie. A grant from the Institute « Rudjer Bošković », Zagreb, is gratefullb acknowledged.

RIASSUNTO (*)

Si espone un trattamento più generale dello scattering nucleare anelastico su nuclei targhetta pari-pari, particolarmente introducendo altri stati collettivi della targhetta oltre a quelli rotazionali, i potenziali nucleari diffusi deformati e di spin-orbita e il potenziale coulombiano del nucleo deformato della targhetta. Con approssimazione di primo ordine si deducono espressioni esplicite per la sezione trasversale differenziale (18) e per la sezione trasversale totale (19) per la transizione $0 \to 2$.

(*) *Traduzione a cura della Redazione.*

IL NUOVO CIMENTO Vol. XVII, N. 3 1° Agosto 1960

A Method for Trapping Muons in Magnetic Fields, and Its Application to a Redetermination of the EDM of the Muon.

G. Charpak (*), L. M. Lederman (**), J. C. Sens and A. Zichichi

CERN - Geneva

(ricevuto il 4 Aprile 1960)

Summary. — A method for trapping muons in magnetic fields is described together with its application to higher accuracy determination of the electric dipole moment of the muon. The value found is:

$$\mathrm{EDM} \leqslant e(5 \pm 5) \cdot 10^{-17} \text{ cm}$$

consistent with time reversal invariance.

1. – Introduction.

The availability of beams of polarized muons with asymmetric decay has stimulated many groups to consider the extension to the case of the muon of the methods used by Louisell, Pidd and Crane [1], to measure the anomalous magnetic moment of the electron.

In this method, one can measure directly $(g-2)$ by storing the particles for some time in a magnetic field and then measuring the relative precession angle between the spin and the momentum, which serves as a reference vector. As in the electron experiments, the prime requirement is to succeed in injecting the muons into a magnetic field so that they circulate on essentially periodic orbits, and to trap them in this field for as large a number of « turns », *i.e.* orbit periods, as possible. The low fluxes, high momenta and large extensions

(*) On leave from Centre National de la Recherche Scientifique, Paris.

(**) Ford Foundation Fellow, on leave from Columbia University. Also J. S. Guggenheim Fellow, 1958-1959.

(1) W. K. H. Louisell, R. W. Pidd and H. R. Crane: *Phys. Rev.*, **94**, 7 (1954).

in position and momentum space (low density in phase space) which the presently available muon beams exhibit in comparison with conventional electron beams present, however, many new difficulties in meeting this requirement. On the other hand, there is one advantage of the muons—it is not necessary to analyze the spin polarization by scattering, since the asymmetric electron decay reveals the spin deviation.

Several practical methods for overcoming these difficulties have been investigated experimentally and/or theoretically over the past year at CERN. We have now succeeded in trapping muons of 85 MeV/c momentum for 28 turns, and our results indicate that minor modifications in the method used should enable one to achieve storage for several hundreds of turns. The main purpose of this note is to describe this method.

As a first application, we have used equipment that was primarily developed for trapping studies, for a redetermination of the electric dipole moment (EDM) of the muon. It is known [2] that elementary particles can possess an EDM only if they have some interaction not invariant under time-reversal. In this sense, a search for an EDM constitutes a test of the validity of this invariance principle. Like previous workers [3] we have found a value for the muon EDM that is zero within the experimental errors. These errors were, however, considerably reduced with respect to those of refs. [3]—mainly in virtue of the much longer time which the muons spend in the field in our arrangement. The second purpose of this note is to discuss our EDM determination and its results.

2. – Injection and trapping.

The principle of our method, to be described with reference to Fig. 1, is to inject a muon beam into the median ($X - Y$) plane of a flat magnet gap (say, along the Y-axis), and to contain it therein by reducing the momentum by means of a moderator M, to a value p, the latter being suited to the mean vertical field B_{z0} and the lateral extension of the gap. The magnetic field configuration is so chosen as to produce a drift of the muon orbits along the X-axis away from M, and to focus them in the median plane. The trapping efficiency obtainable is of course limited by the Liouville theorem.

---

[2] L. LANDAU: *Nucl. Phys.*, **3**, 127 (1957); I. B. ZELDOVICH: *Žurn. Èksp. Teor. Fiz.*, **33**, 1488 (1957). Also T. D. LEE and C. N. YANG: *B.N.L.*, 443 (1957).

[3] D. BERLEY, R. L. GARWIN, G. GIDAL and L. M. LEDERMAN: *Phys. Rev. Lett.*, **1**, 144 (1958); *Annual International Conference on High Energy Physics, CERN* (1958), p. 332; D. BERLEY, G. GIDAL and L. M. LEDERMAN: *Kiev Conf.*, 1959 (to be published). See also R. L. GARWIN and L. M. LEDERMAN: *Nuovo Cimento*, **11**, 776 (1959).

Our field had the form:

$$B_z = B_{z0}(1 + ay - by^2) \tag{1}$$

in the median plane (the exit point of M being taken as the origin). With $ar \ll 1$ and $br^2 \ll 1$, the muons emerging from M will move on nearly circular

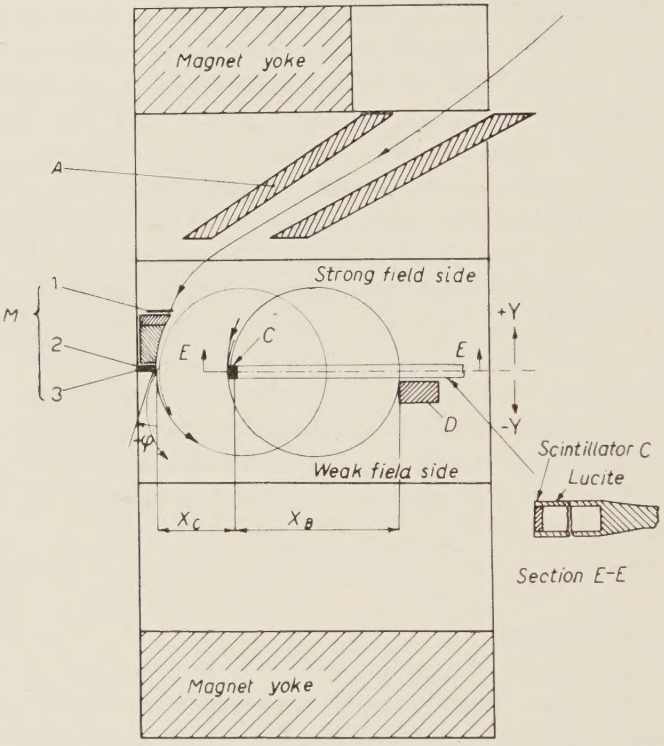

Fig. 1. – Experimental layout. *A*) magnetic channel; *B*) scintillator; *D*) lucite block; *M*) moderator; 1, 2, 3) scintillators.

orbits of radius r. As is well known, a linear gradient alone leads to a drift of these orbits in the X-direction by an amount (« step-size »):

$$s = \pi r^2 \langle \text{grad}\, B_z/B_z \rangle = \pi r^2 a/\text{turn}\,, \tag{2}$$

where $\langle\ \rangle$ denotes average over one orbit loop. This drift enables some of the muons to clear M after their first turn, whereupon they proceed on a trochoidal orbit. The linear gradient produces also a feeble vertical focusing, partly because the field index (n) is larger in the weak field region (vertically focusing) than in the strong field region (vertically defocusing) and partly

because of the « strong focusing » effects of even equal alternating n-values. An accurate analysis (4) gives for the vertical focusing wavelength:

$$\frac{\lambda_v}{2\pi} = \frac{0.76}{a} .$$

This focusing is, however, very *weak* ($\lambda_v/2\pi r \gg 1$), because one wants $r/s \gg 1$ in order to store as large as possible a number of turns in a magnet of given size. With $r/s = 16$ for example, one has one vertical oscillation per 38 turns. Thus, as we could verify experimentally, the vertical divergence, due to multiple scattering of the muons emerging from M, leads to poor storage as long as one provides only a linear gradient. In addition, it is very difficult in such a field to keep the magnetic median plane near the centre of the gap. Should the median plane touch the poles, *all* particles are lost.

As was pointed out by GARWIN, one can improve the vertical focusing while maintaining a given large value of r/s by the addition of the by^2 term. In fact, for the field given by (eq. (1)), one has:

$$\frac{\lambda_v}{2\pi} = (b + 1.74a^2)^{-\frac{1}{2}} \sim \frac{1}{\sqrt{b}} ,$$

while the step-size is still given by eq. (2) for orbits which start out parallel to the Y-axis. By taking, *e.g.* $b = 50a^2$, one can, while maintaining the same r/s above (for such orbits), improve the focusing to 1 oscillation/7 turns. Thus the intensity of stored muons is increased by a factor $38/7 \sim 5$ by the addition of the quadratic term to the field. The by^2 term serves also the useful function of fixing more firmly the magnetic median plane in the centre of the magnet gap. An additional consideration is the location of the edge of the stability bands for orbits in a field of the form (1). The result quoted for $\lambda_v/2\pi$ is of course correct only for small b and a. For large b and a the vertical focusing first improves and then becomes unstable. These questions are treated in reference (4). It is, however, not permissible to choose b arbitrarily large, because this would lead to a spread in step-sizes and hence in storage times—even if a mono-energetic beam could be made to emerge from M. Orbits emerging at an angle Φ with respect to the Y-axis would have a step-size:

$$s(\Phi) = \pi r^2(a - 2b\,r\Phi) \tag{3}$$

---

(4) R. L. GARWIN: *Numerical calculations of the stability bands and solutions of a Hill differential equation*, CERN internal report (October 1959); W. K. H. PANOFSKY: *Orbits in the linear magnet*, CERN internal report (October 1959).

as can be seen by introducing eq. (1) into eq. (2). A spread in Φ is in practice unavoidable, and is reflected in a spread in s according to eq. (3). For a fixed Φ one has, on the other hand, an additional momentum dependence as compared to the case with $b = 0$. Both of these effects depend on b, and its magnitude must be chosen so as to maximize the number of particles stored for a given number of turns.

The field of eq. (1) (with $B_{z0} = 13.1$ kG, $a = 10^{-3}$ cm, $b = 5 \cdot 10^{-5}$ cm^2) was obtained by modifying an existing magnet of gap volume $83 \times 53 \times 10$ cm^3. The linear gradient was produced by inserting wedge-shaped iron plates behind the pole caps. Additional shims served to provide the quadratic term and to correct for field irregularities. Iron bars of suitable profile, mounted along all the edges of the gap, served to increase its useful width and length by cancelling the field fall-off originally present. Out to a distance of 2.5 cm from the edges, the so resulting field agreed to better than 0.2% with the prescribed dependence (eq. (1)).

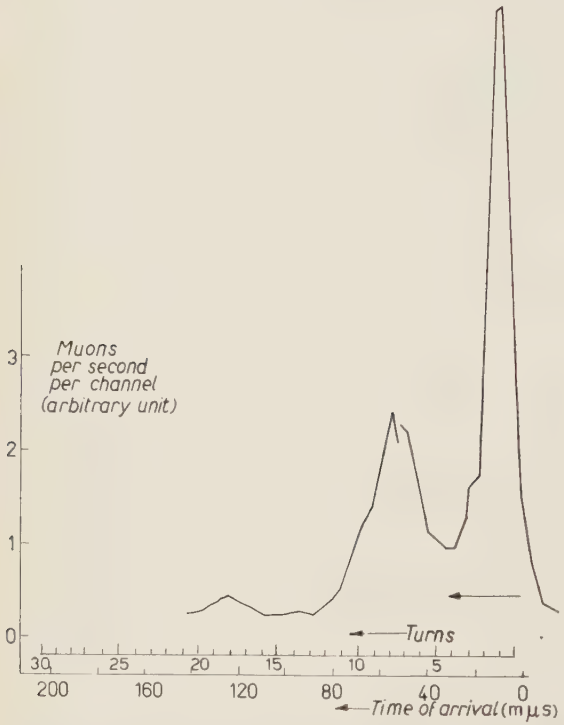

Fig. 2. – Time distribution of the stored muons as displayed on the pulse height analyser, Distance between moderator M and counter C, $x_0 = 13$ cm. C detects muons having completed an integer number of turns.

In the actual experiments, a π^+, μ^+ beam of momentum 150 MeV/c was focused, by means of a pair of quadrupole lenses (not indicated in Fig. 1), through an iron channel, which served to eliminate the fringing field of the magnet, onto the moderator M. The moderator consisted of a Be block of 14.7 g/cm^2 thickness (Be was used because of its low Z and high density), of a few graphite plates for minor range adjustments, and of the three scintillators of counters 1, 2, 3 constituting an injection telescope. The curved shape of this assembly, indicated in Fig. 1, enabled the muons to clear it after their first turn. M reduced the initial momentum to $\overline{p} \approx 85$ MeV/c. A polyethylene bag filled with helium gas at atmospheric pressure served to reduce ionization loss and scattering below that due to air.

Even so, the muon population can be shown to decrease exponentially due to multiple scattering with a decay length of ~ 42 turns.

The storage was studied by placing a scintillator C on the X-axis at a distance X_c from M, and measuring the distribution of the times of arrival of the muons striking C. This distribution is determined by means of a time-to-pulse-height converter (T.C.) system, which had (123) and C for inputs, and was displayed on a many-channel pulse-height analyser (PHA). Figs. 2 and 3*a* are typical examples of two distributions obtained in this way, differing in the position at which counter C was placed.

For $X_c < 2\bar{r}$ (*) one detects in C mostly muons which have completed an integral number of turns (**),

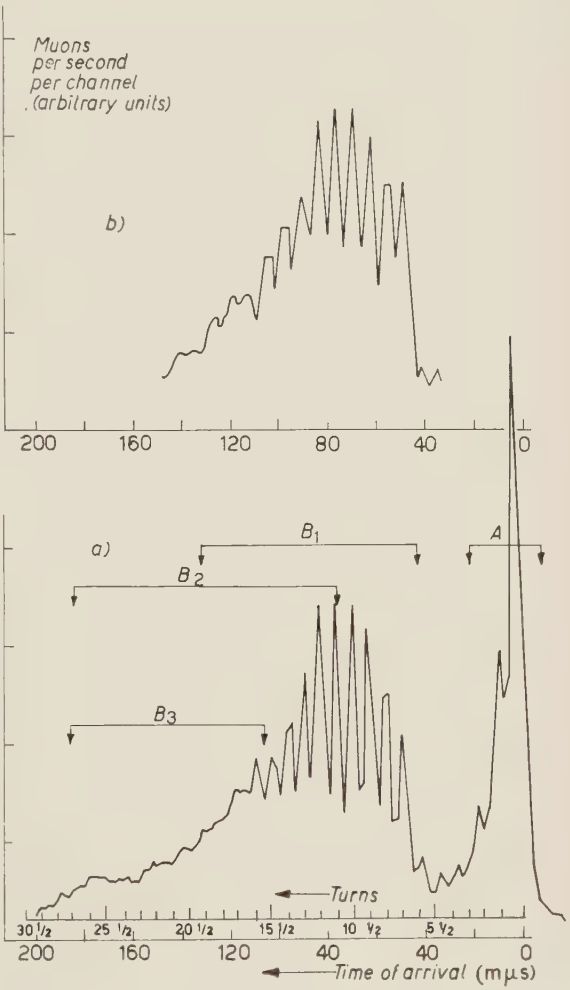

Fig. 3. – *a*) Time distribution of the stored muons displayed on the pluse-height analyser. Distance between moderator M and counter C, $x_c = 66$ cm. C detects muons having completed $n+\frac{1}{2}$ turns, where n is an integer. *Group A*: particles with mean turn number $\langle n \rangle = 1$, reaching C after excursion through the fringing field. *Groups* B_1, B_2, B_3: particles with $\langle n \rangle_1 = 11.5$; $\langle n \rangle_2 = 16.5$; $\langle n \rangle_3 = 19.5$. The arrows indicate the single channel analyser window limits. - *b*) Calculated time distribution. The area of this distribution is normalized to the experimentally obtained area from channel 7 to 20.

(*) From here on we indicate with a bar ($\bar{b}$) all quantities (as for instance, radius, step-size, etc.) corresponding to the momentum $\bar{p}$.

(**) It is possible for muons to cross the X-axis at $X > X_c$ because counter C was built with an « air light-pipe ». The scintillator C was glued to two thin lucite strips on top and bottom of the scintillator itself. This system was wrapped in Al-foil of 4 mg/cm² thickness. The beam traverses therefore ~ 8 mg/cm² per turn.

for $X_c > 2\bar{r}$ one detects muons mostly of a half-odd integral number of turns. The essential features of such distributions, *viz.* *a*) the occurrence of a main peak accompanied by smaller « satellite » peaks, *b*) the time separation between peaks, *c*) the widths of each peak, *d*) the width of the entire group of peaks, and *e*) the relative populations of the peaks, are readily understood on the basis of the following considerations:

Let C be placed at the point x_μ where the muons of momentum $\bar{p}$ cross the X-axis, after having completed an integral number, $\bar{n}$, of turns:

$$x_c = x_\mu = \bar{n}\,\bar{s}\,. \tag{4}$$

For such an x_c, the T.C. distribution will exhibit a main peak at:

$$t_n = \bar{n}\bar{T}, \tag{5}$$

where $\bar{T}$ is the orbital period corresponding to $\bar{p}$, *i.e.* ≈ 7.25 ns in our case.

Since the time of arrival is a function of p, Φ and x_μ: $t = t(p, \Phi, x_\mu)$, a spread in momentum and angle of the beam emerging from M, as well as the finite width « w » of C ($\mathrm{d}x_\mu < w < 2\bar{s}$) will result in a spread $\mathrm{d}t$ in time of arrival. In fact, since:

$$t = nT \qquad \text{and} \qquad x_\mu = ns \tag{6}$$

one has:

$$\mathrm{d}t/t = \mathrm{d}n/n + \mathrm{d}T/T = \mathrm{d}n/n + \beta^2\,\mathrm{d}p/p\,; \qquad (\text{where } \beta = r/c) \tag{7}$$

$$\mathrm{d}x_\mu/x_\mu = \mathrm{d}n/n + \mathrm{d}s/s\,. \tag{8}$$

Substituting into eq. (7) the value of $\mathrm{d}n/n$ obtained from eq. (8) and making use of eq. (3), one obtains:

$$\mathrm{d}t/t = (\beta^2 - A)\,\mathrm{d}p/p - B\,\mathrm{d}\Phi + \mathrm{d}x_\mu/x_\mu\,, \tag{9}$$

where A and B are defined by the relation:

$$\mathrm{d}s/s = A\,\mathrm{d}p/p + B\,\mathrm{d}\Phi\,, \tag{10}$$

with

$$A = 2\left(\frac{a - 3br\Phi}{a - 2br\Phi}\right),$$

and

$$B = -\,2br/(a - 2br\Phi)\,.$$

For example, for a beam with $\bar{p} = 85$ MeV/c, $\bar{\Phi} = 0$, $x_\mu = 8.5$ cm, $|\mathrm{d}x_\mu| = w/2 = 1$ cm, $\mathrm{d}p/p = 10\%$, $\mathrm{d}\Phi = 0.1$ rad, one finds for the relative spread on the T.C. time scale $dt/t = 50\%$. The distribution of times of arrival, however, is not a smooth function but exhibits a peak structure, as can be seen from eq. (8), by noting that $\mathrm{d}n$ must be an integer, say $dn = m$, where m indicates the order of the satellite peak. With eq. (9), one can evaluate the separation between satellites by substituting into eq. (9) the values of $\mathrm{d}p/p$ and $\mathrm{d}\Phi$ that satisfy eq. (8) and eq. (10) for a given $\mathrm{d}n = m$, taking into account the correlated distributions in p and Φ of the stored beam.

The width of each satellite is obtained in the same way, by computing $\mathrm{d}t/t$ for a fixed n; *i.e.* $dn = 0$. From eqs. (8) and (10) we can write:

$$\frac{\mathrm{d}x_\mu}{x_\mu} = \frac{\mathrm{d}n}{n} + \frac{A\,\mathrm{d}p}{p} + B\,\mathrm{d}\Phi\,. \tag{11}$$

If the available $\mathrm{d}p$ are large enough, this equation always can be satisfied for a given $\mathrm{d}x_\mu$ or $\mathrm{d}\Phi$, and we have from eq. (9):

$$\frac{\mathrm{d}t}{t} = \frac{\beta^2}{A}\frac{\mathrm{d}x_\mu}{x_\mu} + \frac{(A-\beta^2)}{A}\frac{\mathrm{d}n}{n} - \frac{\beta^2 B}{A}\,\mathrm{d}\Phi\,. \tag{12}$$

Thus, the width of the n-th turn ($\mathrm{d}n = 0$) is:

$$\left(\frac{\mathrm{d}t}{t}\right)_n = \frac{\beta^2}{A}\frac{\mathrm{d}x_\mu}{x_\mu} - \frac{\beta^2 B}{A}\,\mathrm{d}\Phi\,,$$

(the terms to be added in quadrature, of course). For $\mathrm{d}x_\mu \leqslant s_{\max}$ and $\mathrm{d}\Phi = 0.1$, we have

$$\frac{\mathrm{d}t}{t} = \frac{\beta^2}{A}\left[\left(\frac{1}{n}\right)^2 + (B\,\mathrm{d}\Phi)^2\right]^{\frac{1}{2}},$$

$$\mathrm{d}t = \frac{\beta^2 T}{A}\left[1 + (0.1nb)^2\right]^{\frac{1}{2}} = T\frac{0.4}{2}\left[1 + (0.22n)^2\right]^{\frac{1}{2}}.$$

Numerically the widths of the peaks should be:

$$\mathrm{d}t\,(n = 1) = 0.20\,T\,,$$

$$\mathrm{d}t\,(n = 10) = 0.48\,T\,,$$

$$\mathrm{d}t\,(n = 20) = 0.90\,T\,.$$

The separation between peaks is essentially constant and equal to $\bar{T}$ because of the weak dependence of T on p (eq. (7)).

To find the overall width of the distribution in t, we use eq. (9) with:

$$\frac{\mathrm{d}p}{p} = 0.1\,,$$

$$\mathrm{d}q = 0.1 \text{ rad}$$

$$\mathrm{d}x_\mu = 1 \text{ cm}$$

$$x_\mu = 13 \text{ cm}$$

to find

$$\left(\frac{\mathrm{d}t}{t}\right) = \pm\left\{[(1.6)0.1]^2 + (0.22)^2 + \left(\frac{1}{13}\right)^2\right\}^{\frac{1}{2}} = \pm 0.28\,.$$

Thus far we have considered the case where the counter C was placed such as to accept muons that have completed an integer number, n, of turns. An analogous derivation of the previous formulae can be obtained for the case where C is set to accept muons after $(n+\frac{1}{2})$ number of turns. In this case, one has instead of eq. (6):

$$x_c = x_\mu = (n+\tfrac{1}{2})s + 2r\,; \qquad t = (n+\tfrac{1}{2})T\,.$$

One finds instead of eq. (9):

$$\mathrm{d}t/t = (\beta^2 - A - 2r/(n+\tfrac{1}{2})s)\,\mathrm{d}p/p - B\,\mathrm{d}\Phi + \mathrm{d}x_\mu/(n+\tfrac{1}{2})s\,. \tag{13}$$

By an argument similar to that following eq. (12), we obtain for the width of particular turns:

$$\mathrm{d}t\,(n = \tfrac{1}{2}) = 0.004\,T$$

$$\mathrm{d}t\,(n = 10+\tfrac{1}{2}) = 0.17\;\; T$$

$$\mathrm{d}t\,(n = 20+\tfrac{1}{2}) = 0.36\;\; T$$

$$\mathrm{d}t\,(n = 30+\tfrac{1}{2}) = 0.55\;\; T$$

for the counter position of Fig. 3*a*. The improved visibility of the peak structure of Fig. 3*a* over that of Fig. 2 is thus explained and is, in fact, due to the dispersion of muon orbits according to momentum, for the counter in the « $x_c > 2r$ » position. To find the overall width of the distribution in « t », we use eq. (13) and find:

$$\frac{\mathrm{d}t}{t} = \pm 0.43 \qquad \left(\text{with } \frac{\mathrm{d}p}{p} = 0.1;\;\; \mathrm{d}\varphi = 0.1;\;\; \mathrm{d}x_\mu = 1 \text{ cm};\;\; x_\mu - 2r = 22 \text{ cm}\right),$$

in good agreement with the observed spread. As we can see from Figs. 2 and 3*a*, the overall width of the two distributions is quite different in the two cases, this difference being well explained by eqs. (9) and (13) respectively, as the two numerical examples quoted above show. Fig. 3*a* shows an experimentally observed T.C. picture; Fig. 3*b* presents a distribution calculated on the basis of the measured momentum distribution and of the expected angular spread due to multiple scattering of the beam in the moderator.

The stored rate is measured by the area under the peaks in the T.C. distributions. At an injection (123) rate of $2 \cdot 10^3$ per second, of which about 600 are muons, about 16 muons/s are stored. This ratio 16/600 is in reasonable agreement with the calculated acceptance. The maximum number of turns detected with this arrangement was 28. The most important parameter entering the quantitative predictions of step-size, period, position of C to accept a given turn, etc., is the mean momentum $\bar{p}$ of the circulating muon beam. It can, in principle, be calculated from the value of the initial momentum and the properties of M. It is, however, useful to measure it directly. For this purpose we have measured the mean diameter $2\bar{r}$ of the orbits by intercepting them by means of a lucite block B (Fig. 1) and observing the rate of muons arriving in C. When this block is moved towards M, the rate in C drops for $x_B < x_{B_1} \quad 2\bar{r}$ (for the definition of x_B, see Fig. 1); after intercepting the first turn (at $x_B = x_{B_2} \equiv 2\bar{r} - x_C$), the ratio increases again until for $x_B < 0$, the block cuts into late turns once more. It is from the observed x_{B_1} and x_{B_2} that we conclude that $\bar{p} = 85$ MeV/c; this is in agreement with the value expected from the momentum loss in M.

It might be thought to be advantageous to slow the muons to a smaller momentum than 85 MeV/c. Because of the rapid variation of ionization loss with muon energy, however, the density of muons per unit $\mathrm{d}p/p$ falls like $(\bar{p}/p)^{7/2}$ in the non-relativistic range. In addition multiple scattering increases and the resulting loss in intensity precludes the use of such slow muons.

3. – Electric dipole moment of the muon.

It has been first remarked by LANDAU [2] that the presence of a static electric dipole moment (EDM) for elementary particles can be interpreted only as the simultaneous violation of space (P) and time reversal (T) invariance. Under a P-operation, the electric dipole moment vector $\boldsymbol{D}$ which can be put equal to $k\boldsymbol{\sigma}$, changes sign whereas $\boldsymbol{\sigma}$ does not; under a T-operation, $\boldsymbol{\sigma}$ changes sign but not $\boldsymbol{D}$. Therefore, in a P-conserving interaction, the absence of an EDM would allow no conclusion as to the invariance with respect to time reversal and so it is desirable to look for electric dipole moments in particles known to have characteristics non-invariant with reflection [2]. The deter-

mination of a finite value for the EDM of the muon would provide a lower limit for the non-invariance under T-reversal.

T-non-invariance has been sought in a number of experiments: *a*) the EDM of the neutron [5], was found to be $D < 5 \cdot 10^{-20} \cdot e$ (cm). *b*) in the β-decay of the neutron, any phaseshift due to T-non-invariance has been measured [6] to be less than 0.15 rad. *c*) Recently a series of experiments has established an upper limit to the EDM of the muon [3]. Our measurements were based on the same principle as these latter, as follows:

Assume that longitudinally polarized muons possessing an EDM given by

$$D \equiv f e \frac{\hbar}{mc} \equiv g' \frac{e}{2mc} \frac{\hbar}{2},$$

move in a magnetic field B, in the plane perpendicular to the latter. In their instantaneous rest-frame, they experience an electric field $E' = \gamma \boldsymbol{\beta} \times \boldsymbol{B}$ ($\boldsymbol{\beta} = \boldsymbol{v}/c$; $\gamma = (1 - \beta^2)^{-\frac{1}{2}}$), which causes a precession of $\boldsymbol{D}$. In the laboratory the spin precesses about $\boldsymbol{v} \times \boldsymbol{B}$, *i.e.* out of the orbit plane by an angle:

$$\Theta_s = 2 f \beta \gamma \Theta_0 ,$$

when the orbit has gone through an angle:

$$\Theta_0 = \frac{eB}{mc\gamma} t \ [7] .$$

The polarization (perpendicular to the orbit) thus produced is detected by stopping the muons after a known Θ_0 and measuring the up-downa symmetry (*) of the decay-positron with respect to the orbit plane. It is important to note that the determination of this component of the spin can still be achieved if the muons stop in a strong magnetic field. The present determination differs from that described in ref. [3] only in the magnitude of Θ_0. While in ref. [3] $\Theta_0 < 2\pi$, we used the storage device described here to obtain $\Theta_0 = 2n\pi$, with n up to 28. The arrangement used to detect the decay positron in our measurements is schematically illustrated in Fig. 4. This arrangement consisted of three counters 4, 5 and 6; the scintillator of counter 4, thick enough (3 g/cm^2) to stop the muons incident upon it, lies in the median plane of the magnet, while scintillators 5 and 6 are arranged symmetrically with

[5] J. H. SMITH, E. M. PURCELL and N. F. RAMSEY: *Phys. Rev.*, **108**, 120 (1957).

[6] M. T. BURGY, V. E. KROHN, T. B. NOVEY, G. R. RINGO and V. L. TELEGDI: *Phys. Rev. Lett.*, **1**, 324 (1958).

[7] V. BARGMANN, L. MICHEL and V. L. TELEGDI: *Phys. Rev. Lett.*, **2**, 435 (1959).

(*) The up-down asymmetry is given by $a = (N_{\text{up}} - N_{\text{down}})/(N_{\text{up}} + N_{\text{down}})$.

respect to 4, respectively above (5) and below (6) it. Coincidences (45) or (46) are produced by the positron from muon decay in 4. The assembly (456) was mounted with centre at a distance $x = 66$ cm from M. The injection telescope (123) was as indicated in Fig. 1, and produced a gate of 300 ns duration.

A (123 gated 4) coincidence corresponds to a muon arriving in 4, while we refer to a (45) coincidence as « Top-electron » and to a (46) coincidence as « Bottom-electron ». A system of gate circuits (logic box) was triggered by the arriving muon and enabled one to count for « Top » and « Bottom » separately, « electrons + accidentals » and « accidentals ». Upon arrival of a (123 gated 4)-signal at the input of the logic box, two identical sets of two gate pulses were produced; each set consisted of one prompt pulse (called G_1; duration 5 μs) and one pulse delayed by 6 μs (called G_2; duration also 5 μs). The box had two more inputs: one fed by the « Top-electron signal », the other by the « Bottom-electron signal ». Each of these two signals was delayed by 5.5 μs and then brought into coincidence with one set (G_1 and G_2). In this way a « prompt » event (with respect to the 4 pulse) in Top or Bottom gives no output, since it falls between G_1 and G_2: events occurring between +0.5 and 5.5 μs (electrons + accidentals) pass through G_2; events occurring between — 5.5 and — 0.5 μs (accidentals) pass through G_1. The outputs Top-G_1, Top-G_2, Bottom-G_1 and Bottom-G_2 are split into two: each of them is brought into coincidence with two single channel pulse-height analyser output pulses (A or B). A and B are set to cover different ranges of the pulse-height of the output pulse from the T.C. In this way we select two ranges of time of flight: group A, particles which have made few turns in the magnet (*) and are used for calibration, and group B, particles which have made many turns. By subtracting the two asymmetries thus obtained,

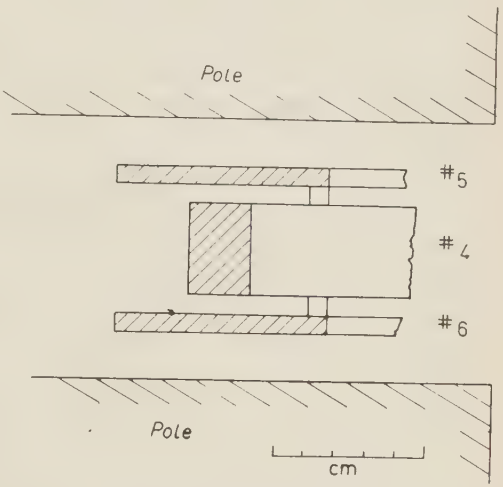

Fig. 4. – Counter layout for the measurement of the electric dipole moment.

(*) In spite of the large distance ($x = 66$ cm) of the EDM telescope from M, some muons reach counter 4 in half turn by going through the fringing field of the magnet. See Fig. 3*a*.

instrumental asymmetry and an up-down asymmetry in the incident beam, are eliminated. One thus measures simultaneously in 8 scalers (see Fig. 5):

Top events
- electrons + accidentals — from Early muons
- electrons + accidentals — from Late muons
- accidentals — from Early muons
- accidentals — from Late muons

Bottom events
- electron + accidentals — from Early muons
- electron + accidentals — from Late muons
- accidentals — from Early muons
- accidentals — from Late muons

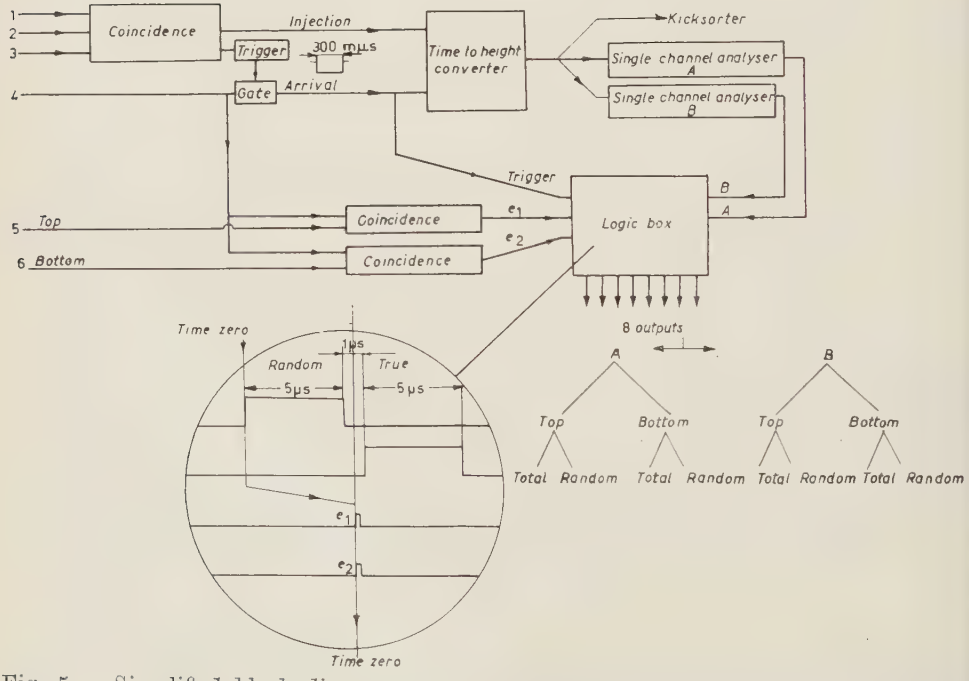

Fig. 5. – Simplified block diagram of the electronics for the electric dipole moment measurement.

Parallel to this the Top and Bottom events are identified as electron from muon decay in no. 4 by measuring the muon life-time in a separate « life-time converter » whose « *startside* » is fed by the gated 4 pulse and « *stopside* » by the (4 5) or (4 6) coincidence.

The results can be divided into 3 groups: Group I in which the up-down asymmetry is measured for muons which have made on the mean, either one [A (« early ») set on $\langle n \rangle = 1$] or 11.5 [B(« late ») set on $\langle n \rangle = 11.5$] turns. Group II with mean turn index 1 and 16.5. Group III with mean turn index 1 and 19.5. For each group the difference in asymmetry Δ between « early » and « late » is evaluated. The angles Θ_s through which the spin has rotated out of the median plane is given by $\Theta_s = \Delta / a_{max}$, where a_{max} is the maximum obtainable asymmetry in this (150 MeV/c) beam (*). The mean spatial angle $\Theta_{orbit} = \langle \omega(t) \cdot t \rangle$ (t is the time of arrival in 4 enclosed by the windows of A resp. B). However, since $\mathrm{d}T/T = |\mathrm{d}\omega/\omega| = \beta^2(\mathrm{d}p/p)$, one finds using eq. (13) that the dependence of ω on t is weak and thus $\Theta_{orbit} \sim \omega \langle t \rangle$. One therefore takes the centre of gravity of the PHA range enclosed by A resp. B. The results are listed in Table I. The errors are statistical.

TABLE I. – *Results obtained for particles which have made, in the mean* 11.5, 16.5 *and* 19.5 *turns* (*Group I, II and III respectively*). a_{early} refers to the asymmetry for muons, which have made, in the mean, one turn (ranging from $\frac{1}{2}$ to $\frac{3}{2}$ turns).

Group	Late turns	a_{early} (%)	a_{late} (%)	$a_{late} - a_{early}$ (%)	$\langle \Theta_{spin} \rangle$ (rad.)	$\langle \Theta_{orbit} \rangle$ (rad.)
I	$6\frac{1}{2} - 18\frac{1}{2}$	8.01 ± 0.84	6.98 ± 0.40	-1.04 ± 0.94	0.062 ± 0.047	66.0
II	$11\frac{1}{2} - 26\frac{1}{2}$	7.28 ± 1.81	7.04 ± 0.87	-0.24 ± 2.00	0.014 ± 0.100	97.0
III	$15\frac{1}{2} - 26\frac{1}{2}$	7.41 ± 1.24	7.19 ± 0.94	-0.22 ± 1.55	0.013 ± 0.080	116

A systematic error could be introduced if the circulating muon beam does not enter 4 symmetrically with respect to the median plane, or if counters 5 and 6 have different efficiencies for detection of the decay electrons. By taking the difference in up-down asymmetry between « early » and « late », both errors are eliminated provided the « early » and « late » fractions of the beam on 4 can be shown to have the same deviations from symmetric incidence. A vertical scan on « early » and « late » turns, arriving in 4, shows no difference in the centre of the intensity profile to 2 mm, while both are ~ 3 mm above

(*) This was measured in Carbon as stopping material. Although the stopping medium in this case is scintillating material which is partly depolarizing, it can be inferred from data on the re-establishment of the polarization in strong magnetic fields that in 13 kG the polarization is restored to 100%. See: J. C. SENS, R. A. SWANSON, V. L. TELEGDI and D. D. YOVANOVITCH: *Phys. Rev.*, **107**, 1465 (1957).

the median plane. No error is thus introduced when taking the differences, but a higher top than bottom rate is to be expected. A better check is obtained by taking data with the EDM telescope displaced with respect to the median plane as shown in Table II. Although the « early » and « late » asymmetries

TABLE II. – *Subdivision of Table I, Group I into asymmetries obtained by placing the EDM assembly at different height with respect to the median plane of the magnet.*

Height above median plane (mm)	a_{early} (%)	a_{late} (%)	$a_{\text{late}} - a_{\text{early}}$ (%)
− 9	10.14 ± 2.40	9.42 ± 1.06	− 0.72 ± 2.60
0	10.25 ± 2.10	7.23 ± 0.80	− 3.02 ± 2.25
+ 2	6.85 ± 1.20	7.12 ± 0.69	+ 0.27 ± 1.39
+ 2.5	9.37 ± 2.10	5.49 ± 0.87	− 3.88 ± 2.28
+ 9	4.00 ± 3.10	5.34 ± 1.38	+ 1.34 ± 3.40

each vary considerably, the variation in the difference has been shown to be insignificant. A second systematic error could be introduced by the longitudinal electric field, which is produced in the rest frame of the particle when it slows down in 4. The error is, however, negligible since it depends on the EDM to second order ([3]). As a separate check on the performance of the apparatus, the time distribution of decay electrons was measured. The life-time for μ^+, deduced from these measurements combining the top and bottom counters, was found to be:

$$\tau_{\mu}^{+} = (2.19 \pm 0.03) \cdot 10^{-6} \text{ s} .$$

Combining the 3 values of $\Theta_{\text{spin}}/\Theta_{\text{orbit}}$ which are listed in Table I, one finds:

$$f = (2.7 \pm 2.8) \cdot 10^{-4} .$$

This corresponds to an upper limit for the EDM of $e \cdot (5.0 \pm 5.0) \cdot 10^{-17}$ cm, and is consistent with time reversal invariance.

This value of « f » is to be compared with:

$$f = (2.0 \pm 1.5) \cdot 10^{-3}$$

obtained (*) in ref. ([3]).

(*) It must be noted that by assuming that the incoming beam has zero polarization transverse in the orbit plane, a value:

$$f = (4 \pm 7) \cdot 10^{-1} ,$$

s obtai ned in ref. ([3]). However, no errors are quoted as to the possible magnitude

* * *

We wish to acknowledge the competent technical assistance of Mr. B. NICOLAI throughout this experiment.

We should also like to thank Drs. C. CAVERSAZIO, F. J. M. FARLEY, R. L. GARWIN, T. MULLER, W. K. H. PANOFSKY, G. TAGLIAFERRI, V. L. TELEGDI and C. M. YORK for their significant contributions and most welcome help in this work.

We would like to express our appreciation to Prof. G. BERNARDINI for his continuous interest and for the action taken at various stages of this experiment.

of the up-down asymmetry caused by misalignment of the cyclotron, etc. A partial discussion of these points is given by G. GIDAL: *Thesis* (Columbia, 1960) (Nevis 83), Appendix II. We believe that the focal point of the beam transport system in this experiment has not been demonstrated not to be above or below the target, which would contribute a vertical component of polarization sufficient to vitiate the second result quoted.

RIASSUNTO

Si descrive un metodo per la cattura di muoni in campi magnetici e la sua applicazione ad una più accurata determinazione del momento di dipolo elettrico del muone. Il valore trovato è:

$$\mathrm{EDM} \leqslant e(5 \pm 5) \cdot 10^{-17} \text{ cm}$$

consistente con l'invarianza rispetto all'inversione del tempo.

Inner Bremsstrahlung-Nuclear Recoil Angular Correlation in K-Capture (*).

S. D. Bloom and J. L. Uretsky (**)

University of California, Lawrence Radiation Laboratory - Livermore, Cal.

(ricevuto l'11 Aprile 1960)

Summary. — It is suggested that a measurement of the inner bremsstrahlung (IB)-nuclear recoil angular correlation in K-capture leads to a method for determining the ratio $|C_A|^2/|C_V|^2$, which is substantially free from dependence on either lifetime or spectral-shape factors, in contrast to the estimates of $|C_A|^2/|C_V|^2$ made from the ft values. So far a determination such as suggested here has been made only in the case of the β decay of aligned neutrons. In the case of ^{7}Be, the only known super-allowed K-capturer, a similar measurement might be of considerable interest since here some fairly dependable calculations of $|M_{GT}|$, the Gamow-Teller matrix element, might be made. (Knowledge of $|M_{GT}|$ is essential in the evaluation of $|C_A|^2/|C_V|^2$). A general formula is derived for the IB-nuclear recoil angular correlation and applied to the particular case of the $^7\mathrm{Be} \xrightarrow{K\text{-capture}} {}^7\mathrm{Li}$ β decay. In addition, it is shown that the formula, which in its general form assumes an initial (arbitrary) polarization for the K-capturing nucleus, offers the possibility of doing an unambiguous time-reversal experiment by looking for a left-right asymmetry in the count rate when polarization, recoil-momentum direction, and IB-direction are all mutually perpendicular.

1. – Proposed experiment.

The discovery of parity breakdown in β-decay [1] has given rise to a complete re-examination of the problem of the form of the β-interaction and, in fact, weak interactions in general. In particular, the work of Feynman and

(*) This work was performed under the auspices of the U. S. Atomic Energy Commission.

(**) LRL, Berkeley; present address: Dept. of Physics, Purdue University, Lafayette, Ind.

(1) T. D. Lee and C. N. Yang: *Phys. Rev.*, **104**, 254 (1956); C. S. Wu, E. Ambler, R. W. Hayward, D. D. Hopper and R. P. Hudson: *Phys. Rev.*, **105**, 1413 (1957); **106**, 1361 (1957); R. L. Garwin, L. M. Lederman and M. Weinrich: *Phys. Rev.*, **105**, 1415 (1957).

GELL-MANN (2), SUDARSHAN and MARSHAK (2), and others strongly suggests that the weak interaction is of the form $(V-A)$. Moreover the experimental evidence, for β-decay at least, very clearly supports this hypothesis, including, for instance, experimental redeterminations of the ^{6}He recoil spectrum (3) and the recent discovery of the $(e+\nu)$ mode (4) of decay for the pion. Calculations of the ratio of the coupling constants, $|C_A|^2/|C_V|^2$, have also been made; to date the most reliable estimates of this ratio are based largely on the *ft* values (5) for super-allowed transitions, using the method proposed and utilized by WINTER and KOFOED-HANSEN (6). Although the theories mentioned above (2) require that the ratio be exactly one, it is to be expected that in the case of complex nuclei corrections due to the virtual pion field will in fact alter this situation. In consonance with this the values so far calculated (5) have varied rather widely, nor merely from the value one, but also from each other, being highest for the neutron decay, 1.42 (5), and going down to a value of around 1.15 for super-allowed β emitters of atomic weight greater than about 15. It might therefore be interesting to make a measurement of this ratio which is independent of either the lifetime or spectral-shape determinations. Actually, such a measurement has been done on one case, the decay of the neutron, where the correlation coefficient between the β-particle momentum and the neutron spin direction leads to a value of 1.56 ± 0.14 for the ratio in question (7). It is interesting to note that this agrees, within statistics, with the value obtained from the newest *ft* value for the neutron decay (5), but the possibility of there being a difference between the two numbers is not beyond consideration. It is clear that another measurement, not relying on measured *ft* values, might well be a useful addendum to present data. A measurement like this would be one such as we propose here, in which one observes an angular

(2) R. P. FEYNMAN and M. GELL-MANN: *Phys. Rev.*, **109**, 193 (1958); E. C. G. SUDARSHAN and R. E. MARSHAK: *Phys. Rev.*, **109**, 1860 (1958); a more recent reference containing a reasonably up-to-date bibliography of work in this area is Y. TANIKAWA and S. WATANABE: *Phys. Rev.*, **113**, 1344 (1959).

(3) The most recent experimental results for β decay may be found in the *Minutes of the Conference on Weak Interactions Held at Gatlinburg, Tenn., Bull. Am. Phys. Soc.*, **4**, 1, 77 (1959) and *Rev. Mod. Phys.*, **31**, 782 (1959).

(4) T. FAZZINI G. FIDECARO, A. W. MERRISCH, H. PAUL and A. V. TOLLESTRUP: *Phys. Rev. Lett.*, **1**, 247 (1958); G. IMPEDUGLIA, R. PLANO, A. PRODELL, N. SAMIOS, M. SCHWARTZ and J. STEINBERGER: *Phys Rev. Lett.*, **1**, 249 (1958); H. L. ANDERSON T. FUJII, R. H. MILLER, and L. TAU: *Phys. Rev. Lett.*, **2**, 53 (1959).

(5) O. C. KISTNER and B. M. RUSTAD: *Phys. Rev.*, **114**, 1329 (1959).

(6) A. WINTHER and O. KOFOED-HANSEN: *Kgl. Dan. Videnskab. Selskab-Fys. Medd.*, **27**, no 14 (1953).

(7) M. T. BURGY, V. E. KROHN, T. B. NOVEY and C. R. RINGO: reported by M. GOLDHABER at the *Annual International Conference on High-Energy Physics at CERN*, July 1958, edited by B. FERRETTI (Geneva, 1958).

correlation between the nuclear recoil and some other detectable particle accompanying the β-decay. The electron-neutrino correlation, or, what is the same thing, the electron-nuclear recoil correlation for super-allowed transitions of the ($J \to J$, $T \to T$) type, wherein both Fermi and Gamow-Teller matrix elements may contribute to the decay, would fall fairly well into this category. This is true in spite of the fact that the correlation is still somewhat dependent on the β spectral shape due to the finite mass of the electron ([8]). However, radio-isotopes of this class that are easily fabricated and also amenable to nuclear-recoil detection, and, morevoer, that have lifetimes long enough to accumulate sufficient data, considering the reduced count rate imposed by the coincidence requirement implied above, are not only few and far between, but also possibly even non-existent ([9]), so far. At any rate, K-capture offers the possibility of doing the equivalent of an electron-neutrino correlation experiment, but with the electron replaced by the inner bremsstrahlung (IB) radiation, which radiation accompanies the K-capture during 10^{-4} to 10^{-3} of the time. Furthermore, the zero mass of the IB photons offers the advantage of eliminating an energy-spectrum dependence present in the case of the ordinary electron-neutrino correlation.

The formula for the IB-neutrino correlation (cf. the following section) is

$$W(\varphi) = \text{Constant} \cdot \nu^2 (k_m - \nu)[1 - \varrho_0 \cos\varphi] , \tag{1}$$

where:

$\varphi \equiv$ the angle between the neutrino and the IB photon,

$\nu \equiv$ the neutrino energy,

$k_m \equiv$ the maximum photon energy,

$\mathrm{d}\Omega_k \equiv$ the photon solid-angle differential,

$\mathrm{d}\Omega_\nu \equiv$ the neutrino solid-angle differential,

$$\varrho_0 \equiv \frac{|M_F|^2(|C_S|^2 - |C_V|^2) - \frac{1}{3}|M_{GT}|^2(|C_T|^2 - |C_A|^2)}{|M_F|^2(|C_S|^2 + |C_V|^2) + |M_{GT}|^2(|C_T|^2 + |C_A|^2)} ,$$

$M_F \equiv$ the Fermi matrix element,

$M_{GT} \equiv$ the Gamow-Teller matrix element,

$C_X \equiv$ the coupling constant as per subscript X.

([8]) J. D. JACKSON, S. B. TREIMAN and H. H. WYLD, Jr.: *Phys. Rev.*, **106**, 517 (1957).

([9]) Nevertheless it is worth while mentioning ^{19}Ne, on which recoil spectrum measurements have been recently made by HERRMANNSFELDT *et al.* (cfr. ref. ([3]), p. 77). Its high β^+ end-point energy (2.18 MeV) minimizes the spectral dependence factor, but its 18 s half-life requires the extended use of an accelerator for manufacturing the radioactivity.

To go from this formula to one for the IB-nuclear recoil angular correlation is a straightforward problem in kinematical and solid-angle transformations. The final result is

$$(2) \qquad W(\Theta) = \text{Constant} \cdot \left[\frac{P^2 k v}{(P + k\cos\Theta)}\right]\left[1 + \varrho_0 \frac{k + P\cos\Theta}{k_m - k}\right] \mathrm{d}k\, \mathrm{d}\Omega_k\, \mathrm{d}\Omega_P ,$$

where: $P \equiv$ the nuclear recoil momentum,

$\Theta \equiv$ the photonuclear recoil angle,

$k \equiv$ the photon momentum.

It is to be noted, just as in any other type of β experimentation, one does not escape here the inevitable linking together of the coupling constants and the matrix elements in the form $C_x M_x$. It is for this reason that one is most inclined to work with a super-allowed decay rather than one that is merely favored, since in the former case one might be able to calculate values for the Gamow-Teller matrix elements, either by the magnetic moment method or by direct computation ([6-10]). Such a super-allowed K-capture is not merely rare but unique, namely, ^{7}Be. The radio-isotope ^{7}Be is unique also in that a good deal of recoil detection work has been done with it ([11]), so that a considerable knowledge has already been built up with respect to that aspect of the problem. Furthermore, the half-life of 53 days, plus the known methods ([12]) for producing copious amounts of the isotope, make it experimentally attractive from the handling point of view, since the accelerator operation produces the source and the source measurement itself is quite separate in the length of time available.

In Fig. 1(a)-(d) we have plotted the ^{7}Be IB-nuclear recoil correlation in the case of a pure Fermi transition, pure Gamow-Teller transition, and also for exact equality of $|C_A|^2|M_{GT}|^2$ and $|C_V|^2|M_F|^2$, assuming the ($V-A$) form for the β interaction. As can be seen the differences between the three cases are quite pronounced. Therefore it is to be hoped that with the advanced

([10]) A. M. Lane: *Proc. Phys. Soc.* (*London*), **68**, 189 (1955); in the Appendix of this paper the work of Lane on the ^{7}Be $-$ ^{7}Li β decay (which is of particular interest here) has been brought up to date and compared with more recent calculations (see ref. ([5])).

([11]) P. B. Smith and J. S. Allen: *Phys. Rev.*, **81**, 381 (1951); R. Davis: *Phys. Rev.*, **86**, 976 (1952).

([12]) F. Ajzenberg and T. Lauritsen: *Rev. Mod. Phys.*, **27**, 77 (1955).

techniques available today a measurement of the sort proposed here is not very far off.

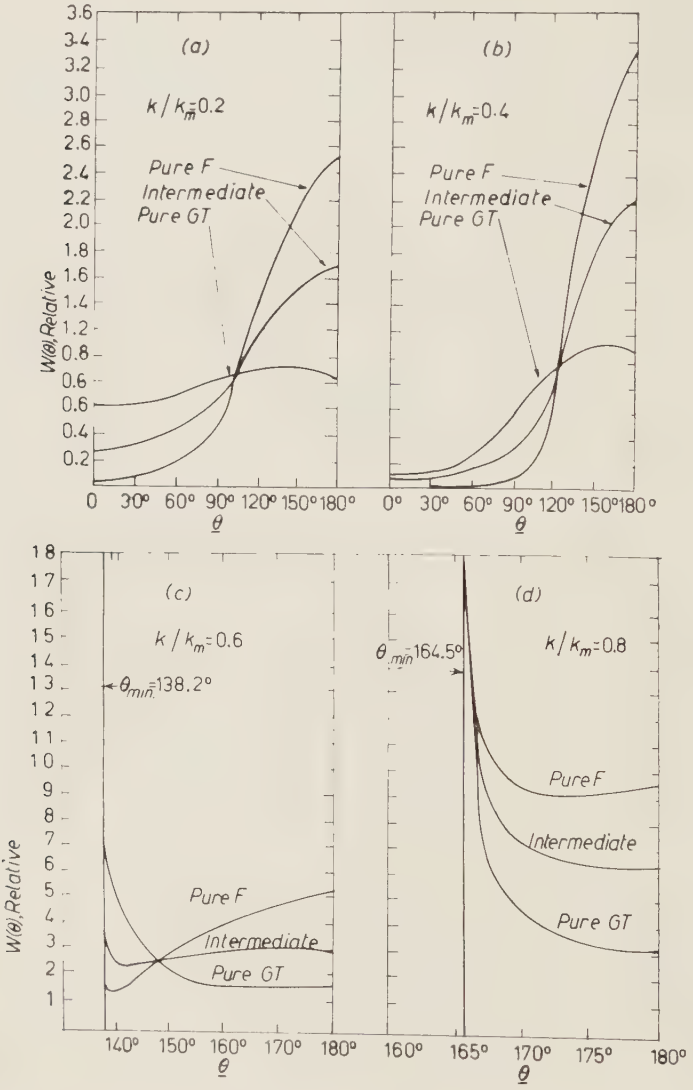

Fig. 1. – Relative IB-nuclear recoil angular correlation in K-capture for four photon energies, assuming the $V-A$ interaction form. It is to be noted for photon energy greater than $k/k_m = 0.5$ there is a minimum angle, $\theta_{\min} = \cos^{-1}[(k^2 - \nu^2)^{\frac{1}{2}}/k]$, beyond which no correlations can be observed, due to simple kinematic relations. Also note all curves have been arbitrarily normalized to the same value for $\theta_{\lambda\nu}$ (angle between IB photon and neutrino) equal to 90°. The three cases plotted for each energy are labeled with regard to the assumptions made, « intermediate » meaning absolute equality of $|C_V|^2|M_F|^2$ and $|C_A|^2|M_{GT}|^2$.

2. – Theory.

The theory of internal bremsstrahlung in K-electron capture has been discussed in much detail by GLAUBER and MARTIN ([13]). Although our calculation follows along the same general lines, there are two points requiring comment: 1) We must be a little more careful with the nuclear kinematics (because we are interested in observing the nuclear recoil), and 2) we can take advantage of GM's results which are based on the assumption that Coulomb effects in intermediate states are negligible. (This treatment is appropriate for high-energy γ-rays to which our interest is confined.)

For the convenience of the reader we repeat some definitions of the GM paper. The radiation and β-decay Hamiltonians are, respectively,

$$H^{\mathrm{r}}(x) = e\bar{\psi}(x)\mathcal{A}(x)\psi(x) \tag{3}$$

and

$$H^{\mathrm{c}}(x) = \sum_{\chi,\lambda} C_{\chi}\bar{\varphi}_{N}(x)\,T_{\chi,\lambda}\varphi_{\mathrm{P}}(x)\cdot\bar{\chi}(x)\,T_{\chi,\lambda}\psi(x) \equiv \bar{\chi}(x)\,\tau(x)\,\psi(x)\,. \tag{4}$$

In these expressions we have introduced the field operators for the electron (ψ), nucleon ($\varphi_{N\text{ or P}}$), neutrino (χ), and electromagnetic ($\mathcal{A}_{\mu}$) fields, as well as the β-coupling operators $T_{\chi\lambda}$ with the concomitant coupling constants C_{χ}. The amplitude for photon emission accompanied by electron capture comes from the second-order S-matrix element,

$$S_2 = -\int \mathrm{d}^4x \int \mathrm{d}^4y\,(H^{\mathrm{r}}(x),\, H^{\mathrm{c}}(y))_{+}\,, \tag{5}$$

where we have used a conventional notation for the time-ordered product. It is to be understood that we are interested in the matrix element of eq. (5) between an initial state with one bound electron of total energy E_r and a final state containing a photon of 4-momentum k_{μ} and a neutrino of 4-momentum ν_{μ}.

The space-time integrals in eq. (5) are evaluated by introducing the field operators for the initial electron state:

$$\left\{\begin{aligned} &\psi_r^{-}(\boldsymbol{x}) = \psi_r(\boldsymbol{x}-\boldsymbol{Y})\exp\left[-iE_r x_0\right]a_r = \\ &\qquad = (2\pi)^{-\frac{3}{2}}a_r\int \mathrm{d}^3q\,\varphi_r(\boldsymbol{q})\exp\left[i[\boldsymbol{q}\cdot(\boldsymbol{x}-\boldsymbol{Y}) - iE_r q_0]\right]\,, \end{aligned}\right. \tag{6a}$$

([13]) R. J. GLAUBER and P. C. MARTIN: *Phys. Rev.*, **104**, 158 (1958); hereinafter this reference will be quoted as (GM); also cfr. P. C. MARTIN and R. J. GLAUBER: *Phys. Rev.*, **109**, 1307 (1958).

which involves the co-ordinate $\boldsymbol{Y}$ of the nuclear center of mass, and the final neutrino state:

$$\bar{\chi}_s^+(\boldsymbol{x}) = (2\pi)^{-\frac{3}{2}} \left(\frac{m_\nu}{\nu_0}\right)^{\frac{1}{2}} \mu_s(\boldsymbol{\nu}) \exp\left[-i\,\boldsymbol{\nu}\cdot\boldsymbol{x}\right] \alpha_s^x(\nu)\,. \tag{6b}$$

The result is

$$\left.\begin{aligned} S_2 = &-\frac{e}{(4\pi)^{\frac{1}{2}}} \left(\frac{m_\nu}{k_0\nu_0}\right)^{\frac{1}{2}} \delta(\boldsymbol{k}+\boldsymbol{\nu}+\boldsymbol{P})\cdot \\ &\cdot \int \mathrm{d}^4p\ \mathrm{d}^3q\ \delta(p_0 - \nu_0 - P_0)\bar{\mu}_s(\nu)\, T(\boldsymbol{p}-\boldsymbol{\nu})\, S_F(p,\ q-k)\ \not{\varepsilon}\ \varphi_r(q) \equiv \\ &\equiv \delta(\boldsymbol{k}+\boldsymbol{\nu}+\boldsymbol{P})\ \delta(E_r - k_0 - \nu_0 - P) M_{fi}\,, \end{aligned}\right\} \tag{7}$$

in which we have introduced the causal propagator $S_F(p, q)$ for an electron in the presence of the nuclear Coulomb field. In order to reach eq. (7) it was necessary to assume that the wave function for a bound electron-nucleus system could be separated into electronic and nuclear co-ordinates. This is equivalent to assuming an infinitely heavy nucleus, and it is expected that the correction terms should be proportional to the ratio of the electronic to nuclear masses. A second approximation is made in performing the sum over intermediate electron states; this is necessary to obtain the propagation function, S_F, since states are included in the summation that are occupied by other electrons. In the GM paper it is argued that this procedure is correct because of the possibility that the intermediate-state electron is captured before the initial-state electron makes a radiative transition. At any rate, we do not expect such considerations to be important in the present case where the γ-ray energy is large compared with the electronic binding energy.

It was shown in the GM paper that the effect of the Coulomb field upon the intermediate-state electron is not important for large γ-ray energies ($k \gg Z\alpha m_e$). Since this is the case in which we shall be interested, we may expand the propagator in powers of the external field and drop all but the first term. We have then

$$S_F(p,\ q-k) = \delta(p-q+k)(ip+m)^{-1} + O(Z\alpha)\,. \tag{8}$$

It is consistent with this approximation to use a non-relativistic form for the initial electron wave function and to evaluate the integrals in eq. (7) only to the lowest order in the parameter $Z\alpha$. For allowed transitions $T(\boldsymbol{p}-\boldsymbol{\nu})$ is independent of its argument, and the integrals give, when evaluated for an initial $(1s)$ state,

$$M_{fi} = \pi \left(\frac{e\varphi_{1s}(0)}{k_0 m_e}\right) \left(\frac{m_\nu}{2k_0\nu_0}\right)^{\frac{1}{2}} \bar{\mu}_s(\nu)\, T(\boldsymbol{p}-\boldsymbol{\nu}=0)\cdot(i\hbar + i\gamma_0 E_r - m_e)\ \not{\varepsilon}\ \Omega_r\,. \tag{9}$$

In the last expression $\varphi_{1s}(0)$ is the non-relativistic electronic wave function evaluated at the origin and Ω is the normalized spinor eigenfunction of γ_4 satisfying

$$\gamma_4 \Omega_r = \Omega_r \,. \tag{10}$$

We next square the expression in eq. (9) and sum over the initial electron spins (the $(1s)$ shell is assumed filled) and the final neutrino spins, and average over final nuclear orientations. After multiplying by the energy-momentum δ-functions and integrating over the neutrino variables and the magnitude of the nuclear recoil momentum, we are left with an expression that is appropriate to an experiment carried out with initially aligned nuclei. The angle between the recoil nucleus and the photon is to be observed along with the magnitude of the photon momentum. If the reference magnetic field is chosen as the Z axis, then the transition probability is

$$\begin{aligned} W_{\mathrm{pol}} \propto \frac{P^2 k(k_m - k)}{P + k\cos\theta}\, \mathrm{d}k\, \mathrm{d}\Omega_k\, \mathrm{d}\Omega_{\boldsymbol{P}}\, \Gamma_0 \cdot \\ \cdot \left\{ 1 + \left(\frac{k^2 + \boldsymbol{k}\cdot\boldsymbol{P}}{k(k_m - k)} \right) \varrho_0 + \left(\frac{1}{3} - \frac{M^2}{J(J+1)} \right) \left[\frac{k^2 - 3k_Z^2 + \boldsymbol{k}\cdot\boldsymbol{P} - 3k_Z P_Z}{k(k_m - k)} \right] \varrho_1 + \right. \\ + (2/\Gamma_0)\ \mathrm{Re}\ M_F^*(M_{\mathrm{GT}})_Z \left[C_S^* C_T \frac{k_m k_Z + k P_Z}{k(k_m - k)} + \right. \\ \left. \left. + C_V^* C_A \frac{k_Z(k_m - 2k) - k P_Z}{k(k_m - k)} + (C_S^* C_T - C_V^* C_A) \frac{(\boldsymbol{k}\times\boldsymbol{P})_Z}{k(k_m - k)} \right] \right\} . \end{aligned} \tag{11}$$

The relevant definitions are

$$\Gamma_0 = (|C_V|^2 + |C_S|^2)\,|M_F|^2 + (|C_A|^2 + |C_T|^2)\,|M_{\mathrm{GT}}|^2$$

$$\Gamma_0 \varrho_0 = (|C_S|^2 - |C_V|^2)\,|M_F|^2 - \tfrac{1}{3}(|C_T|^2 - |C_A|^2)\,|M_{\mathrm{GT}}|^2$$

$$\Gamma_0 \varrho_0 = (|C_A|^2 - |C_T|^2)\,|M_{\mathrm{GT}}|^2 .$$

The factor $|M_{\mathrm{GT}}|^2$ is the square of the Gamow-Teller matrix element after averaging and summing over initial and final orientations.

$$(M_{\mathrm{GT}})_Z = (-)^{J-M} \mathscr{M}_{\mathrm{GT}}(M/J) \,,$$

where $\mathscr{M}_{GT}$ is the Z component of the Gamow-Teller matrix element evaluated in the state where $M = J$. The maximum possible photon energy is denoted by k_m.

When the initial nuclear orientation is not observed we obtain the simpler relation (given in slightly different form in eq. (2)):

$$W = \left[\frac{|\boldsymbol{P}|^2 k(k_m - k)}{P + k\cos\Theta}\right] \mathrm{d}k\,\mathrm{d}\Omega_k\,\mathrm{d}\Omega_p\,\Gamma_0 \cdot \left[1 + \frac{k^2 + \boldsymbol{k}\cdot\boldsymbol{P}}{k(k_m - k)}\,\varrho_0\right]. \tag{12}$$

The equivalent of expression (12) has been previously obtained by YANG, HUANG, and LEE [14] for the special case of μ-meson capture by a nucleon. The relative dependence of W on the angle between $\boldsymbol{k}$ and $\boldsymbol{P}$ is shown in Fig. 1(a)-(d) for the various situations described above.

3. – Time-reversal experiment.

It is worth while to make some additional remarks on the form of eq. (1), which is the correlation function for an IB-recoil experiment where the decaying nuclei are polarized along the Z axis. If we assume the complete validity of the $V-A$ theory and further postulate an experimental configuration such as given in Fig. 2, where the spin polarization direction, the IB direction ($\boldsymbol{k}$), and the recoil direction ($\boldsymbol{P}$) are all mutually perpendicular, eq. (11) takes a very simple form:

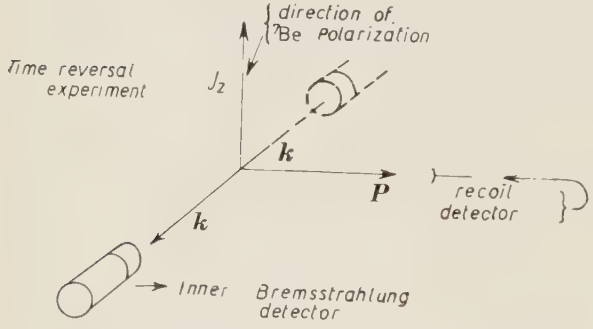

Fig. 2. – A schematic representation of a time-reversal experiment with polarized ^{7}Be nuclei. The solid and dotted vectors for $\boldsymbol{k}$ correspond to the positive and negative signs, respectively, in eqs. (13) and (14).

$$W_{\mathrm{pol}}(\pm 90^\circ) \propto P\,k(k_m - k)\,\mathrm{d}k\,\mathrm{d}\Omega_k\,\mathrm{d}\Omega_p\,\Gamma_0 \cdot \cdot\left\{1 + \frac{k}{k_m - k}\left[\varrho_0 + \frac{1}{3} - \frac{M^2}{J(J+1)} \pm (-)^{J-M-1}\frac{2PM}{kJ}\,\frac{M_F\mathscr{M}_{GT}}{\Gamma_0}\,(C_{VI}C_{AR} - C_{VR}C_{AI})\right]\right\}, \tag{13}$$

[14] K. HUANG, C. N. YANG and T. D. LEE: *Phys. Rev.*, **108**, 1340 (1957).

where the I and R subscripts denote, respectively, the imaginary and real parts of the coupling constants. If we now concentrate our attention simply on the relative count-rate ratio for $\pm 90°$ (plus and minus are as defined in Fig. 2), we find

$$(14) \qquad W_{\text{pol}}(\pm 90°) \propto \left\{\left[1 + \frac{k}{k_m - k}\left(\varrho_0 + \frac{1}{3} - \frac{M^2}{J(J+1)}\right)\right] \pm \right.$$

$$\left. \pm \left[\frac{k}{k_m - k} \cdot (-)^{J-M-1} \frac{2PM}{kJ} \cdot \frac{M_{\text{F}} \mathcal{M}_{\text{GT}}}{\Gamma_0} \cdot (C_{V\text{I}} C_{A\text{R}} - C_{V\text{R}} C_{A\text{I}})\right]\right\} .$$

It is easy to see that roughly speaking the east-west difference in count rate will be of the order $\sim 2(C_{V\text{I}} + C_{A\text{I}})/(|C_V| + |C_A|)$. Here we have taken advantage of the fact that in super-allowed β emitters the matrix elements are necessarily diagonal, *i.e.*, *real*. This is important because it means the existence of an effect is unambiguous proof of the breakdown of time invariance in β-decay, since such an effect would require non-zero values for $C_{V\text{I}}$ and/or $C_{A\text{I}}$. Conversely, it also means the *absence* of an effect would be evidence, to the extent of the precision of the experiment, of the validity of time-reversal invariance in β-decay.

* * *

The authors would like to express their thanks to Mr. Douglas Verdery for his invaluable help in preparing the various versions of the manuscript and to Dr. Ervin M. Schwarcz for his interest and comments during the progress of the writing.

Appendix

In the case of the ground-state decay of ^{7}Be, Lane [10] has made a calculation of the Gamow-Teller matrix element (the Fermi matrix element being simply unity) as a function of the intermediate coupling parameter, a/K. In Fig. 3 we have replotted Lane's results so that $|M_{\text{GT}}|^2$ may be directly read off as a function of y or $(a/K)[y \equiv (a/K)/(5 + a/K)]$. Although Lane compared theoretical *ft* values (as computed by him) with experimental values, it was necessary for him to insert in his theory a value for the Fermi coupling constant, an improved number for which has become available since then (1955). However, in the case of ^{7}Be or ^{7}Li the values over which a/K might range are restricted by many more consistent data than just the *ft* value. Accordingly, in this calculation we will take Lane's estimates for this range: $2 \leqslant a/K \leqslant 4$.

In Fig. 3 the range of values of $|M_{GT}|^2$ corresponding to this range in a/K can be seen to be 1.43 to 1.53. If we use the value of 1.48 ± 0.05 for $|M_{GT}|^2$

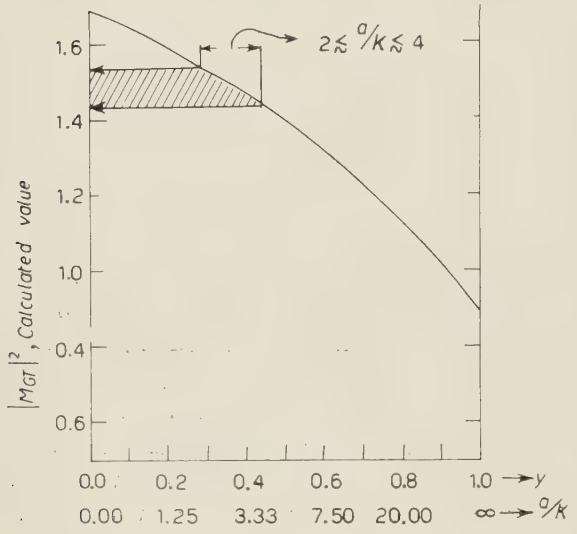

Fig. 3. – A replot of Lane's (see ref. [10]) theoretical computation of $|M_{GT}|^2$ as a function of a/K, the intermediate coupling parameter. Actually the abscissa is laid out in units of y, where $y \equiv (a/K)/(5+a/K)$. From other pieces of data, relating not only to ^{7}Be and ^{7}Li but other p-shell nuclei as well, Lane concludes that a/K must lie somewhere between 2 and 4. As can be seen from our graph this leads to a rather restricted range of values of $|M_{GT}|^2$, namely, 1.43 to 1.53.

in fitting to the Y-X plot of KISTNER and RUSTAD [5], we obtain the results shown in Fig. 4, where it can be seen that the point for the ^{7}Be β-decays fall

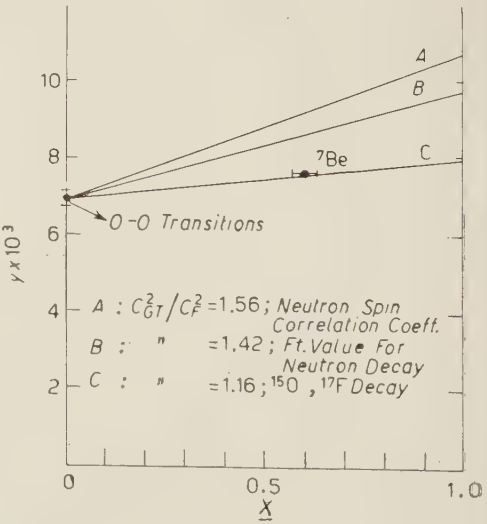

Fig. 4. – A duplication of the Y-X plot of Kistner and Rustad (see ref. [5]), which describes in detail how this representation is achieved). With the exception of the value of C_V^2 obtained from the pure Fermi transition (0-0), the graph does not show the experimental points they used in order to pick the three values for C_{GT}^2/C_F^2 leading to the three different lines. It is clear that a value of C_{GT}^2/C_F^2 of around 1.16 is necessary to account for the *ft* value of ^{7}Be, just as in the other super-allowed cases of ^{15}O and ^{17}F.

essentially right on the Y-X line for the super-allowed β-emitters ^{15}O and ^{17}F. This line corresponds to a ratio for C_{GT}^2/C_F^2 of 1.16. In view of the fact that

$|M_{GT}|^2$ is so very insensitive to large changes in a/K this agreement must be considered as more than fortuitous, therefore lending good support to the validity of the calculated value for $|M_{GT}|^2$.

RIASSUNTO (*)

Si fa l'ipotesi che la correlazione angolare del rinculo (IB)-nucleare della bremsstrahlung interna nella cattura K porti ad un metodo per determinare il rapporto $|C_A|^2/|C_A|^2$, che è sostanzialmente privo di dipendenza sia dalla vita media sia dai fattori di forma spettrale, in contrasto con le valutazioni di $|C_A|^2/|C_V|^2$ dedotto dai valori *ft*. Sinora una determinazione, quale quella qui suggerita, è stata eseguita solo nel caso del decadimento β di neutroni allineati. Nel caso del ^{7}Be, che è il solo elemento superdotato di capacità di cattura K, una misurazione simile potrebbe essere di considerevole interesse poichè in questo caso si potrebbero effettuare alcuni attendibili calcoli di $|M_{GT}|$, l'elemento della matrice Gamow-Teller (La conoscenza di $|M_{GT}|$ è essenziale alla valutazione di $|C_A|^2/|C_V|^2$). Si deduce una formula generale per la correlazione angolare del rinculo IB-nucleare e si applica al caso particolare del decadimento β $^7\mathrm{Be} \xrightarrow{\text{cattura } K} {}^7\mathrm{Li}$. Inoltre si mostra che la formula, che nella sua forma generale postula una polarizzazione iniziale (arbitraria) per il nucleo che esegue la cattura K, offre la possibilità di effettuare un esperimento di inversione del tempo, privo di ambiguità, ricercando una asimmetria sinistra-destra nel conteggio quando la polarizzazione, la direzione dell'impulso di rinculo e la direzione IB sono tutte reciprocamente perpendicolari.

(*) *Traduzione a cura della Redazione.*

^{8}Li Fragments Associated with Nuclear Disintegration (*).

A. Alumkal and A. G. Barkow

Marquette University, Milwaukee, Wisc.

G. Kane

Manhattan College - New York, N. Y.

R. E. McDaniel

New Mexico State University - State College, New Mex.

Z. O'Friel

St. Bonaventure University - St. Bonaventure, N. Y.

(ricevuto il 13 Aprile 1960)

Summary. — This paper is a preliminary report on the emission of heavy fragments in nuclear disintegration. It is assumed that the probability of emission of a heavy fragment depends on the nuclear temperature (T) and the potential barrier (V) of the excited nucleus. It is the purpose of this investigation to study the dependence of the differential energy spectrum on the excitation energy. The data collected were from four stacks of Ilford G-5 emulsions, exposed to (*a*) a stopped pion beam; (*b*) 400 MeV proton beam; (*c*) (4÷5) GeV pion beam and (*d*) cosmic rays with an exposure in Texas, Magnetic latitude of 41° N, and on the Island of Guam at the magnetic equator. In this report emphasis will be placed on the emission of ^{8}Li as the heavy fragment. The results of the experiment indicate that for high excitation energy there is a collimation of lithium and beryllium fragments in the forward direction which may be explained on the basis of evaporation theory by assuming the fragment emission to take place during the flight of a highly excited nucleus. In the case of low excitation energy the angular distribution of ^{8}Li fragments is isotropic and the energy distribution indicates that the majority result from the absorption of a π^--meson by a light nucleus.

(*) Work supported by the National Science Foundation.

1. – Introduction.

Whenever a high energy nucleon collides with a nucleus there occurs within a time interval of about 10^{-23} seconds a series of collisions between this nucleon and the individual nucleons which make up the nucleus. These collisions can be classified into two main groups, radiative and elastic. In all present day theories it is assumed that all collisions are of the nucleon-nucleon type since a nucleon cannot interact with an assemblage of nucleons as a whole. This argument appears reasonable in view of the low binding energy of the nucleons, and also since the wave length of the incident nucleon is small compared with internuclear distance and the range of nuclear forces. However, the experimental observation of energetic fragments of helium, lithium, beryllium and even boron is inconsistent with this simplified hypothesis. Also the rare observation of a « clean » jet indicates that collisions between the incoming nucleon and a nucleon in the nucleus must cause a great disturbance in the nucleus.

Throughout the random exchange of energy by collision we can assume that after some time a definite amount of energy has been transferred to the nucleus leaving it in a highly excited state and that all the fast particles (gray tracks) have already left the nucleus. We can assume that the exchange of energy among the nucleons in the nucleus is completed before the expulsion of any further particles. The disintegration from this excited state may then be treated as quite independent of the process by which it is formed and the disintegration that follows is analogous to a process by evaporation. If this is the case, the energy spectrum of the emitted particles is of Maxwellian form, and their angular distribution should be isotropic.

In this paper we will consider only those particles finally emitted with energies below 30 MeV and they will be observed as « black » tracks and have grain density greater than 6.8 times minimum.

The statistical treatment of nuclear disintegration was initiated by Bohr and Kalckar [1], amplified by Bethe [2], Weisskopf [3] and LeCouteur [4], and leads to some very definite predictions. If 1) the excited nucleus is always in approximate thermodynamic equilibrium, 2) the emission time between successive particles is longer than the time required for the convection of energy across the nucleus, 3) the excitation energy is much less than the total binding energy of the nucleus, then the theory predicts that in the center of

(1) N. Bohr and F. Kalckar: *Kgl. Dan. Vid., Selsk.*, **24**, 10 (1937).
(2) H. A. Bethe: *Rev. Mod. Phys.*, **9**, 69 (1937).
(3) V. Weisskopf: *Phys. Rev.*, **52**, 295 (1937).
(4) K. J. Le Couteur: *Proc. Phys. Soc.* (*London*), A **63**, 259 (1950).

mass system of the evaporating nucleus the probability of a particle being emitted with kinetic energy between E and $E+\mathrm{d}E$ is given by

$$P(E)\,\mathrm{d}E = \frac{E-V}{T^2}\exp\left[-\frac{E-V}{T}\right]\mathrm{d}E\,, \tag{1}$$

where the parameters V and T are the average height of the effective potential barrier and the mean nuclear temperature in MeV.

During the last years numerous reports have been given of the observation of heavy nuclear fragments emitted from stars in photographic emulsions ([5-19]). The study of nuclear disintegration with emission of particles with charge $Z = 3$ has been extensively studied in our laboratory. The program consisted in studying the emission for various excitation energies. The exposures ranged from high energy cosmic rays at the magnetic equator to 140 MeV energy realized in stopped π^- events.

2. – Experimental procedure.

2·1. *Exposures.* – Various stacks of Ilford G-5 emulsions were exposed to radiation of different primary energy and disintegrations, accompanied by heavy fragments, were analysed. These primary beam energies were, 1) stopped π^- beam, 2) 400 MeV beam from the University of Chicago cyclotron, 3) 4.5 GeV pion beam (*) and 4) Cosmic Ray at the magnetic equator, Island of Guam.

([5]) A. Bonetti and C. Dilworth: *Phil. Mag.*, **40**, 585 (1949).
([6]) P. Hodgson and D. H. Perkins: *Nature*, **163**, 439 (1949).
([7]) D. H. Perkins: *Proc. Roy. Soc.* (*London*), A **203**, 399 (1950).
([8]) S. O. Sörensen: *Phil. Mag.*, **42**, 325 (1951).
([9]) J. P. Lonchamp: *Ann. Phys.*, **10**, 201 (1955).
([10]) B. A. Muir: *Phil. Mag.*, **1**, 355 (1956).
([11]) S. J. Goldsack, W. O. Lock and B. A. Munir: *Phil. Mag.*, **2**, 149 (1957).
([12]) S. Nakagawa, E. Tamai, H. Huzita and K. Okudaira: *Journ. Phys. Soc. Japan*, **11**, 191 (1956); **12**, 747 (1957).
([13]) O. Skjeggestad and S. O. Sörensen: *Phys. Rev.*, **113**, 1115 (1959).
([14]) S. Katcoff: *Phys. Rev.*, **114**, 905 (1959).
([15]) R. Hagedorn and W. Macke: *Komische Strahlung* (Berlin, 1953), p. 201.
([16]) R. H. Brown, U. Camerini, P. H. Fowler, H. Heitler, D. T. King and C. F. Powell: *Phil. Mag.*, **40**, 862 (1949).
([17]) M. Teucher: *Komische Strahlung* (Berlin, 1953), p. 69.
([18]) S. Nakagawa, E. Tamai and O. Nomoto: preprint (1958).
([19]) E. Tamai: *Nuovo Cimento*, **14**, 1 (1959).

(*) This stack of emulsions was kindly loaned to us by Professors V. Telegdi and R. Levi Setti of the Enrico Fermi Institute of Nuclear Study, University of Chicago.

The criteria for the selection and measurements of tracks were as follows:

1) Tracks of all particles ended in the emulsion.

2) The angle of dip was less than 30° before processing and range corrections were made for all angles. Width measurements on tracks with different dip angles were made and found to be consistent up to 30°.

3) The complete thickness of the emulsion was scanned. There was no significant change in track width from one emulsion depth to another for particles within these limits.

4) All hammer tracks were assumed to be due to ^{8}Li nuclei stopping in the emulsion. The stacks for all exposures were gridded which permitted tracing back of all observed hammer tracks. Hence, the geometrical correction to the energy spectra for tracks escaping from the emulsion is negligible ([20]).

5) The energies of the fragments were derived from the measured lengths of tracks and range-energy relations for ^{8}Li in nuclear emulsions given by SKJEGGESTAD ([20]) and BARKAS ([21]).

2·2. *Determination of charge of the fragment.* – The charge of heavy fragments was determined by the method employed by NAKAGAWA *et al.* ([12]). The procedure consists in measuring the average width of stopped particles as a function of residual range. By means of a bifilar the average width was obtained every 6 μm of length and when plotted as a function of residual range produced a graph showing a plateau, the ordinate of which is taken as the width of the track. Our calibration consisted in measuring the track width of known particles. These were protons from stopped proton exposure, α tracks from thorium stars and hammer tracks, and Li from ^{8}Li hammer tracks. In the case of lithium fragments the flat portion of the width curve started at about 38 μm, for alpha's at about 30 μm and for protons at about 18 μm. In the identification of fragments it was only necessary to measure the width at every 10 μm. The weighted average width of the ^{8}Li fragments was obtained by finding the centroid of the histogram or

$$\overline{w} = \frac{\sum n_i w_i}{\sum n_i} . \tag{1}$$

Assuming that the width of a track of charge Z varies as $Z^{\frac{1}{2}}$, the average width

([20]) O. S. SKJEGGESTAD: *Nuovo Cimento*, **13**, 927 (1958); *Thesis* (Oslo, no. 289).
([21]) W. H. BARKAS: *Phys. Rev.*, **89**, 1019 (1953).

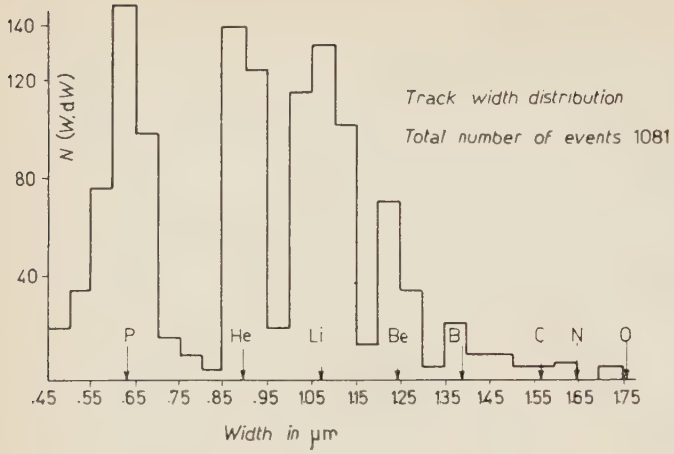

Fig. 1. – Track width distribution of particles from $Z=1$ to $Z=8$. The weighted average track width of ^{8}Li fragments was determined and found to be 1.07 μm. The arrows indicate the estimated track width of other charged particles calculated on the assumption that the track width varies as the square root of the charge.

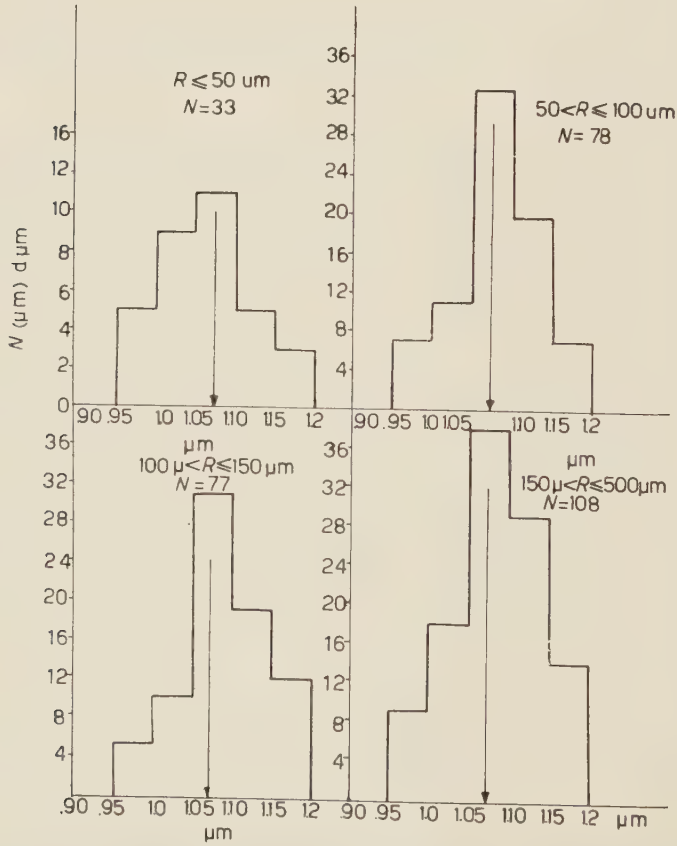

Fig. 2. – Results of the study of track width of lithium fragments of four different range groups.

of any particle of charge Z was obtained and is indicated by arrows in Fig. 1 and the corresponding width with standard deviations is given in Table I.

TABLE I. – *Average track width for fragments of charge $Z=1$ to $Z=8$.*

Z	Average width (μm)	Z	Average width (μm)
1	0.63 ± 0.05	5	1.39 ± 0.03
2	0.89 ± 0.03	6	1.52
3	1.07 ± 0.05	7	1.65
4	1.24 ± 0.04	8	1.76

It is immediately evident that for small Z the method employed becomes a fast and simple way for the determination of charge, but becomes less reliable for Z greater than five. A study of the reliability of track width measurements as a function of the length of the track was made for ^{6,7}Li fragments. The tracks were classified into four groups of ranges up to 500 μm. The results are given in Fig. 2 and show that the width of the track is independent of the range.

3. – Results.

3·1. ^{6}Li, ^{7}Li *and* ^{8}L, *fragments from cosmic ray stars.* – A study was made of the energy distribution of the unstable ^{8}Li and the stable ^{6,7}Li fragments. If the lithium fragments are emitted during the evaporation of a highly excited parent nucleus, then their differential energy spectrum should be of the form [4]

$$N(E)\,\mathrm{d}E = \frac{E-V}{T^2}\exp\left[-\frac{E-V}{T}\right]\mathrm{d}E\,, \tag{2}$$

for $E > V$ and where V is the potential barrier and T is the nuclear temperature both expressed in MeV.

The average $\bar{E}$ for any fragment will be given by

$$\bar{E} = \frac{\int_0^\infty E\cdot N(E)\,\mathrm{d}E}{\int_0^\infty N(E)\,\mathrm{d}E} = 2T + V\,, \tag{3}$$

where the value of V for heavy nuclei was taken to be [15]

$$V = 5.5\,Z\ \text{(MeV)}\,. \tag{4}$$

For each excitation energy E (in MeV) the nuclear temperature T was calculated from the excitation energy E(exc)

$$E(\text{exc}) = KAT^2 , \tag{5}$$

where A is the atomic weight of the excited nucleus, and $K = \pi^2/4G$, where G is the kinetic energy of the highest occupied state in the unexcited nucleus and is taken as 25 MeV. Equation (5) sets an upper limit on the nuclear temperature T of 10 MeV, since the application of the evaporation theory to heavy nuclei requires that the excitation energy be less than the binding energy of the nucleus or about 800 MeV.

The distribution for ^{8}Li and ^{6,7}Li is given in Fig. 3. In all our work it was assumed that the evaporating nucleus came to rest before the fragment was emitted. In this figure we give the distribution of the lithium fragments ob-

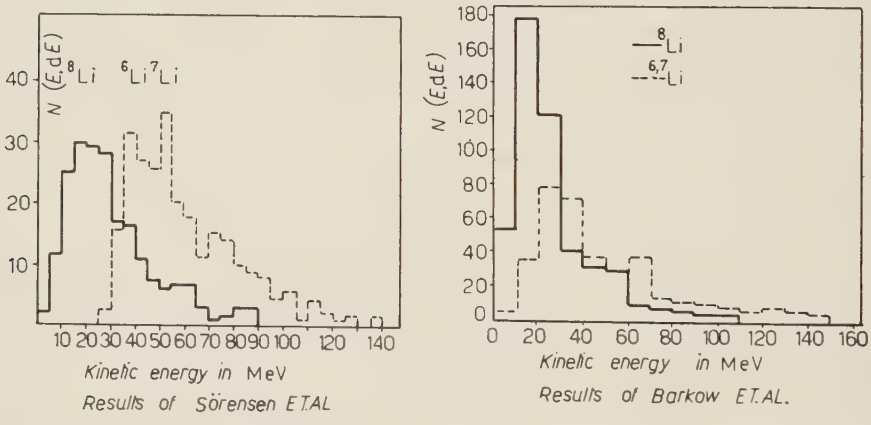

Fig. 3. – The energy distribution of ^{6,7}Li and ^{8}Li from cosmic ray stars. The angle of dip is less than 30°. The ^{6,7}Li distribution is for 340 events giving $T=15$ MeV, $V=12.5$ MeV and E (av)$=44$ MeV. The ^{8}Li distribution is for 467 events giving $T=9.5$ MeV, $V=5$ MeV and E (av)$=24.5$ MeV. In both distributions T and V were obtained by the method of best fit.

served by us and those found by SKJEGGESTAD and SÖRENSEN by the method described in reference ([13]). By means of a projection microscope they draw contours of the fragment tracks and determine the charge by measuring the total area of the last 106 μm of the track with a planimeter. SKJEGGESTAD and SÖRENSEN concluded that the marked difference in the form of the two spectra, position of the maxima, is not real. They believe that the lack of any strong increase in number of stable lithium fragments in the low energy region is due to a considerable loss of short tracks during scanning and the bias imposed by the method used.

Our results bear out these conclusions. Since SKJEGGESTAD and SÖRENSEN required tracks of length 106 μm or greater, their energy cut-off was in the neighborhood of 29 MeV. Employing the method of measuring track width we are sure of identifying particles of charge three, having a range of 38 μm or more which corresponds to a cut-off energy of 16 MeV. The inability of definitely identifying lithium particles of mass 6 and 7 of range less than 38 μm introduces an error in the low energy portion of the distribution. Any increase in number in these two intervals would result in a shift of the theoretical curve to the lower energy region and should give complete agreement between the different isotopes. At the present time profile measurements are being made on short tracks in an effort to actually identify lithium fragments of range shorter than 38 μm.

From the curves the experimental results can be explained qualitatively by assuming that the fragments of lithium of kinetic energy less than 80 MeV are ejected as part of the evaporation process. For energies greater than 80 MeV there is a surplus of fragments over the number predicted by the evaporation theory.

The values of T and V were obtained by getting the best theoretical fit of Eq. (1) to the experimental histogram. This was done by making a plot on transparent paper of $(E-V)$ *vs.* $N(E)\,\mathrm{d}E$ normalized to the total number of observed particles, for various values of T. By superimposing the theoretical graphs on the histogram the best values of T and V can be obtained. For ^{6,7}Li the values obtained by the method described above were $T=15$ MeV and $V=12.5$ MeV, while employing Eq. (2) and (3) we get $T=14$ MeV and $V=16.5$ MeV which gives reasonably close agreement and an $E_{av}=44$ MeV. The E_{av} is biased toward the high energies. However for ^{8}Li the values obtained were $T=9.5$ MeV, $V=5$ compared with $T=4$ MeV and $V=16.5$ and an $E_{av}=24.5$ MeV.

A study was made of the energy distribution of ^{8}Li as a function of the size of the parent star. As a measure of the size of the star we used the number of heavily ionizing prongs N_h defined as the number of tracks with grain density greater than

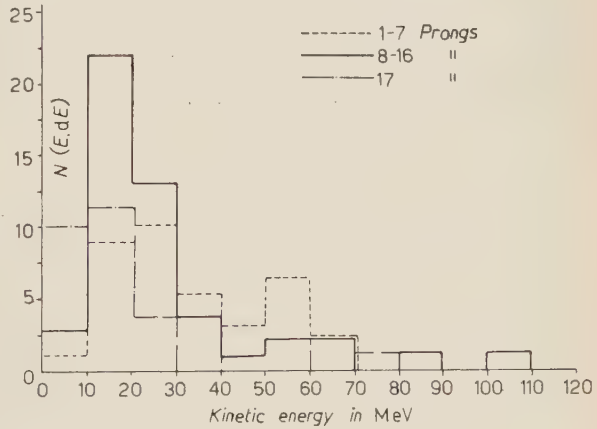

Fig. 4. – Energy distribution of ^{8}Li from cosmic ray stars as a function of the number of black tracks, N_h, of the parent star. The classification was: *a*) (1÷7) prongs; *b*) (8÷16) prongs and *c*) greater than 17 prongs.

1.4 times minimum. Further we have divided the ^{8}Li tracks into three groups with $1 \leqslant N_h \leqslant 7$, $8 \leqslant N_h \leqslant 16$ and $N_h \geqslant 17$. The three energy spectra are plotted in Fig. 4. As seen from the distribution the form of the three spectra does not depend on the energy released in the parent star.

3·2. ^{8}Li *fragments from* 4.5 GeV *pion stars.* – A similar study to that in Section 3·1 was made on ^{8}Li fragments found in 4.5 GeV pion stars. The energy distribution of 363 lithium fragments is plotted in Fig. 5 and the energy

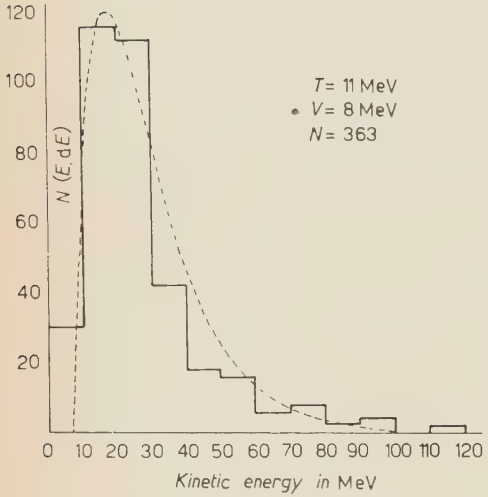

Fig. 5. – The energy distribution of ^{8}Li fragments found in 4.5 GeV pion stars. The distribution is for 363 events, giving $E_{av} = 22.5$ MeV, $T = 11$ MeV and $V = 8$ MeV.

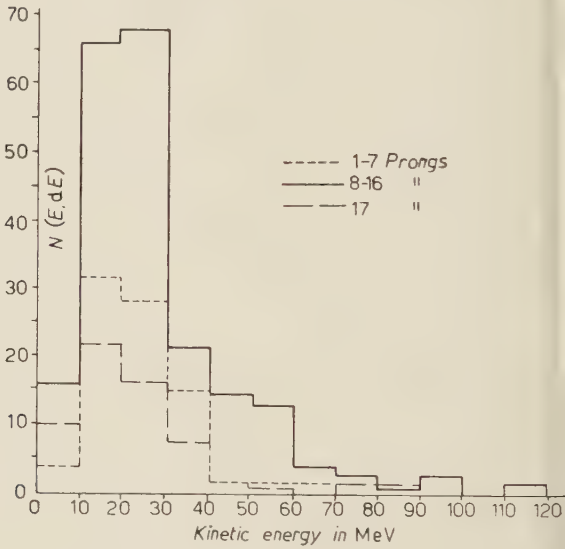

Fig. 6. – Energy distribution of ^{8}Li from 4.5 GeV pion stars as a function of N_h. The classification was: *a*) (1÷7) prongs; *b*) (8÷16) prongs and *c*) greater than 17 prongs.

distribution of the fragments as a function of N_h is given in Fig. 6. The energy distribution gives an $E_{av} = 22.5$ MeV which is in close agreement with the $E_{av} = 24.5$ MeV obtained from cosmic ray stars. The corresponding values $T = 9.5$ MeV and $V = 5$ MeV for ^{8}Li fragments from cosmic ray stars must be compared with $T = 11$ MeV and $V = 8$ MeV for 4.5 GeV pion stars. The energy distribution as in cosmic ray stars is independent of N_h.

3·3. *Beryllium fragments from cosmic ray stars.* – The energy distribution of ^{9}Be fragments from cosmic ray stars is given in Fig. 7. The angular distribution is given in Fig. 8. The observed values of $T = 19$ MeV and $V = 25$ MeV appear to be in good agreement with evaporation theory values obtained from

eq. (2) and (3). The theory gives values of $T = 21$ MeV and $V = 22$ MeV. However it is generally assumed that the evaporation theory breaks down when the energy of excitation approaches the total binding energy of the nucleus. If we assume an average A of 100 for AgBr and a binding energy

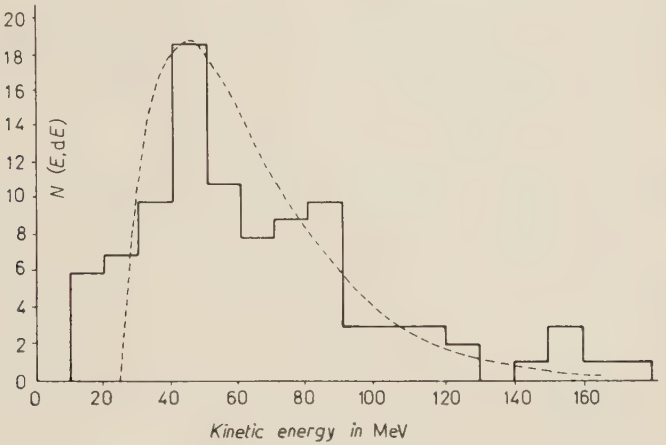

Fig. 7. – The energy distribution for 98 ^{9}Be fragments from cosmic ray stars, with the following results: $E_{av} = 64$ MeV, $T = 19$ MeV and $V = 25$ MeV.

of 8 MeV per nucleon, the upper limit will be of the order of 800 MeV corresponding to a nuclear temperature of about 10 MeV. The value of 21 MeV for the mean temperature is much too high to be acceptable. This conclusion is even further supported by the results of nuclear cascade calculations which give the average excitation energies of the residual nuclei of only a few hundred MeV. We are at a loss to explain the relatively large number of ^{9}Be fragments with kinetic energies less than 22 MeV unless we assume the fragment to be the result of the evapora-

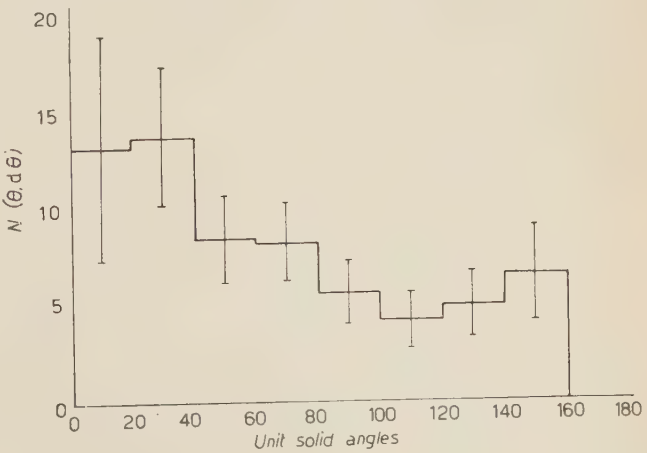

Fig. 8. – Angular distribution of ^{9}Be fragments. A collimation in the forward direction is indicated.

tion of a light nucleus. The minimum energy of an evaporated particle from a heavy nucleus is determined by eq. (4) and for Be should be 21 MeV.

3·4. ^{8}Li *fragments from stopped* π^- *stars.* – In connection with the study of heavy fragments originating from high energy nucleon interaction it was felt advisable to analyse the occurrence of ^{8}Li fragments originating in stopped π^- stars, the thought being that since the excitation energy is known, namely 140 MeV, a study could be made as to the evaporation of ^{8}Li from heavy nuclei contrasted to the evaporation of ^{8}Li from light nuclei. In the case of heavy nuclei, namely silver and bromine, the excitation energy is well below the total binding energy of the respective nuclei and the evaporation theory should apply. However, in the case of light nuclei (C O H N) the excitation energy is greater than the average binding energy of the nuclei.

A stack of 36, (2 × 4) inch, 600 μm G-5 emulsion were exposed to the π^- beam of the cyclotron at the University of Chicago. The beam entered the stack perpendicular to the 4 in. dimension and parallel to the emulsion. After travelling 1.5 cm of emulsion 95 percent of the π^- mesons stopped within a strip of length 2 cm. The pion flux was $4 \cdot 10^4$ π's per cm^2 per minute and the stopped μ^- contamination was less than one percent in the portion of the emulsion where the π^- mesons stopped, or less than one percent of the zero prong stars can be attributed to μ^- absorption. Over 22 308 σ stars were analysed and the following problems emphasized.

3·4.1. Prong distribution of σ stars. – All σ stars found in the stack were catalogued and classified according to prong number. The results are

TABLE II. – *Sigma stars from stopped* π^- *beam ecitation energy* 140 MeV. *Total number of stars*: 22 308.

No. of prongs	ADELMAN and JONES (%)	CHESTON and GOLDFORB (%)	MENON, MUIRHEAD and ROCHET (%) (aver.)	Group from MARSHAK $P-182$ %	BARKOW, ALUMKAL and CHAMANY (no.)	BARKOW, ALUMKAL and CHAMANY %
0	26.8	35.2	19.4	28 ±2	6 684	29.9
1	21.5	13.3	33.4	23.3±0.7	7 389	33.1
2	27.0	21.9	23.4	23.5±0.7	4 444	19.9
3	15.2	18.9	20.1	16.1±0.5	2 624	11.8
4	7.8	8.8	3.7	7.6±0.4	985	4.4
5	1.8	1.9	—	1.4±0.2	175	0.8
6	—	—	—	0.1±0.1	1	—
7	—	—	—	—	3	—
8	—	—	—	—	1	—
No. of stars studied	1 500	500	2 500	4 000	22 308	

tabulated in Table II and compared with results obtained by ADELMAN and JONES ([22]), CHESTON and GOLDFORB ([23]), MENON, MUIRHEAD and ROCHET ([24]) and the average given by MARSHAK ([25]). The possibility of including the recoil nucleus as a prong is very small. For a recoil nucleus of charge $Z = 5$ and mass $M = 10$ to have a range of 2 μm, which is barely visible, required one proton to have energy of nearly 45 MeV. The probability of observing protons with energy greater than 45 MeV is less than two percent and since this is divided between light and heavy nuclei, the actual observing of a light nucleus recoil is less than one percent.

3·4.2. Prong distribution of stars having a ^{8}Li fragment. The frequency distribution and energy distribution of ^{8}Li fragments observed in σ stars were studied. The criteria for selection of events were, 1) all ^{8}Li hammer tracks were assumed to have stopped in the emulsion and their co-linearity checked within 5°; 2) energy of measured ^{8}Li fragments had angle of dip 30° or less in the undeveloped emulsion and 3) all questionable hammer tracks were assumed to be due to ^{8}Li. Three strongly suspicious ^{8}B fragments were observed and are not included in the results. The reason for selecting the 30° dip criterion was to simultaneously check the isotropy of ^{8}Li emission, since the solid angle subtended by the surface area of a sphere from 0° to 60° is equal to that subtended from 60° to 90°. A typical four prong σ star caused by an absorbed stopped π^- is shown in the mosaic photograph in Fig. 9.

The prong distribution of the parent star from which the ^{8}Li fragment originated is syown in Table III, and contains both the data for all ^{8}Li fragments

TABLE III. – *Prong distribution of parent star of* ^{8}Li *fragments (data from over* 235 000 σ *stars).*

No. of prongs	Frequency of ^{8}Li (total)	Frequency of ^{8}Li (dip angle less than 30°)	Percent of total ^{8}Li
1	5	2	1.1
2	51	20	11.4
3	266	139	59.5
4	113	59	25.3
5	12	5	2.7
Total	447	225	100

([22]) F. L. ADELMAN and JONES: *Science*, **3**, 226 (1960); F. L. ADELMAN: *Phys. Rev.*, **85**, 249 (1952).

([23]) W. B. CHESTON and L. J. B. GOLDFARB: *Phys. Rev.*, **78**, 683 (1950).

([24]) M. G. K. MENON, H. MUIRHEAD and O. ROCHAT: *Phil. Mag.*, **41**, 583 (1950).

([25]) R. E. MARSHAK: *Meson Theory* (New York, 1952), p. 182.

Fig. 9. – Mosaic photograph of the capture of a π^--meson by a nucleus resulting in a four prong star, one prong of which is a ^{8}Li fragment.

observed and those that satisfy the 30° dip criterion. The fact that the emission is isotropic for both cases is apparent and this isotropy was verified by an angular distribution plot. From Table III the ^{8}Li fragment favors the environment of two other fragments as 60 percent of the hammer tracks were observed in 3 prong stars.

The energy distribution of ^{8}Li from 3 and 4 prong stars and from all stopped π^- stars is given in Fig. 10 and appears to be independent of the size of the parent star. Since 90 percent of the ^{8}Li fragments have observable energy of 16 MeV or less it is evident that they must have originated from light nuclei. This follows from the fact that 16 MeV is the minimum energy of an evaporated particle from a heavy nucleus.

In an attempt to check this conclusion further we carefully analysed the fragments accompanying the ^{8}Li in three prong stars.

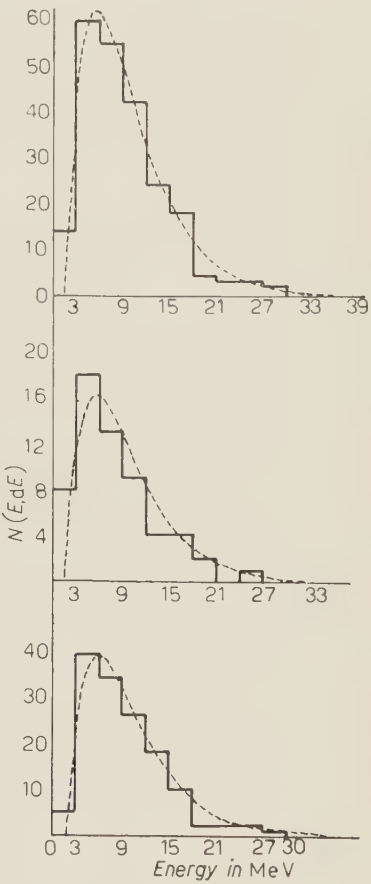

Fig. 10. – Energy distribution of ^{8}Li from stopped π^- stars. The upper curve is the distribution from all stars regardless of the prong number. The middle curve is the distribution of ^{8}Li from 4 prong stars while the bottom curve is the distribution from 3 prong stars. Since the potential barrier for ^{8}Li fragments from heavy nuclei is about 16 MeV, it is evident that 90% of the fragments originated from light nuclei.

TABLE IV. – *Analysis of π^- interactions from three prong stars.*

Identified fragments	No. of events	Reaction scheme	Percent
p, p, $^8_3$Li	9	$\pi^- + {}^{12}_{6}\mathrm{C} \rightarrow 2\,{}^{1}_{1}\mathrm{H} + {}^{8}_{2}\mathrm{Li} + 2\,{}^{1}_{0}\mathrm{n}$	7.5
p, α, $^8_3$Li	48	$\pi^- + {}^{14}_{7}\mathrm{N} \rightarrow {}^{1}_{1}\mathrm{H} + {}^{4}_{2}\mathrm{He} + {}^{8}_{3}\mathrm{Li} + {}^{1}_{0}\mathrm{n}$	39.0
α, α, $^8_3$Li	15	$\pi^- + {}^{16}_{8}\mathrm{O} \rightarrow 2\,{}^{4}_{2}\mathrm{He} + {}^{8}_{3}\mathrm{Li}$	12.5
p, $^{6,7}_3$Li, $^8_3$Li	17	$\pi^- + {}^{16}_{8}\mathrm{O} \rightarrow {}^{1}_{1}\mathrm{H} + {}^{6}_{3}\mathrm{Li} + {}^{8}_{3}\mathrm{Li} + {}^{1}_{0}\mathrm{n}$	14.0
p, $^{6,7}_3$Li, $^8_3$Li	17	$\pi^- + {}^{16}_{8}\mathrm{O} \rightarrow {}^{1}_{1}\mathrm{H} + {}^{7}_{3}\mathrm{Li} + {}^{8}_{3}\mathrm{Li}$	
heavies, $^8_3$Li	32	π^- + heavy	27.0
	121		100

Of the 139 events that satisfied the dip criterion, 121 could be classified as clean stars giving no evidence of a short recoil. The fragments were identified by the method discussed previously with no width corrections made when a fragment had a dip angle greater than 30°. The analysis is given in Table IV and indicates that about 73 percent of the three prong stars could owe their origin to the capture of a π^- meson by a light nucleus.

4. – Conclusion.

At the present time nuclear evaporation is the only theory from which relative frequency, energy spectra and angular distribution of fragments can be calculated. It is generally assumed that evaporation breaks down when the excitation energy of the nucleus exceeds the total binding energy. The upper limit for application of the theory to heavy nuclei (Ag and Br in emulsion) is generally taken as about 800 MeV resulting in a nuclear temperature of about 10 MeV. Hence, any temperature greater than this, like the value of 19 MeV for beryllium fragments is somewhat too high to be accepted. Also the presence of the high energy tail accompanying the distribution and the contribution of the fast nucleon-nucleon knock-on stage which precedes the evaporation process cannot be neglected. The observation of high energy heavy fragments which cannot be explained on the basis of elastic collision ([18]) strongly suggests the presence of hot spots in the nucleus. It is generally accepted that the fair agreement between calculation and experiment in the low energy region is a good indication that the evaporation mechanism is dominant, but that at high energies another mechanism takes over.

For low excitation energy as in the case of the π^- exposure 90 percent of the ^{8}Li were emitted from supposedly light nuclei and the application of evaporation theory for light nuclei becomes questionable. The light nuclear case together with the presence of a small Coulomb barrier is complicated by the additional processes which lead to the formation of ^{8}Li as spallation residues. For a nitrogen target, an average light nucleus in the emulsion of A equal to 14 and Z equal to 7, the concept of evaporation does not apply since the ^{8}Li has about half the mass of the target. In other words, what is the meaning of the potential barrier for a nucleus that absorbs a π^- meson resulting in a 3 prong star whose fragments are ^{8}Li, an α particle and a proton? Results predicted by the evaporation theory especially those relating average energy of the fragment with nuclear temperature and the Coulomb barrier are in good agreement with experimental results (Fig. 10). The frequency of observing a ^{8}Li fragment originating from a heavy nucleus is in agreement with the theoretical consideration of LeCouteur ([26]).

([26]) K. J. Le Couteur: *Nuclear Reactions* (Amsterdam, 1959).

An additional controversy arises in the study of the angular distribution of ^{8}Li from cosmic ray stars and heavy fragments $Z \geqslant 4$. In Fig. 11 we have plotted the combined angular distribution of over 600 heavy fragments of $Z \geqslant 4$, observed in cosmic ray stars, 4.5 GeV pion stars and 400 MeV proton stars. All observed fragments greater than lithium, regardless of whether they were identified or not, are included in the plot. The distribution also includes the 98 fragments identified as ^{9}Be from Fig. 8. At high excitation energy there appears to be a definite collimation of fragments in the forward direction, while for relatively low excitation (140 MeV) the angular distribution indicates an isotropic emission of ^{8}Li fragments. The anisotropy observed in the case of high energy fragments can only be explained on the basis of nuclear evaporation by assuming the fragment emission to take place during the flight of the highly excited rest nucleus formed after the initial nucleon cascade is completed. The theoretical discussion of SKJEGGESTAD and SÖRENSEN ([13]), calculated on the assumption that the evaporating nucleus is in motion predicts a collimation of fragments in the forward direction for high energies and becomes nearly isotropic at energies less than 30 MeV.

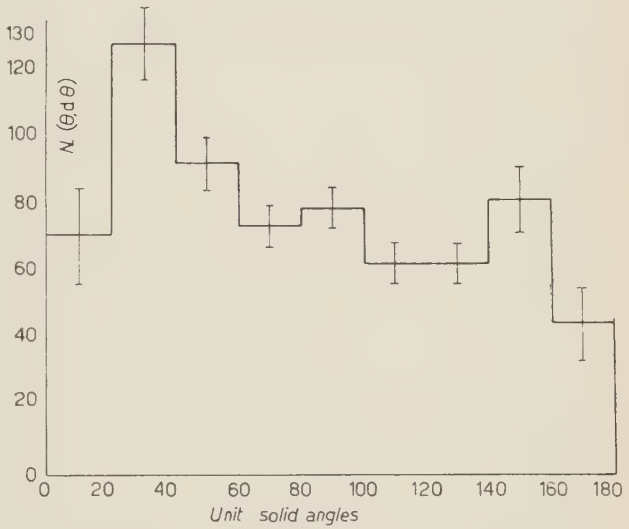

Fig. 11. – Angular distribution of heavy fragments for $Z \geqslant 4$. All observed fragments for Z greater than 3 were plotted regardless of whether they were definitely identified or not.

In communication with LEVI-SETTI and SKJEGGESTAD a very similar distribution of ^{8}Li fragments from stopped K^- stars is being obtained. From preliminary results 90 percent of the ^{8}Li fragments have energy less than 16 MeV and range less than 50 μm.

* * *

The authors are very grateful to Professor MARCEL SCHEIN, of the University of Chicago, for his generous assistance in regard to this problem. It is also a pleasure to thank Drs. ERICK LOHRMANN and MARTIN TEUCHER, of the University of Chicago, for many stimulating discussions.

Appendix

The Le Couteur formula can be obtained if we consider the nucleons within the excited nucleus to follow a Fermi distribution of the form

$$n(E)\,\mathrm{d}E = \frac{\text{constant}\; g(E)\exp\left[-E/kt\right]}{\exp\left[\alpha\right]\exp\left[-E/kt\right]}\,\mathrm{d}E\,, \tag{1}$$

where $n(E)$ is the number of nucleons per energy interval within the nucleus and $g(E)$ the number of levels per energy interval and is proportional to $E^{\frac{1}{2}}$. If $\exp\alpha \gg \exp\left[-E/kt\right]$ and when compared to $\exp\left[-E/kt\right]$ is a slowly varying function of kt and can be considered constant, eq. (1) becomes

$$n(E)\,\mathrm{d}E = C_1 g(E)\exp\left[-\frac{E}{kt}\right]\mathrm{d}E \tag{2}$$

or

$$n(E)\,\mathrm{d}E = C_2 E^{\frac{1}{2}}\exp\left[-\frac{E}{kt}\right]\mathrm{d}E\,. \tag{3}$$

The probability of a nucleon escaping from the nucleus is proportional to $n(E)$, provided the energy of the particle E is greater than the height of the potential barrier V, and also proportional to v the velocity of the particle or to $E^{\frac{1}{2}}$. The probability that a particle of energy between E and $E+\mathrm{d}E$ will escape is given by

$$P(E)\,\mathrm{d}E = C_3 E^{\frac{1}{2}}\cdot E^{\frac{1}{2}}\exp\left[-\frac{E}{kt}\right]\mathrm{d}E$$

or

$$P(E)\,\mathrm{d}E = C_3 E\exp\left[-\frac{E}{T}\right]\mathrm{d}E\,, \tag{4}$$

where T is in units of kt and usually expressed in MeV. If we do not permit leakage through the barrier, the smallest value of E for a nucleon that escapes will be V, the height of the Coulomb potential barrier. Normalizing eq. (4) to obtain C_3 we have

$$C_3\int_V^\infty \mathrm{E}\exp\left[-\frac{E}{T}\right]\mathrm{d}E - 1$$

since the observed energy of a nucleon outside the nucleus is $(E-V)$ we have

$$C_3\int_V^\infty E\exp\left[-\frac{E-V}{T}\right]\mathrm{d}E = 1$$

from which $C_3 = 1/T^2$ or

$$P(E)\,\mathrm{d}E = \frac{E-V}{T^2}\exp\left[-\frac{E-V}{T}\right]\mathrm{d}E \tag{5}$$

which is Le Couteur's formula.

RIASSUNTO (*)

Questo è un rapporto preliminare sulla emissione di frammenti pesanti nella disintegrazione nucleare. Si presuppone che la probabilità di emissione di frammenti pesanti dipenda dalla temperatura nucleare (T) e dalla barriera di potenziale (V) del nucleo eccitato. Lo scopo di questa ricerca è di studiare la dipendenza dello spettro differenziale dell'energia dall'energia di eccitazione. I dati raccolti provenivano da quattro pile di emulsioni Ilford G-5, esposte a: (*a*) un fascio di pioni frenato; (*b*) un fascio di protoni di 400 MeV; (*c*) un fascio di pioni di (4÷5) GeV e (*d*) raggi cosmici con esposizione nel Texas, latitudine magnetica 41° N, e sull'isola di Guam all'equatore magnetico. In questo scritto si sottolinea l'emissione di ^{8}Li come frammento pesante. I risultati dell'esperimento indicano che per elevata energia di eccitazione si ha una collimazione in avanti dei frammenti di litio e berillio, che può spiegarsi sulla base della teoria dell'evaporazione, supponendo che l'emissione dei frammenti abbia luogo durante il volo di un nucleo fortemente eccitato. Nel caso di bassa energia di eccitazione la distribuzione angolare dei frammenti di ^{8}Li è isotropica e la distribuzione dell'energia indica che la maggior parte proviene dall'assorbimento di un mesone π^- in un nucleo leggero.

(*) *Traduzione a cura della Redazione.*

On the Anisotropy of the Cosmic Radiation.

E. W. Kellermann and M. S. Islam

Department of Physics, The University of Leeds - Leeds

(ricevuto il 14 Aprile 1960)

Summary. — An attempt has been made to reproduce some results of McCusker and his coworkers who had reported diurnal effects of cosmic ray showers. The design of the apparatus follows closely that of these workers, but allows more detailed information about each recorded event to be obtained. The main categories of observed events, including those examined by McCusker *et al.*, show no significant diurnal variation. A possible sidereal diurnal variation of a particular group of events is critically examined, and it is concluded that, in spite of strong statistical weight, the implications of accepting the variation as physically real do not at present allow it to be regarded as such.

Many attempts have been made to determine whether an anisotropy of the cosmic radiation, apart from that imposed in the immediate neighbourhood of the earth, can be detected. Although for obvious reasons one would regard as most promising the study of the products of very energetic primaries, a number of workers who report some indication of anisotropy have been concerned with effects due to primaries of much lower energy. Notably, McCusker and his co-workers [1-3] have presented evidence for the detection of a sidereal time variation of large amplitude, and hence a directional anisotropy of incident primaries, with a relatively simple counter arrangement sensitive to penetrating showers. Other workers, too, have reported similar, if smaller

[1] C. B. A. McCusker, J. G. Dardis and B. G. Wilson: *Proc. Phys. Soc.*, A **68**, 585 (1955).

[2] C. B. A. McCusker: *Nuovo Cimento*, **2**, 1340 (1955).

[3] C. B. A. McCusker and R. J. Reid: *The Oxford Conference on Extensive Showers* (Harwell, 1956), p. 58.

effects, and the great difficulty in seeing any reasonable interpretation of these observations must be set against the fact that considerable agreement is to be found in such work regarding the phase of the possible sidereal variations.

The work reported here was prompted by the need for investigation of the large sidereal variation reported by McCusker and of the very large variation in solar time reported by him ([3]) by similarly simple counter arrangements. Data for 14 months are now available, and so a stage has been reached when significant statistical improvement will be slow; they are perhaps now of sufficient interest to justify this report.

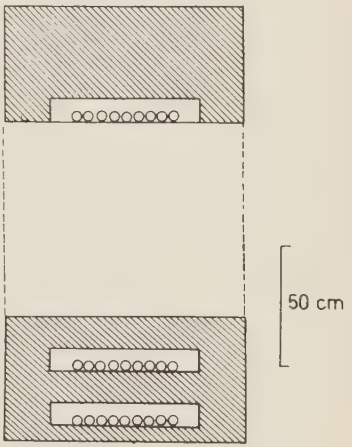

Fig. 1*a*. – The shielded trays *S*.

The experiment is being carried out at Leeds. Following McCusker closely we use a penetrating shower detector of three trays of Geiger tubes (Fig. 1*a*). Each tray contains 9 counters of area 240 cm², and they are respectively shielded vertically by 30, 40 and 50 cm lead while there is 15 cm lead shielding at the sides. This unit is placed at the centre of a triangle (Fig. 1*b*) formed by three unshielded trays of counters each containing two of area 240 cm² and two of 35 cm² area. The discharge of every counter of the array is separately displayed, and the form of a penetrating event together with an estimate of the accompanying electron shower density may be obtained. The selection was made for penetrating showers, involving the discharge of at least two counters in each of the three shielded trays.

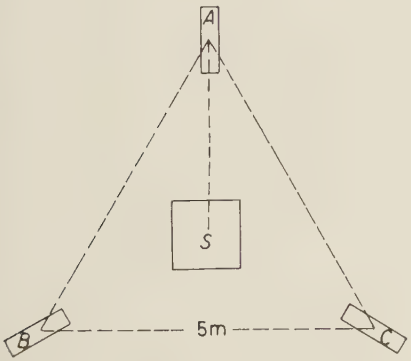

Fig. 1*b*. – The geometry of the shielded trays *S*, and the unshielded trays *A*, *B* and *C*.

The hodoscope arrangement, enabling the discharge pattern to be examined, allowed different kinds of events to be distinguished. Some of these could be compared with observations of other workers, affording a useful check on overall operation; it was felt, too, that any anisotropy found to occur in events of any but extreme energy might belong not to a broad grouping of events, but rather to some small, but perhaps recognisable component. Accordingly, the rates of the separated components making up the total observed group of

« penetrating showers » were analysed both in solar and in sidereal time, tested for fit to isotropic incidence, and only where this failed subjected to Fourier analysis over a solar or sidereal day.

The period of operation reported here was of about 10 000 hours (between February 1958 and June 1959); in it the following events were distinguished:

1) Knock-on events, 4 047 in number.

These, arising from the successive elastic collisions of muons near to each shielded tray were selected from the hodoscope record by inspection. The selected number was later compared with a calculated rate based on the established muon flux. Agreement was reasonable, and the separation of these events is probably good.

2) P_L-showers, 18 482.

Penetrating « local » showers, discharging at least two counters in each of the three shielded layers, by their geometry probably not of type 1) above, and not accompanied by any discharges in the unshielded trays.

3) P_E-showers, 2 455.

Penetrating showers accompanied by at least one counter discharge in the unshielded array.

The pattern of discharges of shielded counters within the central lead shield, represented in Figs. 2(*a*), 2(*b*) by the total number, $6 \leqslant n \leqslant 27$ of these counters discharged, shows a significant difference between P_L and P_E events; the latter yield a very much higher average number of discharged counters, and therefore probably refer to more energetic events.

In the P_E-events (Fig. 2(*b*)) there is a tendency for the frequency-number relation to become constant for a high number of discharged counters. This may represent saturation, but might also be the result of superposition of two effects: the P_E-events have accordingly been divided into the categories

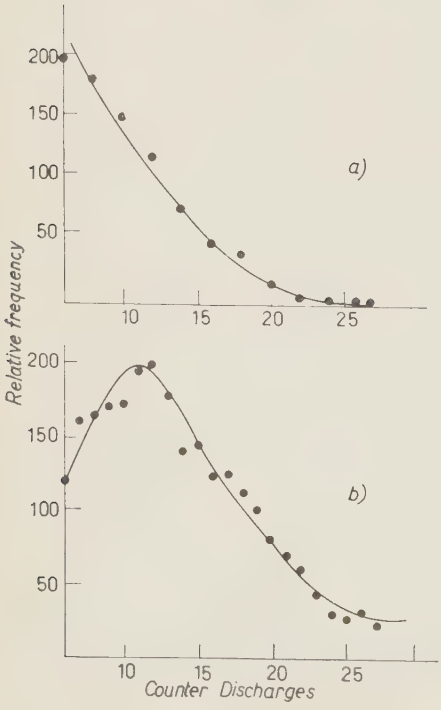

Fig. 2. – The frequency of numbers of shielded counter discharges for: *a*) penetrating local showers P_L; *b*) penetrating extensive showers P_E.

$P_E(\geqslant 19)$ and $P_E(\leqslant 18)$ depending on whether the count does or does not lead to the discharge of at least 19 of the shielded counters. They are the events

(3*a*) $P_E(\geqslant 19)$, 471

and

(3*b*) $P_E(\leqslant 18)$, 1 984 .

A final subdivision of the $P_E(\geqslant 19)$ events was made on the basis of the density of accompanying electronic shower particles as estimated by the detailed discharge pattern in the unshielded counter trays surrounding the central unit (Fig. 3). The figure leads one to make a separation at an electron density of about 50 particles per square metre, and the final subdivision there leads to the categories

(3*a*, *a*) $P_E(\geqslant 19, > 50\ m^{-2})$, 191

and

(3*a*, *b*) $P_E(\geqslant 19, < 50\ m^{-2})$, 280 .

In order to acquire some information comparable to the results published by McCusker [4] referring to showers of high particle density, we selected, for some six months, also events triggered only by the small counters in the unshielded trays, where at least one small counter in each of the trays was discharged. We estimated the average density of these events as larger than 200 particles m^{-2}. About 730 of these high density, H.D., events were registered.

All of the groups listed above were, as has been indicated, tested for compatibility with isotropic incidence in both solar and sidereal time and were

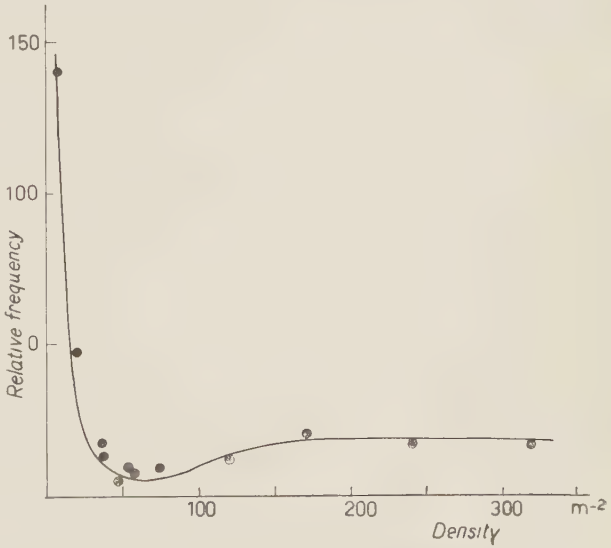

Fig. 3. – The density distributions of the soft component accompanying the $P_E(\geqslant 19)$ events.

[4] C. B. A. McCusker, D. E. Page and R. A. Reid: *Phys. Rev.*, **89**, 1172 (1959).

subjected to harmonic analysis where the level of compatibility was low. The raw data were not corrected for pressure or temperature since such correction would only be possible for recognizable components, and such identification is not possible as yet: moreover, our statistics are not yet sufficient to derive a pressure or temperature coefficient from our data.

The results of the analysis are given in Tables I and II; the compatibility of the data with isotropy is measured by a χ^2-test for constant intensity through a solar and sidereal day respectively, and the probability of fit, P, is given in column 3 of each table; the usual convention of examining the significance of the value of P at the 5%—and at the 1%—level has been adopted.

TABLE I. – *Results of solar time analysis. Total running time* 9803 h *solar time.*

	Type of shower	No. of events	Compatible with st. line	P (%)	1st harmonic		P (%)	2nd harmonic		P (%)
					Amplitude	Phase (h)		Amplitude	Phase (h)	
(1)	Knock-on	4047	?	3	6.4 ± 2.7	2.80 ± 1.5	53	—	—	—
(2)	P_L	18482	Yes	30	—	—	—	—	—	—
(3)	P_E	2455	Yes	36	—	—	—	—	—	—
(3*a*)	P_E (≥ 19)	471	Yes	63	—	—	—	—	—	—
(3*b*)	P_E (≤ 18)	1984	Yes	45	—	—	—	—	—	—
(3*a*, *a*)	P_E (≥ 19, > 50 m^{-2})	191	Yes	50	—	—	—	—	—	—
(3*a*, *b*)	P_E (≥ 19, < 50 m^{-2})	280	Yes	42	—	—	—	—	—	—
(4)	H_D (six months)	729	Yes	70	—	—	—	—	—	—

TABLE II. – *Results of sidereal time analysis. Total running time*: 9830 h *sidereal time.*

	Type of shower	No. of events	Straight line	P (%	1st harmonic		P (%)	2nd harmonic		P (%)
					Amplitude	Phase h G.S.T.		Amplitude	Phase h G.S.T.	
(1)	Knock-on	4047	Yes	87	—	—	—	—	—	—
(2)	P_L	18482	Yes	33	—	—	—	—	—	—
(3)	P_E	2455	Yes	50	—	—	—	—	—	—
(3*a*)	P_E (≥ 19)	471	No	0.05	20.7 ± 7.4	21.6 ± 1.4	7	20.7 ± 6.5	$\frac{12.0 \pm 0.6}{0.0 \pm 0.6}$	5
(3*b*)	P_E (≤ 18)	1984	Yes	10	—	—	—	—	—	—
(3*a*, *a*)	P_E (≥ 19, > 50 m^{-2})	191	No	0.2	30.9 ± 11.3	21.5 ± 1.3	2	35.1 ± 11.9	$\frac{11.5 \pm 0.7}{23.5 \pm 0.7}$	16
(3*a*, *b*)	P_E (≥ 19, < 50 m^{-2})	280	Yes	8.6	—	—	—	—	—	—
(4)	H_D (six months)	729	Yes	40	—	—	—	—	—	—

The solar and sidereal analyses may be commented upon separately; the only indication of a solar effect concerns knock-on events, and even here the significance of the variation is not particularly high. Neither amplitude nor

phase of the possible effect agrees with that established for the general meson component, and there is no reason to postulate a real effect. It should be mentioned here that the combined groups of knock-on and P_L events roughly correspond to the « penetrating local showers » examined by McCusker and Wilson [1].

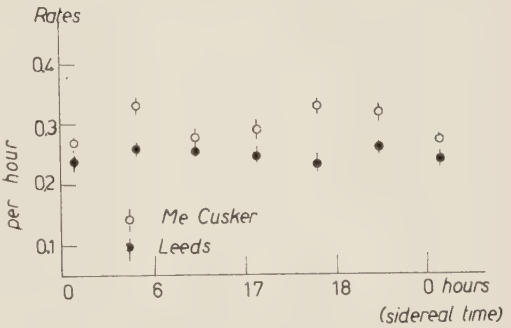

Fig. 4. – The rates of penetrating extensive showers versus sidereal time, as measured by McCusker [3] and in Leeds.

The P_E showers as a whole correspond to the penetrating extensive showers for which McCusker and Reid [3] have reported a sidereal variation. Since our results have statistics comparable to those of McCusker and Reid, both their results and ours have been plotted together in Fig. 4. The figure illustrates the findings in Table I, namely that, as for the local showers, our results confirm neither the phases nor the amplitudes found by these workers.

The possible sidereal effect concerns the results grouped as $P_E(\geqslant 19)$ and, in particular, those related to high density electron showers, $P_E(\geqslant 19, > 50\ \mathrm{m}^{-2})$ rather than those related to lower shower densities, $P_E(\geqslant 19, < 50\ \mathrm{m}^{-2})$ although one must bear in mind that the subdivisions leading to the isolation of the $P_E(\geqslant 19)$ events are arbitrary. The rate of $P_E(\geqslant 19, > 50\ \mathrm{m}^{-2})$ events as a function of sidereal time is plotted in four-hourly and in two-hourly intervals in Fig. 5. The continuous graph is the calculated second harmonic, the dotted line is the first harmonic. For comparison we have plotted, too, the rates in solar time and « antisidereal » time.

The « antisidereal » time scale, first used by Farley and Storey [5], has no physical meaning and is arrived at in a purely formal way. Farley and Storey have pointed out that as the sidereal time can be regarded formally as a modulation of the solar time, so an « antisidereal » time can be obtained by a modulation of solar time opposite in sign. Since this time scale is devoid of physical meaning no variation should be expected and none, as in solar time representation, is in fact found.

The evidence presented in favour of the reality of sidereal variation must be weighed carefully in conjunction with the following arguments:

Firstly: it is important to establish whether the events in question, the $P_E(\geqslant 19, > 50\ \mathrm{m}^{-2})$ are a selection from extensive air showers, (EAS). If

(5) F. J. M. Farley and J. R. Storey: *Proc. Phys. Soc.*, A **67**, 996 (1954).

they are, then in view of all the accumulated knowledge on EAS, the time variation reported here is most likely a statistical fluctuation. Certainly, the rate of the events, ~ 0.5 per day, is about 5% of the rate of showers of den-

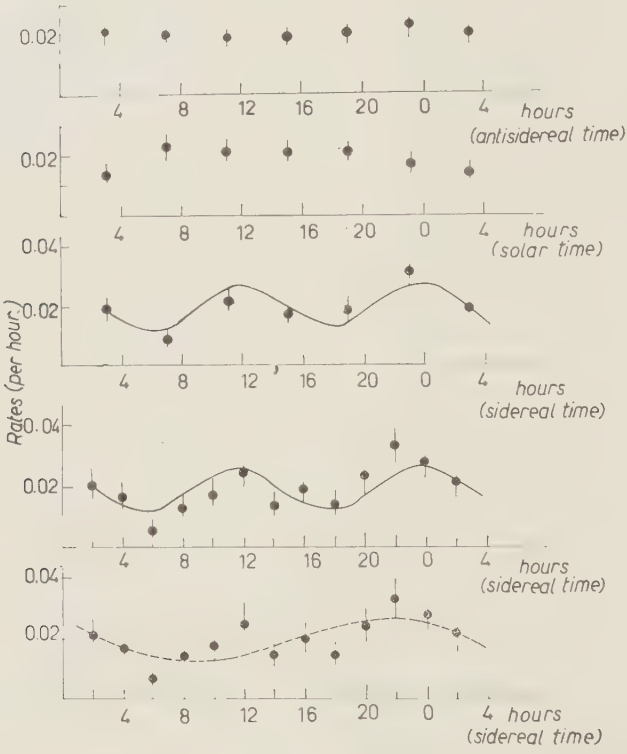

Fig. 5. – $P_E(\geqslant 19, > 50\ \mathrm{m}^{-2})$ events plotted in antisidereal and solar time, and in two-hourly and four-hourly intervals in sidereal time.

sity of $(100 \div 200)$ particles m^{-2} expected, according to the known density spectrum of EAS, to fall on the pile. Such a percentage is not unreasonably high, and the identification of these particular events with a selection from EAS is therefore not ruled out. The energy one would have to associate with the primary giving rise to the events would judged by the rate, be of the order of $(10^{15} \div 10^{16})$ eV.

A further argument against the reality of a sidereal variation is, of course, the amplitude (30%) of the effect which is unplausibly large.

The arguments against the existence of the effect are at least modified by the following:

First, a systematic error is less likely to occur in a sidereal than in a solar analysis. Here, the analysis in solar and in «antisidereal» time shows the expected absence of the effect. There is agreement too, with the results of other workers, but not with McCUSKER, on the absence of a large effect in the group comprising all penetrating extensive showers.

Secondly, the main maximum of the variation reported here (21.5 h) coincides with the phase for which other workers (see for example GREISEN [6], GALBRAITH [7]) have found—albeit not statistically significant—indications.

The size of the variation reported here relates to a separated component and so does not correspond to the total cosmic ray flux investigated by previous workers. In particular, normal observation of extensive air showers would, even if this effect were real, only show it in an extremely diluted form.

However, even if one does assume that one is dealing here not with EAS but with a correctly separated and independent component of the cosmic radiation, there are still great difficulties in accepting the effect as real: such an independent component would have to be due to a neutral particle in order to account for its arrival in a preferred direction and thus to have escaped the diffusion process. At the latitude of Leeds (53.8° N) and at 21.5 h the apparatus faces along a direction near that of the spiral arm of the galaxy. One can see that a neutron of 10^{16} eV, though not any known particle of shorter lifetime, could have a range comparable with galactic distances, but an attempt to connect the effect with the existance of neutrons leads to further implications which are difficult to reconcile.

A strong directional effect implies that if neutrons arose by a charge-exchange of protons after acceleration, this must take place in the neighbourhood of sources rather than after complete diffusion of the protons. Since some concentration of matter is essential for an exchange process, this is in a sense satisfactory, but the implicationt that the maximum intensity should be observed in the direction of maximum concentration of sources does not fit with the observed direction. A further difficulty which still remains is how such a neutron could give rise to effects which are experimentally distinguishable from the main EAS.

All these considerations, therefore, lead us to the conclusion that the reality of the effect remains doubtful in spite of its statistical weight. Certainly, our investigation does not confirm the existence of large time variations as reported by McCUSKER in the case of the total flux of cosmic ray air showers. We are continuing our experiments to examine the small component of cosmic ray showers characterized by high multiplicity under lead.

---

(6) K. GREISEN: *Progr. in Cosmic Ray Phys.* (ed. J. G. WILSON), vol. 3 (Amsterdam 1956), p. 124-125.

(7) W. GALBRAITH: *Extensive Air Showers* (London, 1958), p. 162-163.

* * *

The authors are indebted to Professor E. C. STONER for the facilities provided, and to Professor J. G. WILSON for valuable discussions. M.S.I. wishes to thank the University of Leeds for a grant from the Ackroyd Rund.

RIASSUNTO (*)

Si è fatto un tentativo di riprodurre alcuni risultati ottenuti da McCusker e collaboratori che hanno descritto effetti diurni degli sciami di raggi cosmici. La struttura dell'apparecchio segue da vicino quello di questi autori, ma permette di ottenere informazioni più dettagliate su ciascun evento registrato. Le principali categorie di eventi osservati, comprese quelle esaminate da McCusker *et al.*, non presentano significative variazioni diurne. Una possibile variazione diurna siderea di un particolare gruppo di eventi viene esaminata criticamente, e si conclude che, malgrado il forte peso statistico, le implicazioni derivanti dall'accettare la variazione come fisicamente reale non permettono che essa sia considerata tale.

(*) *Traduzione a cura della Redazione.*

Radio-Frequency Discharges in Magnetic Fields.

F. Bisi and B. De Michelis

Istituto di Fisica del Politecnico - Milano

(ricevuto il 14 Aprile 1960)

Summary. — Measurements on radio-frequency discharges in argon have been performed by using a magnetic field normal to the r.f. electric field. The power absorbed by the discharge has been determined as a function of the pressure inside the chamber and the magnetic fields: different curves have been obtained by increasing or decreasing the pressure. Different geometrical arrangements have been used. The qualitative behaviour of the discharge has been interpreted by using an average electron picture.

1. – Introduction.

Many experiments have been made on electrical discharges in a.c. fields. In the last few years some results on r.f. discharges in magnetic fields have been reported and discussed [1-3]. The essential features of the processes involved are sufficiently known and numerical data can be obtained in some simple configurations by applying the Boltzmann theory that takes into account the electron energy distribution inside the discharge. However due to the large number of discharge parameters involved, some processes have not been adequately studied.

In our measurements we used a magnetic field normal to the r.f. electric field. This arrangement is responsible for some of the observed phenomena, namely the appearance of a high intensity discharge at low pressure, because the electron oscillation amplitude in the direction of the electric field is strongly constricted. We have used different geometrical arrangements of the electrodes.

[1] S. C. Brown: *Basic Data of Plasma Physics* (London, 1959).

[2] L. Goldstein in: *Electronics and Electron Physics*, 7, 399 (1955).

[3] S. C. Brown in: *Rend. del III Congresso Internazionale sui fenomeni di ionizzazione nei gas* (Venezia, 1957), p. 169.

Some preliminary measurements were made on a discharge between parallel plates, so as to have the advantage of a simpler configuration and a better analytical elaboration of the obtained data, but the large drift velocity of the electrons in the direction normal to both electric and magnetic fields prevents the high intensity discharge at low pressure. The phenomenon is encountered in discharge between coaxial cylinders: we have used two different sizes of internal electrode. The results obtained with the smaller electrode are the most significant and most measurements were made in this configuration. We have also studied the discharge with a larger internal electrode, so to approach the condition for a constant electric field, as postulated in the development of the theory. The results are in agreement with the theory, but due to reduced dimensions, only a few discharge states are present. With radial configuration and smaller internal electrode, the discharge shows a different behavior for curves obtained by increasing or decreasing the pressure: in the latter case the experiments do not only show the maintenance of discharge at lower pressure than that of threshold, but also the appearance of new states of discharge not observed when pressure was increased. Using an average electron picture a qualitative interpretation of phenomena is given [1-4].

2. – Apparatus.

Our measurements have been performed in a discharge chamber as in Fig. 1. The discharge was excited inside the cylindrical tube of pyrex by the r.f. field

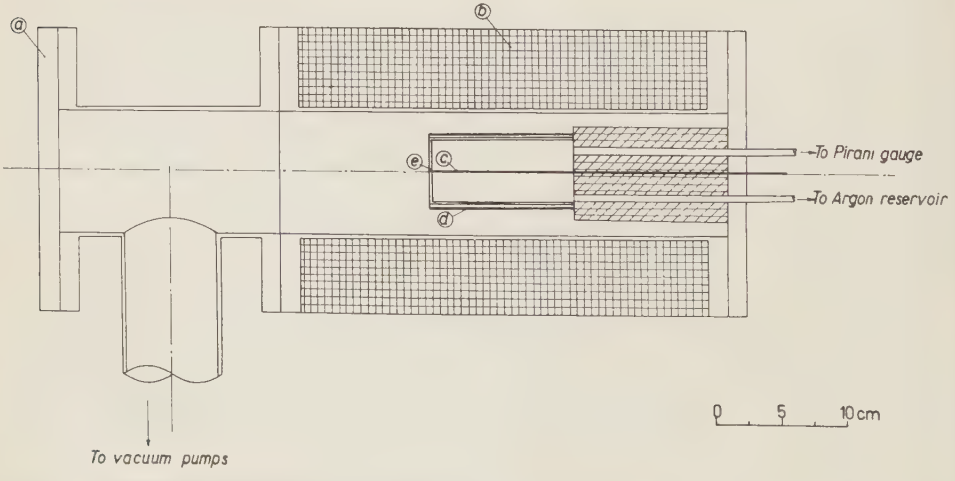

Fig. 1. – Discharge chamber: *a*) plexiglass window; *b*) coils; *c*) axial graphite electrode; *d*) steel mesh; *e*) pirex cylinder.

[4] B. LASE, W. P. ALLIS and S. C. BROWN: *Journ. Appl. Phys.*, **21**, 1297 (1950).

applied between the axial internal electrode of graphite and a steel mesh around the cylinder: the direction of the magnetic field was the same as the axis of the cylinder. The gas used (argon at 99.9%) was introduced by a needle valve and the pressure was read on a Pirani gauge: measurements were made in the pressure range between 1 and 500 μm Hg.

The principal geometric and electric data are reported in Table I.

TABLE I.

Chamber length	120 mm
Chamber diameter	50 mm
Diameter of internal electrode: small.	2 mm
large.	34 mm
Electric field frequency	1 MHz
Oscillator power	100 W
Output voltage	500 V
Maximum magnetic induction	600 G

3. – Results.

In Figs. 2 and 3 are reported the results of our experiments. The power absorbed by the discharge was determined by measuring the variation of the oscillator plate current as a function of the pressure inside the chamber. The voltage between the electrodes, measured by an electronic voltmeter, did not change greatly during the measurements: the small variations were compensated by means of a 1 000 pF capacitance inserted in the discharge circuit. In every position the oscillator was syntonized. The

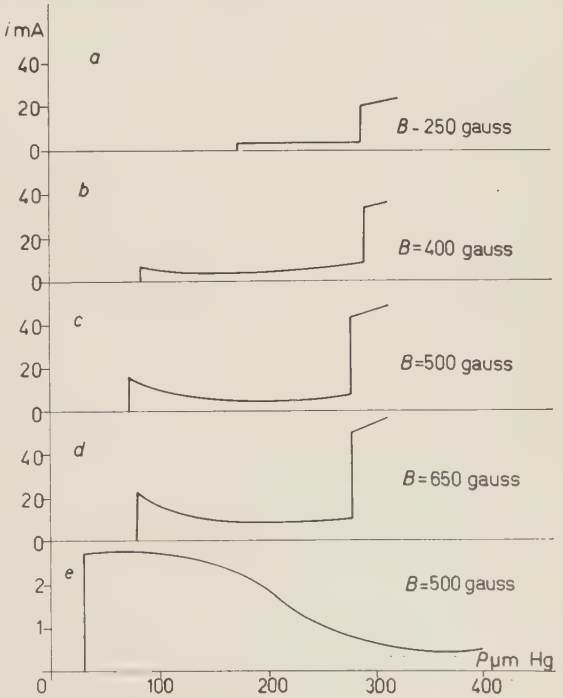

Fig. 2. – Plate current increase as a function of the pressure for different magnetic fields. The curves were obtained by increasing the pressure. In curves *a*), *b*), *c*) and *d*, the small electrode was used; in curve *e*) the large electrode was used.

curves in Figs. 2 and 3 are reported for different values of the magnetic field and were obtained respectively by increasing (Fig. 2)or by decreasing (Fig. 3) the pressure; a small internal electrode was used.

a) *Small electrode-increasing pressure* (Fig. 2). – At magnetic fields under 300 gauss, the curves show two different states of the discharges; a low intensity discharge excited at low pressure is suddenly changed, at higher pressure, into a high intensity discharge, the absorbed power increasing to a higher level. The variation is also visible due to a sharp increase in brigthness.

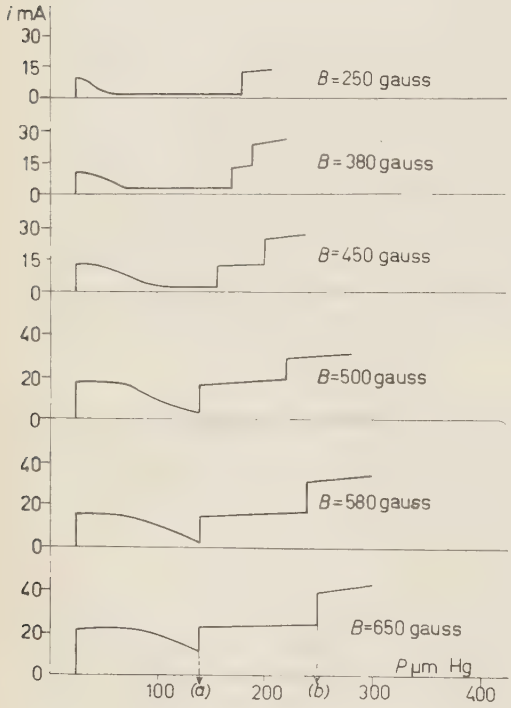

Fig. 3. – Plate current increase as a function of the pressure for different magnetic fields. The small electrode was used. The curves were obtained by decreasing the pressure.

At higher magnetic field the threshold pressure is lower and the initial discharge appears as a high intensity process; however the intensity decreases sharply and a low intensity discharge is maintained at higher pressure. By increasing the pressure, a new threshold is found for a high intensity discharge. The threshold pressure of the first state seems to be indipendent from the value of the magnetic field.

In the high magnetic field curves the initial discharge, displaying a peak, was always preceded by a very low intensity discharge excited at pressures well below the peak threshold. This discharge state, not shown in Fig. 2, is visible as a feeble violet discharge and the correspondent plate current increase of the oscillator is quite negligible. At low magnetic fields the very low intensity discharge disappears.

The data are not well reproducible; the general behavior of the curves does not change, but the values of the threshold pressures can vary with discharge conditions. In particular when the pressure of the residual gas exceeds 10^{-1} mm Hg, it seems to modify the value of minimum pressures required to excite the different states of discharge and to favour the appearance of the very low intensity discharge.

b) *Small electrode-decreasing pressure* (Fig. 3). – In the curve of Fig. 3 the discharge is studied by slowly decreasing pressure. At high magnetic fields a new state of discharge appears and the high pressure, high intensity discharge decreases to the low intensity region by two steps. The high intensity, low pressure region is still visible and the quenching of the discharge is displaced towards lower pressures. At lower magnetic fields the high intensity, low pressure-discharge is observed over a more restricted region and only three states of discharge are present throughout the pressure range.

c) *Large electrode* (Fig. 2*e*). – The results are reported for a magnetic induction of 500 gauss: the curves obtained by increasing or decreasing pressure are quite similar. A net increase of the plate current at low pressure is well visible: then the discharge decreases and no other states are visible in the studied pressure range. Different values of magnetic induction do not change the process: under 300 gauss the discharge is no longer observed.

d) *parallel plates.* – Some measurements were made for a discharge between parallel plates in a gap of 12 mm. A discharge was observed only well above 500 μm Hg: the discharge is not characterized by a high intensity initial state.

4. – Discussion.

A detailed description of the diffusion controlled breakdown and the phenomena accompanying low pressure discharges can be given only by taking into account the electron energy distribution. A physical interpretation of the controlling mechanism can be given more simply by referring to a simple representative electron: however the results are not valuable for the determination of the threshold pressures, because the radial electric field causes a strong asymmetry in the electron energy distribution.

a) *Diffusion processes.* – To describe the breakdown some fundamental variables must be considered, the electric field intensity E, the ionization potential V_i, the diffusion length Λ describing the discharge chamber, the angular frequency ω of the exciting field and the pressure p ([5]).

The simplest breakdown condition is the balance between the loss of electrons by diffusion to the walls and the ionization rate. If the average energy an electron gains in a mean free path λ is u_c, the total energy gain before reaching, the wall, in absence of anelastic collisions, is $u_c(3\Lambda^2/\lambda^2)$.

([5]) S. C. Brown and A. D. MacDonald: *Phys. Rev.*, **76**, 1629 (1949).

The balance condition requires that before the electron strikes the wall it must gain the energy required for ionization:

$$\gamma u_c \frac{3\Lambda^2}{\lambda^2} = eV_i \,. \tag{1}$$

The factor γ, less than one, takes into account the fact that electrons can lose energy in collisions by excitation or processes other than ionization. The energy u_c, depending on collision frequency ν, can be obtained through the kinetic theory and is given by:

$$u_c = \frac{e^2E^2}{m(\nu^2 + \omega_b^2)}$$

when a magnetic field B is present and $\omega \ll \omega_b = eB/m$.

Λ can be calculated from the diffusion equation

$$D\nabla N(r, z) + \nu_i N(r, z) = 0 \,,$$

where D is the diffusion coefficient for electrons, N is the electron density depending on the radial and the axial variables, r and z, and ν_i is the net production rate per electron. By imposing the condition that $N = 0$ on the walls of the discharge chamber, the expression for Λ results the sum of two terms, corresponding to diffusion lengths $\Lambda_\perp$ and $\Lambda_\parallel$ in radial and axial direction:

$$\frac{1}{\Lambda^2} = \frac{1}{\Lambda_\perp^2} + \frac{1}{\Lambda_\parallel^2} \,.$$

In our calculations we used a mean value of the field E: we think that the error introduced by this approximation does not modify the validity of the qualitative conclusions.

Under these conditions the radial solution of the diffusion equation is

$$N(r) = c_1 J_0\left(\frac{r}{\Lambda_\perp}\right) + c_2 Y_0\left(\frac{r}{\Lambda_\perp}\right),$$

where J_0 and Y_0 are the zero Bessel functions of first and second kind. The application of boundary conditions allows a numerical evaluation of Λ, which for our vessel results to be:

$$\Lambda_\perp \sim 0.6 \text{ cm} \quad \text{small internal electrode} \,,$$

$$\Lambda_\perp \sim 0.2 \text{ cm} \quad \text{large internal electrode} \,.$$

The axial solution of equation is

$$N(z) = C \cos\left(\frac{z}{\Lambda_\parallel}\right).$$

The buoundary cindition gives $\Lambda_\parallel = 3.8$ cm.

The presence of a magnetic field in the axial direction strongly reduces the radial diffusion of electrons: the effect can be evaluated by using a diffusion length Λ_b corrected by the presence of the magnetic field so that

$$\frac{1}{\Lambda_b^2} = \frac{\nu^2}{\nu^2 + \omega_b^2}\frac{1}{\Lambda_\perp} + \frac{1}{\Lambda_\parallel^2}.$$

The validity of the diffusion theory is assured when the mean free path is shorter than the diffusion length: therefore equation (1) gives the breakdown equilibrium only wen $\lambda < \Lambda$.

In Fig. 4 and 5 $l = \sqrt{e V_i \lambda^2 / 3\gamma u_c}$, Λ_b and λ_i, the ionization mean free path, are reported as functions of pressure p for two different values of the magnetic

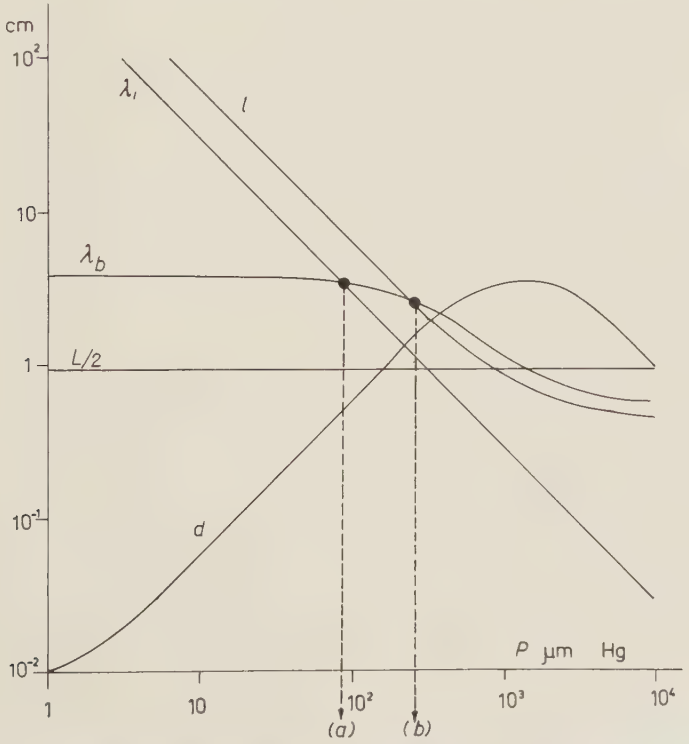

Fig. 4. – l, λ_i, Λ_b, $L/2$ and d as a function of the pressure for $B = 500$ G. Small electrode.

field $B = 250$ gauss and $B = 500$ gauss, assuming a mean diffusion velocity of electrons $w = 3 \cdot 10^8$ cm/s, corresponding to an energy of about 25 eV, and $\gamma = 0.02$.

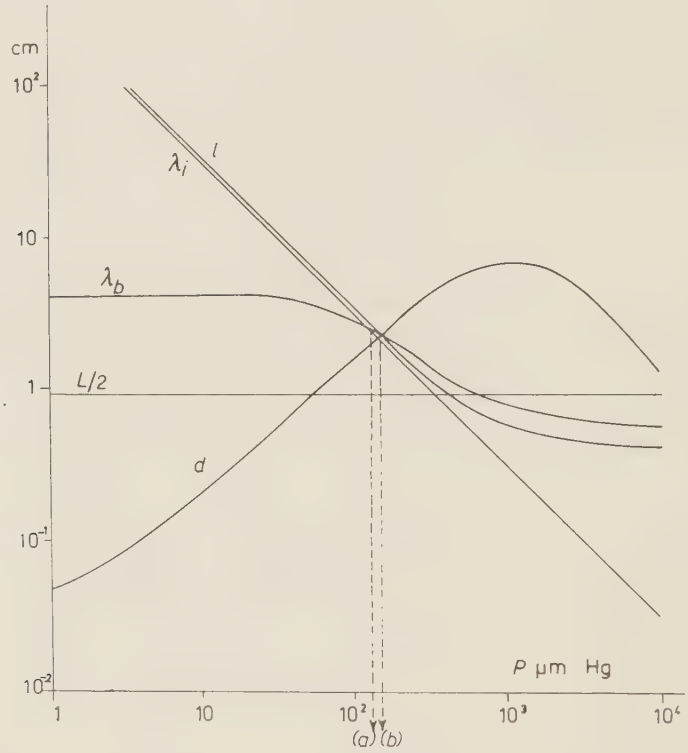

Fig. 5. – l, λ_i, Λ_b, $L/2$ and d as a function of the pressure for $B = 250$ G. Small electrode.

The values of γ and w are only representative and have been chosen in a range of reasonable values so as to have a rough agreement with experimental data: however the values of both w and γ can vary in a fairly large range of values without compromising the validity of the qualitative interpretation of the phenomena. In particular, the mean electron energy used in calculations is largely superior to the effective mean energy of electrons in the discharge; such an approximation is justified by the fact that, due to the presence of a radial electric field, the discharge starts along the axis where the electric field is maximum and is mainly maintained by the contribution of the more energetic axial electrons.

In Fig. 6 are reported the same quantities as in Fig. 4 and 5 for the discharge chamber with the large internal electrode, at $B = 500$ gauss.

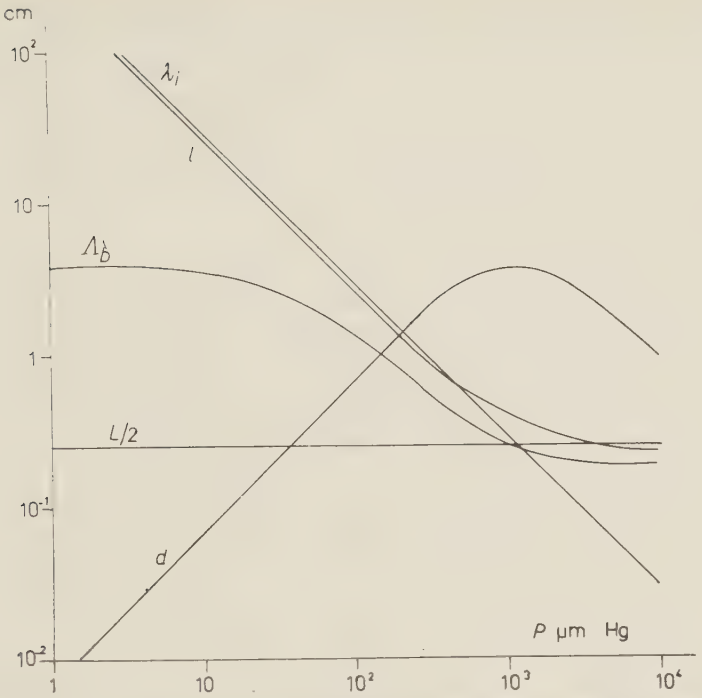

Fig. 6. – l, λ_i, Λ_b, $L/2$ and d as a function of the pressure for $B = 500$ G. Large electrode.

b) *Oscillation amplitude limit.* – When the amplitude of the electron oscillation in the electric field is sufficiently high the electrons can travel across the chamber and be lost at the walls. As a limiting case, all the electrons will hit the walls when the oscillation amplitude is equal to one half of the electrode separation length: at this limit the electron loss to the walls is greatly increased.

The motion equation of an electron in a plane normal to the z axis is:

$$m\frac{\mathrm{d}\boldsymbol{v}}{\mathrm{d}t}(r,\theta) + \nu m\boldsymbol{v}(r,\theta) = -e\boldsymbol{E}(r) - e\left[\boldsymbol{v}(r,\theta)\wedge\boldsymbol{B}\right].$$

In the approximation $E = \text{const}$ and $\omega_b \ll v_0/r$ well verified for magnetic fields higher than 200 gauss, the radial solution of motion equations, for an electron of initial co-ordinates $r = r_0$, $\theta = \theta_0$ is:

$$r = \frac{e^{-\nu t}}{\nu^2+\omega_b^2}\left[C_1(\omega_b \sin\omega_b t - \nu\cos\omega_b t) + (C_2(\omega_b\cos\omega_b t + \nu\sin\omega_b t)\right] +$$
$$+ \frac{(A\omega + B\nu)}{\omega\omega_b}\sin\omega t + \frac{(B\omega - A\nu)}{\omega\omega_b}\cos\omega t + \frac{A\nu - B\omega}{\omega\omega_b} + \frac{C_1\nu - C_2\omega_b}{\nu^2+\omega_b^2} + r_0,$$

where A and B are constants depending on discharge parameters and C_1 and C_2 are evaluated by the initial conditions $v_r = 0$ and $v_\theta = 0$ for $t = 0$.

Omitting the transitory solution, unimportant for $\omega \ll \omega_b$, the oscillation amplitude is:

$$d = \frac{eE}{m\omega} \sqrt{\frac{\nu^2 + \omega^2}{4\nu^2\omega^2 + (\nu^2 + \omega_b^2 - \omega^2)^2}} \tag{2}$$

and has a maximum for $\nu = \omega_b$.

In Fig. 4, 5 and 6 d is reported as a function of p in the same conditions as above; half of the interelectrode length, $L/2$, is also reported.

The physical significance of the oscillation amplitude curves is clear by calculating the path of electrons in crossed magnetic and electric fields. In a plane normal to the z axis the trajectories at low pressure are circles with center on the z axis. When the pressure is increased, the collisions create a radial component of velocity and decrease the tangential drift velocity; the trajectories then become spirals. As pressure increases, the electrons cannot do a complete circuitation at high pressure, the motion is almost rectified; the length of oscillation decreases and the effect of the magnetic field is negligible.

c) Interpretation of the experimental curves. – From the curves in Fig. 4, 5 and 6 a qualitative interpretation of the experimental curves can be tried. It must be noted that only a rough interpretation can be given for three reasons, at least: 1) the negligibility of the true electron energy distribution; 2) the approximation used in the expression of the radial electric field; 3) the uncertainty about the form of the electric field in the plasma that affects the calculation of the thresholds of the different states when the discharge is present.

A net difference can be seen in the experimental curves obtained with the small internal electrode by increasing or decreasing the pressure: in the latter case new states of the discharge can be found. In general a low intensity discharge seems to be maintained in states normally unstable, when it follows a high intensity discharge: the phenomenon is probably due to the contribution of secondary electrons emitted from hot electrodes.

α) Small electrode-increasing pressure. – For magnetic fields strong enough to bend the path of the electrons bringing them to hit the axial electrode, a discharge, probably maintained by a secondary electron resonance process ([6]), can be excited at low pressures, as shown in Fig. 2. The discharge intensity is high because the oscillation amplitude is shorter than the chamber dimensions and the loss of electrons to the walls is strongly reduced.

By increasing the pressure the discharge intensity decreases, because the

([6]) E. W. GILL and A. VON ENGEL: *Proc. Roy. Soc.*, A **169**, 446 (1948).

breakdown resonance conditions are no more satisfied, the loss of electrons to the walls is higher and is not balanced by ionization inside the gas. However, the discharge is maintained probably by electrons extracted from the walls; the internal graphite electrode is heated to a bright red, during the discharge. When the loss of electrons is balanced by ionization in the gas, a high intensity discharge is again excited at pressures corresponding to breakdown diffusion threshold (at $l = \Lambda_b$).

β) Small electrode-increasing pressure. – In the curves of Fig. 3 the high intensity discharged at high pressure decreases abruptly at b) when the diffusion equilibrium is no more maintained. The discharge remains in an excited state until the ionization mean free path becomes longer than diffusion length: under this threshold a) another sharp decrease in intensity allows the maintenance only of a low intensity discharge. A new high intensity discharge is present at lower pressure when the oscillation amplitude becomes shorter than chamber dimensions and a resonance breakdown mechanism is possible; the loss of electrons is also strongly reduced.

An interesting feature of the experimental curves is the behaviour of the two thresholds, indicated as (a) and (b) in Fig. 3, when the magnetic field is varied: the values of such thresholds cannot be obtain by the average electron theory developed above, but the behaviour can be qualitatively explained.

From the curves in Fig. 5 and 6 it can be seen that the threshold (a) varies between two values, given by the intersection of λ_i with the asymptotic values of Λ_b and reaches a constant value for high magnetic fields. The threshold (b) represented by the intersection of l with Λ_b increases with the magnetic field, at least in the studied region: by lowering the magnetic field the two thresholds become identical and one state of discharge is observed. These conclusions are in agreement with the results.

The first state, in the resonance breakdown region, shows a constant quenching pressure and covers a large pressure range at increasing magnetic field. This last result can be justified, as is shown from eq. (2), by the fact that, due to reduced electron diffusion at high magnetic fields, the intersection between oscillation amplitude and interelectrode distance $L/2$ moves towards higher pressures.

γ) Large electrode. – A high intensity, low pressure discharge can be observed, the oscillation amplitude being shorter than the interelectrode distance: a second state of discharge with a sharp threshold is not visible for pressures below 1 mm Hg, because, as shown in Fig. 6, there is no intersection between Λ_b and l and no diffusion equilibrium can be reached. No metastable state of the discharge in the decreasing pressure curves can be observed, because these are possible only when the metastable state follows a higher intensity stable state.

δ) Parallel plates. – No high intensity-low pressure states were observed. In this geometrical arrangement the electron drift velocity, normal to both the electric and the magnetic field, is directed towards the walls of the discharge camber and causes a high electron loss.

The drift velocity v_d is much greater than the velocity in the direction of the electric field, at least in high magnetic fields: $v_d/v = \omega_b/\omega$.

So the electron motion in the drift direction becomes important in discharge processes that are related mainly to its characteristics. The oscillation amplitude of the drift motion is much greater than the chamber dimensions at low pressure: as a function of the pressure it does not shown a maximum but decrease continuosly. These conclusions explain the absence of the phenomena observed in other geometrical arrangements.

* * *

Thanks are due to Prof. G. Bolla and Prof. E. Gatti for their kind interest and helpful criticism.

RIASSUNTO

Sono state studiate scariche a radio-frequenza in argon, usando campi elettrici e magnetici perpendicolari fra loro. La potenza assorbita dalla scarica è stata determinata in funzione della pressione e del campo magnetico. Le curve ottenute aumentando o diminuendo la pressione presentano un diverso andamento: la scarica è stata studiata in diverse disposizioni degli elettrodi. I diversi stati di scarica osservati sono stati qualitativamente interpretati riferendosi al comportamento medio di un elettrone nella scarica.

IL NUOVO CIMENTO Vol. XVII, N. 3 1° Agosto 1960

An Analysis of Infrared Divergences.

E. R. Caianiello and S. Okubo (*)

Istituto di Fisica Teorica dell'Università - Napoli
Istituto Nazionale di Fisica Nucleare - Sottosezione di Napoli

(ricevuto il 15 Aprile 1960)

Summary. — A concise and rigorous treatment is given of the infrared divergences of quantum electrodynamics, by using a technique previously developed in connection with ultraviolet renormalization. The result is essentially equivalent to an extension of the classical Bloch-Nordsieck formula, and is independent of perturbative methods.

1. – Introduction.

The present investigation is intended to provide a concise and rigorous proof, with methods recently developed by one of us [1], of very plausible statements made on the problem of infrared divergences by several authors [2,3] on the basis of the traditional analysis of graphs. It may serve, therefore, also as a test of the effectiveness of different techniques in questions of this nature.

As is well known, unlike the ultraviolet divergences which are caused by short-range effects, the infrared divergences originate from the long-range

(*) This work was done in part at the Ecole Normale Supérieure, Paris. The authors express their warm thanks to Prof. M. Lévy for the kind hospitality they enjoyed there.

« The research reported in this document has been sponsored in part by the Office Chief of Research and Development, U. S. Department of the Army, through its European Office under contract no. DA-91-591-EUC-1096 ».

(1) E. R. Caianiello: *Nuovo Cimento*, **13**, 637 (1959); **14**, 185 (1959).

(2) J. M. Jauch and F. Rohrlich: *Helv. Phys. Acta*, **27**, 613 (1954) and *Theory of Photons and Electrons* (Cambridge, Mass. 1955), pp. 390-405.

(3) D. R. Yennie and H. Suura: *Phys. Rev.*, **105**, 1378 (1957).

interactions among fields; one may say, in the usual phraseology, that the first are related to the innermost, the latter to the outermost part of the structure of the electron. It was shown recently (1) that ultraviolet divergences may be conveniently removed if the ordinary notion of integral is modified in a suitable way (provided the theory is « renormalizable »). We propose to show here that a similar approach permits to take care also of the infrared divergences, although the problem for them is not to remove, but rather to factor out of a matrix element the divergent contributions, so as to achieve an appropriate generalization of the classical results of BLOCH and NORDSIECK (4); our work is thus similar in scope to that by YENNIE and SUURA (3).

We restrict our considerations to the case of electron-electron scattering, with the explicit exclusion of forward scattering; this will suffice, since the generalization to all possible cases is immediate and does not involve, with our method, any complication of the calculations presented here. Reference is made, for notation and results, to the works quoted in Ref. (1), which were primarily concerned with the removal of ultraviolet divergences; since, however, the present problem is very much simpler than the ones treated there, we have tried to render the present work as independent as possible from those referred to, by limiting our quotations to a few preliminary formulae and repeating for the rest the considerations which are relevant for our present purposes. For the same reason, we consider only perturbative expansions and use equations among matrix elements only as short-hand for relations among their expanded forms; this is irrelevant for the final result and expedites our proofs.

The reader will remark that there is in principle no interference between ultraviolet and infrared divergences, except for photon self-energies; only for the latter, indeed, can a continuous chain of short-range vacuum polarizations have an overall long-range effect in our problem. As we deal with a theory which is already freed from ultraviolet infinities by renormalization, any such interference is taken automatically into account by our treatment.

2. – Infrared divergences.

We consider the matrix element for non-forward scattering of two electrons with initial momenta q_1 and q_2 and final momenta p_1 and p_2.

It is given by (5)

$$(1)\qquad M\begin{pmatrix}\overset{\circ}{p}_1 & \overset{\circ}{p}_2\\ \overset{\circ}{q}_1 & \overset{\circ}{q}_2\end{pmatrix} - \sum_{n=0}^{\infty}\frac{\lambda^{2n}}{(2n)!}\int \mathrm{d}\xi_1 \dots \int \mathrm{d}\xi_{2n} \sum \gamma^1 \dots \gamma^{2n} \begin{pmatrix}\overset{\circ}{p}_1 \overset{\circ}{p}_2 & \xi_1 \dots \xi_{2n}\\ \overset{\circ}{q}_1 \overset{\circ}{q}_2 & \xi_1 \dots \xi_{2n}\end{pmatrix} [\xi_1 \dots \xi_{2n}]\,,$$

(4) F. BLOCH and A. NORDSIECK: *Phys. Rev.*, **52**, 54 (1937).

with:

$$(\mathring{p}\,\xi) = \overline{u}_p(\xi)\,; \qquad (\xi\,\mathring{q}) = u_q(\xi)\,; \qquad (\mathring{p}\,\mathring{q}) = 0\,, \tag{2}$$

where $u_q(\xi)$ denotes the wave function of the electron of momentum q.

Ultraviolet renormalization amounts to changing the integrals $\int$ in (1) with a new operation, denoted with the symbol $\overline{\int}$ in Ref. [1]; this was proved in all generality in that work and will be the object of a specific study for electrodynamics in a forthcoming paper. In order to avoid any possible confusion, however, we shall retain here the old integral symbol in (1) and in its consequences; the considerations that follow must be understood, though, as performed with the operations $\overline{\int}$ throughout, and with renormalized values of the parameters λ (charge), etc.

The λ-derivative equation for kernels [5] yields immediately, because of (2):

$$\frac{\mathrm{d}}{\mathrm{d}(\lambda^2/2)}\, M\begin{pmatrix}\mathring{p}_1\,\mathring{p}_2\\ \mathring{q}_1\,\mathring{q}_2\end{pmatrix} = \int \mathrm{d}\xi_1 \int \mathrm{d}\xi_2 \sum \gamma^1\,\gamma^2\,[\xi_1,\xi_2]\, M\begin{pmatrix}\mathring{p}_1\,\mathring{p}_2\,\xi_1\,\xi_2\\ \mathring{q}_1\,\mathring{q}_2\,\xi_1\,\xi_2\end{pmatrix}. \tag{3}$$

The integration $\int \mathrm{d}\xi_1 \int \mathrm{d}\xi_2$ gives infrared divergences whenever ξ_1, ξ_2 are in positions such that:

a) a pair p_1, p_2, or q_1, q_2, is directly connected with ξ_1, ξ_2;

b) a pair p, q is directly connected with ξ_1, ξ_2;

c) one momentum state p or q is connected to itself by ξ_1 or ξ_2 through an ultraviolet self-energy part.

Typical instances of these situations are shown in Fig. 1, to which all those those resulting from the appropriate symmetrizations must be added. *c*) shows the interference of ultraviolet with infrared divergences, which is however taken care of automatically by the use of $\overline{\int}$ ($\equiv$ our $\int$).

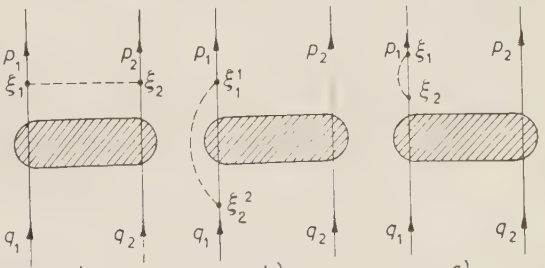

Fig. 1.

In analogy with the nomenclature established in (1) we say that there is a *confluence* of the pair ξ_1, ξ_2, with p_1, p_2, etc., whenever we find factors in the integrand of (3) of the form $(p_1\xi_1)\cdot(p_2\xi_2)\cdot[\xi_1\xi_2]$, etc. The preceding considerations have merely the purpose of illustrating in a familiar language the instances in which such confluences lead to infinite results; in all other cases one obtains finite results.

[5] E. R. Caianiello: *Nuovo Cimento*, **11**, 220 (1954).

We neglect all other integrations which are contained in the perturbative expansion of (3) and decompose $\int d\xi_1 \int d\xi_2$ as follows:

$$\int d\xi_1 \int d\xi_2 f(\xi_1, \xi_2, \ldots) = \hat{\int} d\xi_1 \hat{\int} d\xi_2 f(\xi_1, \xi_2, \ldots) + \hat{D}^{12}(\xi_1, \xi_2, \ldots) \tag{4}$$

$\hat{\int} d\xi_1 \hat{\int} d\xi_2 f$ in (4) will be such that it coincides with $\int d\xi_1 \int d\xi_2 f$ whenever the latter is convergent (and then $\hat{D}^{12} f \equiv 0$); it will stay finite, however, if $\int d\xi_1 \int d\xi_2 f$ is divergent, the divergent part being given by $\hat{D}^{12}$. Since we work with a renormalized theory, there are no other infinities to worry about; it is interesting to remark that for non renormalized, and therefore for all non-renormalizable theories, this treatment of infrared divergences may break down, as will be seen from the fact that all divergent contributions in which λ is the *renormalized* coupling constant are factored out by it as an exponential factor $\exp[-(\lambda^2/2)I]$.

$\hat{\int} d\xi_1 \hat{\int} d\xi_2$ is still far from being uniquely defined at this stage, nor do we wish to discuss here the optimum way to define it for practical purposes. We prefer to take advantage of the fact that our considerations apply as well to perturbative expansions, which permits to use in (4) a definition which agrees entirely with the standard procedure. The comparison of the results obtained by our method with those of the other authors will then be immediate.

With $\int d\xi_1 \int d\xi_2$ we find in (3) always the integrand factor:

$$[\xi_1 \xi_2] = \frac{-i}{(2\pi)^4} \delta_{\mu_1 \mu_2} \int d^4k \, \frac{1}{k^2 - i\varepsilon} \exp[ik(\xi_1 - \xi_2)] : \tag{5}$$

we define

$$\hat{\int} d\xi_1 \hat{\int} d\xi_2 \, \gamma^1 \gamma^2 [\xi_1 \xi_2] g(\xi_1, \xi_2, \ldots) = \lim_{\varrho \to 0} \int d\xi_1 \int d\xi_2 \cdot \tag{6}$$

$$\cdot \gamma^1 \gamma^2 \left\{ -\frac{i}{(2\pi)^4} \delta_{\mu_1 \mu_2} \left[\int_{k > K} d^4k \, \frac{1}{k^2 - i\varepsilon} \exp[ik(\xi_1 - \xi_2)] + \right. \right.$$

$$\left. \left. + \int_{k \gtrless K} d^4k \, \frac{1}{k^2 - i\varepsilon} \left(\exp[ik(\xi_1 - \xi_2)] - \varrho^2 \exp[i\varrho k(\xi_1 - \xi_2)] \right) \right] \right\} g(\xi_1, \xi_2, \ldots) ,$$

$$\hat{D}^{12} \gamma^1 \gamma^2 [\xi_1, \xi_2] g(\xi_1, \xi_2, \ldots) = \lim_{\varrho \to 0} \int d\xi_1 \cdot \int d\xi_2 \cdot \tag{7}$$

$$\cdot \gamma^1 \gamma^2 \cdot \left\{ -\frac{i}{(2\pi)^4} \delta_{\mu_1 \mu_2} \cdot \varrho^2 \cdot \int_{|k| < K} d^4k \, \frac{1}{k^2 - i\varepsilon} \exp[i\varrho k(\xi_1 - \xi_2)] \right\} g(\xi_1, \xi_2, \ldots) ,$$

where K is an arbitrary positive cut-off which is taken to be sufficiently small in the next section.

Elementary computations prove that the def. (6), (7) satisfies all the wanted requirements (6): the new symbol $\int\!\!\!\!\!\!-$ differs from the old one $\int$: $\int\!\!\!\!\!\!-$ only when there are infrared divergences, which are set apart in (8).

We find:

$$(8)\qquad \frac{\mathrm{d}}{\mathrm{d}(\lambda^2/2)} M\begin{pmatrix} \mathring{p}_1 \mathring{p}_2 \\ \mathring{q}_1 \mathring{q}_2 \end{pmatrix} = \int\!\!\!\!\!\!-\hat{\mathrm{d}}\xi_1 \int\!\!\!\!\!\!-\hat{\mathrm{d}}\xi_2 \gamma^1\gamma^2[\xi_1\xi_2] M\begin{pmatrix} \mathring{p}_1 \mathring{p}_2 \xi_1\xi_2 \\ \mathring{q}_1 \mathring{q}_2 \xi_1\xi_2 \end{pmatrix} + \\ + \hat{D}^{12}\gamma^1\gamma^2[\xi_1\xi_2] M\begin{pmatrix} \mathring{p}_1 \mathring{p}_2 \xi_1\xi_2 \\ \mathring{q}_1 \mathring{q}_2 \xi_1\xi_2 \end{pmatrix},$$

where the divergent term is computed explicitly from (1), (3) and (7), since the terms in the expansion of

$$\begin{pmatrix} \mathring{p}_1 \mathring{p}_2 & \xi_1 \dots \xi_{2n+2} \\ \mathring{q}_1 \mathring{q}_2 & \xi_1 \dots \xi_{2n+2} \end{pmatrix}$$

which give rise to infrared infinities such as a), b), c) of Fig. 1, can be easily studied one by one.

A straightforward calculation gives then (6):

$$(9)\qquad \hat{D}^{12}\gamma^1\gamma^2[\xi_1\xi_2] M\begin{pmatrix} \mathring{p}_1 \mathring{p}_2 \xi_1\xi_2 \\ \mathring{q}_1 \mathring{q}_2 \xi_1\xi_2 \end{pmatrix} = -I\cdot M\begin{pmatrix} \mathring{p}_1 \mathring{p}_2 \\ \mathring{q}_1 \mathring{q}_2 \end{pmatrix},$$

with

$$(10)\quad I \equiv J(p_1, p_2) + J(q_1, q_2) - J(p_1, q_1) - J(p_2, q_2) - J(p_1, q_2) - J(p_2, q_1) + \\ + \tfrac{1}{2}[J(p_1, p_1) + J(p_2, p_2) + J(q_1, q_1) + J(q_2, q_2)],$$

where

$$(11)\qquad J(p, q) = -\frac{2i}{(2\pi)^4}(p, q)\cdot \int_{|k|<K} \mathrm{d}^4k \,\frac{1}{k^2}\cdot\frac{1}{(p\cdot k)}\cdot\frac{1}{(q\cdot k)}\,.$$

---

(6) For example, in the case of the confluence of pair ξ_1 and ξ_2 with p_1 and p_2, we have

$$\hat{D}^{12}_{(p_1p_2)}\gamma^1\gamma^2[\xi_1\xi_2] M\begin{pmatrix} \mathring{p}_1\mathring{p}_2 \ \xi_1\xi_2 \\ \mathring{q}_1\mathring{q}_2 \ \xi_1\xi_2 \end{pmatrix} = \frac{+i}{(2\pi)^4}\,\overline{u}(p_1)\overline{u}(p_2)\gamma^1_\mu\cdot\gamma^2_\mu\cdot\lim_{\varrho\to 0}\varrho^2\int_{|k|<K}\mathrm{d}^4k\cdot\frac{1}{k^2}\cdot \\ \cdot\frac{i\gamma^1(p_1-\varrho k)-m}{(p_1-\varrho k)^2+m^2}\cdot\frac{i\gamma^2(p_2+\varrho k)-m}{(p_2+\varrho k)^2+m^2}\cdot\widetilde{M}\begin{pmatrix} p_1-\varrho k, & p_2+\varrho k \\ q_1\ , & q_2 \end{pmatrix} - -J(p_1, p_2)\cdot M\begin{pmatrix} \mathring{p}_1\mathring{p}_2 \\ \mathring{q}_1\mathring{q}_2 \end{pmatrix},$$

where $\widetilde{M}$ has he same structure as M except for the absence of the Dirac matrices, $\overline{u}(p_1)$ and $\overline{u}(p_2)$.

I is therefore given by

$$I = -\frac{i}{(2\pi)^4}\int_{|k|<K} \mathrm{d}^4k\,\frac{1}{k^2 - i\varepsilon}\,Q^2(k)\,, \tag{12}$$

with

$$Q(k) = \frac{p_1}{(p_1\cdot k)} + \frac{p_2}{(p_2\cdot k)} - \frac{q_1}{(q_1\cdot k)} - \frac{q_2}{(q_2\cdot k)}\,. \tag{13}$$

Exactly with the same arguments one would find, more generally:

$$\frac{\mathrm{d}}{\mathrm{d}(\lambda^2/2)}\,M\begin{pmatrix}\mathring{p}_1\,\mathring{p}_2 & x_1 \dots x_r\\ \mathring{q}_1\,\mathring{q}_2 & y_1 \dots y_r\end{pmatrix} = \hat{\int}\mathrm{d}\xi_1\hat{\int}\mathrm{d}\xi_2\;\gamma^1\gamma^2[\xi_1\xi_2]\cdot \tag{14}$$

$$\cdot\, M\begin{pmatrix}\mathring{p}_1\,\mathring{p}_2 & \xi_1\,\xi_2 & x_1 \dots x_r\\ \mathring{q}_1\,\mathring{q}_2 & \xi_1\,\xi_2 & y_1 \dots y_r\end{pmatrix} - I\cdot M\begin{pmatrix}\mathring{p}_1\,\mathring{p}_2 & x_1 \dots x_r\\ \mathring{q}_1\,\mathring{q}_2 & y_1 \dots y_r\end{pmatrix},$$

which is true also if $y_k \equiv x_k$.

3. – Factorization of divergent contributions.

We can regard the r.h.s. of (3) as the result of an operation Θ performed on $M\begin{pmatrix}\mathring{p}_1\,\mathring{p}_2\\ \mathring{q}_1\,\mathring{q}_2\end{pmatrix}$ and write

$$\frac{\mathrm{d}}{\mathrm{d}(\lambda^2/2)}\,M\begin{pmatrix}\mathring{p}_1\,\mathring{p}_2\\ \mathring{q}_1\,\mathring{q}_2\end{pmatrix} = \Theta\cdot M\begin{pmatrix}\mathring{p}_1\,\mathring{p}_2\\ \mathring{q}_1\,\mathring{q}_2\end{pmatrix}; \tag{15}$$

Θ could be easily written down explicitly by means of functional derivatives, but this is unnecessary here.

The decomposition (8) of Θ, which we may symbolically express with

$$\frac{\mathrm{d}}{\mathrm{d}(\lambda^2/2)}\,M\begin{pmatrix}\mathring{p}_1\,\mathring{p}_2\\ \mathring{q}_1\,\mathring{q}_2\end{pmatrix} = \hat{\Theta}\cdot M\begin{pmatrix}\mathring{p}_1\,\mathring{p}_2\\ \mathring{q}_1\,\mathring{q}_2\end{pmatrix} + \hat{D}\cdot M\begin{pmatrix}\mathring{p}_1\,\mathring{p}_2\\ \mathring{q}_1\,\mathring{q}_2\end{pmatrix}, \tag{16}$$

leads immediately, if we define

$$M_c\begin{pmatrix}\mathring{p}_1\,\mathring{p}_2\\ \mathring{q}_1\,\mathring{q}_2\end{pmatrix} = \exp\left[-\frac{\lambda^2}{2}\cdot\hat{D}\right]\cdot M\begin{pmatrix}\mathring{p}_1\,\mathring{p}_2\\ \mathring{q}_1\,\mathring{q}_2\end{pmatrix}, \tag{17}$$

to

$$\frac{\mathrm{d}}{\mathrm{d}(\lambda^2/2)} M_c\begin{pmatrix}\mathring{p}_1\,\mathring{p}_2\\ \mathring{q}_1\,\mathring{q}_2\end{pmatrix} - \left[\exp\left[\frac{\lambda^2}{2}\hat{D}\right]\Theta\exp\left[\frac{\lambda^2}{2}\hat{D}\right]\right]\cdot M_c\begin{pmatrix}\mathring{p}_1\,\mathring{p}_2\\ \mathring{q}_1\,\mathring{q}_2\end{pmatrix}, \tag{18}$$

or

$$\frac{\mathrm{d}}{\mathrm{d}(\lambda^2/2)} M_c\begin{pmatrix}\mathring{p}_1\,\mathring{p}_2\\ \mathring{q}_1\,\mathring{q}_2\end{pmatrix} = \hat{\int}\mathrm{d}\xi_1\hat{\int}\mathrm{d}\xi_2\gamma^1\gamma^2[\xi_1\xi_2]\, M_c\begin{pmatrix}\mathring{p}_1\,\mathring{p}_2 & \xi_1\,\xi_2\\ \mathring{q}_1\,\mathring{q}_2 & \xi_1\,\xi_2\end{pmatrix}, \tag{19}$$

if

$$\hat{\Theta}\hat{D}\cdot M = \hat{D}\cdot\hat{\Theta}\cdot M\,. \tag{20}$$

The relation (20) is certainly verified by our prescription (6), (7); it suffices to use (14) to calculate first $(\mathrm{d}/\mathrm{d}(\lambda^2/2))\,\hat{\Theta}\cdot M$ and then $\hat{\Theta}\cdot(\mathrm{d}/\mathrm{d}(\lambda^2/2))M$: (20) follows by equating the two expressions thus obtained, due to the symmetry properties of the integrands.

We conclude that the perturbative solution of (19), by iteration of $\hat{\int}\mathrm{d}\xi_1\hat{\int}\mathrm{d}\xi_2$ is entirely free from infrared divergences, and that the original matrix element is related to the one thus calculated by:

$$M\begin{pmatrix}\mathring{p}_1\,\mathring{p}_2\\ \mathring{q}_1\,\mathring{q}_2\end{pmatrix} = \exp\left[-\frac{\lambda^2}{2}\cdot I\right]\cdot M_c\begin{pmatrix}\mathring{p}_1\,\mathring{p}_2\\ \mathring{q}_1\,\mathring{q}_2\end{pmatrix}, \tag{21}$$

as a consequence of (9) and (17), with I given by (12). This proves that infrared divergences, computed with the prescription used here (which is the close counter-part of the one usually followed), can indeed by factored out in an exponential factor. This result is furthermore independent of perturbative methods, because entirely similar considerations can be made directly on the branching equations (1).

4. – Soft-photon emission.

It follows from (21) that the cross-section for the process is:

$$\sigma = \exp\left[-\lambda^2\cdot I\right]\cdot\sigma_c\,. \tag{22}$$

We must consider now the cross-section for the emission of n photons with

momenta $k_1, \ldots, k_n$ respectively. The corresponding matrix element is given by

$$M\left(\begin{matrix}\mathring{p}_1 \mathring{p}_2 \\ \mathring{q}_1 \mathring{q}_2\end{matrix}\middle| k_1 \ldots k_n\right) = \lambda^n \int \mathrm{d}\xi_1 \ldots \int \mathrm{d}\xi_n \sum \gamma^1 \ldots \gamma^n \bar{Z}_{k_1}(\xi_1) \ldots \bar{Z}_{k_n}(\xi_n) \cdot \cdot M\left(\begin{matrix}\mathring{p}_1 \mathring{p}_2 & \xi_1 \ldots \xi_{2n} \\ \mathring{q}_1 \mathring{q}_2 & \end{matrix}\right). \tag{23}$$

We are interested in the limit for vanishing $k_1 \ldots k_n$. Using the same terminology as before divergences with respect to ξ_1 when $k_1 \to 0$ may appear in the cross-section when ξ_1 has confluences with either of the external p_1, p_2, q_1 and q_2. We define, similarly,

$$\int \mathrm{d}\xi_1 = \hat{\int} \mathrm{d}\xi_1 + \hat{D}^1, \tag{24}$$

and neglect the finite contributions from $\hat{\int} \mathrm{d}\xi_1$. The remaining divergent part is easily calculated from (23) and (24), with considerations identical to those made previously, as

$$\frac{\lambda}{(2\pi)^{\frac{3}{2}}} \frac{1}{(2k_1^0)^{\frac{1}{2}}} \left[\frac{(p_1 \cdot \varepsilon_1)}{(p_1 \cdot k_1)} + \frac{(p_2 \cdot \varepsilon_1)}{(p_2 \cdot k_1)} - \frac{(q_1 \cdot \varepsilon_1)}{(q_1 \cdot k_1)} - \frac{(q_2 \cdot \varepsilon_1)}{(q_2 \cdot k_1)}\right] M\left(\begin{matrix}\mathring{p}_1 \mathring{p}_2 \\ \mathring{q}_1 \mathring{q}_2\end{matrix}\middle| k_2 \ldots k_n\right), \tag{25}$$

where ε_1 is the polarization vector of the photon k_1. By induction we find that the divergent part of (24) is given by:

$$\frac{\lambda^n}{(2\pi)^{3n/2}} \prod_{j=1}^{n} \frac{1}{(2k_j^0)^{\frac{1}{2}}} \cdot \left[\frac{(p_1 \cdot \varepsilon_j)}{(p_1 \cdot k_j)} + \frac{(p_2 \cdot \varepsilon_j)}{(p_2 \cdot k_j)} - \frac{(q_1 \cdot \varepsilon_j)}{(q_1 \cdot k_j)} - \frac{(q_2 \cdot \varepsilon_j)}{(q_2 \cdot k_j)}\right] \cdot M\left(\begin{matrix}\mathring{p}_1 \mathring{p}_2 \\ \mathring{q}_1 \mathring{q}_2\end{matrix}\right), \tag{26}$$

so that the cross-section for n soft-photon emission has a divergent part given by

$$\sigma_n = \frac{f^n}{n!} \exp\left[-\lambda^2 \cdot I\right] \cdot \sigma_c, \tag{27}$$

where

$$f = \frac{\lambda^2}{(2\pi)^3} \sum_{\text{pol.}} \int_{|\boldsymbol{k}|<K} \mathrm{d}^3\boldsymbol{k} \, \frac{1}{2k_0} (Q \cdot \varepsilon)^2, \tag{28}$$

with Q given by eq. (13). It is then easy to see that

$$f = \lambda^2 \cdot I \tag{29}$$

because, since $Q \cdot k = 0$, $\sum_{\text{pol.}} (Q \cdot \varepsilon)^2 = Q^2$.

Eq. (27) reduces thus to

$$\sigma_n = \frac{f^n}{n!} \exp[-f] \cdot \sigma_c \,, \tag{30}$$

which is the desired Poisson distribution originally given by BLOCK and NORDSIECK (4). The total cross-section is obviously:

$$\sigma_{\text{total}} = \sum_{n=0}^{\infty} \sigma_n = \sigma_c \,, \tag{31}$$

which exhibits the cancellation of the infrared divergences against the divergent contributions due to soft-photon emission.

Energy conservation is neglected in eq. (31). The condition $K \to 0$ is unrealistic; if we impose, instead, for all n,

$$\sum_{i=1}^{n} k_i^0 < \Delta E \,, \tag{32}$$

we have

$$\sigma_{\text{tot.}}(\Delta E) \simeq F(\beta) \cdot \exp\left[\beta \log \frac{\Delta E}{K}\right] \cdot \sigma_c \,, \tag{33}$$

where

$$\beta = \frac{\lambda^2}{2(2\pi)^3} \int \mathrm{d}\Omega_{\boldsymbol{k}} \cdot |\boldsymbol{k}|^2 \cdot Q^2, \tag{34}$$

and

$$F(\beta) = \frac{1}{2\pi i} \int_{-\infty}^{+\infty} \mathrm{d}t \frac{\exp[it]}{t - i\varepsilon} \exp\left[\beta \cdot \int_0^1 \mathrm{d}x \frac{\exp[-itx] - 1}{x}\right] = \tag{35}$$

$$= 1 - \frac{\pi^2}{12} \beta^2 + O(\beta^4) \,,$$

so that the divergent term

$$f = \beta \cdot \int_0^k \mathrm{d}k \frac{1}{k} \,. \tag{36}$$

disappears.

The derivation of eq. (33) is almost the same as that given by YENNIE and SUURA (3) and JAUCH and ROHRLICH (2), and need not be repeated here.

In conclusion, we wish to emphasize that our aim has been here solely to give a rigorous and relatively simple derivation of eq. (21). We have limited our considerations to perturbative expansions and to the prescription (6), (7) in order to simplify the discussion as much as possible; neither restriction appears however to be necessary, and it may well be that other subtraction rules prove more advantageous. The prescription (6), as it is, could be taken, for computational purposes, as a formal re-definition of the free photon propagator (which includes the additional limiting process $\varrho \to 0$): it is easy to see that, if everything is calculated with (6), performing the limit $\varrho \to 0$ *before* the integrations gives M, performing it *afterwards* gives M_c.

One of us (S. O.) presents separately ([7]), for purposes of comparison, a more conventional treatment of this subject based upon use of (6) in momentum space, yelding identical results, although with less generality.

RIASSUNTO

Le divergenze infrarosse della elettrodinamica quantistica vengono trattate in modo rigoroso e conciso, mediante tecniche elaborate a scopo rinormalizzativo. Si ottiene, in modo indipendente da metodi perturbativi, la naturale estensione della formula classica di Bloch-Nordsieck.

Photoneutrons from Bismuth.

V. Emma, C. Milone and A. Rubbino

Istituto di Fisica dell'Università - Catania
Centro Siciliano di Fisica Nucleare - Catania

R. Malvano

Istituto di Fisica dell'Università - Torino
Istituto Nazionale di Fisica Nucleare - Sezione di Torino

(ricevuto il 16 Aprile 1960)

Summary. — The energy spectrum of photoneutrons from bismuth irradiated with 31 MeV bremsstrahlung is studied at ϑ angles of 30°, 60°, 90°, 120° and 150°, by means of nuclear emulsion. A comparison between the experimental energy spectra and an evaporative spectrum calculated according the expression $F(E_n) = kE_n \exp[-E_n/T]$, shows a surprisingly high contribution of high energy neutrons around $\vartheta = 90°$. The angular distribution is isotropic in the region $(2 < E_n \leqslant 4)$ MeV, is approximatively of the form $1 + 0.7 \sin^2 \vartheta$ for $(4 < E_n \leqslant 5)$ MeV, and shows back and front asimmetry for $E_n > 5$ MeV. The contribution of the photoneutrons arising from the Bi$(\gamma, 2n)$ process is evaluated.

1. – Introduction.

The energy spectra of photoneutrons from Bi irradiated with bremsstrahlung have been studied by Price [1] at $E_{\gamma max} = 22$ MeV, by Zatsepina *et al.* [2] at $E_{\gamma max} = 18.9$ MeV, and by Bertozzi *et al.* [3] at $E_{\gamma max} = 14.3$ and 15.8 MeV. These spectra show a greater contribution of high energy neutrons

(1) G. A. Price: *Phys. Rev.*, **93**, 1279 (1954).
(2) G. N. Zatsepina, L. E. Lazareva and A. N. Pospelov: *Sov. Phys. JETP*, **5**, 21 (1957).
(3) W. Bertozzi, F. R. Paolini and C. P. Sargent: *Phys. Rev.*, **110**, 790 (1958).

($E_n > (3 \div 4)$ MeV) which cannot be accounted for by an evaporative process than that found for instance in the photoneutron spectrum from Au [4]. A remarkable contribution of high energy neutrons has been found also in the photoneutron spectrum from Ta [5], but this contribution is explained as being due to neutrons emitted by direct interaction and coming in part from a second resonance in the (γ, n) cross-section. In the case of Bi, the known cross-sections [6-8] give no evidence of a second resonance as in the case of Cr, As, I, Ta [5-9]. So the high percentage of high energy neutrons from Bi seemes to be a peculiarity of this element.

In the present experiment the energy spectra and the angular distribution of the photoneutrons from bismuth are studied by irradiation with a 30 MeV bremsstrahlung beam. At this irradiation energy, the study of the photoneutrons includes a large region beyond the giant resonance in the $\sigma(\gamma, n)$ process so that, far from the giant resonance, the contribution of other processes may also be investigated.

2. – Experimental procedure.

A cylindrical target of Bi was irradiated by a collimated γ-ray beam from the Betatron of the University of Turin, working at the maximum energy of 30 MeV. The photoneutrons emitted at ϑ angles of 30°, 60°, 90°, 120° and 150° with the photon beam where recorded by means of proton recoil tracks in L4 plates 400 μm thick.

The experimental arrangement was analogous to that used in a previous work [10]. The only difference being the substitution of the water wall—screening the plates against the neutrons from the betatron—with a paraffin moderator as shown in Fig. 1.

The scanning of the plates exposed with no target in the beam shows that the background was negligible (<1%).

---

(4) S. CAVALLARO, V. EMMA, C. MILONE and A. RUBBINO: *Nuovo Cimento*, **9**, 736 (1958).

(5) G. CORTINI, C. MILONE, A. RUBBINO and F. FERRERO: *Nuovo Cimento*, **9**, 85 (1958).

(6) J. HALPERN, R. NATHANS and A. K. MANN: *Phys. Rev.*, **88**, 679 (1952).

(7) R. MONTALBETTI, L. KATZ and J. GOLDENBERG: *Phys. Rev.*, **91**, 659 (1953).

(8) F. FERRERO, A. O. HANSON, R. MALVANO and C. TRIBUNO: *Nuovo Cimento*, **4**, 418 (1956).

(9) F. FERRERO, R. MALVANO and C. TRIBUNO: *Nuovo Cimento*, **6**, 385 (1957).

(10) C. MILONE and A. RUBBINO: *Nuovo Cimento*, **13**, 1035 (1959).

The experimental data are summarized in Table I.

TABLE I.

Element	^{209}Bi (100%)				
(γ, n) threshold (MeV)	7.44				
Energy of the cross-section peak (MeV)	13.5 [8] ÷ 14 [7]				
$E_{\gamma max}$ (MeV)	30				
Dose (Roentgen)	2960				
ϑ	30°	60°	90°	120°	150°
Scanned volume (mm^3)	50	54	88	57	54
Slow scanning. Number of experimentally accepted tracks $E_n \leq 5$ MeV	246	299	489	251	264
Slow and fast scanning. Number of experimentally accepted tracks $E_n > 5$ MeV	46	91	148	79	36

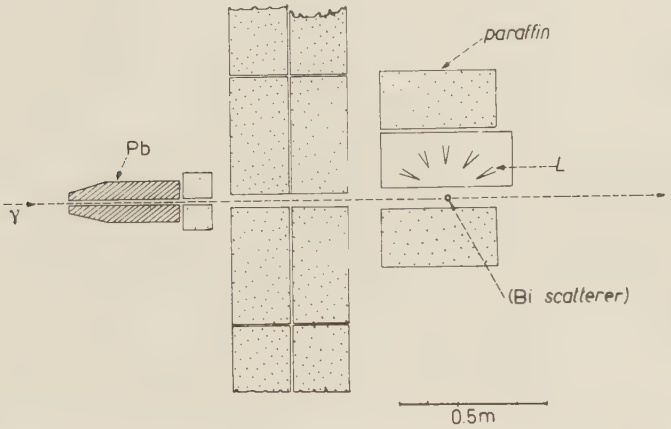

Fig. 1. – Experimental arrangement; Pb: lead collimator; Paraffin (moderator) screen against neutrons from the betatron; L: photoplates; Bi: target of Bismuth.

The experimental data on the observed recoil protons have been treated following the standard method [10] in order to derive the neutron energy and angular distributions.

3. – Results and discussion.

3·1. *Energy spectra.* – The experimental spectra obtained at different θ angles are shown in Fig. 2. The curves reported in the same figure are calculated according the following expression, for evaporated neutrons [11-13]

$$F(E)_n = \text{const}\, E_n \exp\left[-E_n/T\right],$$

assuming for the nuclear temperature the value $T = 0.8$ corresponding to the T values found by many authors [13-15].

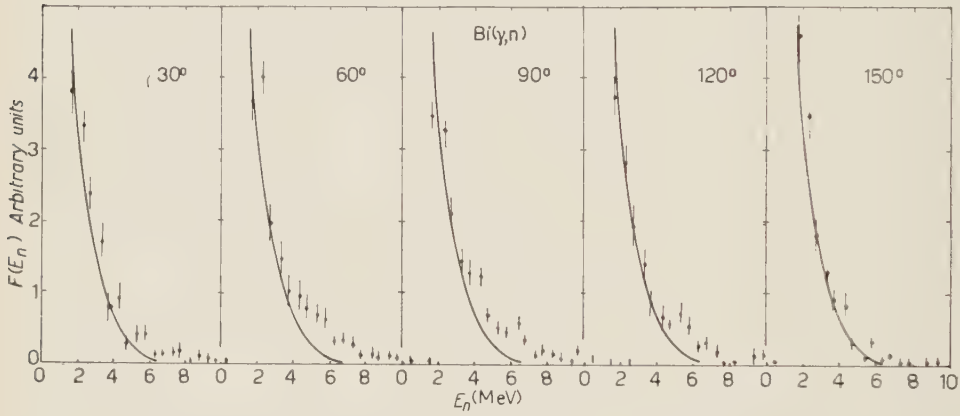

Fig. 2. – Energy spectra of the photoneutrons from Bi at angles $\vartheta = 30°$, 60°, 90°, 120° and 150°. The continuous curve is the calculated evaporative spectrum (see text).

The evaporative curve (Fig. 2) is normalized to the average of the experimental figures around $E_n = 2$ MeV relative to all five experimental spectra.

A remarkable contribution of high energy neutrons outside the evaporative curve is shown in Fig. 2. The amount of these neutrons divided by the total neutron number over $E_n = 2$ MeV is reported in Table II as « neutron fraction F » [16].

[11] V. F. Weisshopf and D. H. Ewing: *Phys. Rev.*, **57**, 472 (1940).
[12] D. L. Livesey: *Can. Journ. Phys.*, **33**, 391 (1955).
[13] G. Cortini, C. Milone, T. Papa and R. Rinzivillo: *Nuovo Cimento*, **14**, 54 (1959).
[14] P. C. Gugelot: *Phys. Rev.*, **81**, 51 (1951).
[15] L. Colli, U. Facchini, I. Iori, M. G. Marcazzan and A. M. Sona: *Nuovo Cimento*, **13**, 730 (1959).
[16] V. Emma, C. Milone and R. Rinzivillo: *Nuovo Cimento*, **14**, 1149 (1959).

TABLE II. – « *Neutron fraction F* » *at* $E_n > 2$ MeV *for* Bi *irradiated with* 30 MeV *and* 18.9 MeV *bremsstrahlung.*

ϑ angle	30° and 150°	60° and 120°	90°	References
« *F* » (30 MeV)	0.22	0.32	0.38	Present work
« *F* » (18.9 MeV)	0.44		0.58	(2)

In Table II is also reported the neutron fraction F relative to the experiment at $E_{\gamma max} = 18.9$ MeV (2). The evaporative curve and the point of normalization are the same as in the experiment at 30 MeV. This fraction F, is surprisingly high in a nucleus as heavy as bismuth.

Yet, the contribution of high energy neutrons in our experimental spectrum is lower than that found by ZATSEPINA *et al.* (2) at $\vartheta = 90°$ and 270° with 18.9 MeV bremsstrahlung. This may be seen in Fig. 3 where the two experimental spectra obtained at $E_{\gamma max}$=20 and 18.9 MeV are compared after normalization in the energy range $5 \leqslant E_n \leqslant 8$ MeV (see below). In Fig. 3 is also shown the energy spectrum of photoneutrons from Bi obtained by PRICE (1) with irradiation at $E_{\gamma max} = 22$ MeV.

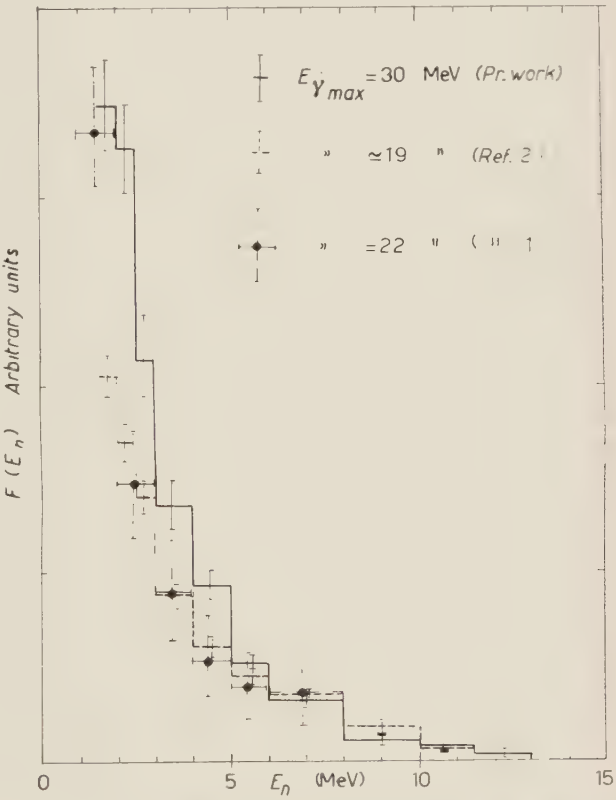

Fig. 3. – Comparison between the experimental spectra obtained at $E_{\gamma max}$=18.9 (2), 22 (1) and 30 MeV after normalization in the energy range ($5 \leqslant E_n < 8$) MeV (see Sect. 3·3).

We will show in Section 3·3 that this different behaviour is due to the Bi(γ, 2n) process that for $E_{\gamma max} = 30$ MeV gives a considerable number of neutrons with energy $E_n < 5$ MeV.

We consider the $(\gamma, 2n)$ process as the only process competing with the (γ, n) in the neutron emission. Indeed at the excitation energy that we have used, the (γ, np) process is negligible respect to the $(\gamma, 2n)$ because the emission of a charged particles is strongly inhibited by the Coulomb barrier, and the Bi$(\gamma, 3n)$ process is not appreciable at this energy.

3·2. *Angular distribution.* – The angular distributions are reported separately in Fig. 4 for the following neutron groups: $2 < E_n < 4$ MeV, $4 < E_n < 5$ MeV and $E_n > 5$ MeV. The experimental results are normalized to unity for $\vartheta = 90°$.

Neutron group $2 \leqslant E_n < 4$ MeV: The angular distribution is isotropic inside the experimental errors, as expected, the emission of the neutrons being due principally to evaporation in this interval of energy.

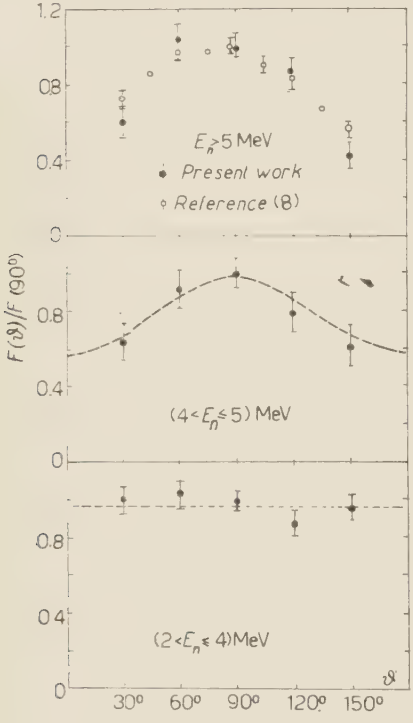

Fig. 4. – Experimental angular distribution of photoneutrons from bismuth for the various neutron groups.

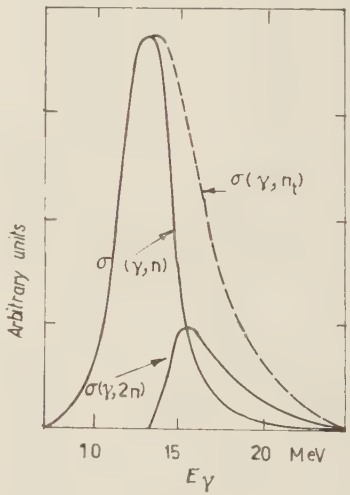

Fig. 5. – Bi(γ, n) and Bi$(\gamma, 2n)$ cross sections deduced by the total photoneutron cross sections assuming the statistical theory of nuclear reactions.

Neutron group $4 \leqslant E_n < 5$ MeV: These photoneutrons may be attributed prevalently to γ absorption in the region of the giant resonance; see the behaviour of the $\sigma(\gamma, n)$ in Fig. 5.

An angular distribution of the form $A + B \sin^2 \vartheta$ should be expected for electric dipole transition. The experimental figures may be fitted by a curve of the form $A + B \sin^2 \vartheta$ with $(B/A) \simeq 0.7$.

Neutron group $E_n > 5$ MeV: A back and front asymmetry appears evident in agreement with a similar result found previously ([8]) with Si(n, p) detectors (Fig. 4).

3·3. *Contribution of the* Bi(γ, 2n) *process.* – The competition between the (γ, n) and (γ, 2n) process can be predicted by the statistical theory of nuclear reactions ([11-17]) and we use as a good approximation the following expression ([17])

$$(1) \qquad \frac{\sigma(\gamma, 2n)}{\sigma(\gamma, n_t)} = 1 - \left[1 + \sqrt{\frac{a}{E}}(E - E_b)\right] \exp\left[-\sqrt{\frac{a}{E}}(E - E_b)\right],$$

where a is a constant for a given A, E is the energy of excitation, E_b is the threshold energy for the (γ, 2n) process and $\sigma(\gamma, n_t) = \sigma(\gamma, n) + \sigma(\gamma, 2n)$ according to our previous discussion.

This expression compares the (γ, 2n) contribution to the (γ, n) cross-section in heavy nuclei; it may be observed that the calculated ratios $\sigma(\gamma, 2n)/\sigma(\gamma, n_t)$ are in fair agreement with the experimental results ([7,18,19]).

The experimental total neutron cross-section curves, $\sigma_{\text{Exper}}(\gamma, n_t)$, for the photoneutron emission from bismuth are given by several authors: up to 20 MeV ([7,8]) and up to 25 MeV ([6]); so the unknown $\sigma(\gamma, 2n)$ cross-section may be calculated according to expression (1). Let

$$\frac{\sigma(\gamma, 2n)}{\sigma(\gamma, n_t)} \simeq \frac{\sigma(\gamma, 2n)}{\sigma(\gamma, n) + \sigma(\gamma, 2n)} = f(E_\gamma),$$

and being

$$\frac{\sigma_{\text{Exper}}(\gamma, n)}{\sigma(\gamma, 2n)} \simeq \frac{\sigma(\gamma, n) + 2\sigma(\gamma, 2n)}{\sigma(\gamma, 2n)}.$$

We then have

$$\sigma(\gamma, 2n) = \sigma_{\text{Exper}}(\gamma, n_t)\left(\frac{f(E_\gamma)}{1 + f(E_\gamma)}\right),$$

$$\sigma(\gamma, n) = \sigma_{\text{Exper}}(\gamma, n_t)\left(\frac{1 - f(E_\gamma)}{1 + f(E_\gamma)}\right).$$

We have introduced for this calculation the values of the $\sigma_{\text{Exper}}(\gamma, n_t)$ found by FERRERO *et al.* ([8]) up to $E_{\gamma\max} = 20$ MeV, that are in very good agreement

([17]) B. T. FELD, H. FERSHBACH, M. L. GOLDBERGER, H. GOLDSTEIN and V. F. WEISSKOPF: *Final report on the fast neutron project*, USAEC NYO 636 (1958).

([18]) J. GOLDENBERG and L. KATZ: *Phys. Rev.*, **90**, 308 (1953).

([19]) E. SILVA, J. GOLDENBERG, P. B. SMITH and L. MARQUEZ: *Nuovo Cimento*, **9**, 17 (1958).

with that obtained by MONTALBETTI *et al.* (7). For E_γ between 20 and 25 MeV we have adopted the values given by HALPERN *et al.* (6).

The ratio

$$\int_0^{E\gamma max} \sigma(\gamma, n)\, dE_\gamma \Big/ \int_0^{E\gamma max} \sigma(\gamma, 2n)\, dE_\gamma,$$

so calculated is reported in Table III. In the same Table, the experimentally known ratios for ^{181}Ta (20), ^{141}Pr (21), ^{93}Nb (19) and ^{63}Cu (21) are also reported. As Table III shows, the calculated ratio for Bi is very near to the experimental ratio for Ta as theoretically predicted. This result gives assurance of the reliability of the calculated Bi(γ, 2n) cross-section taking into account that the behaviour of the $\sigma(\gamma, n)$ cross-sections are very similar for Bi and for Ta (20).

TABLE III.

Element		^{63}Cu	^{93}Nb	^{141}Pr		^{181}Ta		^{209}Bi
$E_s(\gamma, n)$	(MeV)	10.6	8.7	10.0		7.6		7.44
E_γ for $\sigma_{\gamma,n}$ max	(MeV)	17.6	17.2	15.2		14.0		13.3
$E_s(\gamma, 2n)$	(MeV)	20.0	17.3	18.3		14.0		13.3
E_γ for $\sigma_{\gamma,2n}$ max	(MeV)	25.5	19.3	20		15		15.5
$E_s(\gamma, 2n) - E_s(\gamma, n)$	(MeV)	9.4	8.6	8.3		6.4		5.9
$E_{\gamma max}$	(MeV)	35	22	31		31	25	25
$\int_0^{E\gamma max} \sigma(\gamma, n)\, dE_\gamma \Big/ \int_0^{E\gamma max} \sigma(\gamma, 2n)\, dE_\gamma$		Experimental						Calculated
		6.80	6.25	5.5	3	2.7 ± 0.3	2.65 ± 0.3	2.9
References		(22)	(19)	(21)	(23)	(20)		Pres. work

The deduced curves of the B i(γ, n) and Bi(γ, 2n) cross-sections are shown in Fig. 5 together with the $\sigma(\gamma, n_i)$ obtained by FERRERO *et al.* (8) up to $E_\gamma = 20$ MeV and by HALPERN *et al.* (6) for $E_\gamma > 20$ MeV.

(20) J. H. CARVER and W. TURCHINETZ: *Proc. Phys. Soc.*, **71**, 613 (1958).
(21) J. H. CARVER and W. TURCHINETZ: *Proc. Phys. Soc.*, **73**, 110 (1959).
(22) A. J. BERMAN and K. L. BROWN: *Phys. Rev.*, **96**, 83 (1954).
(23) F. FERRERO, R. MALVANO, E. SILVA, J. GOLDEMBERG and G. MOSCATI: *Nucl. Phys.*, **10**, 423 (1959).

Now in order to show and confirm that the different behaviour of the spectra reported in Fig. 3 is due to the contribution of photoneutrons arising from the $(\gamma, 2n)$ process, our spectra and Soviet group's spectra observed at $\vartheta = 90°$ are connected by the following functions:

$$a_{30} = \sigma(\gamma, \mathrm{n}) \cdot I(E_\gamma, 30) \; ; \qquad a_{19} = \sigma(\gamma, \mathrm{n}) \cdot I(E_\gamma, 19) \; ;$$

$$b_{30} = 2\sigma(\gamma, 2\mathrm{n}) \cdot I(E_\gamma, 30) \; ; \qquad b_{19} = 2\sigma(\gamma, 2n) \cdot I(E_\gamma, 19) \, .$$

Normalizing these functions so that a_{30} and a_{19} assume the same maximum value we observe that the curve a_{30} nearly coincides with the normalized curve $a_{19}^{(\mathrm{n})}$ (Fig. 6). Taking into account this result, we have normalized the two experimental spectra in the energy range $5 \leqslant E_\mathrm{n} \leqslant 8$ MeV; the lower limit ($E_\mathrm{n} \geqslant 5$ MeV) selects the neutrons arising almost exclusively from the (γ, n) reaction, while the higher limit ($E_\mathrm{n} \leqslant 8$ MeV) excludes the low contribution of neutrons coming certainly from the region in which a_{30} becomes different from a_{19} (Fig. 6).

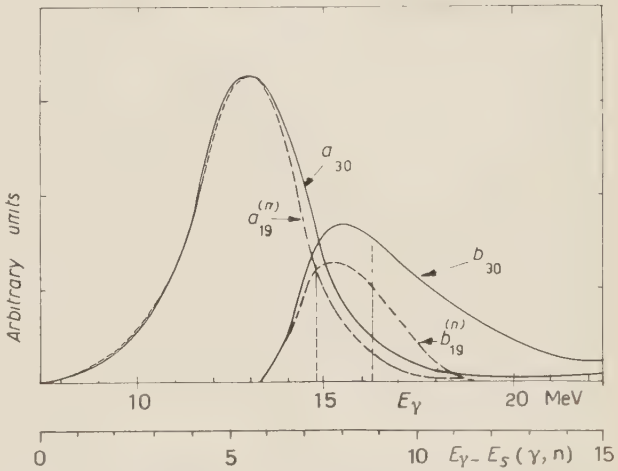

Fig. 6. – Functions $a_{E_{\gamma\max}}$ and $a^{(\mathrm{n})}_{E_{\gamma\max}}$ as defined in Sect. 3·3.

Now, if $F(E_\mathrm{n})$ is the flux of neutrons of energy E_n, we have

$$\frac{\int_0^{30 - E_s(\gamma,\,\mathrm{n})} F_{30}(E_\mathrm{n})\,\mathrm{d}E_\mathrm{n}}{\int_0^{19 - E_s(\gamma,\,\mathrm{n})} F_{19}^{(\mathrm{n})}(E_\mathrm{n})\,\mathrm{d}E_\mathrm{n}} = \frac{\int_{E_s(\gamma,\,\mathrm{n})}^{30} (a_{30} + b_{30})\,\mathrm{d}E_\gamma}{\int_{E_s(\gamma,\,\mathrm{n})}^{19} (a_{19}^{(\mathrm{n})} + b_{19}^{(\mathrm{n})})\,\mathrm{d}E_\gamma} \, .$$

Ignoring the negligibles values of the integrals

$$\int_{E_s(\gamma,\,\mathrm{n})}^{E_s(\gamma,\,\mathrm{n})+1.5} a\,\mathrm{d}E_\gamma \, , \qquad \int_{25}^{30} a_{30}\,\mathrm{d}E_\gamma \qquad \text{and} \qquad \int_{25}^{30} b_{30}\,\mathrm{d}E_\gamma \, , \quad \text{(Fig. 5)};$$

taking no account of the

$$\int_{E_s(\gamma,\,2n)}^{E_s(\gamma,\,2n)+3} b\,\mathrm{d}E_\gamma$$

values that give prevalently neutrons of energy less than 1.5 MeV; and observing that the $F(E_n)$ values for $E_n < 1.5$ MeV are connected to the $F(E_n)$ values in the energy range ($1.5 \leqslant E_n \leqslant 5$ MeV), we have with good approximation:

$$R_1 = \frac{\int_{1.5}^{30-E_s(\gamma,\,n)} F_{3}(E_n)\,\mathrm{d}E_n}{\int_{1.5}^{19-E_s(\gamma,\,n)} F_{19}^{(n)}(E_n)\,\mathrm{d}E_n} = \frac{\int_{E_s(\gamma,\,n)+1.5}^{25} a_{30}\,\mathrm{d}E_\gamma + \int_{E_s(\gamma,\,2n)+3}^{25} b_{30}\,\mathrm{d}E_\gamma}{\int_{E_s(\gamma,\,n)+1.5}^{19} a_{19}^{(n)}\mathrm{d}E_\gamma + \int_{E_s(\gamma,\,2n)+3}^{19} b_{19}^{(n)}\mathrm{d}E_\gamma} = R_2\,.$$

In our case the ratios R_1 and R_2 obtained from the curves reported in Fig. 3 and Fig. 6 assume respectively the values 1.4 and 1.3. This confirms that the different behaviour between our and the Soviet group's spectra, in the energy range $E_n < 5$ MeV, is due to the different contributions of the $(\gamma, 2n)$ process.

4. – Conclusions.

a) Photoneutron spectrum from Bismuth shows around 90° a surprisingly high contribution of neutrons outside the calculated evaporative spectrum.

b) The angular distribution is isotropic for $E_n \leqslant 4$ MeV, is approximately of the form $1+0.7\sin^2\vartheta$ for $(4 < E_n \leqslant 5)$ MeV while a back and front asymmetry appears for $E_n > 5$ MeV.

c) Evidence and evaluation are given of the photoneutrons from $(\gamma, 2n)$ processes.

RIASSUNTO

Si studia lo spettro a 30°, 60°, 90°, 120° e 150° dei fotoneutroni emessi dal bismuto irradiato con bremsstrahlung di 30 MeV. Un confronto degli spettri sperimentali con uno spettro evaporativo calcolato secondo l'espressione $F(E_n) = \mathrm{cost}\cdot E_n\cdot\exp[-E_n/T]$ mette in evidenza intorno a 90° un contributo di fotoneutroni, al di sopra della curva evaporativa, sorprendentemente alto per un nucleo così pesante. La distribuzione angolare risulta praticamente isotropa per neutroni con energia inferiore a 4 MeV. Nell'intervallo $(4 < E_n \leqslant 5)$ MeV si ha $F(\vartheta) \simeq 1+0.7\sin^2\vartheta$ mentre sopra 5 MeV si nota una evidente asimmetria avanti indietro. Si valuta il contributo dei neutroni provenienti della reazione Bi$(\gamma, 2n)$.

Quantum Electrodynamics in an Expanding Universe (*).

F. L. Scarf

University of Washington - Seattle, Wash.

(ricevuto il 19 Aprile 1960)

Summary. — The equations of quantum electrodynamics are investigated in an expanding universe characterized by a de Sitter metric. It is assumed that the expansion occurs on a microscopic level and that $\hbar$, the bare electron mass and the bare charge are all constant. For a particular coordinate system the operators may be expressed in terms of coupled flat-space fields which have m replaced by $mR(t)$. The equivalent quantized field problem is soluble using standard perturbation theory with modified commutators and Green's functions. As a first approxmation, adiabatic changes caused by the expansion are evaluated by imaking the replacement $m \to mR$ in all final formulae. Renormalization effects are examined using asymptotic expressions which contain ultraviolet cut-offs. Assuming that the cutoff procedures are meaningful and are related to the structure of the physical electron, it is noted that the renormalized mass and charge could vary with time for a particular kind of cut-off process.

1. – Introduction.

It is customary to interpret the observed red shift of stellar spectra as a Doppler effect associated with a large-scale expansion of the universe. This expansion has been described as a Newtonian phenomenon, and it also has been discussed using a curved space-time metric such as

$$ds^2 = dt^2 - R^2(t)[dx^2 + dy^2 + dz^2], \qquad R(0) = 1 \quad (1). \tag{1}$$

(*) Supported in part by the U. S. Atomic Energy Commission.

(1) The velocity of light is defined by this metric; it is then equal to unity and independent of cosmic time in the conformally flat T-system introduced below. Furthermore, we assume that $\hbar$ is the same universal constant of unit magnitude in all systems.

For macroscopic motions the two points of view predict the same effects (2). This note is concerned with a comparison of the two theories on a *microscopic level*; we shall examine the consequences of an assumption that the relativistic expansion occurs for atomic and subatomic phenomena.

In order to have any observable red shift for electromagnetic radiation, some unit of length (that is, a third scale factor to go with c, $\hbar$) must be independent of the cosmic time t. In the past it has usually been implicitly assumed that the bare electron mass is the meter stick which defines ($\mathrm{d}x$) of eq. (1) and we shall accordingly take m_0 and e_0 (bare charge) as parameters which are constant in all systems.

Ordinary quantum mechanics then predicts that only the standard red shift will be seen, even if the Bohr orbits expand; when the co-ordinates in the Schrödinger equation,

$$E\psi = [p^2/2m_0 - Ze_i^2/r]\psi \,, \tag{2}$$

undergo an adiabatic variation which is consistent with eq. (1), r is replaced by $R(t)\,r(0)$ $[(\mathrm{d}r^2) \to R^2(t)(dx^2+dy^2+\mathrm{d}z^2)]$ and p_k by $p_k(0)/R(t)$ (the latter follows from invariance of the phase integrals). This leads to

$$E_n(t,\, m_0) = E_n(0,\, m_0 R(t))/R(t) + 0(\mathrm{d}R/\mathrm{d}t) \,, \tag{3}$$

but for a Coulomb force,

$$E_n(0,\, m') = m' f(e_0,\, \hbar,\, n) \,, \tag{4}$$

so that $E_n(t,\, m_0)$ is the same constant *at* each star, if $\mathrm{d}R/\mathrm{d}t$ terms are negligible. The only appreciable modifications of the observed spectrum stem from the relative velocities of source and observer. The same result follows when the adiabatic variation is applied in the classical relativistic hamiltonian. In fact, one finds that E_n is independent of $R(t)$ to first order using only the virial theorem for the Coulomb potential.

Although these simple arguments might seem reliable when applied to determinations of atomic energy levels, there are several uncertainties connected with the above discussion. The results, eqs. (3), (4), depend in a detailed way on the form of the potential. It would be desirable to have a formalism which can treat any problem in electrodynamics, including those with magnetic forces, spin-orbit forces, etc. Furthermore, the Schrödinger and Dirac equations must be regarded as approximate relations which follow

(2) H. Bondi: *Cosmology* (Cambridge, 1952), chap. 9; W. H. McCrea: *Rep. Progr. Phys.*, **16**, 331 (1953).

from the complete quantized theory of interacting electron and photon fields. Accordingly, in the next section the general equations of quantum electrodynamics are examined for a geometry characterized by eq. (1). It is found that the original problem may be mapped onto one having effective flat-space fields with $m_0^{\text{eff}} = m_0 R(t)$.

In the third section the analysis is completed with a discussion of renormalization effects. It is noted that another fundamental length (the cut-off, Λ) enters at this point and the renormalized charges and masses are functions of (Λ/m_0). For some cut-off models, Λ has a value which depends on $R(t)$. We conclude that the quantized field theory may lead to results which are not contained in the single particle picture, and that frequency variations other than Doppler shifts could be observable even if the parameters for bare fields are constants.

2. – Field quantization.

In a Riemannian space with metric $g_{\mu\nu}$, the equations of electrodynamics are

$$i\gamma^\mu \nabla_\mu \psi + m_0 \psi = e_0 \gamma^\mu A_\mu \psi \,, \tag{5}$$

$$\{\gamma^\mu, \gamma^\nu\} = 2g^{\mu\nu} \,, \tag{6}$$

$$(-g)^{-\frac{1}{2}} \partial_\mu \left[(-g)^{\frac{1}{2}} F^{\mu\nu}\right] = e_0 \overline{\psi}\gamma^\nu \psi \,, \tag{7}$$

$$F_{\mu\nu} = \partial_\mu A_\nu - \partial_\nu A_\mu \,, \tag{8}$$

($g = \det g_{\mu\nu}$). The covariant spinor derivative is defined so that ∇_μ acting on $\overline{\psi}\psi$ or $\overline{\psi}\gamma^\nu\psi$ gives the ordinary gradient of a scalar or vector, respectively. One finds [3] $\nabla_\mu \psi = \partial_\mu \psi - \Gamma_\mu \psi$,

$$\Gamma_\mu = \tfrac{1}{4}(\gamma^\nu \Gamma^\alpha_{\mu\nu}\, \gamma_\alpha - \gamma^\nu \partial_\mu \gamma_\nu) \,, \tag{9}$$

where $\Gamma^\alpha_{\mu\nu}$ is an ordinary Christoffel symbol.

For the present it is convenient to consider these equations in a co-ordinate system (T-frame) with

$$\mathrm{d}s^2 = h(T)\,[\mathrm{d}T^2 - \mathrm{d}x^2 - \mathrm{d}y^2 - \mathrm{d}z^2] \,, \tag{10}$$

$t = \int_0^T h^{\frac{1}{2}}(T)\,\mathrm{d}T$, $h(T) = R^2(t)$. Then $g_{\mu\nu} = h(T)\tilde{g}_{\mu\nu}$ ($\tilde{g}_{\mu\nu}$ is flat) and eq. (6) may be

---

[3] D. R. Brill and J. A. Wheeler: *Rev. Mod. Phys.*, **29**, 465 (1957).

satisfied by $\gamma^\mu = h^{-\frac{1}{2}}(T)\tilde{\gamma}^\mu$ ($\tilde{\gamma}^\mu$ is flat). In this T-frame the spinor derivative also has a simple form, $\gamma^\mu \nabla_\mu \psi = h^{-5/4}\tilde{\gamma}^\mu \partial_\mu (h^{\frac{3}{4}}\psi)$, and eq. (65) becomes

$$i\tilde{\gamma}^\mu \partial_\mu \varphi + h^{\frac{1}{2}}(T) m_0 \varphi = e_0 \tilde{\gamma}^\mu A_\mu \varphi \,, \tag{11}$$

with $\varphi = h^{\frac{3}{4}}\psi$. In the same system eq. (7) reduces to

$$\partial_\mu (h^2 F^{\mu\nu}) = e_0(\bar{\varphi}\tilde{\gamma}^\nu \varphi) \,. \tag{12}$$

The tensor $F^{\mu\nu}$ must be expressed in terms of $F_{\mu\nu}$, the quantity which defines A_μ. The transition is quite straightforward: $\partial_\mu = \partial^\alpha \tilde{g}_{\mu\alpha}$ ($\tilde{g}_{\mu\alpha}$ is constant) so that the left-hand side of eq. (12) is $\partial^\nu(\tilde{g}_{\nu\mu} h^2 F^{\mu\nu})$. If the entire equation is multiplied through by $\tilde{g}_{\beta\nu}$, the new source term, $e_0(\bar{\varphi}\tilde{\gamma}_\beta \varphi)$, is equal to $\partial^\alpha(\tilde{g}_{\alpha\mu}\tilde{g}_{\beta\nu} F^{\mu\nu} h^2)$. However, $F_{\alpha\beta} = g_{\alpha\mu} g_{\beta\nu} F_{\mu\nu}$ and $g_{\alpha\nu} = \tilde{g}_{\alpha\nu} h$, so that

$$\partial^\mu \partial_\mu A_\nu = e_0(\bar{\varphi}\tilde{\gamma}_\nu \varphi) \tag{13}$$

if we require that $\partial^\nu A_\nu$ be zero in this particular co-ordinate system [4].

The last condition is not covariant and therefore it is not the Lorentz condition ($A_\nu{}^{;\nu} = 0$). However, although eqs. (11), (13) are equations of motion for field operators, the gauge condition is only a subsidiary condition on the state vectors, $(\partial^\nu A_\nu)^{(+)}|n\rangle = 0$. Moreover, the definitions of all state vectors, positive and negative frequencies, etc., shall be made with respect to a particular co-ordinate system, and our subsidiary condition does not introduce a new lack of general covariance. (We shall not speculate here on the fundamental problem of reconciling the non-covariance of quantum field theory with the general covariance of the relativistic scheme; we merely note that this difficulty is common to all theories [see ref. (7)].) In the T-frame it insures that the things which are ordinarily called longitudinal photons are eliminated, but the « energy » of the free photon field is not positive definite [5]. Since the concept of energy is degraded in a curved space we believe that the effect is not necessarily significant. At any rate the quantization of this field theory is straightforward and consistent although it may not correspond to the gene-

[4] SCHRÖDINGER has mapped the source-free electromagnetic *field strengths* into flat space quantities for conformally flat spaces (E. SCHRÖDINGER: *Proc. Irish Acad.*, **46**, 25 (1940); see also M. VON LAUE: *Helv. Phys. Acta, Suppl.*, **4**, 42 (1956)).

[5] GUTZWILLER has examined these equations in terms of a potential $\overline{A}$ defined by $F^{\mu\nu} = \partial^\mu \overline{A}^\nu - \partial^\nu \overline{A}^\mu$ (M. GUTZWILLER: *Helv. Phys. Acta*, **29**, 313 (1956)). His $\overline{A}$ is *not* related to our A by any simple equation such as $\overline{A}^\mu = g_{\mu\nu} A_\nu$. Furthermore, in this work the condition $A^\nu{}_{;\nu} = 0$ was used so that the final equation for $\overline{A}$ involves $g_{\mu\nu}$ in an explicit and complex manner.

ralization of ordinary electrodynamics. It should be noted, however, that in the relevant adiabatic limit of $\dot{h} \to 0$, the two conditions are actually identical.

The coupled equations for φ and A have flat-space derivatives and matrices and are identical to the flat-space equations for a φ-electron field with the single modification $m_\varphi = m_0 h^{\frac{1}{2}}(T)$. In the T-frame it is possible to quantize eqs. (11) and (13) by imposing the commutation rules

$$[A_\mu^{\text{in}}(x), A_\nu^{\text{in}}(x')] = ig_{\mu\nu} D(x-x') = i\tilde{g}_{\mu\nu} \tilde{D}(x-x') , \tag{14}$$

and

$$\{\varphi_\alpha^{\text{in}}(x), \overline{\varphi}_\beta^{\text{in}}(x')\} = iS_{\alpha\beta}(x-x') . \tag{15}$$

Here $\tilde{D}$, which satisfies $\Box\tilde{D} = 0$, is the ordinary flat-space photon commutator. The anticommutator S is not the conventional S function, but is a solution of $[i\tilde{\gamma}_\mu \partial_\mu + m(T)]S = 0$ with the usual boundary values. (If we had required $A_\nu{}^{;\nu} = 0$, the $\tilde{D}$ function in eq. (14) would be a solution of $L(\partial_\mu, h)\tilde{D} = 0$.)

The quantization in the T-frame is completed by setting up Schrödinger equations for the operator representatives of the classical constants of motion. The action principle which gives the equations of motion leads to

$$\partial_\mu \mathscr{T}_\nu^\mu = \tfrac{1}{2}\mathscr{T}^{\alpha\beta}(\partial g_{\alpha\beta}/\partial x^\nu) , \tag{16}$$

where $\mathscr{T}_\nu^\mu = \sqrt{-g}\, T_\nu^\mu$ has the usual form with covariant derivatives replacing the flat-space quantities. Since $h = h(T)$, the spatial component S of the total momentum,

$$P_\alpha = \int \mathrm{d}^3x \sqrt{-g}\, T_x^0 \qquad (\alpha = 1, 2, 3), \tag{17}$$

are constants of motion (in both the t and T system) although P_0 and P^r are not. The state vectors in the T-frame are thus the simultaneous eigenstates of P_α and

$$Q = \int \mathrm{d}^3x\, \tilde{j}_0 \quad (\partial^\mu \tilde{j}_\mu = 0) , \tag{18}$$

and they may be constructed in the customary manner. For instance, the renormalized in-state with a single physical electron is [6]

$$\left| \begin{matrix} \mathrm{e} \\ \mathrm{in} \end{matrix} \right\rangle = \lim_{T \to -\infty} \int \mathrm{d}\sigma_\mu\, \overline{\varphi}_r(\boldsymbol{x}, T) |0\rangle \tilde{\gamma}^\mu v_r^{(+)}(\boldsymbol{x}, T) , \tag{19}$$

[6] W. THIRRING: *Principles of Quantum Electrodynamics* (New York, 1958), p. 177.

where $v_r^{(+)}$ is a positive frequency c-number solution of $[i\tilde{\gamma}^\mu \partial_\mu + m(T)]v_r = 0$. The vacuum is defined so that the above is zero when $v_r^{(+)} \to v_r^{(-)}$, and $v_r^{(\pm)}$ are given by

$$v_r^{\pm)}(T, \boldsymbol{x}) = \frac{1}{2\pi i} \int_{-\infty}^{\infty} \frac{\mathrm{d}T' \, v_r(\boldsymbol{x}, T')}{(T' - T \pm i\varepsilon)} \,. \tag{20}$$

If the gauge condition $\partial^i A_i = 0$ is used, the photon states are defined in the conventional manner. In the above scheme all state vectors are constructed in terms of entities which are not spinors or vectors under general co-ordinate transformations. This means that a special kind of time keeping is required for the decomposition into positive and negative frequencies ([7]).

The general perturbation treatment of quantum electrodynamics is again valid for this theory with modified S function and suitably modified propagators. Since energy is not conserved, the out-state has additional pairs and photons and the matter production is proportional to $(dh/\mathrm{d}T)$ (eq. (17) with $\nu - 0$). We are primarily interested in the adiabatic limit because $\dot{h}$ is extremely small for the actual universe. Therefore, it is of interest to compare the predictions of the theory for two values of h, neglecting terms of order $\dot{h}$. (Again note that in this adiabatic limit $\partial^\nu A_\nu = 0$, does not differ from the conventional Lorentz condition.)

If $\dot{h}$ is very small, P_0 depends on T only through the adiabatic variation of m_φ, and therefore $P_0(T, m_0) = P_0(0, m_0 h^{\frac{1}{2}}) + 0(\dot{h})$. However, $P^0 = g^{00} P_0$ varies as h^{-1}; in order to have a meaningful definition of energy we must transform to a system such as the t-frame with $g^{00} = 1$, $g^{0\alpha} = 0$. In the t-frame the energy is $P_0' = P^{0'} = P_0/R(t)$ and thus the adiabatic limiting process applied to the field theoretical problem again gives eq. (3), but it is now meaningful for *any* electromagnetic phenomenon. The result is more general than was indicated by the original deduction and it is valid for hyperfine splittings with anomalous g-factors, radiative corrections and so forth.

3. – Renormalization.

All properties of the physical particles (ψ-field) are given in terms of the observed (renormalized) charge and mass with $e = Z^{\frac{1}{2}} e_0$ and $m = m_0 + \delta m$. We assume that m_0 and e_0 are finite and find, as usual, that δm and Z are represented by divergent integrals. Several authors have suggested that there may

([7]) For many forms of $R(t)$ the out-state has unusual properties in at least one of the two frames. A discussion of this point shall appear in the *Proceedings of the Royaumont Conference on Gravitation* (C.N.R.S., Paris, 1960).

be some degree of meaning associated with the introduction of an ultra-violet cut-off although there is no unique way to perform the operation. We shall assume that observations ($|e| > 0$, $m < \infty$) imply that the true theory does contain an additional length in some unknown manner; we also assume (with much less foundation) that a cut-off theory has significance as a phenomenological way of accounting for this new parameter with dimension of length.

These ideas may be used to speculate on the possible effects of a microscopic relativistic expansion on Z, δm. LANDAU [8] has argued that formulae of a certain type are meaningful so that, for instance, in the T-frame ($\dot{h}$ small) the renormalization constant for the (effective) φ-field is

$$Z = \left(\frac{e}{e_0}\right)^2 = \exp\left[-2e_0^2 \ln\left(\Lambda_\varphi/m_\varphi\right)\right], \tag{21}$$

where m_φ is the slowly varying effective mass for the φ^{in} field and Λ_φ is an effective cut-off energy for the virtual quanta of the bare φ and A fields.

Some physical meaning must be attached to Λ_φ in order to complete the analysis for an expanding universe. A plausible suggestion is that Λ_φ is a constant multiple of the effective bare electron rest mass and that it corresponds to the maximum energy of the effective virtual electrons. Then $\Lambda_\psi = km_0$ is constant and $\Lambda_\varphi = km_\varphi = h^{\frac{1}{2}}(T)km_0$, so that $\Lambda_\psi/m_\psi = \Lambda_\varphi/m_\varphi = k$ and Z is independent of T. If this were true, there would be no real difference between the predictions of the single particle and second quantized theories. (One argument in favor of this choice is based on the observation that all charged particles have the same value for e. This suggests that Z should indeed be a universal constant. However bosons have the same e, but eq. (21) does not describe their renormalization.)

On the other hand, Λ_φ might represent a maximum energy independent of T (that is, Λ_ψ might change). For instance, Λ_φ could be the energy associated with a critical photon frequency or field strength, $\hbar\nu_{\text{cr.t.}}$ (the photon properties are independent of T for $\dot{h} \to 0$ but the $\psi - A$ coupling term contains $h(T)$; on the other hand, the $\varphi - A$ coupling is independent of h). It is not unreasonable to associate the cut-off for the electron charge with some property of the photon field since the divergence is certainly an aspect of the interaction between the two fields. In this case $Z(T) = Z'(t)$ is a scalar function of x_k which depends only on time in the two special frames under consideration.

While the second suggestion may be highly improbable, it is of some in-

---

[8] L. D. LANDAU: *Niels Bohs and the Development of Physics* (New York, 1955), pp. 52-69. A somewhat different form for Z is given in this reference.

terest to note that the variation

$$Z(t) = \exp\left[-\frac{2}{137}\,[Z\,(\text{present})]^{-1}\ln\,[k/R(t)]\right] \tag{22}$$

will give an increase in e with time (the present value of $(137)^{-1}$ has been inserted for α and k is defined as $\hbar\omega_{\text{crit}}/m_0$). This would mean a decrease with retardation (distance) for the atomic frequencies in stellar spectra. Such a decrease could be separated from the ordinary Doppler shift by examining the ratios of fine structure frequencies to principal frequencies for sources of discrete spectra such as planetary nebulae. If one inserts $R(t) = \exp\,[t/\tau]$, eq. (22) becomes

$$Z(t) = Z(0)\,\exp\,[2t/137\,\tau Z(\tau)] \tag{23}$$

and the maximum frequency variation over the observable universe corresponds to $t_{\text{initial}} \simeq 0$, $t_{\text{present}} \simeq \tau$ (9). The self energy also varies with time if Λ_φ is constant, but these changes cannot be isolated from the standard Doppler shift.

4. – Conclusions.

If all lengths and times, except for the bare electron Compton wavelength (λ_η), expand uniformly (*e.g.*, $\Delta r = k^{\frac{1}{2}}\,\Delta r_0$, $-\Delta T = k^{\frac{1}{2}}\,\Delta T_0$) one might expect that electrodynamics could be connected with a theory in which *only* the effective electron Compton wave (λ_q) decreases while other lengths remain fixed ($\Delta r' = \Delta r_0$, $\Delta T' = \Delta T_0$). We have shown that this reasoning is indeed correct if a special non-covariant generalization of the Lorentz condition is imposed, but that the connection does not exist in general (unless $\dot{k}$ is negligible).

It has also been noted that the renormalization « constants » of quantum electrodynamics might be functions of time, even in the adiabatic limit. In

(9) A frivolous estimate of the greatest permissible variation in e^2 can be made using these formulae if one assumes that $kR^{-1}(t)$ had its maximum real value (no ghosts), at $t=0$. Then $Z(0)=\exp\,[-2\,(\ln k/137)\,Z(\tau)]$ and $Z(\tau)=\exp\,[2(1-\ln k)/137\,Z(\tau)]$. Setting $Z(\tau)=CZ(0)$ we get $Z(0)\ln Z(0) = -2\ln k/137C$. The smallest real value of $Z\ln Z$ (largest real k) is $-\varepsilon^{-1} = -0.368$. The equation for $Z(\tau)$ then yields $C\ln C = 2\varepsilon/137$ or $C = 1.34$. This magnitude for C gives a maximum $\Delta\nu$ comparable with ordinary Doppler shifts, but any numerical result is, of course, extremely sensitive to the functional form of the cut-off factor.

order for this to occur the ultraviolet cut-off must represent some maximum energy for the virtual photons; if the cut-off is correlated with a maximum bare electron energy the renormalization constants are time-independent in this limit.

* * *

I am grateful to Professors E. Henley and L. Wilets for several helpful discussions.

RIASSUNTO (*)

Si esaminano le equazioni dell'elettrodinamica quantistica in un universo in espansione caratterizzato da una metrica di de Sitter. Si suppone che l'espansione avvenga a livello microscopico e che $\hbar$, la massa nuda dell'elettrone e la carica nuda siano tutte costanti. Per un particolare sistema di coordinate gli operatori possono essere espressi in termini di campi accoppiati dello spazio piano che hanno m sostituito da $mR(t)$. Il problema equivalente del campo quantizzato si risolve usando la teoria standard della perturbazione con commutatori e funzioni di Green modificati. In prima approssimazione i cambiamenti adiabatici prodotti dall'espansione vengono valutati facendo la sostituzione $m \to mR$ in tutte le formule finali. Gli effetti di rinormalizzazione vengono esaminati usando espressioni asintotiche che contengono tagli ultravioletti. Supponendo che i procedimenti di taglio siano significativi e siano in rapporto alla struttura dell'elettrone fisico, si nota che la massa e la carica rinormalizzate possono variare col tempo per un tipo particolare di procedimenti di taglio.

(*) *Traduzione a cura della Redazione.*

IL NUOVO CIMENTO Vol. XVII, N. 3 1° Agosto 1960

Tripole Ghosts in Field Theory.

K. L. Nagy

Istituto di Fisica e Scuola di Perfezionamento in Fisica Nucleare dell'Università - Roma (*)

(ricevuto il 22 Aprile 1960)

Summary. — An appropriate modification of the Lee model is discussed. For a definite set of parameters beside the dipole ghost state also a tripole ghost is to be found. Using the Källén-Lehmann method contributions of tripole ghost states, supposed to exist in a relativistic quantum field theory, are calculated.

1. – Introduction.

According to the general properties of a state vector space with an indefinite metric even in a finite dimensional space, it is not sure that the eigenvectors of a hermitian operator (in Heisenberg's nomenclature pseudo-hermitian) form a complete system. The necessary and sufficient condition of the completeness is that the minimum polynomial $m(P)$ (*i.e.* the polynom having the least possible degree for which $m(P) = 0$) of the operator P to be considered should have the form [1]

$$m(P) = (P - p_1) \dots (P - p_k), \qquad p_i \neq p_k \text{ if } i \neq k$$

Since the characteristic polynomial $M(P)$ of P is, of course, equal to zero and has the form

$$M(P) = (P - p_1)^{\alpha_1} \dots (P - p_k)^{\alpha_k},$$

(*) On leave of absence from Institute for Theoretical Physics of the R. Eötvös University, Budapest.

(1) L. K. Pandit: *Suppl. Nuovo Cimento*, **11**, 157 (1959).

where $\alpha_1+\ldots+\alpha_k$ is the dimension of the vector space, the minimum polynomial can always be written as

$$m(P) = (P-p_1)^{\beta_1} \ldots (P-p_k)^{\beta_k}, \qquad \beta_i \leqslant \alpha_i .$$

But if at least one of the β's, let us say $\beta_i > 1$, the eigenvector $|p_i\rangle$ corresponding to the eigenvalue p_i has necessarily zero norm. If $\beta_i = 2$, a state vector different from 0, satisfying

$$(P-p_i)\,|D\rangle = |p_i\rangle , \tag{1}$$

also exist and has to be added to the eigenvectors, for completing the vector space. The state $|D\rangle$ was called by Heisenberg dipole ghost. If $\beta_i = 3$ beside $|D\rangle$ another state vector $|T\rangle$ defined by

$$(P-p_i)\,|T\rangle = |D\rangle \tag{2}$$

has also to be added to the set, and so on, depending on the degree of the minimum polynomial. $|T\rangle$ may be called « tripole » ghost.

Choosing the parameters of the model appropriately, a dipole ghost state can be found in the Lee model ([2]). Ghost states with higher pole order emerge ([3]) in a proposed model theory of Froissart ([4]), but in the sector containing higher number of particles.

Here a modification of the Lee model will be treated resulting in dipole and tripole ghost states. The modification was originally made in Teodorovich's work ([5]), but there the consequences were analysed in a completely wrong way. Next we calculate the contribution to the propagators of tripole ghost states supposed to exist in a relativistic field theory.

2. – The model.

The modified Lee model starts with the Hamiltonian

$$H = -m_{\mathrm{V}}\int \psi^*_{\mathrm{V}}\psi_{\mathrm{V}}\,\mathrm{d}\boldsymbol{p} + m\int \varphi^*\varphi\,\mathrm{d}\boldsymbol{p} + \int \omega(\boldsymbol{k})\,a^*(\boldsymbol{k})\,a(\boldsymbol{k})\,\mathrm{d}\boldsymbol{k} - \tag{3}$$

$$- \frac{g_0}{\sqrt{4\pi}}\int \frac{1}{\sqrt{2\omega}}\,\delta(\boldsymbol{p}-\boldsymbol{q}-\boldsymbol{k})\{\psi^*_{\mathrm{N}}(\boldsymbol{q})\psi_{\mathrm{V}}(\boldsymbol{p})\,a^*(\boldsymbol{k}) - \psi^*_{\mathrm{V}}(\boldsymbol{p})\,\psi_{\mathrm{N}}(\boldsymbol{q})\,a(\boldsymbol{k})\}\,\mathrm{d}\boldsymbol{p}\,\mathrm{d}\boldsymbol{q}\,\mathrm{d}\boldsymbol{k} +$$

$$+ e_0\int \{\varphi^*\psi_{\mathrm{V}} - \psi_{\mathrm{V}}\varphi\}\,\mathrm{d}\boldsymbol{p}\,, \qquad \omega = \sqrt{\boldsymbol{k}^2 + m_0^2}\,,$$

([2]) W. Heisenberg: *Nucl. Phys.*, **4**, 532 (1957).
([3]) K. L. Nagy: preprint.
([4]) M. Froissart: *Suppl. Nuovo Cimento*, **14**, 197 (1959).
([5]) E. V. Teodorovich: *Dokl. Akad. Nauk SSSR*, **126**, 1236 (1959).

where ψ_V, ψ_N and a stand for the field operators of the V, N and 0 particles. φ describes another fermion, with bare mass m. g_0 and e_0 are pure imaginary numbers. The commutation relations are the usual ones, except for ψ_V, for which

$$\{\psi_V(\boldsymbol{p}), \psi_V^*(\boldsymbol{p}')\} = -\delta(\boldsymbol{p}-\boldsymbol{p}'), \tag{4}$$

which gives rise to an indefinite metric:

$$\langle N_V, N_N, N_\varphi, N_\theta | N_V', N_N', N_\varphi', N_\theta' \rangle = (-1)^{N_V} \delta_{N,N'} .$$

The real vacuum and N particle states are the corresponding bare states, the dressed V, φ states have to be determined from

$$\boldsymbol{H}|E\rangle = E|E\rangle , \tag{5}$$

where $|E\rangle$ has the form

$$|E\rangle = \left(-\alpha\psi_V - \beta\varphi^* + \psi_N^* \int \Phi(\boldsymbol{k})\, a^*(\boldsymbol{k})\, \mathrm{d}\boldsymbol{k}\right)|0\rangle \tag{6}$$

considering the Hamiltonian (3). (5) and (6) give

$$\begin{cases} (m_V - E)\alpha - e_0\beta = \dfrac{g_0}{\sqrt{4\pi}} \displaystyle\int \frac{1}{\sqrt{2\omega}}\, \Phi(\boldsymbol{k})\, \mathrm{d}\boldsymbol{k} , \\ (\omega - E)\, \Phi(\boldsymbol{k}) = \alpha \dfrac{g_0}{\sqrt{4\pi}} \dfrac{1}{\sqrt{2\omega}} , \\ e_0\alpha + (E - m)\beta = 0 . \end{cases} \tag{7}$$

If $E = \omega$ one obtains the scattering states, all of them have positive norm. We are interested in bound real particle states for which $E \neq \omega$. In this case

$$\begin{cases} \beta = \dfrac{e_0\alpha}{m - E} , \\ \Phi(\boldsymbol{k}) = \dfrac{\alpha g_0}{\sqrt{4\pi}} \dfrac{1}{\sqrt{2\omega}\,(\omega - E)} , \end{cases} \tag{8}$$

and the eigenvalues have to be determined from

$$m_V - E + \frac{e_0^2}{E - m} = g_0^2 \int \frac{k^2\, \mathrm{d}k}{2\omega(\omega - E)} . \tag{9}$$

Using the identity

$$\frac{1}{\omega - z} = \frac{1}{\omega} + \frac{z}{\omega^2} + \frac{z^2}{\omega^2(\omega - z)},$$

and defining the function $H(z)$

$$(10) \quad H(z) = \frac{z - m_{\mathrm{V}}}{g_0^2} + \int \frac{k^2\,\mathrm{d}k}{2\omega(\omega - z)} + \frac{e}{m - z} = \\ = a + bz + G(z)z^2 + e\,\frac{1}{m - z} = h(z) + e\,\frac{1}{m - z},$$

where

$$(11) \quad a = -\frac{m_{\mathrm{V}}}{g_0^2} + \int \frac{k^2\,\mathrm{d}k}{2\omega^2}, \quad b = \frac{1}{g_0^2} + \int \frac{k^2\,\mathrm{d}k}{2\omega^3}, \quad e = \frac{e_0^2}{g_0^2}, \quad G(z) = \int \frac{k^2\,\mathrm{d}k}{2\omega^3(\omega - z)},$$

the energy eigenvalues are given from (9) by the zeros of $H(z)$. In this model a, b, e and m are finite parameters, therefore

$$e_0^2 \sim g_0^2 \sim \frac{-1}{\log \hat{\omega}}, \qquad m_{\mathrm{V}} \sim -\frac{\hat{\omega}}{\log \hat{\omega}},$$

$\hat{\omega}$ is the cut off energy. $h(z)$ is the corresponding function in the Lee model. Considering (10) there are three different cases:

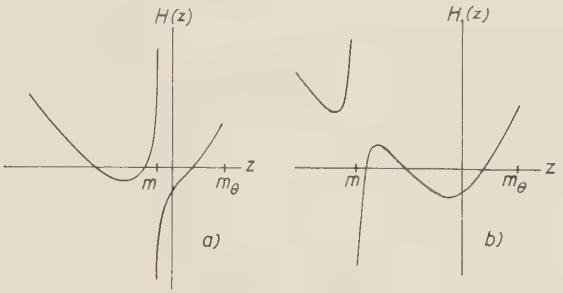

Fig. 1 *a*, *b*. – Discrete ghost case.

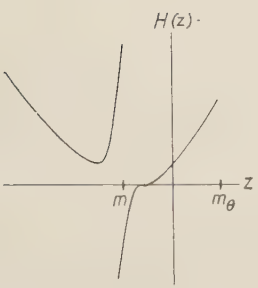

Fig. 2. – Tripole ghost case.

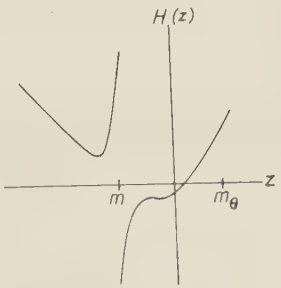

Fig. 3. – Complex ghost case

For E_i real, from (6), (8) and (10) one obtains

$$\langle E_i | E_j \rangle = \delta_{ij} |\alpha g_0|^2 \frac{\mathrm{d}H}{\mathrm{d}z}\bigg|_{E_i}, \tag{12}$$

therefore in the discrete ghost case two of the states have positive, one has negative norm. This is the ghost state. In the tripole ghost case there is only one eigenvalue E_0 and one eigenvector. It has zero norm, since there $\mathrm{d}H/\mathrm{d}z = 0$. $|E_0\rangle$ is orthogonal to the scattering states having real eigenvalues and since the metric is not degenerate (*i.e.* a state orthogonal to all state vectors of the space, including the vector itself does not exist; cf. [1]) at least one state $|D\rangle$ satisfying (1)

$$(H - E_0)|D\rangle = |E_0\rangle \tag{13}$$

necessarily exists. Indeed substituting (6) and

$$|D\rangle = \left(-\gamma\psi_{\mathrm{V}}^* - \delta\varphi^* + \psi_{\mathrm{N}}^* \int \varrho(\boldsymbol{k})\, a^*(\boldsymbol{k})\, \mathrm{d}\boldsymbol{k}\right)|0\rangle \tag{14}$$

into (13) one finds

$$\begin{cases} (m_{\mathrm{V}} - E_0)\gamma - e_0\delta = \dfrac{g_0}{\sqrt{4\pi}} \displaystyle\int \frac{1}{\sqrt{2\omega}}\, \varrho(\boldsymbol{k})\, \mathrm{d}\boldsymbol{k} + \alpha\,, \\ (\omega - E_0)\, \varrho(\boldsymbol{k}) = \gamma \dfrac{g_0}{\sqrt{4\pi}} \dfrac{1}{\sqrt{2\omega}} + \Phi(\boldsymbol{k})\,, \\ e_0\gamma + (E_0 - m)\delta = -\beta\,. \end{cases} \tag{15}$$

From (8) and (15)

$$\begin{cases} \delta = \dfrac{e_0}{m - E_0}\left(\gamma + \dfrac{\alpha}{m - E_0}\right), \\ \varrho(\boldsymbol{k}) = \dfrac{g_0}{\sqrt{8\pi\omega}\,(\omega - E_0)}\left(\gamma + \dfrac{\alpha}{m - E_0}\right). \end{cases} \tag{16}$$

Substituting (16) into the first equation of (15) and collecting the terms to one side, using (10) one obtains

$$g_0^2 \left\{ H(E_0)\gamma + \frac{\mathrm{d}H}{\mathrm{d}z}\bigg|_{E_0} \alpha \right\}, \tag{17}$$

which is equal to zero, showing that the dipole ghost $|D\rangle$ indeed exists with

an arbitrary α and γ. From (6), (8), (14) and (16) an explicit calculation gives

$$\langle E_0 | D \rangle = \alpha^* \gamma |g_0|^2 \frac{\mathrm{d}H}{\mathrm{d}z}\bigg|_{E_0} + \frac{|\alpha g_0|^2}{2} \frac{\mathrm{d}^2 H}{\mathrm{d}z^2}\bigg|_{E_0} = 0 \tag{18}$$

thus the dipole ghost $|D\rangle$ and $|E_0\rangle$ are orthogonal. Similarly

$$\langle D | D \rangle = |\gamma g_0|^2 \frac{\mathrm{d}H}{\mathrm{d}z}\bigg|_{E_0} + \frac{\alpha^*\gamma + \alpha\gamma^*}{2} |g_0|^2 \frac{\mathrm{d}^2 H}{\mathrm{d}z^2}\bigg|_{E_0} + \frac{1}{6} |\alpha g_0|^2 \frac{\mathrm{d}^3 H}{\mathrm{d}z^3}\bigg|_{E_0} = \tag{19}$$

$$= \frac{|\alpha g_0|^2}{6} \frac{\mathrm{d}^3 H}{\mathrm{d}z^3}\bigg|_{E_0} > 0 \,.$$

Therefore choosing $|\alpha|^2$ equal to

$$|\alpha|^2 = \frac{6}{|g_0|^2 \dfrac{\mathrm{d}^3 H}{\mathrm{d}z^3}_{E_0}} \,, \tag{20}$$

$|D\rangle$ can be normalized to $+1$. It is interesting to note that the normalization coefficient α of $|E_0\rangle$ is determined by the normalization of $|D\rangle$. Since $|E_0\rangle$ and $|D\rangle$ are orthogonal, the supposition of a non-degenerate metric requires that a state $|T\rangle$ satisfying the equation

$$(H - E_0)|T\rangle = |D\rangle \tag{21}$$

exist. Substituting as before $|T\rangle$ and $|D\rangle$

$$|T\rangle = \left(- \varepsilon \psi_{\mathrm{V}}^* - \lambda \varphi^* + \psi_{\mathrm{N}}^* \int x(\boldsymbol{k})\, a^*(\boldsymbol{k})\, \mathrm{d}\boldsymbol{k} \right) |0\rangle \,, \tag{22}$$

one obtains

$$\begin{cases} (m_{\mathrm{V}} - E_0)\varepsilon - e_0 \lambda = \dfrac{g_0}{\sqrt{4\pi}} \displaystyle\int \frac{1}{\sqrt{2\omega}} x(\boldsymbol{k})\, \mathrm{d}\boldsymbol{k} + \gamma \,, \\ (\omega - E_0)\, x(\boldsymbol{k}) = \varepsilon \dfrac{g_0}{\sqrt{4\pi}} \dfrac{1}{\sqrt{2\omega}} + \varrho(\boldsymbol{k}) \,, \\ e_0 \varepsilon + (E_0 - m)\lambda = - \delta \,, \end{cases} \tag{23}$$

from which

$$\begin{cases} \lambda = \dfrac{e_0}{m - E_0} \left(\varepsilon + \dfrac{\gamma}{m - E_0} + \dfrac{\alpha}{(m - E_0)^2} \right), \\ x(\boldsymbol{k}) = \dfrac{g_0}{\sqrt{8\pi\omega}\,(\omega - E_0)} \left(\varepsilon + \dfrac{\gamma}{\omega - E_0} + \dfrac{\alpha}{(\omega - E_0)^2} \right). \end{cases} \tag{24}$$

Substituting these into the first equation of (23) and ordering it again as in (17) one obtains

$$g_0^2\left(H(E_0)\varepsilon + \left.\frac{\mathrm{d}H}{\mathrm{d}z}\right|_{E_0}\gamma + \frac{1}{2}\left.\frac{\mathrm{d}^2H}{\mathrm{d}z^2}\right|_{E_0}\alpha\right), \tag{25}$$

so $|T\rangle$ exists indeed with an arbitrary ε and γ. An explicit calculation gives

$$\langle T|T\rangle = (\gamma\gamma^* + \varepsilon\alpha^* + \alpha\varepsilon^*)\left.\frac{|g_0|^2}{6}\frac{\mathrm{d}^3H}{\mathrm{d}z^3}\right|_{E_0} + (\alpha^*\gamma + \gamma\alpha^*)\left.\frac{|g_0|^2}{24}\frac{\mathrm{d}^4H}{\mathrm{d}z^4}\right|_{E_0} +$$

$$+ \left.\frac{|\alpha g_0|^2}{120}\frac{\mathrm{d}^5H}{\mathrm{d}z^5}\right|_{E_0}.$$

By choosing ε appropriately one can therefore make

$$\langle T|T\rangle = 0\,. \tag{26}$$

Similarly

$$\langle T|D\rangle = |g_0|^2\left\{\left.\frac{\alpha^*\gamma + \gamma^*\alpha}{6}\frac{\mathrm{d}^3H}{\mathrm{d}z^3}\right|_{E_0} + \left.\frac{|\alpha|^2}{24}\frac{\mathrm{d}^4H}{\mathrm{d}z^4}\right|_{E_0}\right\},$$

and now fixing γ one can also prescribe

$$\langle T|D\rangle = 0\,. \tag{27}$$

Finally

$$\langle E_0|T\rangle = \left.\frac{|\alpha g_0|^2}{6}\frac{\mathrm{d}^3H}{\mathrm{d}z^3}\right|_{E_0}. \tag{28}$$

Here $\mathrm{d}H/\mathrm{d}z|_{E_0} = \mathrm{d}^2H/\mathrm{d}z^2|_{E_0} = 0$ was taken into account. Thus fixing the parameters α, γ and ε according to the equations (20), (26) and (27), respectively, we have

$$\begin{cases} \langle E_0|E_0\rangle = \langle T|T\rangle = \langle E_0|D\rangle = \langle T|D\rangle = 0\,, \\ \langle E_0|T\rangle - \langle D|D\rangle = 1\,. \end{cases} \tag{29}$$

These equations being results of an explicit calculation are, of course, in agreement with the general properties. Indeed, let us suppose that there exist

three vectors, satisfying

$$(H-E_0)|E_0\rangle = 0\,,$$

$$(H-E_0)|D\rangle = |E_0\rangle\,,$$

$$(H-E_0)|T\rangle = |D\rangle\,.$$

In this case $\langle E_0|E_0\rangle = 0$ since just this was the necessary condition for the system of eigenfunctions being incomplete. From the third equation $\langle E_0|(H-E_0)|T\rangle = \langle E_0|D\rangle$, from the first $\langle T|(H-E_0)|E_0\rangle = 0$. Thus $\langle E_0|D\rangle = 0$. But in this case $\langle E_0|T\rangle \neq 0$ since the metric is non-degenerate. From the third equation $\langle D|(H-E_0)|T\rangle = \langle D|D\rangle$, from the second $\langle T|(H-E_0)|D\rangle = \langle T|E_0\rangle$, from which $\langle D|D\rangle = \langle E_0|T\rangle \neq 0$. Now $\langle T|D\rangle$ and $\langle T|T\rangle$ can be chosen equal to zero without violating the requirement of the non-degenerate character of the metric.

Supposing that another state $|Q\rangle$ would be needed to complete the system, then

$$(H-E_0)|Q\rangle = |T\rangle\,,$$

and repeating the procedure as in (17) or (25) we obtain that such a state would exist only if

$$\frac{\mathrm{d}^3H}{\mathrm{d}z^3}\bigg|_{E_0}$$

were also zero. In this model it is positive, showing that the system $|E_0\rangle$, $|D\rangle$, $|T\rangle$ is complete, and the minimum polynomial in this subspace is

$$m(H) = (H-E_0)^3\,.$$

Similarly it follows that $|E_0\rangle$, $|D\rangle$ and $|T\rangle$ are orthogonal to an eigenstate $|E'\rangle$ if $E' \neq E_0$ (scattering eigenstates). So the projection operator to to this subspace has the form

$$P = |D\rangle\langle D| + |E_0\rangle\langle T| + |T\rangle\langle E_0| \tag{30}$$

showing that one can meet negative norm only if a state contains both $|E_0\rangle$ and $|T\rangle$.

In the complex ghost case $H(z)$ has two complex roots E, E' and a real root E_0. E and E' are complex conjugated. The corresponding states have

the properties

$$\langle E_0 | E \rangle = \langle E_0 | E' \rangle = \langle E | E \rangle = \langle E' | E' \rangle = 0 ,$$
$$\langle E | E' \rangle \neq 0$$

as also follows from general principles.

The probabilistic interpretation of this model is the same as that of the Lee model; in the discrete ghost case ([6]) and in the complex ghost case ([7]) they are not probabilistically interpretable since in the higher sectors negative scattering probabilities occur. The tripole ghost case is interpretable only in the absence of bound states with negative norms in the higher sectors.

3. – Tripole ghost contribution to propagators.

If, for the sake of simplicity, in the case of a simple relativistic scalar (pseudoscalar) field there are discrete ghost states, the contribution of these states to the propagators is simply

$$\int \varrho(\mu^2)\, \Delta(x - x';\, \mu^2)\, \mathrm{d}\mu^2$$

but ϱ is negative. In the dipole ghost case one finds the contribution ([8])

$$\int \varrho_1(\mu^2)\, \Delta(x - x';\, \mu^2)\, \mathrm{d}\mu^2 + \int \varrho_2(\mu^2)(x - x')_\mu\, \partial_\mu \Delta(x - x';\, \mu^2)\, \mathrm{d}\mu^2 ,$$

where ϱ_1 and ϱ_2 may be $\gtrless 0$.

Now we wish to find the tripole ghost contribution. The method applied here is the same as in ([8]), according to which we suppose:

a) there exist a four momentum operator with the property

$$[P_\mu, \varphi(x)] = i\, \partial_\mu \varphi(x) , \tag{31}$$

b) indefinite metric, with tripole ghost,

c) and require relativistic invariance.

The supposition *b*) in the spirit of the general principles and the preceeding model means: the eigenvectors of P_μ do not form a complete system. To obtain

([6]) G. Källén and W. Pauli: *Mat. Fys. Medd. Dan. Vid. Selsk*, **30**, no. 7 (1955).
([7]) R. Ascoli and E. Minardi: *Nuovo Cimento*, **14**, 1254 (1959).
([8]) K. L. Nagy: *Nuovo Cimento*, **15**, 993 (1960)

such a set one has to consider all the states defined by

$$(32)\qquad (P_\mu - p_\mu)|p\rangle = 0\,, \qquad \langle p|p'\rangle - 0\,, \qquad p^2 - -\mu^2\,, \qquad p_0 > 0\,,$$

$$(33)\qquad (P_\mu - p_\mu)|Dp\rangle = c_\mu|p\rangle\,, \qquad \langle Dp|Dp'\rangle = \varepsilon\,\delta_{pp'}\,,$$

$$(34)\qquad (P_\mu - p_\mu)|Tp\rangle = C_\mu|Dp\rangle\,, \quad \langle Tp|Tp'\rangle = 0\,.$$

Here because of relativistic invariance

$$(35)\qquad c_\mu = f(p^2)p_\mu\,, \qquad C_\mu = g(p^2)p_\mu\,, \qquad C_\mu c_\nu = C_\nu c_\mu\,.$$

According to the indefinite metric $\varepsilon = \pm 1$. $|p\rangle$ and $|Tp\rangle$ are not orthogonal

$$(36)\qquad \langle Tp|p'\rangle = a\,\delta_{pp'}\,,$$

but $|Dp\rangle$ is orthogonal to $|p\rangle$ and $|Tp\rangle$.

As in the general part, from (34) $Dp|(P_\mu - p_\mu)|Tp\rangle = C_\mu\langle Dp|Dp\rangle$, from (33) $\langle Tp|(P_\mu - p_\mu)|Dp\rangle = c_\mu\langle Tp|p\rangle$, thus

$$(37)\qquad g(p^2)\varepsilon = f^*(p^2)a^*\,.$$

The projection operator to this subspace is (cf. (30))

$$(38)\qquad P = \sum\left\{|Dp\rangle\frac{1}{\varepsilon}\langle Dp| + |p\rangle\frac{1}{a}\langle Tp| + |Tp\rangle\frac{1}{a^*}\langle p|\right\},$$

and the contribution of these states to Δ'

$$(39)\qquad \Delta' \sim \sum\left\{\langle 0|\varphi(x)|Dp\rangle\frac{1}{\varepsilon}\langle Dp|\varphi(x')|0\rangle + \langle 0|\varphi(x)|p\rangle\frac{1}{a}\langle Tp|\varphi(x')|0\rangle + \right.$$
$$\left. + \langle 0|\varphi(x)|Tp\rangle\frac{1}{a^*}\langle p|\varphi(x')|0\rangle\right\} - \{x \rightleftarrows x'\}\,.$$

From (31) and (32)

$$(40)\qquad \langle 0|\varphi(x)|p\rangle = \langle 0|\varphi(0)|p\rangle\exp[ipx],$$

from (31) and (33)

$$(41)\qquad \langle 0|\varphi(x)|Dp\rangle = \{\langle 0|\varphi(0)|Dp\rangle + ix_\mu c_\mu\langle 0|\varphi(0)|p\rangle\}\exp[ipx]\,.$$

and from (31), (34) and (35)

$$(42)\qquad \langle 0|\varphi(x)|Tp\rangle = \left\{\langle 0|\varphi(0)|Tp\rangle + iC\ x_\mu\left(\langle 0|\varphi(0)|Dp\rangle + \right.\right.$$
$$\left.\left. + \frac{ic_\lambda x_\lambda}{2}\langle 0|\varphi(0)|p\rangle\right)\right\}\exp[ipx]\,.$$

Substituting these matrix elements into (39), and requiring again relativistic invariance one obtains

$$\Delta'(x-x') \sim C_1 \Delta(x-x') + C_2 (x-x')_\mu \partial_\mu \Delta(x-x') + \\ + C_3 (x-x')_\mu (x-x')_\nu \partial_\mu \partial_\nu \Delta(x-x') \,, \tag{43}$$

where (37) was also used. Each coefficient C_i is real and may be negative. From (43) it follows that the Fourier transform of the tripole ghost contribution has the form

$$\Delta'(p) \sim \int \varrho_1(\mu^2) \frac{1}{p^2 + \mu^2} \, \mathrm{d}\mu^2 + \int \varrho_2(\mu^2) \frac{\mu^2}{(p^2 + \mu^2)^2} \, \mathrm{d}\mu^2 + \int \varrho_3(\mu^2) \frac{\mu^4}{(p^2 + \mu^2)^3} \, \mathrm{d}\mu^2 \,; \tag{44}$$

each function ϱ_i may be negative.

The contributions from ghost of higher pole order can be calculated similarly. Here new and new derivates of Δ multiplied by the distances emerge.

Since theories with discrete or complex ghosts do not seem to be interpretable, the general properties of a state vector space mentioned in the introduction and the probabilistic interpretability together seem to allow only pole-type propagators, *i.e.* the form (44) having as many terms as the « pole order » of the ghost.

Nevertheless one has to be careful in applying the general results of a state vector space to the vector spaces of quantum field theories, which are constructed from the direct products of an infinite number of vector spaces.

* * *

The author is greatly indebted to the Scuola di Perfezionamento in Fisica Nucleare dell'Università, Rome, for financial support which made possible for him to work in the stimulating atmosphere of the Institute.

RIASSUNTO (*)

Si discute una modifica appropriata del modello di Lee. Per un definito gruppo di parametri si trova, oltre allo stato fantasma dipolare, anche un fantasma tripolare. Usando il metodo di Källén-Lehmann si calcolano i contributi degli stati fantasmi tripolari, che si suppongono esistere in una teoria relativistica del campo quantistico.

(*) *Traduzione a cura della Redazione.*

IL NUOVO CIMENTO Vol. XVII, N. 3 1° Agosto 1960

Polarization Phenomena for Positron Annihilation-in-Flight (*).

W. H. McMaster

Lawrence Radiation Laboratory, University of California - Livermore, Cal.

(ricevuto il 23 Aprile 1960)

Summary. — A method is presented for solving the Dirac equation for the annihilation of positrons using the Pauli spinors in such a way that all the polarization features are retained. Several specific examples of the polarization features are discussed, and finally the annihilation equation is put into matrix form for use with the Stokes parameters. This later representation is particularly convenient in that it readily points out the general features of the annihilation process.

1. – Introduction.

The computation of the differential cross-section for positron annihilation can be accomplished without the usual averaging over the positron-electron spins and summing [1] over photon polarizations by the use of the two-component Pauli spinors. Thus the wave function can be written in a form that greatly simplifies the calculation and leads to results that are given in terms of the positron and electron spin vectors [2]. The final results of this computation are similar to those obtained by Page [3], but are presented in a more general form.

The computation is carried out in the center-of-mass system for a two-quantum annihilation. In this system the energies of the two photons, the electron, and the positron are identical. The geometry being discussed is shown

(*) This work was performed under the auspices of the U. S. Atomic Energy Commission.

(1) See W. Heitler: *Quantum Theory of Radiation*, 3rd ed. (Oxford, 1954), p. 269.

(2) H. Olsen and L. C. Maximon: *Phys. Rev.*, **114**, 887 (1959). The author is grateful for having received a pre-publication copy of this paper. See also the Appendix:

(3) L. A. Page: *Phys. Rev.*, **106**, 394 (1957).

in Fig. 1. For a transformation to the laboratory system one utilizes the standard formulae:

$$E = 2\varepsilon^2 - 1\,, \qquad \beta = \left(\frac{E-1}{E+1}\right)^{\frac{1}{2}}, \quad \text{and} \quad \theta_{\text{lab}} = \theta + \text{tg}^{-1}\left(\frac{\beta \sin\theta}{2 - \beta\cos\theta}\right),$$

where β is given in the c-m system; E and ε are the total energies in units of mc^2 in the lab. and c-m system, respectively.

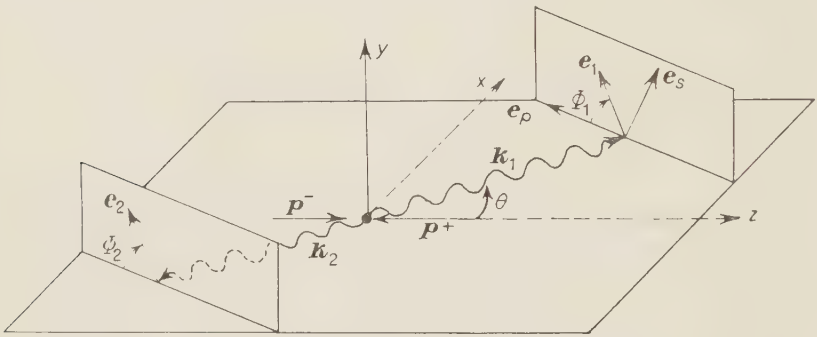

Fig. 1. – Center-of-mass system for the two-quanta annihilation of positrons. The angles φ_1 and φ_2 give the angle between the polarization vectors of the two quanta $\boldsymbol{k}_1$ and $\boldsymbol{k}_2$ and the plane of interaction (x-z plane).

2. – Computation of the cross-section.

2·1. *Evaluation of matrix elements.* – The two-quanta-annihilation differential cross-section is given by [1]

$$\frac{\mathrm{d}\sigma}{\mathrm{d}\Omega} = \frac{r_0^2}{4\beta}|H|^2\,, \tag{1}$$

where the matrix element responsible for the annihilation process is

$$H = -\sum\left[\frac{(u_0^*\alpha_1 u')(u'^*\alpha_2 u)}{\varepsilon'} + \frac{(u_0^*\alpha_2 u'')(u''^*\alpha_1 u)}{\varepsilon''}\right], \tag{2}$$

and the summation is to be carried out over all spin directions and energy signs in the intermediate states. The quantity $\alpha_1 = \boldsymbol{\alpha}\cdot\boldsymbol{e}_1$, with $\boldsymbol{e}_1$ being a unit vector in the direction of polarization of photon $\boldsymbol{k}_1$, and, similarly, $\alpha_2 = \boldsymbol{\alpha}\cdot\boldsymbol{e}_2$ for the second photon $\boldsymbol{k}_2$. The quantities ε' and ε'' are the total energies in units of mc^2 of the electron in the intermediate states, where $\boldsymbol{k}_1$, and $\boldsymbol{k}_2$, respectively, are given off first.

Since the denominators are sensitive to the sign of the intermediate state we can use the relations $H'u' = \varepsilon' u'$ and $H''u'' = \varepsilon'' u''$ to rewrite eq. (2) as

$$H = -\sum \left[\frac{(u_0^* \alpha_1 H' u')(u'^* \alpha_2 u)}{\varepsilon'^2} + \frac{(u^* \alpha_2 H'' u)(u''^* \alpha_1 u)}{\varepsilon''^2} \right]. \tag{3}$$

Momentum is conserved in the intermediate states, so we have $\boldsymbol{p}' = \boldsymbol{p} - \boldsymbol{k}_1$ and $\boldsymbol{p}'' = \boldsymbol{p} - \boldsymbol{k}_2$, where $\boldsymbol{p}$ is the momentum of the initial electron. Since $\boldsymbol{k}_1 = -\boldsymbol{k}_2$ and $k_1 = k_2 = \varepsilon$, we find $\varepsilon'^2 = 2\varepsilon^2(1 - \beta \cos\theta)$ and $\varepsilon''^2 = 2\varepsilon^2(1 + \beta \cos\theta)$. Thus the matrix element becomes

$$2\varepsilon^2(1 - \beta^2 \cos^2\theta) H = -\sum [(1 + \beta \cos\theta)(u_0^* \alpha_1 H' u')(u'^* \alpha_2 u) + (1 - \beta \cos\theta)(u_0^* \alpha_2 H'' u'')(u''^* \alpha_1 u)] \tag{4}$$

The sum over the intermediate states can now be carried out in the usual manner, resulting in

$$2\varepsilon^2(1 - \beta^2 \cos^2\theta) H = -[(1 + \beta \cos\theta)(u_0^* \alpha_1 H' \alpha_2 u) + (1 - \beta \cos\theta)(u_0^* \alpha_2 H' \alpha_1 u)]. \tag{5}$$

To evaluate the matrix elements we will follow the spin formalism used by Olsen and Maximon [2], which gives the result directly in terms of the spin vectors of the positron and electron. The initial (electron)—and final (positron)—state wave functions satisfying the Dirac equation are

$$\left\{ \begin{array}{l} u_0 = \left(\dfrac{\varepsilon + 1}{2\varepsilon} \right)^{\frac{1}{2}} \begin{pmatrix} 1 \\ \dfrac{\boldsymbol{\sigma} \cdot \boldsymbol{p}}{\varepsilon + 1} \end{pmatrix} v_0(\boldsymbol{S}), \\ \text{and} \\ u = \left(\dfrac{\varepsilon - 1}{2\varepsilon} \right)^{\frac{1}{2}} \begin{pmatrix} 1 \\ \dfrac{-\boldsymbol{\sigma} \cdot \boldsymbol{p}}{\varepsilon - 1} \end{pmatrix} v(-\boldsymbol{P}), \end{array} \right. \tag{6}$$

where $v_0(\boldsymbol{S})$ and $v(-\boldsymbol{P})$ are the Pauli spinors, with $\boldsymbol{S}$ and $\boldsymbol{P}$ being the electron and positron spin vectors, respectively. The positron's momentum is represented by $-\boldsymbol{p}$ since it is moving in the negative z direction.

Using these wave functions, we have

$$(u_0^* \alpha_1 H' \alpha_2 u) = \frac{(\varepsilon^2 - 1)^{\frac{1}{2}}}{2\varepsilon} \left\{ v_0^* 1 \overbrace{\frac{\boldsymbol{\sigma} \cdot \boldsymbol{p}}{\varepsilon + 1}} [\alpha_1 (\boldsymbol{\alpha} \cdot \boldsymbol{p}' + \beta) \alpha_2] \begin{pmatrix} 1 \\ \dfrac{-\boldsymbol{\sigma} \cdot \boldsymbol{p}}{\varepsilon - 1} \end{pmatrix} v \right\}, \tag{7}$$

and similarly for $(u_0^*\alpha_2 H''\alpha_1 u)$ where we have used the Dirac Hamiltonians:

$$H' = \boldsymbol{\alpha}\cdot\boldsymbol{p}' + \beta \qquad \text{and} \qquad H'' = \boldsymbol{\alpha}\cdot\boldsymbol{p}'' + \beta\,.$$

Multiplying out the terms in eq. (7), one finds

$$2p\varepsilon(u_0^*\alpha_1 H'\alpha_2 u) = v_0^*[(\varepsilon-1)\boldsymbol{\sigma}\cdot\boldsymbol{p}\,\boldsymbol{\sigma}\cdot\boldsymbol{e}_1\boldsymbol{\sigma}\cdot\boldsymbol{p}'\,\boldsymbol{\sigma}\cdot\boldsymbol{e}_2 - (\varepsilon+1)\boldsymbol{\sigma}\cdot\boldsymbol{e}_1\boldsymbol{\sigma}\cdot\boldsymbol{p}'\,\boldsymbol{\sigma}\cdot\boldsymbol{e}_2\boldsymbol{\sigma}\cdot\boldsymbol{p} - \\ - p^2\boldsymbol{\sigma}\cdot\boldsymbol{e}_1\boldsymbol{\sigma}\cdot\boldsymbol{e}_2 - \boldsymbol{\sigma}\cdot\boldsymbol{p}\,\boldsymbol{\sigma}\cdot\boldsymbol{e}_1\boldsymbol{\sigma}\cdot\boldsymbol{e}_2\boldsymbol{\sigma}\cdot\boldsymbol{p}]v\,,$$

and similarly:

$$2p\varepsilon(u_0^*\alpha_2 H''\alpha_1 u) = v_0^*[(\varepsilon-1)\boldsymbol{\sigma}\cdot\boldsymbol{p}\,\boldsymbol{\sigma}\cdot\boldsymbol{e}_2\boldsymbol{\sigma}\cdot\boldsymbol{p}''\,\boldsymbol{\sigma}\cdot\boldsymbol{e}_1 - (\varepsilon+1)\boldsymbol{\sigma}\cdot\boldsymbol{e}_2\boldsymbol{\sigma}\cdot\boldsymbol{p}''\,\boldsymbol{\sigma}\cdot\boldsymbol{e}_1\boldsymbol{\sigma}\cdot\boldsymbol{p} - \\ - p^2\boldsymbol{\sigma}\cdot\boldsymbol{e}_2\boldsymbol{\sigma}\cdot\boldsymbol{e}_1 - \boldsymbol{\sigma}\cdot\boldsymbol{p}\,\boldsymbol{\sigma}\cdot\boldsymbol{e}_2\boldsymbol{\sigma}\cdot\boldsymbol{e}_1\boldsymbol{\sigma}\cdot\boldsymbol{p}]v\,.$$

Combining, to obtain the complete expression for the matrix element, we find

$$(8)\quad 4p\varepsilon^3(1-\beta^2\cos^2\theta)H = v_0^*\{[(\varepsilon+1)(\boldsymbol{\sigma}\cdot\boldsymbol{e}_1\boldsymbol{\sigma}\cdot\boldsymbol{p}'\,\boldsymbol{\sigma}\cdot\boldsymbol{e}_2\boldsymbol{\sigma}\cdot\boldsymbol{p} + \boldsymbol{\sigma}\cdot\boldsymbol{e}_2\boldsymbol{\sigma}\cdot\boldsymbol{p}''\,\boldsymbol{\sigma}\cdot\boldsymbol{e}_1\boldsymbol{\sigma}\cdot\boldsymbol{p}) - \\ - (\varepsilon-1)(\boldsymbol{\sigma}\cdot\boldsymbol{p}\,\boldsymbol{\sigma}\cdot\boldsymbol{e}_1\boldsymbol{\sigma}\cdot\boldsymbol{p}'\,\boldsymbol{\sigma}\cdot\boldsymbol{e}_2 + \boldsymbol{\sigma}\cdot\boldsymbol{p}\,\boldsymbol{\sigma}\cdot\boldsymbol{e}_2\boldsymbol{\sigma}\cdot\boldsymbol{p}''\,\boldsymbol{\sigma}\cdot\boldsymbol{e}_1) + \\ + p^2(\boldsymbol{\sigma}\cdot\boldsymbol{e}_1\boldsymbol{\sigma}\cdot\boldsymbol{e}_2 + \boldsymbol{\sigma}\cdot\boldsymbol{e}_2\boldsymbol{\sigma}\cdot\boldsymbol{e}_1) + \\ + (\boldsymbol{\sigma}\cdot\boldsymbol{p}\,\boldsymbol{\sigma}\cdot\boldsymbol{e}_1\boldsymbol{\sigma}\cdot\boldsymbol{e}_2\boldsymbol{\sigma}\cdot\boldsymbol{p} + \boldsymbol{\sigma}\cdot\boldsymbol{p}\,\boldsymbol{\sigma}\cdot\boldsymbol{e}_2\boldsymbol{\sigma}\cdot\boldsymbol{e}_1\boldsymbol{\sigma}\cdot\boldsymbol{p})] + \\ + \beta\cos\theta[(\varepsilon+1)(\boldsymbol{\sigma}\cdot\boldsymbol{e}_1\boldsymbol{\sigma}\cdot\boldsymbol{p}'\,\boldsymbol{\sigma}\cdot\boldsymbol{e}_2\boldsymbol{\sigma}\cdot\boldsymbol{p} - \boldsymbol{\sigma}\cdot\boldsymbol{e}_2\,\boldsymbol{\sigma}\cdot\boldsymbol{p}''\,\boldsymbol{\sigma}\cdot\boldsymbol{e}_1\boldsymbol{\sigma}\cdot\boldsymbol{p}) \\ - (\varepsilon-1)(\boldsymbol{\sigma}\cdot\boldsymbol{p}\,\boldsymbol{\sigma}\cdot\boldsymbol{e}_1\boldsymbol{\sigma}\cdot\boldsymbol{p}'\,\boldsymbol{\sigma}\cdot\boldsymbol{e}_2 - \boldsymbol{\sigma}\cdot\boldsymbol{p}\,\boldsymbol{\sigma}\cdot\boldsymbol{e}_2\boldsymbol{\sigma}\cdot\boldsymbol{p}''\,\boldsymbol{\sigma}\cdot\boldsymbol{e}_1) + \\ + p^2(\boldsymbol{\sigma}\cdot\boldsymbol{e}_1\boldsymbol{\sigma}\cdot\boldsymbol{e}_2 - \boldsymbol{\sigma}\cdot\boldsymbol{e}_2\boldsymbol{\sigma}\cdot\boldsymbol{e}_1) + \\ + (\boldsymbol{\sigma}\cdot\boldsymbol{p}\,\boldsymbol{\sigma}\cdot\boldsymbol{e}_1\boldsymbol{\sigma}\cdot\boldsymbol{e}_2\boldsymbol{\sigma}\cdot\boldsymbol{p} - \boldsymbol{\sigma}\cdot\boldsymbol{p}\,\boldsymbol{\sigma}\cdot\boldsymbol{e}_2\boldsymbol{\sigma}\cdot\boldsymbol{e}_1\boldsymbol{\sigma}\cdot\boldsymbol{p})]\}v\,.$$

In multiplying out the terms in eq. (8) we make use of the relation

$$(\boldsymbol{\sigma}\cdot\boldsymbol{A})(\boldsymbol{\sigma}\cdot\boldsymbol{B}) = \boldsymbol{A}\cdot\boldsymbol{B} + i\,\boldsymbol{\sigma}\cdot(\boldsymbol{A}\times\boldsymbol{B})$$

which follows from the properties of the Pauli spin matrices.

The result can be put in a simple form if we define a set of functions dependent upon the photon polarizations as

$$(9a)\quad \begin{cases} \varrho_0 = \exp[i\delta_1]\sin\varphi_2\cos\varphi_1 - \exp[i\delta_2]\cos\varphi_2\sin\varphi_1\,, \\ \varrho_1 = \exp[i\delta_2]\sin\varphi_2\cos\varphi_1 - \exp[i\delta_1]\cos\varphi_2\sin\varphi_1\,, \\ \varrho_2 = \cos\varphi_2\cos\varphi_1 + \exp[i(\delta_1+\delta_2)]\sin\varphi_2\sin\varphi_1\,, \\ \varrho_3 = \cos\varphi_2\cos\varphi_1 - \exp[i(\delta_1+\delta_2)]\sin\varphi_2\sin\varphi_1\,. \end{cases}$$

where we are representing the electric vector of the photon by $\boldsymbol{e} = \cos\varphi \boldsymbol{e}_p + + \sin\varphi \exp[i\delta]\boldsymbol{e}_s$, with $\boldsymbol{e}_p$ and $\boldsymbol{e}_s$ being unit vectors in the plane of interaction and perpendicular to it, respectively, and δ is the phase angle. For linear polarization ($\delta = 0$), we see that eqs. (9*a*) reduce to

$$(9b) \qquad \begin{cases} \varrho_0 = \sin(\varphi_2 - \varphi_1) \\ \varrho_1 = \sin(\varphi_2 + \varphi_1) \\ \varrho_2 = \cos(\varphi_2 - \varphi_1) = (\boldsymbol{e}_1 \cdot \boldsymbol{e}_2) \\ \varrho_3 = \cos(\varphi_2 + \varphi_1) = \left[\dfrac{2(\boldsymbol{p}\cdot\boldsymbol{e}_1)(\boldsymbol{p}\cdot\boldsymbol{e}_2)}{p^2 \sin^2\theta} - (\boldsymbol{e}_1\cdot\boldsymbol{e}_2)\right]. \end{cases}$$

With these conventions, eq. (8) reduces to

$$(10a) \qquad \varepsilon(1 - \beta^2\cos^2\theta)\boldsymbol{H} = v_0^*(H_0 + i\boldsymbol{H}\cdot\boldsymbol{\sigma})v\,,$$

where

$$(10b) \qquad \begin{cases} H_0 = \dfrac{\beta}{\varepsilon}(\varrho_2 + \varrho_3 \sin^2\theta) \\ H_x = -\varrho_1 \beta \sin\theta \\ H_y = \varrho_3 \beta \sin\theta\cos\theta \\ H_1 = \dfrac{\varrho_0}{\varepsilon}\,. \end{cases}$$

2·2. *The cross-section in general form.* – Upon substitution of the matrxi elements of eq. (10) into eq. (1) we find the differential cross-section

$$(11) \qquad \frac{\mathrm{d}\sigma}{\mathrm{d}\Omega} = \frac{r_0^2}{4\beta}\frac{1}{\varepsilon^2(1-\beta^2\cos^2\theta)^2}\{v^*(H_0 - i\boldsymbol{H}^*\cdot\boldsymbol{\sigma})\, r_0 r_0^*(H_0 + i\boldsymbol{H}\cdot\boldsymbol{\sigma})v\}\,;$$

$$(12) \qquad v_0 v_0^* = \tfrac{1}{2}(1 + \boldsymbol{S}\cdot\boldsymbol{\sigma})\,,$$

however, is the projection operator for the electron.

Therefore, the term in brackets in eq. (11) becomes

$$(13) \qquad \tfrac{1}{2}\{v^*(H_0 - i\boldsymbol{H}^*\cdot\boldsymbol{\sigma})(1 + \boldsymbol{S}\cdot\boldsymbol{\sigma})(H_0 + i\boldsymbol{H}\cdot\boldsymbol{\sigma})v\}\,.$$

Upon expansion we utilize the properties of the positron spinors, *i.e.*,

$$v^*v = 1 \qquad \text{and} \qquad v^*\boldsymbol{\sigma}v = -\boldsymbol{P}\,,$$

where $\boldsymbol{P}$ has the components $P_x = -\sin\chi\cos\omega$, $P_y = -\sin\chi\sin\omega$, and $P_z = \cos\chi$ (see Appendix, eqs. (A.14)). Thus the differential cross-section is given by

$$(14)\qquad \frac{8\beta\varepsilon^2(1-\beta^2\cos^2\theta)^2}{r}\frac{\mathrm{d}\sigma}{\mathrm{d}\Omega} = H_0' + H^2 - (H_0^2 - H^2)(\boldsymbol{P}\cdot\boldsymbol{S}) - [(\boldsymbol{S}\cdot\boldsymbol{H})(\boldsymbol{P}\cdot\boldsymbol{H}^*) + (\boldsymbol{S}\cdot\boldsymbol{H}^*)(\boldsymbol{P}\cdot\boldsymbol{H})] - iH_0[(\boldsymbol{S}\cdot\boldsymbol{H}^*) - (\boldsymbol{S}\cdot\boldsymbol{H})] - iH_0[(\boldsymbol{P}\cdot\boldsymbol{H}) - (\boldsymbol{P}\cdot\boldsymbol{H}^*)] + i[\boldsymbol{S}\cdot(\boldsymbol{H}\times\boldsymbol{H}^*) + \boldsymbol{P}\cdot(\boldsymbol{H}\times\boldsymbol{H}^*)] - H_0[(\boldsymbol{S}\times\boldsymbol{P})\cdot(\boldsymbol{H}+\boldsymbol{H}^*)]\,.$$

For the special case of plane polarization, where $\boldsymbol{H}^* = \boldsymbol{H}$ and $H_0^* = H_0$, eq. (14) reduces to

$$(15)\qquad \frac{\mathrm{d}\sigma}{\mathrm{d}\Omega} = \frac{r_0^2}{8\beta\varepsilon^2(1-\beta^2\cos^2\theta)^2}\cdot \{H_0^2 + H^2 - (H_0^2 - H^2)(\boldsymbol{P}\cdot\boldsymbol{S}) - 2(\boldsymbol{S}\cdot\boldsymbol{H})(\boldsymbol{P}\cdot\boldsymbol{H}) - 2H\,(\boldsymbol{S}\times\boldsymbol{P})\cdot\boldsymbol{H}\}.$$

2·3. *Special case of longitudinal spin.* – For the special case of longitudinal spin along the z axis it is instructive to rewrite eq. (10*a*) in the form

$$(16a)\qquad \varepsilon(1-\beta^2\cos^2\theta)H = v_0^*\begin{pmatrix} H_{11} & H_{12} \\ H_{21} & H_{22}\end{pmatrix} v\,,$$

where

$$(16b)\qquad \begin{cases} H_{11} = \dfrac{1}{\varepsilon}\,(i\varrho_0 + \beta\varrho_2 + \beta\varrho_3\sin^2\theta)\,, \\ H_{22} = \dfrac{1}{\varepsilon}\,(-i\varrho_0 + \beta\varrho_2 + \beta\varrho_3\sin^2\theta)\,, \\ H_{12} = -\beta\sin\theta(i\varrho_1 - \varrho_3\cos\theta)\,, \\ H_{21} = -\beta\sin\theta(i\varrho_1 + \varrho_3\cos\theta)\,. \end{cases}$$

In this case the spin spinors have the simple forms:

$v_0^* = \widehat{10}$: electron spin along the positive z axis

$v^* = \widehat{01}$: electron spin along the negative z axis .

$v = \begin{pmatrix}0\\1\end{pmatrix}$: positron spin along the positive z axis

$v = \begin{pmatrix}1\\0\end{pmatrix}$: positron spin along the negative z axis .

Using these spinors, one readily finds that the matrix elements of eq. (16*a*)

refer to the following alignment of electron-positron spins:

$$\begin{aligned} H_{11}&: \quad +-, \quad (\uparrow\downarrow) \\ H_{22}&: \quad -+, \quad (\downarrow\uparrow) \\ H_{12}&: \quad ++, \quad (\uparrow\uparrow) \\ H_{21}&: \quad --, \quad (\downarrow\downarrow) \end{aligned}$$

This form of the cross-section, then, is similar to that presented by PAGE [3].

2·4. *Photon polarization.* – The cross-section depends upon photon polarization through the ϱ-functions defined by eqs. (9*a*). For a complete description of the polarizations of the two photons $\boldsymbol{k}_1$ and $\boldsymbol{k}_2$ we can specify the ϱ's in either a set of plane-polarizations tates or circular-polarization states. From the definition of the ϱ's one sees that for circular polarization ϱ_0 and ϱ_1 are pure imaginary. To avoid confusion it is convenient to rewrite the matrix elements for the circular-polarization de- scription as

$$\text{(17)} \qquad \begin{cases} H_0 = \dfrac{\beta}{\varepsilon}(\varrho_2 + \varrho_3 \sin^2\theta) \\ H_x = i\varrho_1\beta \sin\theta \\ H_y = \varrho_3\beta \sin\theta\cos\theta \\ H_1 = -i\varrho_0/\varepsilon \end{cases}$$

and

$$\text{(18)} \qquad \begin{cases} H_{11} = \dfrac{1}{\varepsilon}(\varrho_0 + \beta\varrho_2 + \beta\varrho_3 \sin^2\theta) & : \quad (\uparrow\downarrow) \\ H_{22} = \dfrac{1}{\varepsilon}(-\varrho_0 + \beta\varrho_2 + \beta\varrho_3 \sin^2\theta) & : \quad (\downarrow\uparrow) \\ H_{12} = -\beta \sin\theta(\varrho_1 - \varrho_3\cos\theta) & : \quad (\uparrow\uparrow) \\ H_{21} = -\beta \sin\theta(\varrho_1 + \varrho_3\cos\theta) & : \quad (\downarrow\downarrow) \end{cases}$$

For the plane-polarization description, let p and s refer to polarization in and perpendicular to the plane of interaction, respectively. For the circular-polarization description, let R and L indicate right and left circular polarization, respectively [4]. With these conventions, the values of the ϱ's for each set are given in Table I.

[4] In this representation, *e.g.*, right circular polarization of both photons is specified by the vectors $\boldsymbol{e}_1 = \frac{1}{2}(\boldsymbol{e}_p - i\boldsymbol{e}_s)$ and $\boldsymbol{e}_2 = \frac{1}{2}(\boldsymbol{e}_p + i\boldsymbol{e}_s)$; thus each photon advances as a right-hand screw.

TABLE I. – *Photon polarization states.*

State	Linear				Circular			
	pp	*ss*	*ps*	*sp*	*RR*	*LL*	*RL*	*LR*
ϱ_0	0	0	1	−1	1	−1	0	0
ϱ_1	0	0	1	1	0	0	−1	1
ϱ_2	1	1	0	0	1	1	0	0
ϱ_3	1	−1	0	0	0	0	1	1

3. – Discussion of the cross section.

3·1. *Unpolarized electrons and positrons.* – The differential cross-section for unpolarized initial and final spins is obtained directly from eq. (14) as $\mathrm{d}\sigma \sim (H_0^2 + H^2)$ or from eq. (16*b*) and (18) by averaging over the spin combinations; *i.e.*, $\mathrm{d}\sigma \sim \frac{1}{4}(H_{11}^2 + H_{22}^2 + H_{12}^2 + H_{21}^2)$. The result is

$$(19) \qquad \frac{\mathrm{d}\sigma}{\mathrm{d}\Omega} = \frac{r_0^2}{8\beta\varepsilon^2}\frac{1}{(1-\beta^2\cos^2\theta)^2}\cdot \left\{\frac{1}{\varepsilon^2}\left[\varrho_0^2 + \beta^2(\varrho_2 + \varrho_3\sin^2\theta)^2\right] + \beta^2\sin^2\theta(\varrho^2 + \varrho_3^2\cos^2\theta)\right\},$$

for both the linear—and circular—polarization descriptions. From this equation it is seen that in the low-energy limit ($\beta \to 0$) the photons tend to be cross polarized (*ps* and *sp*). In the circular-polarization description the photons are *RR* and *LL*, *i.e.*, there is no net angular momentum.

If the polarizations of the two photons are not observed, then one obtains the differential cross-section by summing over all directions of photon polarization as given in Table I, and obtains

$$\frac{\mathrm{d}\sigma}{\mathrm{d}\Omega} = \frac{r_0^2}{4\beta\varepsilon^2}\left[\frac{1 + 2\beta^2\sin^2\theta - \beta^4 - \beta^4\sin^4\theta}{(1-\beta^2\cos^2\theta)^2}\right].$$

As a check on eq. (19) we can substitute the vector forms of ϱ_2 and ϱ_3 as given by eq. (9*b*) and make use of the fact that $\varrho_0^2 = 1 - \varrho_2^2$ and $\varrho_1^2 = 1 - \varrho_3^2$. Then eq. (19) becomes

$$\frac{\mathrm{d}\sigma}{\mathrm{d}\Omega} = \frac{r_0^2}{8\beta\varepsilon^2}\left[\frac{\varepsilon^2 - (\varepsilon^2 - p^2\cos^2\theta)(\boldsymbol{e}_1\cdot\boldsymbol{e}_2) + 4(\boldsymbol{p}\cdot\boldsymbol{e}_1)(\boldsymbol{p}\cdot\boldsymbol{e}_2)(\boldsymbol{e}_1\cdot\boldsymbol{e}_2)}{(\varepsilon^2 - p^2\cos^2\theta)} - \frac{4(\boldsymbol{p}\cdot\boldsymbol{e}_1)^2(\boldsymbol{p}\cdot\boldsymbol{e}_2)^2}{(\varepsilon^2 - p^2\cos^2\theta)^2}\right],$$

which is Heitler's formula.

Let us now investigate the possibility of producing a polarized γ-ray beam using an unpolarized positron source and an unpolarized electron target. The experiment would consist of measuring the polarization of the lower-energy γ in the laboratory system, which would then determine the degree of polarization of the high-energy γ. We will define the polarization correlation through the equation

$$P = \frac{\sigma_\perp - \sigma_\parallel}{\sigma_\perp + \sigma_\parallel},$$

where $\sigma_\perp = \sigma_{ps} + \sigma_{sp}$ gives the cross-section for cross-polarized γ's, and $\sigma_\parallel = -\sigma_{pp} + \sigma_{ss}$ gives the cross-section for parallel polarization. Thus, using eq. (19) we have

$$P = \frac{1 - 2\beta^2 + \beta^4 + \beta^4 \sin^4\theta}{1 + 2\beta^2 \sin^2\theta - \beta^4 - \beta^4 \sin^4\theta},$$

and for the two limiting cases:

$$P(\pi/2) = \frac{1 - 2\beta^2(1-\beta^2)}{1 + 2\beta^2(1-\beta^2)} \qquad \text{and} \qquad P(0) = \frac{1-\beta^2}{1+\beta^2}.$$

Thus we see that at high energies ($\beta \sim 1$) the cross-polarization correlation increases from zero at $\theta = 0$ to complete cross polarization at $\pi/2$. This does not seem to be a good source of polarized annihilation radiation since the cross section at $\pi/2$ is quite small and the value of P does not increase above ~ 0.1 until θ is greater than about 30° for energies of interest.

3·2. *Longitudinal spins.*

3·2.1. Plane-polarized photons. – The cross-section for antiparallel longitudinal spins is given directly by eq. (15) as $d\sigma \sim 2(H_0^2 + H_z^2)$, or can be obtained from eqs. (16*b*) by averaging over the two spin orientations; *i.e.*, $d\sigma \sim \frac{1}{2}(H_{11}^2 + H_{22}^2)$. The result is

$$\left(\frac{d\sigma}{d\Omega}\right)_{opp} = \frac{r}{4\beta\varepsilon^2} \frac{1}{(1-\beta^2\cos^2\theta)^2} \frac{1}{\varepsilon^2} [\varrho_0^2 + \beta^2(\varrho_2 + \varrho_3 \sin^2\theta)^2]. \tag{20a}$$

Summing over photon polarizations, one has

$$\left(\frac{d\sigma}{d\Omega}\right)_{opp} = \frac{r^2}{2\beta\varepsilon^2} \frac{(1-\beta^2)}{(1-\beta^2\cos^2\theta)^2} [1 + \beta^2 + \beta^2 \sin^4\theta]. \tag{20b}$$

Similarly for parallel spins, we have from eq. (15) that $d\sigma \sim 2(H^2 - H_z^2) = 2(H_x^2 + H_y^2)$, or from eqs. (16*b*) that $d\sigma \sim \frac{1}{2}(H_{12}^2 + H_{21}^2)$. The result is

$$\left(\frac{d\sigma}{d\Omega}\right) = \frac{r_0^2}{4\beta\varepsilon^2} \frac{\beta^2 \sin^2\theta}{(1-\beta^2\cos^2\theta)^2} [\varrho_1^2 + \varrho_3^2 \cos^2\theta] . \tag{21a}$$

Summing over photon polarizations, one has

$$\left(\frac{d\sigma}{d\Omega}\right)_{ar} = \frac{r_0^2}{2\beta\varepsilon^2} \frac{\beta^2 \sin^2\theta(1+\cos^2\theta)}{(1-\beta^2\cos^2\theta)^2} . \tag{21b}$$

From these equations we see that at low energies the annihilation takes place with spins opposed, while at high energies annihilation with parallel spins predominates. In both cases the γ-rays tend to be cross polarized. Note, however, that for $\theta = 0$, $(d\sigma/d\Omega)_{par} = 0$. This feature has been used experimentally to measure the longitudinal polarization of positrons in β-decay ([5]).

3·2.2. Circular polarization. – For the case of antiparallel longitudinal spins, the cross-section as derived from eq. (14) is $d\sigma \sim (H_0^2 + H_z^2 + 2iH_0H_z) = (1/\varepsilon^2)[\mp \varrho_0 + \beta(\varrho_2 + \varrho_3 \sin^2\theta)]^2$, where the upper sign refers to the case where the positron spin is in the $+z$ direction, and is just H_{22}^2 of eqs. (18). The four cases are then

$$\begin{cases} d\sigma_{RR} \sim (1-\beta^2)(1 \mp \beta)^2 , \\ d\sigma_{LL} \sim (1-\beta^2)(1 \pm \beta)^2 , \\ d\sigma_{RL} \sim (1-\beta^2)\beta^2 \sin^4\theta , \\ d\sigma_{LR} \sim (1-\beta^2)\beta^2 \sin^4\theta , \end{cases} \tag{22}$$

where the upper and lower signs refer to positron spin in the positive and negative z directions, respectively. For positrons polarized in the positive z direction the ratio of right circular polarization (RCP) to left circular polarization (LCP) for photons $\boldsymbol{k}_1$ and $\boldsymbol{k}_2$ is given by

$$\begin{matrix} \text{RCP} \\ \text{LCP} \end{matrix} \quad \frac{(1-\beta)^2 + \beta^2 \sin^4\theta}{(1+\beta)^2 + \beta^2 \sin^4\theta} ,$$

from which we see that at low energies ($\beta \to 0$) the photons are unpolarized, while at high energies these photons are mainly LCP. The reverse is true if

([5]) See for example: S. FRANKEL, P. G. HANSEN, O. NATHAN and G. M. TEMMER *Phys. Rev.*, **108**, 1099 (1957).

the positron is polarized in the negative z direction. These results are illustrated in Fig. 2 where we see that photon $\boldsymbol{k}$ tends to pick up the spin of the particle whose momentum is nearly parallel to $\boldsymbol{k}$.

(*a*) Positive positron spin, H_{22} (*b*) Negative positron spin, H_{11}

Fig. 2. – Circular-polarization correlations at high energy for antiparallel-longitudinal spin. Case (*a*) with positive positron spin corresponds to matrix element H_{22}, and Case (*b*) corresponds to H_{11}. Two values of θ are illustrated: one less than $\pi/2$ and one greater than $\pi/2$. In practice $\boldsymbol{k}_1$ and $\boldsymbol{k}_2'$ are undistinguishable. The solid arrows designate the spin directions of the electrons and positrons.

For the case of parallel-longitudinal spins, the cross-section as derived from eq. (14) is $\mathrm{d}\sigma \sim (H_x^2 + H_y^2 \pm 2iH_xH_y) = \beta^2 \sin^2\theta(\varrho_1 \mp \varrho_3 \cos\theta)^2$, where the upper sign again refers to a positron with spin in the positive z direction and is just H_{12}^2 of eqs. (18). The four cases are then

$$\text{(24)} \qquad \begin{cases} \mathrm{d}\sigma_{RR} = \mathrm{d}\sigma_{LL} = 0\,, \\ \mathrm{d}\sigma_{RL} = \beta^2 \sin^2\theta(1 \pm \cos\theta)^2\,, \\ \mathrm{d}\sigma_{LR} = \beta^2 \sin^2\theta(1 \mp \cos\theta)^2\,. \end{cases}$$

For positrons polarized in the positive z direction, the ratio of polarizations of photons $\boldsymbol{k}_1$ is given by

$$\frac{\mathrm{RCP}}{\mathrm{LCP}} = \frac{(1 \pm \cos\theta)^2}{(1 \mp \cos\theta)^2}\,,$$

and for photon $\boldsymbol{k}_2$, by the inverse. Since $\boldsymbol{k}_1$ for $\theta < \pi/2$ and $\boldsymbol{k}_2$ for $\theta > \pi/2$ are undistinguishable, if we look at the photon for angles $0 < \theta < \pi/2$, then the ratio at high energies becomes

$$\text{(25)} \qquad \frac{\mathrm{RCP}}{\mathrm{LCP}} = \frac{(1 + \cos\theta)^2}{(1 - \cos\theta)^2}\,,$$

and we see that these photons are predominately right circularly polarized.

These results are illustrated in Fig. 3, where again the photon tends to pick up the spin of the particle whose momentum is parallel with the photon.

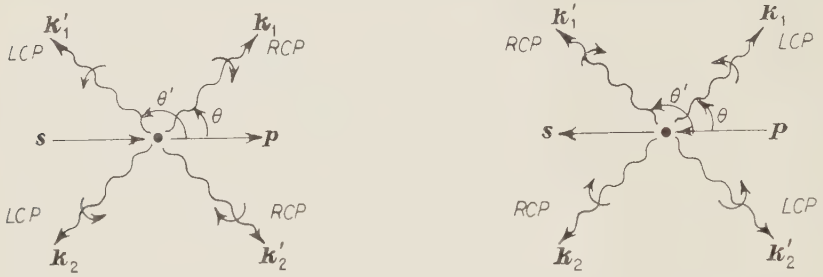

(*a*) Positive positron spin, H_{12} (*b*) Negative positron spin, H_{12}

Fig. 3. – Circular-polarization correlations at high energy for parallel-longitudinal spin

Many times an experiment will be conducted with just one of the particles polarized. We will discuss two such cases ([3]): *a*) A polarized positron beam incident on an unpolarized electron target. This type of experiment might be done to study positron polarization in β-decay when parity is not conserved *b*) An unpolarized positron beam incident upon a polarized electron target, where the electrons are aligned by a magnetic field either parallel or anti-parallel to the positron's momentum. In both cases we will limit observation to the higher-energy photon in the direction of the positron's momentum.

For the case of the polarized positrons incident on unpolarized electrons, let the positrons be polarized in the negative z direction, which covers the case of polarized positrons from β-decay. Then the cross-section is given by eq. (14) as $\mathrm{d}\sigma \sim H_0^2 + H^2 + 2iH_0H_z - 2iH_xH_y$, or from eq. (18) as $\mathrm{d}\sigma \sim H_{11}^2 + H_{21}^2$; that is,

$$\mathrm{d}\sigma \sim (1-\beta^2)(\varrho_0 + \beta\varrho_2 + \beta\varrho_3 \sin^2\theta)^2 + \beta^2 \sin^2\theta(\varrho_1 + \varrho_3 \cos\theta)^2 .$$

The four cases are then

$$(26) \qquad \begin{cases} \mathrm{d}\sigma_{RR} \sim (1-\beta^2)(1+\beta)^2 , \\ \mathrm{d}\sigma_{LL} \sim (1-\beta^2)(1-\beta)^2 , \\ \mathrm{d}\sigma_{RL} \sim (1-\beta^2)\beta^2 \sin^4\theta + \beta^2 \sin^2\theta(1-\cos\theta)^2 , \\ \mathrm{d}\sigma_{LR} \sim (1-\beta^2)\beta^2 \sin^4\theta + \beta^2 \sin^2\theta(1+\cos\theta)^2 . \end{cases}$$

Observing the high energy photon means we are restricting ourselves to $\boldsymbol{k}_1$ when $\pi/2 < \theta < \pi$, and $\boldsymbol{k}_2$ when $0 < \theta < \pi/2$. Let us then redefine the angle θ

as being the angle between the direction of motion of the positron and the observed photon ($0 < \theta < \pi/2$). The polarization ratio is then determined from eqs. (26) as

$$\frac{\mathrm{RCP}}{\mathrm{LCP}} = \frac{(1-\beta^2)\,[(1+\beta)^2 + \beta^2 \sin^4\theta] + \beta^2 \sin^2\theta(1+\cos\theta)^2}{(1-\beta)^2\,[(1-\beta)^2 + \beta^2 \sin^4\theta] + \beta^2 \sin^2\theta(1-\cos\theta)^2}\,, \tag{27}$$

from which we see that at all energies the observed photons are predominantly RCP. This process is shown in Fig. 4*a*.

(*a*) Polarized positrons, unpolarized target

(*b*) Unpolarized positrons, polarized target

Fig. 4. – Circular polarization produced by high-energy positron annihilation-in-flight when one of the particles is unpolarized.

When the target electrons are polarized in the positive z direction and the incident positrons are unpolarized, then the cross section is given by eq. (14) as $\mathrm{d}\sigma \sim H_0^2 + H^2 + 2iH_6H_z + 2iH_xH_y$, or from eqs. (18) as $\mathrm{d}\sigma \sim H_{11}^2 + H_{12}^2$, that is

$$\mathrm{d}\sigma \sim (1-\beta^2)(\varrho_0 + \beta\varrho_2 + \beta\varrho_3 \sin^2\theta)^2 + \beta^2 \sin^2\theta(\varrho_1 - \varrho_3 \cos\theta)^2\,.$$

The four cases are then

$$\begin{cases} \mathrm{d}\sigma_{RR} \sim (1-\beta^2)(1+\beta)^2\,, \\ \mathrm{d}\sigma_{LL} \sim (1-\beta^2)(1-\beta)^2\,, \\ \mathrm{d}\sigma_{RL} \sim (1-\beta^2)\beta^2 \sin^4\theta + \beta^2 \sin^2\theta(1+\cos\theta)^2\,, \\ \mathrm{d}\sigma_{LR} \sim (1-\beta^2)\beta^2 \sin^4\theta + \beta^2 \sin^2\theta(1-\cos\theta)^2\,. \end{cases} \tag{28}$$

Again we shall restrict ourselves to observing the high-energy photon in the lab system, and thus redefine the angle θ as before. The polarization ratio is then determined from eqs. (28) as

$$\frac{\mathrm{RCP}}{\mathrm{LCP}} = \frac{(1-\beta^2)\,[(1+\beta)^2 + \beta^2 \sin^4\theta] + \beta^2 \sin^2\theta(1-\cos\theta)^2}{(1-\beta^2)\,[(1+\beta)^2 + \beta^2 \sin^4\theta] + \beta^2 \sin^2\theta(1+\cos\theta)^2}\,, \tag{29}$$

from which we see that at $\beta = 0$ the photons are unpolarized, at high energies they are LCP, and for an intermediate range they are RCP. This process is shown in Fig. 4*b*.

3·3. *Transverse spins.*

3·3.1. General. – Let us now consider the case where the electron and positron are polarized transverse to the direction of motion at azimuthal angles ω_1 and ω_2 from the x axis. Then, recalling eqs. (A.14), we find that eq. (14) becomes:

$$(30a)\quad \frac{\mathrm{d}\sigma}{\mathrm{d}\Omega}\sim H_0+H^2+(H_0^2-H^2)(\cos\omega_1\cos\omega_2+\sin\omega_1\sin\omega_2)+2H_x^2\cos\omega_1\cos\omega_2+ \\ +2H_y^2\sin\omega_1\sin\omega_2-iH_0(H_x^*-H_x)(\cos\omega_1-\cos\omega_2)\,,$$

where we have utilized the values of ϱ given in Table I to eliminate those terms that are alway zero. Thus,

$$(30b)\quad \frac{4\beta\varepsilon^2(1-\beta^2\cos^2\theta)^2}{r_0^2}\frac{\mathrm{d}\sigma}{\mathrm{d}\Omega}=H_0^2\cos^2\left(\frac{\omega_1-\omega_2}{2}\right)+H_x^2\cos^2\left(\frac{\omega_1+\omega_2}{2}\right)+ \\ +H_y^2\sin^2\left(\frac{\omega_1+\omega_2}{2}\right)+H_z^2\sin^2\left(\frac{\omega_1-\omega_2}{2}\right)-\frac{iH_0}{2}(H^*-H_x)(\cos\omega_1+\cos\omega_2)\,,$$

where the last term is non-zero only for the circular-polarization description when it becomes $(\beta^2/\varepsilon)\varrho_1\varrho_3\sin^3\theta(\cos\omega_1+\cos\omega_2)$. If one averages over photon spins, then only the first four terms remain and lead to Page's [3] formula

$$(31)\quad \frac{\mathrm{d}\sigma}{\mathrm{d}\Omega}\sim\sin^2\left(\frac{\omega_1-\omega_2}{2}\right)+\beta^2(1+\sin^4\theta)\cos^2\left(\frac{\omega_1-\omega_2}{2}\right)+ \\ +\beta^2\varepsilon^2\sin^2\theta\left[\cos^2\left(\frac{\omega_1+\omega_2}{2}\right)+\cos^2\theta\sin^2\left(\frac{\omega_1+\omega_2}{2}\right)\right].$$

For antiparallel spins, $\omega_1-\omega_2=\pi$, we have

$$(32a)\quad \left(\frac{\mathrm{d}\sigma}{\mathrm{d}\Omega}\right)_{\mathrm{opp}}\sim(1-\beta^2)+\beta^2\sin^2\theta[\sin^2\omega_1+\cos^2\theta\cos^2\omega_2]\,,$$

and for parallel spins, $\omega_1=\omega_2$, we have

$$(32b)\quad \left(\frac{\mathrm{d}\sigma}{\mathrm{d}\Omega}\right)_{\mathrm{par}}\sim\beta^2(1-\beta^2)(1+\sin^4\theta)+\beta^2\sin^2\theta[\cos^2\omega_1+\cos^2\theta\sin^2\omega_1]\,.$$

From eqs. (32) we see that in the low-energy limit, $\beta=0$, the annihilation process occurs only for antiparallel spins, which agrees with that found for longitudinal spins.

A close look at eq. (30) shows that the forward γ-rays are unpolarized. The only polarization that can occur arises from the H_0^2 term, and in this case

the polarization is found to be in the plane of interaction with a maximum at $\theta = \pi/2$. This polarization is a maximum at low energies ($\beta \neq 0$) and decreases with increasing positron energy.

3·3.2. Polarization correlation when one particle is polarized. – Let us consider the case where one particle is polarized in the plane of annihilation, $\omega = 0$, and the other particle is unpolarized. Then from eq. (30*a*) we find that

$$\frac{\mathrm{d}\sigma}{\mathrm{d}\Omega} \sim H_2^0 + H^2 - iH_0(H_x^* - H_x)\,,$$

which states immediately that there is no plane polarization correlations, since $H_x^* - H_x$ in this description. If we conisder circular polarization, however, then we have

$$\frac{\mathrm{d}\sigma}{\mathrm{d}\Omega} \sim H_0^2 + H^2 + 2iH_\zeta H_x\,. \tag{33}$$

From this equation we find that the maximum polarization effect occurs for $\theta = \pi/2$, and if we define the degree of polarization in the usual manner as

$$P = \frac{\mathrm{d}\sigma_R - \mathrm{d}\sigma_L}{\mathrm{d}\sigma_R + \mathrm{d}\sigma_L}\,, \tag{34}$$

where $\mathrm{d}\sigma_R = \frac{1}{2}(\mathrm{d}\sigma_{RR} + \mathrm{d}\sigma_{RL})$ and $\mathrm{d}\sigma_L = \frac{1}{2}(\mathrm{d}\sigma_{LL} + \mathrm{d}\sigma_{LR})$, then one finds

$$P = \frac{2\beta}{[1 + 2\beta^2(1 - \beta^2)]}\,, \tag{35}$$

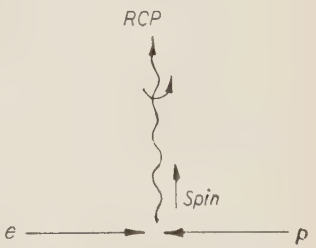

Fig. 5. – Annihilation when one of the particles is transversely polarized. The γ-ray given off in the direction of spin has the same helicity.

which states that the γ-ray is predominantly RCP and thus partakes in the helicity of the polarized particle. This situation is shown in Fig. 5.

On the other hand, if one of the particles is polarized perpendicular to the plane of annihilation, no polarization correlation exists.

4. – Matrix representation of the cross section.

If one uses the Stokes parameters to describe the polarization states of the electron and positron, then it is possible to write the annihilation cross-section

in matrix form ([6]). This form of the cross-section is very convenient for the description of the polarization phenomena in that the general features of the interaction are readily determined.

The initial particles are described by the two four-vectors

$$(36) \qquad \left(\frac{1}{\boldsymbol{S}}\right) = \begin{pmatrix} 1 \\ S_z \\ S_x \\ S_y \end{pmatrix} \quad \text{and} \quad \left(\frac{1}{\boldsymbol{P}}\right) = \begin{pmatrix} 1 \\ P_z \\ P_x \\ P_y \end{pmatrix}$$

for the electron and positron, respectively, where positive values of the components refer to spin in the positive z, x, and y directions. With this notation, eq. (14) can be written in the particularly simple form:

$$(37) \qquad \frac{\mathrm{d}\sigma}{\mathrm{d}\Omega} = \overbrace{1, \boldsymbol{S}}\, T \left(\frac{1}{\boldsymbol{P}}\right),$$

where

$$(38) \qquad T = \frac{r_0^2}{8\beta\varepsilon^2\,(1-\beta^2\cos^2\theta)^2} \cdot$$

$$\cdot \begin{pmatrix} H_0^2+H^2 & 2i(H_xH_y-H_0H_z) & 2iH_0H_x & 0 \\ 2i(H_0H_z+H_xH_y) & H^2-2H_z^2-H_0^2 & 0 & 0 \\ 2iH_0H_x & 0 & H_0^2-H^2+2H_x^2 & 0 \\ 0 & 0 & 0 & H_0^2-H^2+2H_y^2 \end{pmatrix}$$

for the description of circular-polarization states of the annihilation quanta, and

$$(39) \qquad T = \frac{r_0^2}{8\beta\varepsilon^2(1-\beta^2\cos^2\theta)^2} \cdot$$

$$\cdot \begin{pmatrix} H_0^2+H^2 & 0 & 0 & 0 \\ 0 & H^2-2H_z^2-H_0^2 & 2H_xH_z & 0 \\ 0 & 2H_xH_z & H_0^2-H^2+2H_x^2 & 0 \\ 0 & 0 & 0 & H_0^2-H^2+2H_y^2 \end{pmatrix}$$

for the description of plane-polarization states of the annihilation quanta.

([6]) W. H. MCMASTER: *Matrix Representation of Polarization*, University of California Radiation Laboratory Report UCRL-5496, 1959. (To be published in *Rev. Mod. Phys.*).

Appendix

Spin formalism.

The Dirac Equation, $(\boldsymbol{\alpha}\cdot\boldsymbol{p}+\beta-\varepsilon)u=0$ can be written in matrix form as

$$\begin{pmatrix} 1 & \boldsymbol{\sigma}\cdot\boldsymbol{p} \\ \boldsymbol{\sigma}\cdot\boldsymbol{p} & -1 \end{pmatrix} u = \varepsilon u \,. \tag{A.1}$$

Now let us write the four-component wave function in a form in which the two-component Pauli spinor v appears explicitly;

$$u = N\begin{pmatrix} v \\ y \end{pmatrix}, \tag{A.2}$$

where N is a normalization factor. With this notation, the Dirac equation reduces to the two equat ons

$$(\boldsymbol{\sigma}\cdot\boldsymbol{p})y + (1-\varepsilon)v = 0\,,$$

$$(\boldsymbol{\sigma}\cdot\boldsymbol{p})v - (1+\varepsilon)y = 0\,,$$

from which we find $y=(\boldsymbol{\sigma}\cdot\boldsymbol{p})v/(\varepsilon+1)$. The normalization, $u^*u=1$, determines the value of N, and we obtain our wave function in the form

$$u = \left(\frac{\varepsilon+1}{2\varepsilon}\right)^{\frac{1}{2}} \begin{pmatrix} 1 \\ \dfrac{\boldsymbol{\sigma}\cdot\boldsymbol{p}}{\varepsilon+1} \end{pmatrix} v(\boldsymbol{S})\,. \tag{A.3}$$

The Pauli spinor, $v(\boldsymbol{S})$, satisfies the spin equation for electrons:

$$(\boldsymbol{S}\cdot\boldsymbol{\sigma})\,v(\boldsymbol{S}) = v(\boldsymbol{S})\,,$$

whose solution specifies the spin direction of the electron through the equation

$$\frac{v_2}{v_1} = \operatorname{tg}\frac{\chi}{2}\exp[i\omega]\,,$$

where χ is the polar angle and ω the azimuthal angle. Thus a particular representation would be

$$v_0 = v(\boldsymbol{S}) = \begin{pmatrix} \cos\frac{\chi}{2}\exp[-i\omega] \\ \sin\frac{\chi}{2} \end{pmatrix} \tag{A.4}$$

from which we find the particularly useful forms

$$v_0^+ = \begin{pmatrix} 1 \\ 0 \end{pmatrix} \qquad \text{and} \qquad v_0^- = \begin{pmatrix} 0 \\ 1 \end{pmatrix}$$

for spins in the positive and negative z directions, respectively; that is, the electron is said to have a positive longitudinal spin (right helicity) when the spin and momentum vectors are parallel.

The Pauli spinor can be written in forms that display the three components of the spin explicitly; *i.e.*,

$$v(\boldsymbol{S}) = [2(1+S_z)]^{-\frac{1}{2}} \begin{pmatrix} 1+S_z \\ S_x + iS_y \end{pmatrix} \tag{A.5}$$

for positive spin directions, and

$$v(\boldsymbol{S}) = [2(1-S_z)]^{-\frac{1}{2}} \begin{pmatrix} S_x - iS_y \\ 1-S_z \end{pmatrix}$$

for negative spin directions. In addition to the normalization equation $v_0^* v_0 = 1$, one obtains the projection operator

$$v_0 v_0^* = \tfrac{1}{2}(1 + \boldsymbol{S}\cdot\boldsymbol{\sigma}) \tag{A.6}$$

from the adjoint equation

$$v_0^*(\boldsymbol{S}\cdot\boldsymbol{\sigma}) = -v_0^* .$$

From these spinors it is found that

$$v_0^* \boldsymbol{\sigma} v_0 = \boldsymbol{S} . \tag{A.7}$$

The negative energy state of the electron, *i.e.*, the positron, satisfies the Dirac equation with the signs of the energy, momentum, and spin changed [7]; *i.e.*,

$$(-\boldsymbol{\alpha}\cdot\boldsymbol{p} + \beta + \varepsilon)u = 0 , \tag{A.8}$$

---

[7] S. S. SCHWEBER, H. A. BETHE and F. DE HOFFMANN: *Mesons and Fields*, vol. 1 (New York, 1955), p. 142.

which has the solution

$$u = \left(\frac{\varepsilon - 1}{2\varepsilon}\right)^{\frac{1}{2}} \begin{pmatrix} 1 \\ \\ \dfrac{\boldsymbol{\sigma}\cdot\boldsymbol{p}}{\varepsilon - 1} \end{pmatrix} v(-\boldsymbol{S}) , \tag{A.9}$$

where the Pauli spinor now satisfies the spin equation

$$(\boldsymbol{S}\cdot\boldsymbol{\sigma})\, v(-\boldsymbol{S}) = -\, v(-\boldsymbol{S}) . \tag{A.10}$$

This leads to the result that

$$v^{*}\boldsymbol{\sigma} v = -\boldsymbol{S} , \tag{A.11}$$

where again S_z is positive when it is parallel to the momentum. For the case of positron annihilation under discussion, we have chosen the positron to move in the negative z direction; therefore, we must change the sign of $\boldsymbol{p}$ and $\boldsymbol{S}$ above so that eqs. (A.9) and (A.11) become,

$$u = \left(\frac{\varepsilon - 1}{2\varepsilon}\right)^{\frac{1}{2}} \begin{pmatrix} 1 \\ \\ \dfrac{-\boldsymbol{\sigma}\cdot\boldsymbol{p}}{\varepsilon - 1} \end{pmatrix} v(\boldsymbol{S}) , \tag{A.12}$$

and

$$v^{*}\boldsymbol{\sigma} v = \boldsymbol{S} . \tag{A.13}$$

The solutions of the spin equa ion are then given by eqs. (A.5); we must now recall, however, that $S_z - 1$ means spin in the negative z direction. Thus we find that now

$$v^{+} = \begin{pmatrix} 0 \\ 1 \end{pmatrix} \qquad \text{and} \qquad v^{-} = \begin{pmatrix} 1 \\ 0 \end{pmatrix}$$

are the particular solutions for positron spins in the positive and negative z directions, respectively.

Since most of our interest will center around longitudinal spins, let us now respecify the positron's spin vector so that the sign of the longitudinal spin will be explicit, *i.e.*, $\boldsymbol{P} = -\boldsymbol{S}$, *i.e.*,

$$\begin{cases} P_x = -\sin\chi\cos\omega , \\ P_y = -\sin\chi\sin\omega , \\ P_z = \cos\chi . \end{cases} \tag{A.14}$$

Equation (A.13) then becomes

$$v_0^* \boldsymbol{\sigma} v = -\boldsymbol{P}. \tag{A.15}$$

RIASSUNTO (*)

Si presenta un metodo per risolvere l'equazione di Dirac per l'annichilazione dei positroni, usando gli spinori di Pauli in modo da conservare tutte le caratteristiche della polarizzazione. Si discutono diversi esempi specifici delle caratteristiche di polarizzazione, ed infine l'equazione di annichilazione viene scritta in forma di matrice per usarla con i parametri di Stokes. Quest'ultima rappresentazione è particolarmente utile in quanto rivela le caratteristiche generali del processo di annichilazione.

(*) *Traduzione a cura della Redazione.*

IL NUOVO CIMENTO Vol. XVII, N. 3 1° Agosto 1960

Non-Spontaneous Disintegration of Hypernuclei in Flight (*) (**).

H. Neumann and H. S. Valk (***)

Department of Physics, University of Oregon - Eugene, Oreg.

(ricevuto il 26 Aprile 1960)

Summary. — On the basis of a binary model, expressions are obtained for the probability of hypernuclear disintegration in flight. Numerical calculations for 50 MeV $^5He_\Lambda$ slowing in liquid hydrogen, oxygen, and xenon indicate that such processes are most prevalent for medium-Z media. Of the two processes considered, stripping and electric dissociation, the former appears to dominate in the medium- and large-Z range.

1. – Introduction.

The expansion of programs to observe hypernuclei in bubble chambers makes it interesting to study theoretically some of the less frequent hypernuclear processes. The recent, successful treatment of many hypernuclei as lightly-bound, binary associations [1] of a Λ_0-hyperon and a nuclear core implies that such associations can be disintegrated in flight. As in the case of the deuteron, the two dominant disintegration processes are stripping and electric dissociation. These processes both produce free hyperons, whose subsequent spontaneous decays are observable. The tracks of the freed hypernuclear cores, which will retain most of the initial kinetic energy of the hyper-

(*) A preliminary report of this work was given at the Los Angeles meeting of the American Physical Society, H. Neumann and H. S. Valk: *Bull. Am. Phys. Soc.*, Ser. II, **3**, 402 (1958).

(**) This paper is based on a thesis submitted to the Graduate School, University of Oregon, by H. Neumann in partial fulfilment of the requirements for the degree of Master of Arts.

(***) Temporary address: National Science Foundation, Washington 25, D.C.

(1) R. H. Dalitz and B. W. Downs: *Phys. Rev.*, **111**, 967 (1958).

nuclei, should also be visible. In this paper we obtain expressions for the cross-sections for these phenomena. In order to estimate the efficiency of various bubble chamber liquids in producing such events, we consider in detail the example of a 50 MeV $^5He_\Lambda$ slowing in liquid hydrogen, oxygen, and xenon and compare its rate of disintegration in flight with its spontaneous decay rate.

2. – Binary hypernuclear model.

Among the possibilities for the origin of the Λ_0-nucleon force are *a*) the exchange of two pions (corresponding to a Yukawa potential with a range of .71 fermi), *b*) the exchange of a K-meson (range, .40 fermi), and *c*) the exchange of combinations of K-mesons and pions. In the present paper we employ *b*). Since we limit our attention to low-energy disintegrations (within an energy range for which an effective range theory is valid), the choice is not critical.

For definiteness we treat $^5He_\Lambda$, although the methods can be generalized. The hypernucleus $^5He_\Lambda$ is one of the most frequently observed ([2]), and the tight binding of its core is especially favorable to the binary assumption.

If we assume that both the triplet and the single Λ_0-nucleon potentials have the same shape function, $v(\boldsymbol{r})$, the average potential for the Λ_0 over $A-1$ core nucleons is ([1])

$$u(\boldsymbol{R}) = V\int v(|\boldsymbol{R}-\boldsymbol{R}'|)\,\varrho(\boldsymbol{R}'/R_c)\,\mathrm{d}\boldsymbol{R}'\,, \tag{1}$$

where V is the volume integral of the Λ_0 interaction with the core and $\varrho(\boldsymbol{R}'/R_c)$ is the density of nucleons in the core. According to electron scattering experiments ([3]), the density function can be taken as a Gaussian, with root-mean-square radius $R_c = 1.44$ fermi, for ^{4}He. However, because the Λ_0 is presumably in the hypernucleus in a $(1s)$ orbital, it should bind the core more tightly than in free ^{4}He. The effect is to reduce R_c by a small amount, taken to be six per cent ([1]). To evaluate (1) the Yukawa Λ_0-nucleon potential is replaced with an equivalent Gaussian, by use of effective range theory ([4]). The interaction $u(\boldsymbol{R})$ thus becomes a Gaussian, with r.m.s. radius 1.54 fermi.

For the electric dissociation calculation, it is more convenient to take the interaction between the Λ_0 and the core in the form of a square well.

([2]) W. F. Fry: *Ann. Rev. Nucl. Sci.*, **8**, 105 (1958).

([3]) R. Hofstadter: *Ann. Rev. Nucl. Sci.*, **7**, 231 (1957).

([4]) J. M. Blatt and V. F. Weisskopf: *Theoretical Nuclear Physics* (New York, 1952), p. 56.

Applying effective range theory again, we find that the radius of the equivalent square well is $R_0 = 1.80$ fermi. The binding energy of the Λ_0 to the ^{4}He core is taken to be 2.9 MeV (1). From the usual two-particle square well quantum condition, the well depth is then found to be $V_0 = 28.0$ MeV.

3. – Stripping.

The most obvious nuclear reaction that leads to the production of free hyperons is stripping, in which the hypernuclear core strikes a target nucleus and the hyperon continues on. The reverse situation, in which the hyperon strikes the target and the core does not, will probably lead to another hypernucleus. If the entire hypernucleus collides with the target at the high kinetic energies of interest in the present paper, the target will become highly excited. If a hyperon is torn loose in this last process, it will probably knock out a fragment from the target and become attached to it (5).

To obtain an estimate, we assume that the stripping cross-section σ_s is the product of the probability P that an incident core strike the target while the hyperon miss and the cross-section σ_c for compound nucleus formation by the core and target, so that $\sigma_s = P\sigma_c$. This semiclassical model (6) really requires that the collision take place in a time short compared with the oscillation period of the hypernuclear system. Since this condition is not well met at the kinetic energies considered here, we assume that our results give only an upper limit for the cross-section (*).

The probability P can be computed from geometrical considerations and is given by

$$(2) \qquad P = 1 + (\varrho/\pi a)\,[1 - (\varrho/2a)^2]^{\frac{1}{2}} - (2/\pi)\,\sin^{-1}\,[1 - (\varrho/2a)^2]^{\frac{1}{2}} \sim 2\varrho/\pi a\,,$$

where a is the sum of the target and core radii and ϱ is the projection on the plane perpendicular to the projectile path of the vector $\boldsymbol{R}$ connecting the two segments of the hypernucleus. Let $\Psi(\boldsymbol{R})$ be the wave function for the binary hypernucleus. Then the probability averaged over all projections is

$$(3) \qquad P = (4/a)\int_0^\infty\int_{-\infty}^{\infty} \varrho^2\,|\Psi|^2\,\mathrm{d}z\,\mathrm{d}\varrho = (2\pi/a)\int_0^\infty R^3\,|\Psi|^2\,\mathrm{d}R = \bar{R}/2a\,,$$

(5) Such a mechanism seems to have been involved in the production of many of the hypernuclei that have been observed: E. M. Silverstein: *Suppl. Nuovo Cimento*, **10**, 41 (1958).

(6) K. Mather and P. Swan: *Nuclear Scattering* (Cambridge, 1958), pp. 354-359.

(*) We also neglect small diffractional effects such as those considered by A. I. Akhieser and A. G. Sitenko: *Phys. Rev.*, **106**, 1236 (1957).

where $\bar{R}$ is the mean separation of the hyperon and core (for $^5He_\Lambda$, computed to be 2.24 fermi). The location of the core relative to the target is undefined to approximately $\lambda\!\!\!^{-}$, the reduced wavelength of the core relative to the target. The estimate for P can be corrected approximately for this effect by replacing a with $a+\lambda\!\!\!^{-}$.

The cross-section for compound nucleus formation by ^4He projectiles on various targets is given by BLATT and WEISSKOPF ([7]).

4. – Electric dissociation.

The general theory for the electric dissociation of binary nuclear systems has been developed by DANCOFF ([8]), MULLIN and GUTH ([9]), and others ([10]). Here we follow MULLIN and GUTH and consider an interaction energy

$$V=\begin{cases} 0\,, & |\boldsymbol{r}|\leqslant r_0, \\ \sum_i \dfrac{Z_i Z e^2}{|\boldsymbol{r}-\boldsymbol{r}_i|} & |\boldsymbol{r}_i|\geqslant r_0, \end{cases} \tag{4}$$

where r_0 is the sum of the r.m.s. radius of the hypernucleus (for $^5He_\Lambda$, computed to be 2.71 fermi) and the ordinary radius of the target nucleus, eZ_i is the charge of the i-th hypernuclear segment, eZ is the target charge, $\boldsymbol{r}$ is the vector from the hypernuclear mass center to the target, and $\boldsymbol{r}_i$ is the vector from the hypernuclear mass center to the i-th hypernuclear charge. The interaction is cut off at r_0 to exclude direct interactions of the type considered in Section 3.

Since a multipole expansion of V converges rapidly, we retain only the dipole term, so that the cross-section per unit disintegration energy for electric dissociation of a binary hypernucleus described by a square well potential, as in Section 2, is ([9])

$$\frac{\mathrm{d}\sigma}{\mathrm{d}\varepsilon_1}=8\pi[\mu(Z_c/M_c)(Ze^2/\hbar v_1)]^2 B_1 F_1 F_2 \exp\left[2\pi(n_1-n_2)\right], \tag{5}$$

([7]) J. M. BLATT and V. F. WEISSKOPF: *Theoretical Nuclear Physics* (New York, 1952), p. 353.

([8]) S. M. DANCOFF: *Phys. Rev.*, **72**, 1017 (1947).

([9]) C. J. MULLIN and E. GUTH: *Phys. Rev.*, **82**, 141 (1951).

([10]) V. I. MAMASAKHLISOV and G. A. CHILASHVILI: *Soviet Physics. J.E.T.P.*, **5**, 661 (1957).

where

$$B_1 = f[2(k_1 + k_2)r_0] - f[2(k_1 - k_2)r_0]\,,$$

$$f(x) = Ci(x) - (\cos x - x \sin x - 1)/x^2\,,$$

$$Ci(x) = -\int_x^\infty s^{-1} \cos s \, \mathrm{d}s\,,$$

$$F_1 = [(4\hbar^2\beta^2 V_0 R_0^2/3\pi\mu(1 + \alpha R_0)][(\varepsilon_0\varepsilon_1)^{\frac{1}{2}}/(\varepsilon_0 + \varepsilon_1)^4]\,,$$

$$F_2 = (kR_0)^2\{(kR_0)^2[(\gamma R_0)\, j_0(\gamma R_0)/j_1(\gamma R_0)]^2 + \\ + [(kR_0)^2 - (\gamma R_0)\, j_0(\gamma R_0)/j_1(\gamma R_0)]^2\}^{-1}\,,$$

$$n_i = Z_c Z e^2/\hbar v_i\,, \qquad \alpha^2 = 2\mu\varepsilon_0/\hbar^2\,,$$

$$\beta^2 = 2\mu(V_0 - \varepsilon_0)/\hbar^2\,, \qquad \gamma^2 = 2\mu(V_0 + \varepsilon_1)/\hbar^2\,,$$

$$k^2 = 2\mu\varepsilon_1/\hbar^2\,,$$

$$r_0 = \left[4\pi\int_0^\infty R^4 |\Psi|^2 \, \mathrm{d}R\right]^{\frac{1}{2}} + 1.25\, A^{\frac{1}{3}} f\,.$$

Here k_1 and k_2 are the initial and final state relative propagation vectors between the target and the hypernuclear mass center; v_1 and v_2 are the corresponding relative speeds; Z_c and M_c are the charge and mass of hypernuclear core; μ is the reduced mass of the hyperon and core; ε_0 is the binding energy of the hyperon and the core; ε_1 is the relative energy after disintegration of these hypernuclear segments; and A is the atomic mass number of the target. To obtain the total cross-section, expression (5) must be integrated numerically.

The effect of using Coulomb wave functions rather than plane wave functions to describe the relative motion of the hypernucleus and the target is contained (in approximation) in the exponential factor in expression (5) [9]. The plane wave (Born) approximation consists in setting the exponential to unity; this yields an upper limit estimate for the cross-section.

5. – Numerical evaluation; discussion.

As hypernuclei traverse a detecting medium, they lose energy rapidly by ionizing the atoms of the medium (*). A sufficiently accurate expression for the slowing down time from an initial energy E_0 to an energy E (obtained by

(*) Elastic collisions may be neglected, since the cross section is small for light nuclei, and the energy loss per collision is small for heavy nuclei.

integrating the classical Bohr stopping power formula ([11])) is

$$(6)\qquad \begin{cases} t(E) = (m/4\pi Z_e^2 Z N e^4)(MI/4m)^{\frac{3}{2}}(2/M)^{\frac{1}{2}} G\,, \\ G = \overline{Ei}[(\tfrac{3}{2})\ln(4mE_0/MI)] - \overline{Ei}[(\tfrac{3}{2})\ln(4mE/MI)]\,, \end{cases}$$

where N is the atomic density of the medium, m is the electronic mass, M is the hypernuclear mass, I is a mean ionization energy for the atoms of the medium, taken to be $13.5Z$ eV, and the function contained in G is

$$\overline{Ei}(\ln x) = \int_0^x (\ln t)^{-1}\,\mathrm{d}t\,.$$

After the hypernuclei are degraded sufficiently in energy, they can decay only spontaneously, and at all energies considered in the present paper spontaneous disintegration is much more probable than non-spontaneous. Therefore the probability for a particular kind of non-spontaneous event relative to spontaneous disintegration, taken over the entire history of a hypernucleus in the medium in question, is

$$(7)\qquad N\int \exp[-t/\tau]\sigma v\,\mathrm{d}t\,,$$

where v is the hypernuclear speed at time t, σ is the appropriate cross-section and τ is the mean life-time for spontaneous disintegration (for ${}^5\mathrm{He}_\Lambda$, taken to be $1\cdot 10^{-10}$ s).

These calculations have been carried out for ${}^5\mathrm{He}_\Lambda$ hypernuclei degrading from a kinetic energy of 50 MeV to 10 MeV in three liquid media: hydrogen, oxygen, and xenon. Characteristics of the slowing down are given in Table I.

TABLE I. – *Characteristics of the slowing down of* ${}^5\mathrm{He}_\Lambda$ *from* 50 MeV *to* 10 MeV.

Stopping liquid	Density	Slowing down distance	Slowing down time $\cdot 10^{10}$
Hydrogen	.05 g/cm^{-3}	1.18 cm	3.57 s
Oxygen	1.15	.146	.436
Xenon	2.3	.148	.449

([11]) See, for example, E. FERMI: *Nuclear Physics* (Chicago, 1950), p. 30.

The stripping cross-sections and the electric dissociation cross-sections (both with and without the exponential factor) are presented in Table II.

TABLE II. – *Disintegration cross sections for* $^5He_\Lambda$.

Stopping liquid	Hydrogen		Oxygen			Xenon		
Energy (MeV)	σ_{epw} (mb)	σ_{ec} (mb)	σ_{epw} (mb)	σ_{ec} (mb)	σ_s (mb)	σ_{epw} (mb)	σ_{ec} (mb)	σ_s (mb)
10	0	0	1.14	~ 0	85	37	~ 0	~ 0
20	.014	.001	2.9	.60	128	47	.28	11
30	.066	.010	3.5	1.6	142	53	1.7	72
40	.10	.028	3.8	2.2	148	59	7.2	122
50	.12	.053	3.9	2.7	152	66	14	157

σ_{epw}: electric dissociation cross section, plane wave approximation.
σ_{ec}: electric dissociation cross section, Coulomb wave functions.
σ_s: stripping cross section.

The use of Coulomb wave functions is seen to be important even at energies several times the Coulomb barrier, $Z_C Ze^2/r_0$. In the case of stripping, this is partly due to the fact that as the projectile approaches the target, some of its energy is transferred into Coulomb field energy, and it becomes more difficult to transfer energy and momentum to the hypernuclear system. For both stripping and electric dissociation, Coulomb wave functions describe how the Coulomb field reduces the probability for close approaches, while plane wave functions do not.

The relative probabilities for the various disintegration events are listed in Table III.

TABLE III. – *Results of disintegration of* $^5He_\Lambda$.

Stopping liquid	Electric dissociation threshold	Electric dissociation probability (*) (plane wave approximation)	Electric dissociation probability (*) (Coulomb wave functions)	Stripping probability (*)
Hydrogen	17.8 MeV	$1.18 \cdot 10^{-6}$	$4.03 \cdot 10^{-7}$	—
Oxygen	3.84	$1.85 \cdot 10^{-5}$	$9.35 \cdot 10^{-6}$	$7.41 \cdot 10^{-4}$
Xenon	3.02	$7.25 \cdot 10^{-5}$	$7.04 \cdot 10^{-6}$	$1.16 \cdot 10^{-4}$

(*) Relative to spontaneous disintegration probability.

Several conclusions may be drawn: *a*) in the cases considered here, the relative disintegration probabilities are small, consistent with the fact that

such events have not been observed; *b*) stripping appears more likely than electric dissociation in those media in which the release of hyperons is most probable; *c*) non-spontaneous disintegration appears most probable for moderate-Z targets. For low-Z targets, the Coulomb field is too weak to produce many electric dissociation events, and the target nuclear size is too small to produce many stripping events. For high-Z targets, the Coulomb field makes close approaches relatively improbable. These conclusions are, of course, valid only for those hypernuclei for which the binary model is reasonable (where there is not severe distortion of the core or very strong binding of the hyperon to the core).

Although the relative probabilities for non-spontaneous events appear to be very small, it seems possible that increased use of short-radiation-length detectors and rapid scanning techniques could lead to their observation. The appearance of such Coulomb and stripping events would, of course, lend additional support to the credibility of the binary model for certain hypernuclei.

* * *

The authors would like to thank Mr. G. A. WILKINS for his aid with the calculations. One of us (H.S.V.) would also like to thank Drs. H. PRIMAKOFF and M. FRIEDLANDER for valuable comments.

RIASSUNTO (*)

Sulla base di un modello binario si ottengono alcune espressioni della probabilità della disintegrazione degli ipernuclei in volo. I calcoli numerici per $^5He_\Lambda$ da 50 MeV rallentato in idrogeno, ossigeno ed elio liquidi indicano che tali processi dominano maggiormente in mezzi con Z medio. Dei due processi considerati, lo stripping e la dissociazione elettrica, il primo sembra predominare nel campo dei Z medi e grandi.

(*) *Traduzione a cura della Redazione.*

On the Photonic Decay of the Hyperons.

L. Tenaglia

Istituto di Fisica dell'Università - Bari

(ricevuto il 26 Aprile 1960)

Summary. — We have evaluated the matrix element for the photonic decay of the hyperons: it is given as a function of the matrix element for the pion-photoproduction by nucleons. The results we have obtained (namely, the branching ratio between photonic and pionic decay of the hyperons) agree with the few experimental data known at present.

Three examples of photonic decay of hyperons (precisely, of the Σ^0-particle) have been recently found by Quareni [1] *et al.* who deduced from an approximate analysis of the events that the branching ratio R between photonic and pionic decay of the Σ^+-hyperon has the value $\approx 10^{-2}$.

The photonic decay rate has been evaluated in relativistic perturbation theory by Kawaguchi and Nishijima, by Iso and Kawaguchi and by Behrends [2]. The results obtained by these authors are sensibly different; they depend strongly on the nature of the interactions taken into account and do not give the experimental branching ratio R. Moreover, such results are not directly connected with the isotopic spin I and orbital angular momentum l states of the final system. An evaluation which should be more reliable, from a physical point of view, can be performed starting from the matrix elements of pion photoproduction which we know from the Chew-Goldberger-

---

[1] G. Quareni, A. Quareni-Vignudelli, G. Dascola and G. Mora: *Nuovo Cimento*, **5**, 1179 (1959).

[2] M. Kawaguchi and K. Nishijima: *Progr. Theor. Phys.*, **15**, 182 (1956); C. Iso and M. Kawaguchi: *Progr. Theor. Phys.*, **16**, 177 (1956); R. E. Behrends: *Phys. Rev.*, **111**, 1691 (1958).

2631

Low and Nambu analysis [3]. Such a procedure, used in the following evaluation, is not free from some objections, since it is necessary to extrapolate the CGLN matrix elements, which are in good agreement with the experimental data at low energies, to the higher energy values which appear in the intermediate states. In addition, the matrix elements for the pionic decay of the hyperons are not known for any values of I and l, a fact which turns out to be very important in the present case: the only (very scarce) information relative to such a process are also restricted to the low energy region.

For such reasons, in the following we shall be compelled to make some rough approximations. However, even a calculation of this kind leads to a correct order of magnitude for the branching ratio R and, moreover, it allows to single out the angular momentum l and isotopic spin I states for which we can presume that the decay ratios dominate.

The matrix element relative to the photonic decay of a hyperon, $\Upsilon \to \mathcal{N} + \gamma$, is given [4] by:

$$(1)\qquad \begin{cases} S_\nu = i\left(\dfrac{M}{Q_0}\right)^{\frac{1}{2}} (2\pi)^4 \delta(P + k - Q)\, \mathscr{M}_\nu\,, \\ \mathscr{M}_\nu = \dfrac{i}{(2k_0)^{\frac{1}{2}}} \int dy \exp\left[-iky\right] \langle N \,|\, T\big(j_\nu(y)\, I_\Upsilon(0)\big) \,|\, 0\rangle\, u_\Upsilon\,, \\ T\big(j_\nu(y)\, I_\Upsilon(0)\big) = [j_\nu(y), I_\Upsilon(0)]\vartheta(y) + I_\Upsilon(0)\, j_\nu(y)\,, \end{cases}$$

where P, k, Q stand for the energy-momentum of the nucleon, the photon and of the hyperon, respectively: T indicates the Wick ordered product; j_ν, I_Υ are the current densities, sources of the photonic and of the hyperonic fields.

With respect to that relative to the process $\Upsilon \to \mathcal{N} + \pi \to \mathcal{N} + \gamma$, all the other matrix elements are assumed to be negligible. As a matter of fact, it is difficult to estimate, in the present case, the relative orders of magnitude of the different matrix elements of which $\mathscr{M}_\nu$ is the sum. With the only aim to have a tentative comparison, we have performed a relativistic perturbative evaluation of the matrix element for the processes

$$(2)\qquad \Sigma^+ \to \mathcal{N} + \pi \to \mathrm{p} + \gamma\,,$$

$$(2')\qquad \Sigma^+ \to \Sigma'^+ + \gamma\,, \qquad \Sigma'^+ \to (\mathcal{N} + \overline{\mathcal{N}} + \mathcal{N}') \to (\pi + \mathcal{N}') \to \mathrm{p}$$

[3] G. F. Chew, M. L. Goldberger, F. E. Low and Y. Nambu: *Phys. Rev.*, **106**, 1345 (1958); in the following indicated by CGLN.

[4] ν indicates the polarization of the emitted photon, the electromagnetic potential of which is $\boldsymbol{A} = \boldsymbol{e}(2k_0)^{-\frac{1}{2}} \exp[ikx]$. We use natural units $\hbar = c = m_\pi = 1$.

and we have verified that, at least in this approximation, the matrix element for the process (2) is much bigger (by a factor > 10) than the matrix element for the process (2′).

Assuming to be sufficient to take into account only the process (2), one gets

$$(3) \qquad \mathscr{M}_\nu = (2\pi)^3 \sum \delta(\boldsymbol{P} + \boldsymbol{k} - \boldsymbol{P}_n)\,\delta_-(P_{0n} - P_0 - k_0)\langle N|j_\nu|n\rangle\langle n|I_Y|0\rangle u_Y\,.$$

The matrix element $\langle N|j_\nu|n\rangle$ is known, at least for small values of $|(P+k-P_n)|$, from the CGLN analysis. We can also write [5]

$$(4) \qquad \langle n|I_Y|0\rangle u_Y = \left(\frac{M}{2\omega p_0}\right)^{\frac{1}{2}} \sum_I \chi_{N_{nI}} \left(a_{sI} + ib_{pI}\frac{\boldsymbol{\sigma}\cdot\boldsymbol{q}}{a}\right)\chi_Y\,,$$

where χ stands for a Pauli spinor: a_{sI}, b_{pI} represent the amplitudes of the virtual states (in the center of mass system) relative to the eigenstates of orbital angular momentum $l=0$ and $l=1$ (in the present case only the states with angular momentum $J=\frac{1}{2}$ are possible).

Introducing the density of the intermediate states, as a function of the pion energy-momentum, the matrix element of eq. (4) becomes

$$(5) \qquad \mathscr{M}_\nu\varepsilon_\nu = \frac{i}{2(2\pi)^2}\sum_I \bar{\chi}_N\left[q\omega\,\delta_{\omega k_0} + \frac{\mathscr{P}}{\pi i}\int\frac{q^2\,\mathrm{d}q}{E' + \omega - k_0 - P_0}\right]\int \mathrm{d}\Omega\cdot$$

$$\cdot f^*(\boldsymbol{P},\boldsymbol{k},\boldsymbol{q})\frac{M}{p_0}\frac{1}{(2\omega)^{\frac{1}{2}}}\left(a_{sI} + ib_{pI}\frac{\boldsymbol{\sigma}\cdot\boldsymbol{q}}{q}\right)\chi_Y\,,$$

where $f(\boldsymbol{P},\boldsymbol{q},\boldsymbol{k})$ is the photoproduction matrix element. The following symbols are used:

$$\omega = (q^2+1)^{\frac{1}{2}}\,, \qquad E' = [M^2 + |\boldsymbol{P}+\boldsymbol{k}-\boldsymbol{q}|^2]^{\frac{1}{2}}\,, \qquad k_0' = k_0 + P_0 - E'\,;$$

Ω is the solid angle in the $\boldsymbol{q}$ space; $\mathscr{P}$ represents the Cauchy principal value.

In the CGLN analysis, the nucleon recoil is approximately taken into account in the photoproduction: in this approximation one gets

$$(6) \qquad \mathscr{M}_\nu\varepsilon_\nu \simeq \frac{i}{2(2\pi)^2}\sum_I \bar{\chi}_N\int\mathrm{d}\Omega\left[q\omega\,\delta_{\omega k_0''} + \frac{\mathscr{P}}{\pi i}\int\frac{\omega q\,\mathrm{d}\omega}{\omega - k_0 + 2\omega/M}\right] f^*(\boldsymbol{k},\boldsymbol{q})\cdot$$

$$\cdot\frac{M}{p_0(2\omega)^{\frac{1}{2}}}\cdot\left(a_{sI} + ib_{pI}\frac{\boldsymbol{\sigma}\cdot\boldsymbol{q}}{a}\right)\chi_Y\,,$$

with $k_0'' = \omega(1 + 2/M)$.

---

[5] R. P. Dalitz: *Phys. Rev.*, **105**, 605 (1958).

a_{sI} and b_{pI} are functions of ω and of $p_0 = (1+q^2/M^2)^{\frac{1}{2}}$: as a matter of fact, it is very difficult to determine with a good approximation the dependence of a_{sI} and b_{pI} on ω. This is important in connection to the renormalization corrections for the weak interaction coupling constants. In fact, $\mathcal{M}_\nu$ can be evaluated by means of dispersion relations, having taken into account only the matrix element relative to the process (2). A good knowledge of the quantities which appear in the higher order interactions would allow to evaluate the corrections to the Fermi interaction constants, both for the appearance of form factors and for the presence of induced terms (*e.g.* a *PS* interaction can arise from the $V-A$ theory, as it was proved by GOLDBERGER and TREIMAN) (6).

All these corrections are functions of the released energy-momentum, $(P_n - Q)^2$.

The assumption that a_{sI} and b_{pI} are constants is equivalent, in the evaluation of the branching ratio between the photonic and the pionic decay, to the hypothesis that such corrections have the same value both at the low energies for the pionic decay and at the high energies of the virtual states which occur in the matrix element (6). A rather approximate analysis, carried out by means of the Goldberger and Treiman (6) procedure, shows that a_{sI} and b_{pI} can strongly decrease at high values of the energy-momentum released, $(P_n - Q)^2$. It can be also observed that the CGLN photoproduction matrix element cannot be corrected at high values of $|P+k-P_n|$. In fact, if one evaluates the photoproduction cross-section with the preceding function $f(\boldsymbol{P}, \boldsymbol{q}, \boldsymbol{k})$ —including only $J=\frac{1}{2}$ states—one obtains a value which is increasing with the energy, in disagreement (*) with the experimental data. For this reason, in the evaluation of the matrix element (2), which involves divergent integrals, one must assume that the product $f^*(a_{sI}+b_{pI})$ tends to zero for $\omega > \omega_0$, where ω_0 is a convenient maximum energy. This can be accomplished by introducing a cut-off function and, with such approximation, one can take into account the decrease of the amplitudes a_{sI} and b_{pI} at high energies.

(6) M. L. GOLDBERGER and S. B. TREIMAN: *Phys. Rev.*, **110**, 1178 (1958); **111**, 354 (1958).

(*) In fact, from the values reported by CGLN one deduces that the photoproduction cross section, in the angular momentum state $J=\frac{1}{2}$, is a mixture of terms which are decreasing or constants with increasing q, and of terms of the type

$$\frac{q^5}{k\omega^2}, \qquad \frac{q^4}{\omega^2(\omega+\omega_p)},$$

which increase with q. They derive from those matrix elements which make divergent, in the present calculation, the integral over the intermediate states.

From the matrix element (6), keeping a_{sI} and b_{pI} constants, one gets:

$$\mathscr{M}_\gamma \varepsilon_\gamma = \sum_I (a_{sI}\alpha_I + b_{pI}\beta_I)\,. \tag{7}$$

The term $N^+(\omega)$, which does not give an appreciable contribution, has been omitted from the CGLN matrix elements $\mathscr{F}^+$, $\mathscr{F}^-$ and $\mathscr{F}^0$, the sum of which is $f(\boldsymbol{q}, \boldsymbol{k})$, aside from a factor 2π. One obtains in this way

$$\begin{cases} \alpha_I = \boldsymbol{\sigma}\cdot\boldsymbol{\epsilon}\left\{F(k'') + \dfrac{1}{\pi i}\displaystyle\int \frac{F(q)\,\mathrm{d}\omega}{\omega - k_0 + 2\omega/M}\right\}, \\ \beta_I = i\,\boldsymbol{\sigma}\cdot\boldsymbol{k}\times\boldsymbol{\epsilon}\left\{\mathscr{G}(k'') + \dfrac{1}{\pi i}\displaystyle\int \frac{\mathscr{G}(q)\,\mathrm{d}\omega}{\omega - k_0 + 2\omega/M}\right\}, \end{cases} \tag{8}$$

$$F(q) = fe q\omega/[2\omega(1 + q^2/M^2)]^{\frac{1}{2}}\left\{\left[\frac{2}{3}\,i(\delta_1 + \delta_3)\,F_s + q^2/3M\omega\right]J^- + \right.$$
$$\left. + \left[\frac{1}{1+\omega/M} - \frac{i}{3}(2\delta_1 + \delta_3)F_s - q^2/3M\omega\right]J^- + \left[q^2/6M\omega - \frac{g_P + g_N}{2M}\right]J^0\right\}. \tag{9}$$

In the function $F(q)$, only the terms proportional to the magnetic dipole transitions (that is, the terms proportional to $q^2/3M\omega$) diverges linearly, but, owing to the factor $(3M)^{-1}$, their contribution is small for $\omega < 6m_\pi$. The other factors are convergent or they diverge logarithmically: the value of ω_0 has not practical influence on them.

As far as $G(q)$ is concerned, it is very small: assuming, for its evaluation, $\omega_0 = 6m_\pi$ we have verified that the contribution of $G(q)$ is of the order of 10^{-3} with respect to the contribution of $F(q)$. We can also say that the choice of ω_0, in the present case, is not very critical; a variation $\Delta\omega_0 \simeq m_\pi$ does not alter sensibly the results.

For the sake of convenience we put

$$\alpha_I = -\,\boldsymbol{\sigma}\cdot\boldsymbol{\epsilon}\,3^{-\frac{1}{2}}\{[A_2^+ - A_3^+ + i(B_1^+ + B_3^+)]J^+ + [A_1^- + A_3^- + i(B_1^- + B_3^-)]J^- + i\,A^0 J^0\}\,, \tag{10}$$

$$\beta_I = -\,i\,\boldsymbol{\sigma}\cdot\boldsymbol{k}\times\boldsymbol{\epsilon}\,3^{-\frac{1}{2}}(C + iC^0)(J^+ + J^-)\,, \tag{11}$$

where the indices I in $A_I^\pm$, $B_I^\pm$, ... refer to the I isotopic spin states. The matrix element for the decay of the Σ^+-hyperon is given by

$$\mathscr{M}_{\Sigma^+,\mathrm{p}\gamma} = \mathscr{M}_{\Sigma^+,\mathrm{p}\pi^0\mathrm{p}\,\gamma} + \mathscr{M}_{\Sigma^+,\pi^+\mathrm{n},\mathrm{p}\gamma}\,. \tag{12}$$

The two processes contribute coherently to the decay: one can then write

$$3^{\frac{1}{2}}\mathscr{M}_{\Sigma^+,\mathrm{p}\gamma} = -\,\boldsymbol{\sigma}\cdot\boldsymbol{\epsilon}\{a_{s1}[2A_1^- + A_1^+ + i(2B_1^- + B_1^+ + 3A^0)] - \tag{13}$$
$$- 2^{\frac{1}{2}}a_{s3}\cdot[A_3^+ + A_3^- + i(B_3^+ - B_3^-)]\} - i\,\boldsymbol{\sigma}\cdot\boldsymbol{k}\times\boldsymbol{\epsilon}(C + iC^0)(3b_{p1} + 2^{-\frac{1}{2}}b_{p3})\,.$$

A not very different expression is obtained for the matrix element of the Σ^0 and Λ-decays. In the evaluation of the decay probabilities there appear four distinct amplitudes: notoriously, they cannot be determined from the mean lives only.

By putting

$$x = \frac{a_{s3}}{a_{s1}}, \qquad y_1 = \frac{b_{p1}}{a_{s1}}, \qquad y_2 = \frac{b_{p3}}{a_{s1}}, \qquad A^{-1} = 1 + x^2 + y_1^2 + y_2^2$$

we get, for the evaluated branching ratios,

$$(14) \qquad \begin{cases} R_{\Sigma^+} = 0.30 \cdot 10^{-2}(1 - 0.52x + 0.068x^2)A\,, \\ R_{\Sigma^0} = 0.29 \cdot 10^{-2}(1 - 0.51x + 0.065x^2)A\,, \\ R_{\Lambda} = 0.685 \cdot 10^{-2}(1 + 0.85x + 0.21\ x^2)A\,. \end{cases}$$

The sensible difference between R_{Σ^+}, R_{Σ^0} and R_{Λ} is due essentially to the much more limited value of the available energy, in the last case.

One can at last observe that many examples of pionic decay of the Λ have been already found, but no photonic decays have been observed up to now: on the contrary, the only photonic decay detected is the Σ^+-decay. Besides the experimental difficulties, it is obvious how a value $x \simeq 1$ can modify the branching ratio by a factor $\sim 7 \sim 8$ respect to the value at $x \simeq -1$. From this point of view, even if the relation (14) could be affected by an error of about 20%, it is always evident the clear difference of the behaviour of R_{Σ^+}, R_{Σ^0} and R_{Λ} with the variation of the sign of x, for $|x| \simeq 1$.

* * *

I am very glad to thank Prof. M. Cini and Prof. R. Gatto who kindly revised the draught of this elvaluation.

RIASSUNTO

Si calcola il rapporto fra la probabilità di decay fotonico e pionico degli iperoni. L'elemento di matrice pel decadimento fotonico è espresso in funzione di quello di fotoproduzione di pioni da nucleoni. I risultati ottenuti sono in buon accordo con i pochi dati sperimentali attualmente noti.

Triggered Spark Counter Arrays of Large Area (Square meters) for Experiments on Very High Energy Cosmic Ray Particles.

N. B. Mistry (*), G. T. Murthy, P. V. Ramana Murthy, and B. V. Sreekantan

Tata Institute of Fundamental Research - Bombay

(ricevuto il 23 Giugno 1960)

Summary. — The constructional and operational features of triggered spark counters of large area are described. These counters are being used, in conjunction with nuclear emulsions, in current experiments in this laboratory on high energy nuclear interacting particles which arrive simultaneously over large areas, sometimes associated and at other times unassociated with air showers. For these experiments the spark counters and emulsions are being used in arrays covering an area of a few square meters.

1. – Introduction.

Experiments are in progress in this laboratory to study in detail the frequency, multiplicity, energy distribution and lateral separation of high energy nuclear interacting p rticles associated and unassociated with extensive air showers. The frequency of these events is so low that it is necessary to have large detecting areas, of the order of several square meters, in order to record a sufficient number of events in a reasonable time of operation. Because of this requirement of a large area it is not practicable to use multiplate cloud chambers for a comprehensive investigation. In looking for an ideal detector that can give information on all the aspects mentioned above and which can be built economically to cover large areas, it was realized that this could be achieved with a suitable combination of spark counters and photographic

(*) Now at Columbia University, U.S.A.

emulsions (*). For this it would be necessary to construct large area spark counters in which a visible spark would be produced at the position at which a beam of extremely collimated charged particles passed through it. The set-up that was envisaged was the following. The nuclear interacting particles would interact in an absorber and produce a narrow jet of charged and neutral pions; the γ-rays resulting from the decay of the neutral pions would, on passing through a lead converter below, give rise to a collimated beam of electrons; the beam of electrons and mesons then passes through a thin horizontal layer of nuclear emulsions followed by a spark counter immediately below. If the spark counter produces a visible spark at the position at which the beam of particles passed through it, then the co-ordinates of the beam in the emulsions would be known; the number of electrons in the beam can be counted in the emulsion and the approximate size of the interaction determined; a system of two spark counters one below the other, would enable a determination of the direction of the jet and would also fix the co-ordinates in the emulsion more accurately; the occurrence of simultaneous parallel sparks would reveal the presence of multiple nuclear active particles; the system could be put in association with an extensive air shower (EAS) array and the size and core position of the associated shower determined; if the core of the EAS passed through the area of the spark counters, then a very precise location of the position of the core would be possible; it is obvious that this system would work only at very high energies where the particles would be produced with the necessary collimation. These very attractive features prompted a detailed experimental investigation on large area spark counters.

In the first instance a spark counter comprising a metal plate on one side and a set of parallel wires on the other was constructed with a sensitive area 50 cm $\times$ 27 cm and was operated with a continuous (D.C.) voltage. This counter had an excellent response to α-particles but there were two serious disadvantages. Firstly, there were quite a number of spurious spark breakdowns and secondly, the ozone produced as a result of the large corona discharge attacked all parts of the spark counter. To get over these disadvantages, an attempt was made to operate this type of counter on pulsed voltages. A polonium α-source was deposited on the plate of the spark counter and a mica window proportional counter fixed opposite to this source. The voltage was pulsed on the spark counter whenever on α-particle entered the proportional counter after passing through the gap of the spark counter. It was

(*) This system is, in principle, similar to the one reported by GRIGOROV *et al.* [1] who have used photographic emulsions in conjunction with ionisation chambers for the investigation of high energy interactions.

[1] S. I. BRIKKER, N. L. GRIGOROV, M. A. KONDRATEVA, A. V. PODGURSKAJA, A. I. SAVELEVA, V. A. SOBINJAKOV and V. Y. SESTOPEROV: *Suppl. Nuovo Cimento*, **2**, 733 (1958).

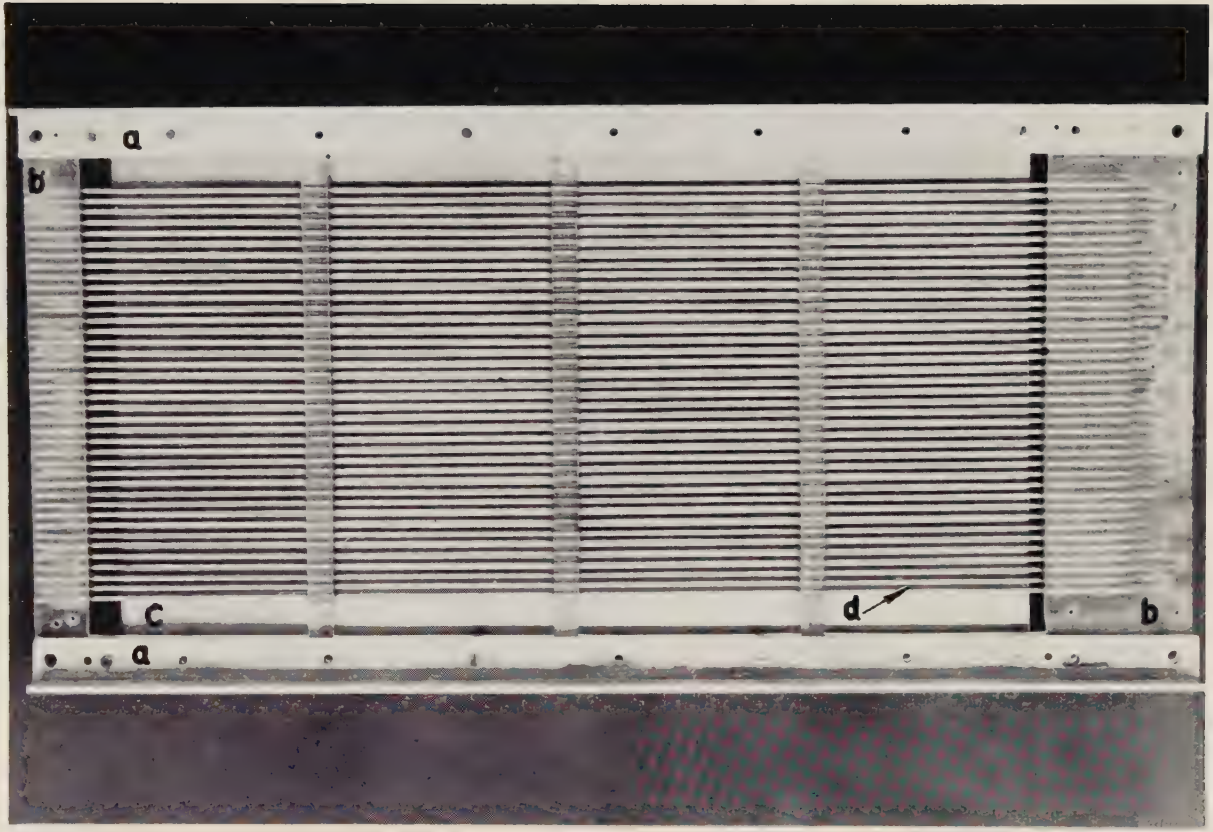

Plate I. – Photograph of a completely assembled spark counter: *a*) aluminium angles to keep the plastic frame straight; *b*) plastic frame 60 cm × 30 cm; *c*) stainless steel plate 50 cm × 30 cm × 3 mm; *d*) brass welding rods 58 cm long, 3 mm diameter.

found that with pulsed voltages the spark counter did not respond to α-particles. All possible parameters like spacing, wire diameter and clearing field, as also the amplitude, duration and rise time of the pulsed voltage etc., were tried but the response was still negative.

After considerable experimentation a design was evolved which met with all the requirements stated above and which was found most suitable from the point of view of construction and operation and also from the point of view of convenience in photographing the sparks. In this paper, are given the details regarding the constructional and operational features of such spark counters developed in this laboratory.

References to earlier work on spark counters are listed below ([2]).

2. – Constructional features.

Specially chosen cylindrical brass welding rods of good surface and linearity, each 60 cm long and 3 mm in diameter, are placed parallel to each other on a plastic frame 60 cm $\times$ 30 cm with a spacing of 3 mm between the rods; the rods are permanently stuck to the frame with araldite. Aluminium angles are fixed to the frame to keep it straight. A highly polished stainless steel plate of thickness 3 mm and of size 50 cm $\times$ 30 cm is treated with dilute hydrochloric acid to remove surface contamination and then washed and dried. This plate is fixed to the frame by means of 2 BA screws and nuts, with a spacing of about 3 mm between the rods and the plate; the spacing can be varied by changing the washers. A transparent plastic sheet is fixed over the frame to prevent dust from settling down in the gap of the spark counter. All the rods are connected together by wires. A photograph of the spark counter is given in Plate I.

3. – Operational features.

3·1. *Pulsing.* – The stainless steel plate is connected to earth and a negative voltage pulse whose amplitude could be varied from 2 to 5 kV, is applied to the rods whenever required. The rise time of the pulse is kept less than

---

([2]) W. Y. Chang and S. Rosenblum: *Phys. Rev.*, **67**, 22 (1945); A. Ryts: *Helv. Phys. Acta*, **22**, 1 (1949); R. D. Connor: *Proc. Phys. Soc.*, B **64**, 30 (1951); N. K. Saha and Narendra Nath: *Nucleonics*, **15**, 94 (June, 1957); M. J. Swetnick and N. G. Anton: *Nucleonics*, **15**, 93 (June, 1957); R. W. Pidd and L. Madansky: *Phys. Rev.*, **75**, 1175 (1949); J. W. Keuffel: *Rev. Sci. Instr.*, **20**, 202 (1949); E. Robinson: A **66**, 73 (1953); F. Bella and C. Franzinetti: *Nuovo Cimento, Proc. Phys. Soc.*, **10**, 1461 (1953); T. E. Cranshaw and J. F. de Beer: *Nuovo Cimento*, **5**, 1107 (1957).

0.05 μs to have a high efficiency of response, and the decay time kept of the order of one microsecond to minimize spurious breakdowns. The pulsing is done using a thyratron circuit similar to the one described by CRANSHAW and DE BEER (2). A low clearing field (~ 20 V) is maintained continuously between the rods and the plate for removing old ions; this helps in reducing spurious breakdowns. The counter is operated in complete darkness to minimize breakdowns due to photoelectric effects.

With a higher voltage of (10÷14) kV, obtained from a pulse-transformer, it is found that the same spark counter can be operated with a spacing ~ 6 mm, which is almost double the previous value of 3 mm. It is of importance to operate the spark counter with a larger spacing, since the requirement of uniformity of spacing is then less stringent. This makes it possible to build individual spark counters of very large area about half to one square meter.

3·2. *Photography.* – The chief advantage of this type of spark counter over parallel plate spark counters is the convenience and simplicity in the photography of the sparks. In parallel plate spark counters, the spark has to be necessarily photographed through the gap; for this the alignment of the cameras has to be very accurate, and also a very large depth of focus is involved. The latter requirement can be met by using pinhole apertures, but for this the intensity of the spark has to be very great. It is not desirable to increase the intensity of the spark, since the surface will be damaged and spurious breakdowns will be greater. For these reasons spark photography in parallel plate

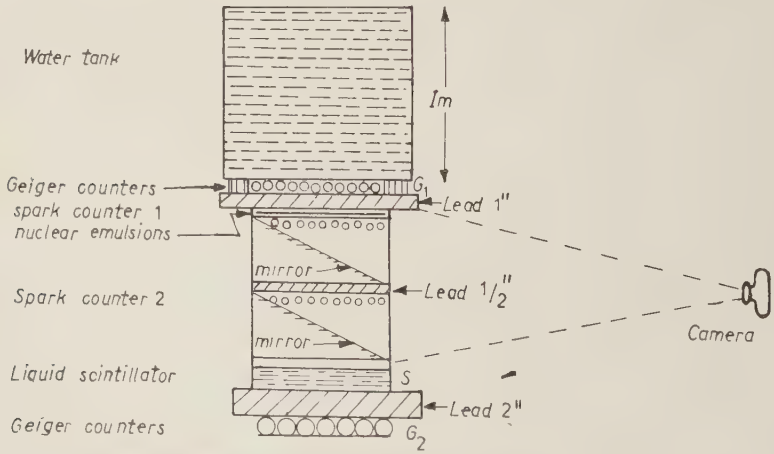

Fig. 1. – Experimental arrangement to test the feasibility of employing nuclear emulsions in conjunction with double spark counter array for the study of high energy jets. The coincidence $G_1 S G_2$ selects nuclear interactions produced mostly in the water tank. The lead plates above the spark counter are meant for the rapid development of the cascades. The direction and co-ordinates of the jets are given by the position of the sparks in the two spark counters.

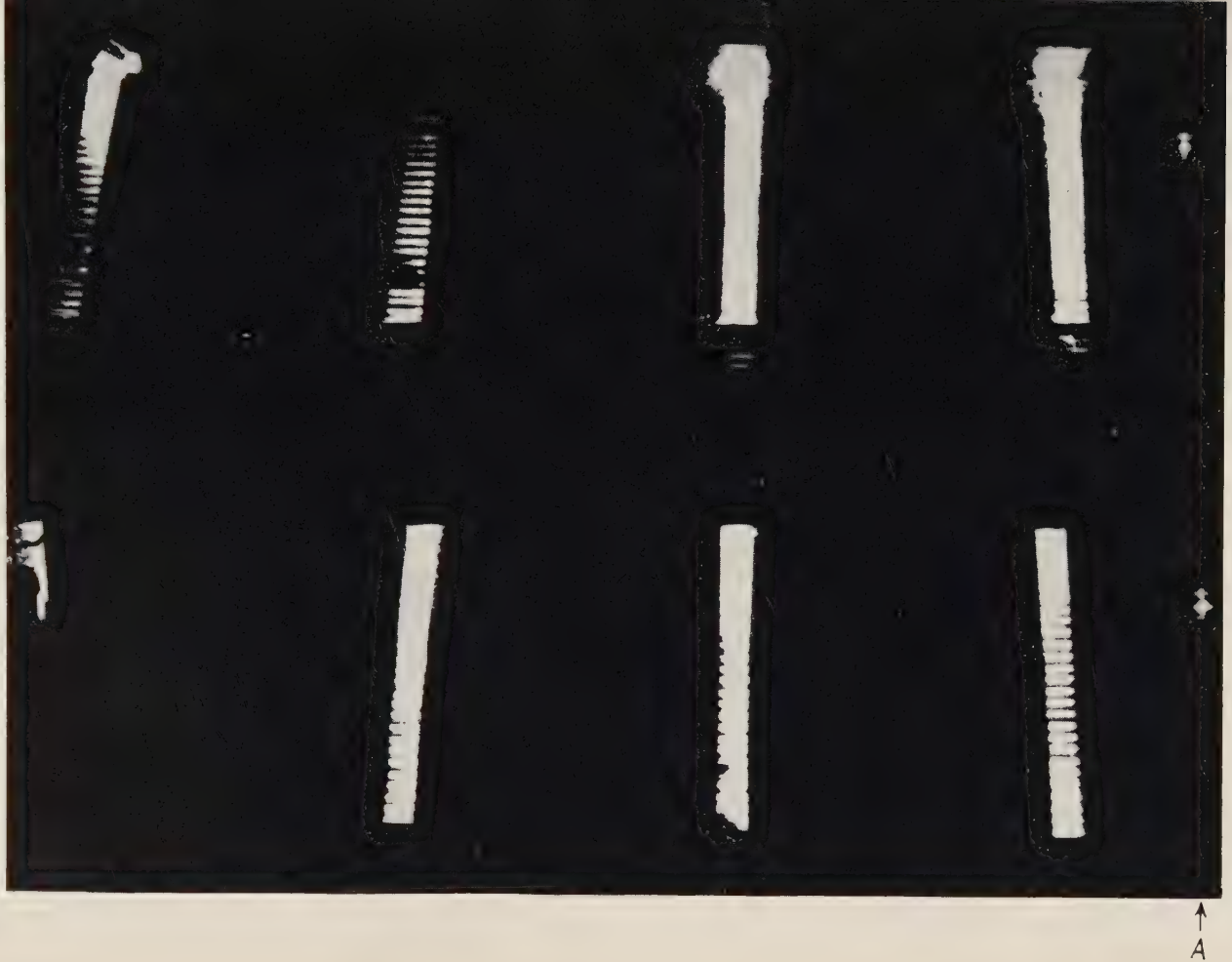

Plate II. – Photograph of a typical double spark event. The sparks have occurred (shown AA) in the right extreme compartment in both the counters. The bright strips seen in the photograph correspond to the portions of brass rods below the ribs of the plastic frame illuminated for a short time, immediately after photographing the sparks but before advancing the film. This serves as a convenient reference frame for locating sparks.

counters of large area poses very difficult technical problems. Moreover, to get the spatial co-ordinates accurately, stereoscopic photographs have to be taken, or else the sparks have to be photographed from two perpendicular directions. In the present spark counters the photography is done with just one camera and in a very simple way using a system of mirrors suitably inclined, as shown in Fig. 1.

The sparks can be located to an accuracy of (3 mm × 3 mm) which is sufficient for the experiments envisated. A typical photograph of a spark is shown in Plate II.

This type of photography using mirrors imposes one limitation, namely, if two spark counters are used one below the other, then the spacing between them cannot be reduced below a limit. However, this is not a serious disadvantage since a certain minimum spacing between the spark counters is essential for an accurate determination of the direction of the jet and also for establishing the parallelism of the jets when there are multiple nuclear interacting particles incident.

3.3. *Efficiency.*

i) Response to singly charged particles at minimum ionization: To determine the operational characteristics for minimum ionizing singly charged particles, the spark counter was placed between two geiger counters registering the passage of cosmic ray particles. The voltage on the spark counter was pulsed whenever there was a coincidence between the Geiger counters. It was observed that sparking took place almost always (99%) in the region covered by the Geiger counter telescope and very rarely (1%) outside. The percentage of spurious breakdowns as obtained from this observation and by random triggering was less than 1%, at normal operating voltages. The efficiency of the spark counter, defined as the ratio of the number of spark breakdowns to the number of double coincidences, was determined as a function of the applied voltage, the clearing field voltage and the delay in the application of the pulse. The results are shown in Figs. 2 and 3 for a particular spark counter. It was found that by careful adjustment of spacing and applied vol-

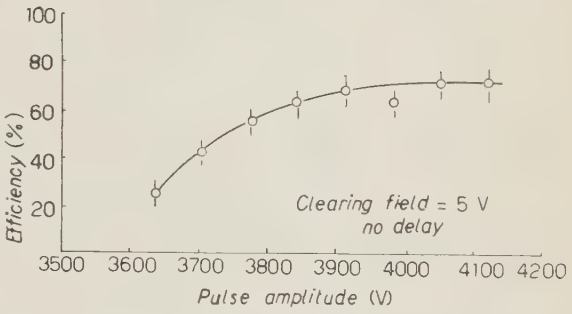

Fig. 2. – Variation of the efficiency of the spark counter for single cosmic ray charged particles, as a function of the pulsed voltage.

tage the efficiency for single particles can be pushed up to almost 90%. The counter was found to be equally sensitive whether the particles passed through the rods or in the gaps between the rods.

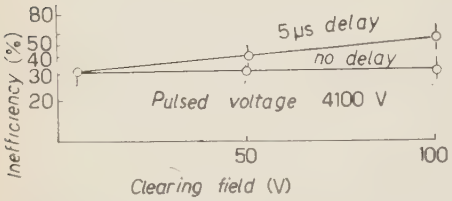

Fig. 3. – Inefficiency as a function of clearing field, and delay in the application of the pulsed voltage.

ii) Response to α-particles: With the same counter, when the operating voltage was adjusted for an efficiency of about 5% for singly charged minimum ionizing particles, the efficiency of response to α-particles was almost 100%. This was checked by depositing a thin film of a polonium α-source on the plate and pulsing the voltage by a proportional counter as before (see Section 1). This experiment shows that by a suitable adjustment of the efficiency, it is possible to make the spark counter respond preferentially to collimated jets that to some extent simulate α-particles in ionization.

4. – Operation with other particle detectors.

To determine the optimum conditions of operation of the spark counter for the detection and location of high energy jets produced by cosmic ray particles, the spark counter was operated in conjunction with a multiplate cloud chamber and with nuclear emulsions. The experiments were carried out at Ootcamund (2.2 km above mean sea level).

4·1. *Operation with the multiplate cloud chamber.* – The spark counter was mounted above the multiplate cloud chamber. Above the spark counter was kept a lead block of 10 cm thickness in which nuclear interactions were produced and which also served as a medium in which the nuclear and electromagnetic cascades developed. The spark counter was set to operate at an efficiency of $\sim 0.2\%$ for singly charged minimum ionizing particles. The cloud chamber and the spark counter were triggered for penetrating showers, with a scintillator-geiger counter selection system; since the selection system was not very rigorous, it responded to penetrating showers and air showers. The cloud chamber photographs provided visual evidence regarding the type of events which actuated sparks in the spark counter. It was found that the spark counter responded to high energy penetrating showers as expected; it was also found to respond sometimes to air showers. The response to air showers could not be explained in terms of the efficiency for single particles, since the

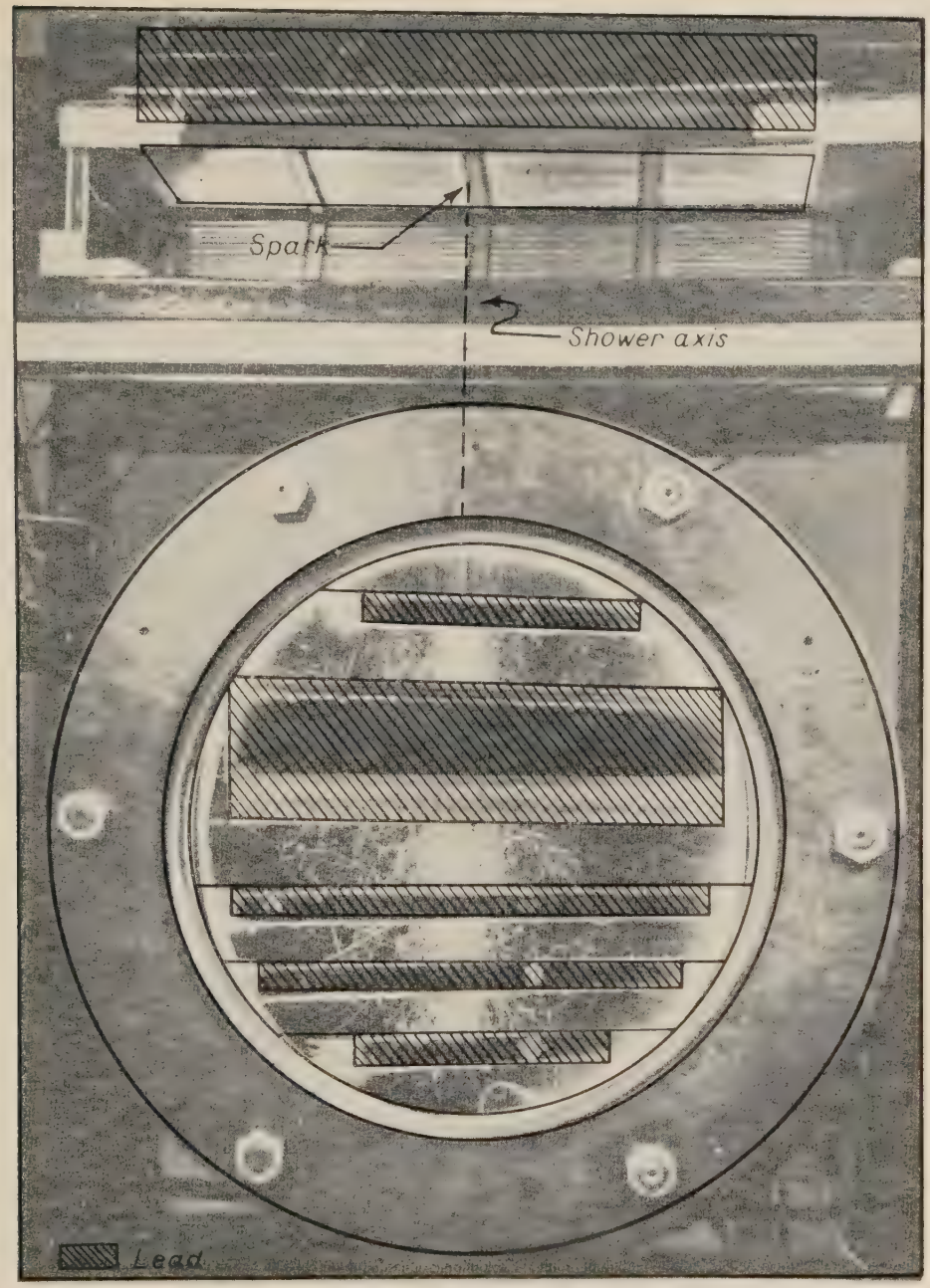

Plate III. - Cloud chamber photograph of a high energy penetrating shower produced in the lead block above the chamber and developing further in the lead plates inside. A spark was seen in the spark counter in the region through which the axis of the shower passed the spark counter (see the superposed illustration).

number of such particles passing through the spark counter was small, as seen in the corresponding cloud chamber photographs. The response is due most probably to heavily ionizing fragments and collimated showers of the type commonly seen emerging from the plates in multiplate cloud chambers. To ensure that the spark counter responds only to high energy penetrating showers, and to reduce considerably its response to air showers in which the high energy nuclear active particles do not pass through the spark counter area, a system of two spark counters one below the other can be employed. Correlated sparks in the two spark counters can only be due to high energy penetrating showers. The double spark counter system also has the additional advantage of giving the direction of the jet and of establishing parallelism in the case of simultaneous jets.

4·2. *Operation with nuclear emulsions.* – A system of two spark counters was operated at Ootacamund, in conjunction with a penetrating shower selection system as shown in Fig. 1. A layer of Ilford G-5 200 μm thick nuclear emulsions was placed above the top spark counter. The spark counter voltage was pulsed whenever there was a coincidence of the type $G_1 S G_2$. The scintillator was biased such that the $G_1 S G_2$ coincidence rate was about 2/hr. These coincidences are mostly due to penetrating showers with energies ≥ 20 GeV. Air showers in which the nuclear active particles do not pass directly through the array will not be admitted by this triggering system. The results are given in the following Table I.

TABLE I.

Time of operation (h)	Pulsed voltage (V)	Efficiency of spark counter for single particles		Number of triggers	Sparks		
		Top spark counter	Bottom spark counter		In top counter only	In bottom counter only	In both counters
28	4070	4.7%	8.5%	41	10	6	4
42	3850	4.1%	4.0%	69	12	5	10
42	3740	0.5%	1.5%	70	7	3	5

It follows from the table that when the efficiency of each spark counter is adjusted to about 5% for singly charged minimum ionizing particles, the efficiency of the system for penetrating showers, *i.e.* that one or both spark counters are triggered, is more than 50%. As already mentioned, the triggering rate of 2/hr corresponds to penetrating showers of energy about 20 GeV, and at this energy the collimation of the particles is poor and the number of electrons

produced by the development of γ-rays is also small. An efficiency of 100% cannot therefore be expected. The double sparks, which correspond to very high energy penetrating showers constitute about 10% of the number of triggering pulses. If the latter are due to showers of energy $\geqslant 20$ GeV, as previously stated, the double sparks should be attributed to showers of energy > 100 GeV. In all cases where double sparks were recorded a search was made in the emulsions at the places (5 mm$\times$5 mm) indicated by the spark counters and in the direction defined by the line joining the sparks, for multiple parallel tracks due to the collimated nuclear electro-magnetic cascades. In some cases, (5÷15) tracks confined within a radius of ~ 50 μm were observed. One can expect 5 tracks confined within a circle of 50 μm under about 5 radiation lengths of lead when the energy of the γ-rays is more than 50 GeV. Such γ-rays will in general arise from nuclear interactions involving energies of about 10^{12} eV. It is difficult to detect in the emulsions events in which the number of tracks is < 5 in a circle of radius 50 μm. Thus the lower limit to the energy of the nuclear interacting particles that can be detected with the combined system of spark counters and nuclear emulsions is about 10^{12} eV. Because of this, in all recorded cases of double sparks the corresponding events have not been detected in the emulsions. Nuclear emulsions of 50 μm thickness would reduce the cost considerably if they could be used. On trials, however, they were found to be unsuitable; because of their small thickness it was difficult to observe the tracks and establish definitely their parallelism. It should be feasible to use a thickness < 200 μm, possibly ~ 100 μm. It may also be emphasized that only those squares of emulsions need be taken out for examination through which jets have passed as indicated by the double sparks.

An important experimental observation is that even though all the rods were connected together electrically, simultaneous multiple sparks were recorded, sometimes quite close to each other (few cm). Therefore, it is not necessary to use many pulsing circuits.

5. – Conclusions.

It is feasible to construct triggered spark counters with areas of the order of half to one square meter, which respond preferentially to high energy jets ($>$ a few hundred GeV) produced by cosmic ray particles. Double spark counter systems can be used to give the position and direction of high energy jets and will be particularly useful in the study of simultaneous high energy nuclear interacting particles ([3,4]) associated and unassociated with air showers.

([3]) N. L. GRIGOROV, V. Y. SHESTOPEROV, V. A. SOBINYAKOV and A. V. PODGURSKAYA: *Žurn. Èksp. Teor. Fiz.*, **33**, 1099 (1957).

([4]) S. NARANAN, R. RAGHAVAN, P. V. RAMANAMURTY, B. V. SREEKANTAN and A. SUBRAMANIAN: *Nuovo Cimento*, **16**, 401 (1960).

Nuclear emulsions can be used in conjunction with such double spark counter system to obtain estimates of the energies of the nuclear interacting particles. Areas of the order of several square meters can be covered with an array of such large area spark counters and nuclear emulsions.

* * *

We have great pleasure in expressing our gratitude to Professor B. PETERS for his interest and encouragement in this investigation. We are thankful to Professor M. G. K. MENON for helpful discussions. We are indebted to Dr. M. S. SWAMY for help in the work connected with the use of nuclear emulsions. Our thanks are due to Messrs. F. GONSALVES and A. R. APTE who have helped us in preparing the spark counters and in operating the cloud chamber.

RIASSUNTO (*)

Si descrivono le caratteristiche costruttive di contatori a scintillazione di grande superficie. Questi contatori vengono usati, in unione con emulsioni nucleari, per esperimenti correnti in questo laboratorio su particelle ad alta energia da interazioni che arrivano simultaneamente su larghe aree, alcune volte in associazione con sciami dell'aria ed altre volte senza associazione con questi ultimi. Per questi esperimenti i contatori a scintillazione e le emulsioni sono usati in disposizioni che coprono un'area di alcuni metri quadrati.

(*) *Traduzione a cura della Redazione.*

Effect of Lepton Non-Conservation on π-Decay.

P. K. KABIR

Saha Institute of Nuclear Physics - University of Calcutta

(ricevuto il 20 Giugno 1960)

It has been pointed out by PAULI [1] that first-order processes throw no light whatever on the question of lepton conservation, a principle which is more or less taken for granted in almost all discussions of leptonic processes. The experiments on second-order processes, like neutrino capture and double β-decay, which could decide the question, present extreme experimental difficulties and provide only a very rough limit of the amount of possible lepton non-conservation. Consequently, it is desirable to examine other processes in which the law of lepton conservation can be tested. It is the purpose of this note to show that the branching ratio of π-e to π-μ decays is a sensitive test for the presence of a particular type of lepton non-conserving interaction.

The branching ratio R of π-e to π-μ decays is found to be [2]

$$R_{\text{exp}} = \frac{W(\pi^+ \to e^+ + \nu)}{W(\pi^+ \to \mu^+ + \nu)} = 1 \cdot 10^{-4} , \tag{1}$$

with a quoted error of less than 20%. We know that pions interact strongly with nucleons and also that nucleons possess weak interactions with muons and with electrons. To understand the pion decay, therefore, it is not necessary to invoke any direct interaction between pions and leptons; in fact, according to the general principles of quantum mechanics, we should expect the pion to decay through a two-stage process whereby the pion first dissociates through its strong interaction virtually into a nucleon-antinucleon pair which trasforms into a lepton and a neutrino through the weak interaction.

Since there is no experimental evidence which requires us to postulate a direct decay coupling between pions and leptons, we shall assume that there is no such direct interaction. Assuming that the pion-nucleon interaction conserves parity and that the pion field is pseudoscalar, it follows from general invariance arguments that the decay proceeds only through the P and A forms of the Fermi interaction.

[1] W. PAULI: *Nuovo Cimento*, **6**, 205 (1957).
[2] H. ANDERSON, T. FUJII, R. H. MILLER and L. TAU: *Phys. Rev. Lett.*, **2**, 53 (1959).

Unfortunately, we cannot in general calculate the decay rates of either of the two modes because of the presence of the strongly interacting particles in the intermediate state [3]. However, for the case of either pure P or pure A interaction, the branching ratio becomes independent of the strong interactions because the effect of the strong interactions may then be represented by a constant factor which is the same for both modes. Assuming lepton conservation and equal coupling constants for β-decay and muon absorption, the calculated ratio for the first case is far in excess of that observed, (1), but for the A case, the ratio is [4]

$$R_0 = \frac{m_e^2}{m_\mu^2}\left[\frac{1 - m_e^2/m_\pi^2}{1 - m_\mu^2/m_\pi^2}\right] = 1.28 \cdot 10^{-4}\,, \tag{2}$$

which is in surprisingly good agreement with (1). Further, inclusion of electrodynamic radiative corrections [5] reduces R by about 11% for an energy resolution of 1 MeV.

It is of course possible that the agreement between (1) and (2) is purely accidental but we shall not adopt that view, particularly since we note that β-decay certainly contains A interactions [6] and it appears that the Hamiltonian for muon-absorption does too [7]; the strengths are known to be comparable. Also, there is no positive evidence for P interaction in either case. From the agreement of (1) and (2), we may exclude the possibility of any P interaction, or more accurately any P interaction with a coupling constant of the order of, or exceeding, 10^{-3} times the A coupling constant [8]. Strictly speaking, we cannot calculate the ratio R for any mixture of interactions but we quote this figure because a perturbation-theory estimate with a cut-off at the nucleon mass indicates that, for equal coupling constants, the amplitude for decay due to P interaction exceeds that due to A by a factor of the order of 10^3. To understand how the introduction of lepton–non-conserving interactions affects R, we recall briefly why the old lepton-conserving theory gave the small value (2) instead of the much larger number which we should expect from phase-space arguments. The expression in square brackets in (2), which is greater than unity, is essentially this factor.

It is a feature of the A interaction (and the opposite for P) that if we describe the neutrino, which we assume to be massless [9], in terms of handed states, negatons are emitted preferentially with the same handedness as the neutrino (which we define by $n \to p + e^- + \bar{\nu}$) and positons the opposite; the probability of the favoured spin-state being $\frac{1}{2}(1+v/c)$ as compared to $\frac{1}{2}(1-v/c)$ for the other. Therefore, since the decay $\pi^+ \to e^+ + \nu$ produces extremely relativistic electrons (electron energy = 70 MeV) the probability of emission of positons with handedness opposite to that

[3] Nevertheless, M. L. Goldberger and S. B. Treiman have succeeded in obtaining a remarkably good estimate of the absolute decay rate on the-basis of certain plausible assumptions: *Phys. Rev.*, **110**, 1178 (1958) and **111**, 354 (1958).

[4] M. Ruderman and R. J. Finkelstein: *Phys. Rev.*, **76**, 1458 (1949).

[5] S. Berman: *Phys. Rev. Lett.*, **1**, 468 (1958).

[6] C. S. Wu: *Rev. Mod. Phys.*, **31**, 783 (1959).

[7] V. Telegdi: see J. Polkinghorne: *Phys. Today*, **12**, 12, 36 (1959).

[8] It is possible for a small P admixture of this order to *reduce* the ratio R through destructive interference, and this was pointed out by Huang and Low at a time when it appeared that π-e decay was even more rare than (1). We do not consider this pathological possibility.

[9] This is only to simplify the discussion, and is not essential to the argument. The assumption of a finite rest-mass (compatible with other experimental evidence) would not affect the principal conclusion.

of the neutrino, is almost unity. But consideration of angular momentum conservation in the rest system of the pion ($J=0$), in which the positon and the neutrino go in opposite directions, requires both particles to have the same handedness; since the probability of emission of such positons is so small, the decay occurs very seldom. In the case of the muon-decay mode, the muon is quite non-relativistic (muon energy = 4 MeV) and the probability of either handed state is almost equal. There is therefore no inhibition due to the angular momentum condition and the decay proceeds at a « normal » rate. Notice that no assumption was made about a particular handedness for the neutrino, thus the argument does not depend on parity non-conservation or on the two-component theory of the neutrino.

But now we see that the argument rests on the assumption that positive pion decay involves the emission of a neutrino and not of an antineutrino, for which the electronic decay mode would again occur at a « normal » rate. Thus a slight relaxation of the law of lepton conservation would have a large effect on the branching ratio R. The general theory of Fermi interactions including possible lepton non-conservation has been given by PAULI ([1]); the β-decay Hamiltonian, for instance, takes the form

$$(3) \qquad \mathscr{H}_{\text{int}} = \sum_i (\overline{\psi}_n \Gamma_i \psi_p) \left[\{\overline{\psi}_\nu (g_i \Gamma_i + g_i' \gamma_5 \Gamma_i) \psi_e\} + \{\psi_\nu C (f_i \Gamma_i + f_i' \gamma_5 \Gamma_i) \psi_e\} \right] + \text{h.c.} ,$$

where the first term in the square brackets represents the conventional Hamiltonian, including parity–non-conserving terms. Taking the pseudoscalar coupling constants as zero ([10]), the branching ratio calculated from interactions of the form (3) for muon-absorption and β-decay is also independent of the strong couplings:

$$(4) \qquad R' = \frac{C_e^2 + m_\pi^2/m_e^2 D_e^2}{C_\mu^2 + m_\pi^2/m_\mu^2 D_\mu^2} ,$$

where

$$C^2 = |g_A|^2 + |g_A'|^2 , \qquad D^2 = |f_A|^2 + |f_A'|^2 .$$

If we take the muon and electron coupling constants as equal and consider the relative strength $\varepsilon = D^2/C^2$ of the lepton–non-conserving interaction as small, (4) can be rewritten as

$$R' = (1 + N\varepsilon) R_0 , \qquad N = \frac{m_\pi^2}{m_e^2} = 7.45 \cdot 10^4 .$$

Thus we see that an admixture of 10^{-5} of lepton–non-conserving A interaction would almost double the branching ratio R, and we may conclude from the agreement between R_0 and R_{exp} that any such admixture *must be considerably smaller or non-existent.* The selection rule which prevents S, V and T interactions from contributing to pion

([10]) The argument given earlier for the smallness of the P coupling constant applies equally to lepton-conserving and non-conserving interactions. However, in the lepton–non-conserving case, a small P admixture would manifest itself as much in enhancing the total decay rate as in changing the branching ratio R.

decay also prevents us from drawing any conclusions about possible lepton-conserving terms of those forms. Similar arguments apply to the $K_{e2}/K_{\mu 2}$ branching ratio, although the greater experimental uncertainty in this case permits only the weaker restriction $\varepsilon < 10^{-3}$.

It should be remarked that another requirement for the agreement of (1) with (2) is the exact or near-exact equivalence of muon and electron with respect to weak interactions with all baryons. The nucleon pair which we assumed in the virtual intermediate state may equally well be replaced by some heavier hyperon pair (consistent with the strong interaction conservation laws) and if these particles contribute appreciably to the decay process, we must require their couplings to electron and muons to be the same if we are to leave R unchanged. In particular, if the interaction constants for hyperon β-decay are smaller than the nuclear β-decay constant, as some authors have suggested, than the coupling constants for muonic decay of hyperons must be smaller in the same ratio.

* * *

This investigation arose from a remark by A. Sirlin. I would also like to thank Prof. R. E. Peierls for helpful comments, and H. Banerjee for checking the calculations.

IL NUOVO CIMENTO Vol. XVII, N. 3 1° Agosto 1960

High-Energy Pion-Nucleon Collisions and Isotopic Properties of the Pion-Pion Interaction.

A. Krzywicki

Institute for Nuclear Research - Warsaw

(ricevuto il 23 Giugno 1960)

The aim of this note is to present a short account of obtained results, concerning the high-energy ($E_\pi^{(\mathrm{lab})} > 4$ GeV) pion-nucleon interaction. The detailed explanation and justification of approximations made will be contained in a (larger) paper, being in publication.

1. – Our essential assumptions are as follows. We adopt the idea of strong pion-pion interaction. We limit ourselves to peripheral pion-nucleon collisions, that is the quantities whose behaviour will be discussed correspond to certain selected events. We identify peripheral collisions with such collisions where only a small amount of momentum of one incident particle is transferred to the other by a single intermediate pion [1]. At the same time we assume that by selecting experimentally observed stars according to properties which are typical for peripheral collisions, we really get a sample of stars in which the contamination of stars due to non-peripheral collisions is small. Concerning the interaction mechanism we assume that the incident pion interacts with one and only one pion of the virtual cloud surrounding the target nucleon, but this interaction can lead to the excitation of the whole nucleon. Moreover we assume that only the pion-pion interaction and the decay of the produced isobar are responsible for the production of additional pions in peripheral pion-nucleon collisions. In calculations we use Dremin and Cerniavski's method and assume that the peripheral pion-nucleon collision is characterized by the scattering of the incident and virtual pions in a low relative angular momentum state and that the pion-pion scattering amplitude weakly depends on energy. The upper limit of the energy to which our calculations are applicable is fixed by the assumption that we can neglect the probability of production of more than two additional pions in a peripheral pion-nucleon collision. The following notation is used (we

[1] I. M. Dremin and D. S. Černiavski: *Žurn. Èksp. Teor. Fiz.*, **38**, 229 (1960).

work in cm):

$\boldsymbol{p}, p_0$ momentum and energy of the incident proton;

$\boldsymbol{q}, \omega_0$ momentum and energy of the incident pion;

$\boldsymbol{P}, P_0$ momentum and energy of the isobar;

$\boldsymbol{k}, \omega$ momentum and energy of the virtual pion;

$\boldsymbol{t}, t_0$ momentum and energy of the final nucleon;

$\boldsymbol{k}_i, \omega_i$ momenta and energies of final pions;

M, m, μ isobar, nucleon and pion masses.

2. – First we examine the problem, whether one can obtain the branching ratio

$$R = \frac{(\pi^- + \mathrm{p} \to \pi^0 + \pi^- + \mathrm{p})}{(\pi^- + \mathrm{p} \to \pi^0 + \pi^- + \mathrm{n})},$$

from the experimental branching ratio

$$R^{(\mathrm{exp})} = \frac{(\pi^- + \mathrm{p} \to \pi^- + \mathrm{p} + ?)}{(\pi^- + \mathrm{p} \to \pi^- + \pi^+ + \mathrm{n} + ?)}.$$

Let us consider an experiment which consists of counting the relative frequency of occurrence of two kinds of stars (in the lab. system), first with two energetic prongs and second with one energetic and one relatively slow prong identifiable as a proton. The following restrictions are imposed on the momenta (in cm) of final charged particles, in order to ensure the peripheral character of selected events.

$$(1) \qquad \begin{cases} |\boldsymbol{k}_i| > h_i(\boldsymbol{k}_i), & \text{for final charged mesons,} \\ |\boldsymbol{t}| > h_3(\boldsymbol{t}), & \text{for final protons,} \end{cases}$$

h_i are chosen in such a way that (1) excludes $\boldsymbol{k}_i \cdot \boldsymbol{q} < 0$, $\boldsymbol{t} \cdot \boldsymbol{p} < 0$. (1) must also imply that the charged meson did not result from the decay of the isobar. h_3 is such that we do not take into account protons which could be produced by the isobar and emitted backward in the isobar rest frame. We assume here that $|\boldsymbol{p} - \boldsymbol{P}|/\mu$ is limited and its maximum value is of the order of magnitude of unity. The simplest choice of h_1 and h_2 is:

$$(2) \qquad h_i(\boldsymbol{k}_i) = \begin{cases} r = \mathrm{const}, & \text{for } \boldsymbol{k}_i \cdot \boldsymbol{q} > 0, \\ |\boldsymbol{k}_i^{(\max)}|, & \text{for } \boldsymbol{k}_i \cdot \boldsymbol{q} < 0, \end{cases}$$

where r is larger than the maximal momentum of a pion flying forward (in cm) and emitted by the decaying isobar flying backward (in cm).

For events selected in such a way, one can calculate $R^{(\mathrm{exp})}/R$. One obtains:

$$(3) \qquad R^{(\mathrm{exp})}/R = (1 + c_1)/(1 + c_2),$$

where

$$(4)\qquad \begin{cases} c_1 = \dfrac{-1}{2\pi^2(g^2/4\pi)} \cdot \dfrac{\int \mathrm{d}_4 P \left([p_0\omega I_{\pi\pi}\sigma(\omega; p\pi^0 \to p\pi^0)]/[(P-p)^2+\mu^2]^2\right) F_1(P)}{\int\limits_{|\boldsymbol{t}|\gtrsim h_3} \mathrm{d}_3 t \left[(m^2+(pt))/t_0[(t-p)^2+\mu^2]^2\right) F_1(t)}\,, \\ c_2 = \dfrac{-1}{4\pi^2(g^2/4\pi)} \cdot \dfrac{\int \mathrm{d}_4 P \left([p_0\omega I_{\pi\pi}\sigma(\omega; p\pi^0 \to n\pi^0)]/[(P-p)^2+\mu^2]^2\right) F_2(P)}{\int \mathrm{d}_3 \boldsymbol{t} \left((m^2+(pt))/t_0[(t-p)^2+\mu^2]^2\right) F_2(t)}\,, \end{cases}$$

(the restrictions imposed on the integration with respect to P are not written explicitly here) F_1 and F_2 denote certain kinematical factors corresponding respectively to cases when in the final state we have proton or neutron. F's are defined by the expression:

$$(5)\qquad F(x) = \int \frac{\mathrm{d}_3 \boldsymbol{k}_1}{\omega_1} \int \frac{\mathrm{d}_3 \boldsymbol{k}_2}{\omega_2} \delta_4(p+q-x-k_1-k_2)\,, \qquad |\boldsymbol{k}_1| > h_1\,,\ \ |\boldsymbol{k}_2| > h_2,$$

(in the case when k_i denotes momentum of a neutral pion $h_i \equiv 0$). We have also [1]

$$(6)\qquad p_0\omega I_{\pi\pi}\sigma(\omega) = \tfrac{1}{2}(M^2 - m^2 - \mu^2)^2 - 4m^2\mu^2]^{\frac{1}{2}}\sigma(M^2)\,.$$

A very rough calculation gives (we assume that only a $\frac{3}{2}$, $\frac{3}{2}$ isobar is produced):

$$(7)\qquad \frac{9}{8}c_1 \sim \frac{9}{2}c_2 \sim \frac{p_0^2}{(g^2/4\pi)(\Delta p)_{\max}^3}\left[3.7\cdot(\Delta p)_{\max} - \frac{9.3\cdot\mu\cdot m}{p_0+\omega_0}\right].$$

$(\Delta p)_{\max}$ denotes the maximal momentum transfer in a peripheral collision, is of the order of μ and plays here the role of a parameter. One can verify that for Walker's experiment [2], at 4.5 GeV, c_1 is of the order of 10, so that $R^{(\exp)}/R$ is not far from 4.

Using the approximate formula (A denotes pion-pion scattering amplitude)

$$(8)\qquad R \sim \frac{|A(\pi^0\pi^- \to \pi^0\pi^-)|^2}{2|A(\pi^+\pi^- \to \pi^+\pi^-)|^2}\,,$$

we calculated R for seven extreme cases (the index at A refers to the isotopic spin of the two-pion system):

$|A^{(0)}| \gg |A^{(1)}|,\ |A^{(2)}|$; $\qquad |A^{(1)}| \gg |A^{(0)}|,\ |A^{(2)}|$; $\qquad |A^{(2)}| \gg |A^{(0)}|,\ |A^{(1)}|$;

$|A^{(0)}| \sim |A^{(1)}| \gg |A^{(2)}|$; $\qquad |A^{(0)}| \sim |A^{(2)}| \gg |A^{(1)}|$;

$|A^{(1)}| \sim |A^{(2)}| \gg |A^{(0)}|$; $\qquad |A^{(0)}| \sim |A^{(1)}| \sim |A^{(2)}|$.

Table I gives R. The first line of the table shows isotopic spins which characterise «large» $A^{(i)}$'s, *e.g.* to the case $|A^{(1)}| \sim |A^{(2)}| \gg |A^{(0)}|$ corresponds the symbol (1, 2) in the first line.

[2] W. D. Walker: *Phys. Rev.*, **108**, 872 (1957).

TABLE I.

T	(0)	(1)	(2)	(0, 1)	(0, 2)	(1, 2)	(0, 1, 2)
R	0	0.5	4.5	0.18	0.5	1.125	0.5

3. – Consider the process $\pi^- + p \to \pi^- + \pi^- + \pi^+ + p$ occuring in a bubble chamber. We take into account only 4-prong stars where three particles are very energetic and one relatively slow (in the lab. system) where the momentum is balanced and the slow particle is identifiable as a pion. This slow pion was emitted backward in cm. We assume that at least two fast particles are collimated forward in cm (peripherality condition). Relative frequency of occurence of stars with slow pion being positive or negative can be measured (we denote this quantity by R_1 and assume that only one $\frac{3}{2}, \frac{3}{2}$ isobar was produced)

$$R_1 \sim \frac{9\,|A(\pi^-\pi^- \to \pi^-\pi^-)|^2}{|A(\pi^-\pi^+ \to \pi^-\pi^+)|^2}\,. \tag{9}$$

Table II shows R_1 in seven extreme cases, when the dependence of $A^{(i)}$ on other variables than iso-spin is neglected.

TABLE II.

T	(0)	(1)	(2)	(0, 1)	(0, 2)	(1, 2)	(0, 1, 2)
R_1	0	0	324	0	36	20,25	9

The cross section for the peripheral process $\pi^- + p \to \pi^- + \pi^- + \pi^+ + p$ when π^- is emitted backward is

$$\sigma_{\substack{\text{periph.}\\ \pi^- \text{ back.}}}(\pi^- p \to 2\pi^-\pi^+ p) = \text{const}\,\frac{p^2}{p_0^2\omega_0}\left[3.7\,(\Delta p)_{\max} - \frac{9.3\cdot\mu\cdot m}{p_0 + \omega_0}\right]. \tag{10}$$

One can show that $\sigma_{\substack{\text{periph.}\\ \pi^- \text{ back.}}}(\pi^- p \to 2\pi^-\pi^+ p)$ corresponding to $E_\pi^{(\text{lab})} = 4.5$ GeV is of the order of, or somewhat smaller than $\sigma_{\text{periph.}}(\pi^- p \to \pi^-\pi^+ n)$ so that it is probably of the order of 1 mb.

* * *

I should like to offer my sincere thanks to prof. Z. KOBA for advice.

Die elastische und inelastische Streuung von negativen K-Mesonen an freien Protonen bei Energien bis 90 MeV.

H. Göing

Max-Planck-Institut für Physik und Astrophysik - München

Nuovo Cimento, **16**, 848 (1960)

ADDENDUM

In der genannten Arbeit wurde erwähnt, daß 55% der wom Verfasser analysierten Ereignisse von den Instituten in Bologna, Paris un Parma beigesteuert worden waren; es war jedoch versehentlich der Hinweis darauf unterlassen worden, daß die analysierten Ereignisse zum größten Teil mit denen identisch sind, die auch in der Gemeinschaftsarbeit von Alles *et al.* [1] behandelt wurden. Der Verfasser dankt seinen Kollegen in Bologna, Paris, Parma und München für ihre Hilfe und Mitarbeit.

---

[1] W. Alles, N. N. Biswas, M. Ceccarelli, R. Gessaroli, G. Quareni, H. Göoing, K. Gottstein, W. Püschel, J. Tietge, G. T. Zorn, J. Crussard, J. Hennessy, G. Dascola und S. Mora: *Nuovo Cimento*, **11**, 771 (1959).

LIBRI RICEVUTI E RECENSIONI

M. R. Wehr and J. A. Richards jr. – *Physics of the atom*. Addison-Wesley Publishing Company, Inc. (Reading, Mass., and London), 1960, pp. XI-420, prezzo dollari 8,50.

Il volume, si dice esplicitamente ma forse un po' troppo genericamente nella prefazione, non vuole essere una rassegna, nè un trattato, ma un vero e proprio libro di testo destinato a colmare la lacuna fra la fisica classica ed il fronte attuale della ricerca. Esso viene quindi ad aggiungersi a parecchie altre opere pubblicate, particolarmente negli Stati Uniti, con simile, e non facile, dichiarato intendimento.

La mole di materia trattata è veramente grande. I primi tre temi sono così enunciati dagli autori, nell'ordine: concezione atomica della materia, dell'elettricità, della radiazione. Seguono, sempre traducendo letteralmente i titoli: modelli atomici di Rutherford e Bohr, relatività, raggi X, onde e corpuscoli, concezione atomica dei solidi, radioattività naturale, reazioni nucleari e radioattività artificiale, energia nucleare ed infine raggi cosmici e particelle elementari. Ogni capitolo è corredato da ampi riferimenti bibliografici e da una ricca serie di problemi, per metà dei quali è offerta la soluzione: notevole l'uso quasi esclusivo del sistema di misura MKS.

Il piano generale dell'opera non soddisfa del tutto sia per numerose divagazioni dal fine prefisso, sia per il criterio con cui le nozioni si susseguono, ben spesso accavallandosi: inoltre, se è vero che una certa superficialità nella trattazione è annunciata e scontata, essa si spinge non di rado ad un punto tale da chiedersi se non sarebbe stato meglio escludere del tutto alcuni argomenti, specie di natura teorica.

A facili critiche si prestano poi le fantasiose analogie, di cui il testo abbonda, troppo spesso suscettibili di indurre in equivoci anche gravi un lettore inesperto; così, mentre il libro è senza dubbio elementare, non se ne può consigliare la lettura che a persone di una certa esperienza, come vivace riepilogo di nozioni già maturate.

Piacevole lo stile, americano come non mai, dell'esposizione e certamente lodevoli così l'attenzione per i protagonisti della ricerca, che rivivono spesso in aneddoti, come la sollecitudine dimostrata per l'avvenire scientifico dei lettori. Risentono di questa singolare attitudine umanistica già la prefazione in cui si ammonisce che le conquiste maggiori si devono a ricercatori in giovane età, e perfino le prime due delle otto appendici: in una si riepilogano in ordine cronologico le principali scoperte nel campo dell'atomismo dando particolare rilievo tipografico ai nomi degli autori riportati con completezza insolita, nell'altra si elencano tutti i premi Nobel per la Fisica e per la Chimica.

A. Loria

S. S. PENNER – *Quantitative Molecular Spectroscopy and Gas Emissivities*. Addison-Wesley Publ. Co., Reading, Mass. Pergamon Press, London-Paris, 1959. Pagine XV-587.

Trattasi di un libro particolarmente destinato a coloro che desiderano specializzarsi nello studio dei moderni motori di propulsione a reazione, e richiede già una certa preparazione di fondo di matematica, di spettroscopia e di meccanica quantistica ed ondulatoria. Esso esamina in generale problemi, relativi all'energia radiante, che di solito non sono svolti nelle opere classiche di spettroscopia o di ottica radiante, in quanto il campo di temperatura particolarmente considerato è intermedio tra quello della spettroscopia molecolare abituale e quello peculiare agli studi astrofisici.

La materia esposta è suddivisa in 19 capitoli i quali trattano nell'ordine: la radiazione termica; i coefficienti e le intensità di Einstein; i profili spettrali; la radiazione da righe spettrali isolate; la misura della trasparenza e dell'assorbimento per righe spettrali isolate; la determinazione sperimentale delle intensità assolute; calcoli teorici di intensità assolute e relative; la misura sperimentale in spettri IR della semi-ampiezza di dispersione; la misura diretta della larghezza delle righe; la dispersione ottica; calcoli teorici del potere di emissione IR a temperatura moderata da parte di gas in stato di equilibrio; calcoli teorici di assorbimento isotermico delle radiazioni del corpo nero; la formulazione matematica per problemi di trasferimento radiante di gas non uniformi; il potere di emissione di aria riscaldata; stima del potere di emissione da parte di atomi di idrogeno; la temperatura di popolazione e la temperatura di traslazione di radicali liberi in fiamma; l'effetto della radiazione sulla combustione e sulla velocità di propellenti solidi; stima del trasferimento di calore radiante e delle variazioni di temperatura in propellenti liquidi per missili.

La trattazione della materia, tenendo presente il livello medio presunto dei lettori interessati, è abbastanza piana e non difficile. In ogni caso questo libro raccoglie una notevole massa di informazioni non facilmente reperibili nei trattati classici e, pertanto, esso è raccomandabile nella biblioteca di ogni spettroscopista.

La presentazione tipografica è ottima per chiarezza sia del testo che delle figure.

G. MILAZZO

Direttore responsabile: G. POLVANI Tipografia Compositori - Bologna
Questo fascicolo è stato licenziato dai torchi il 12-VIII-1960